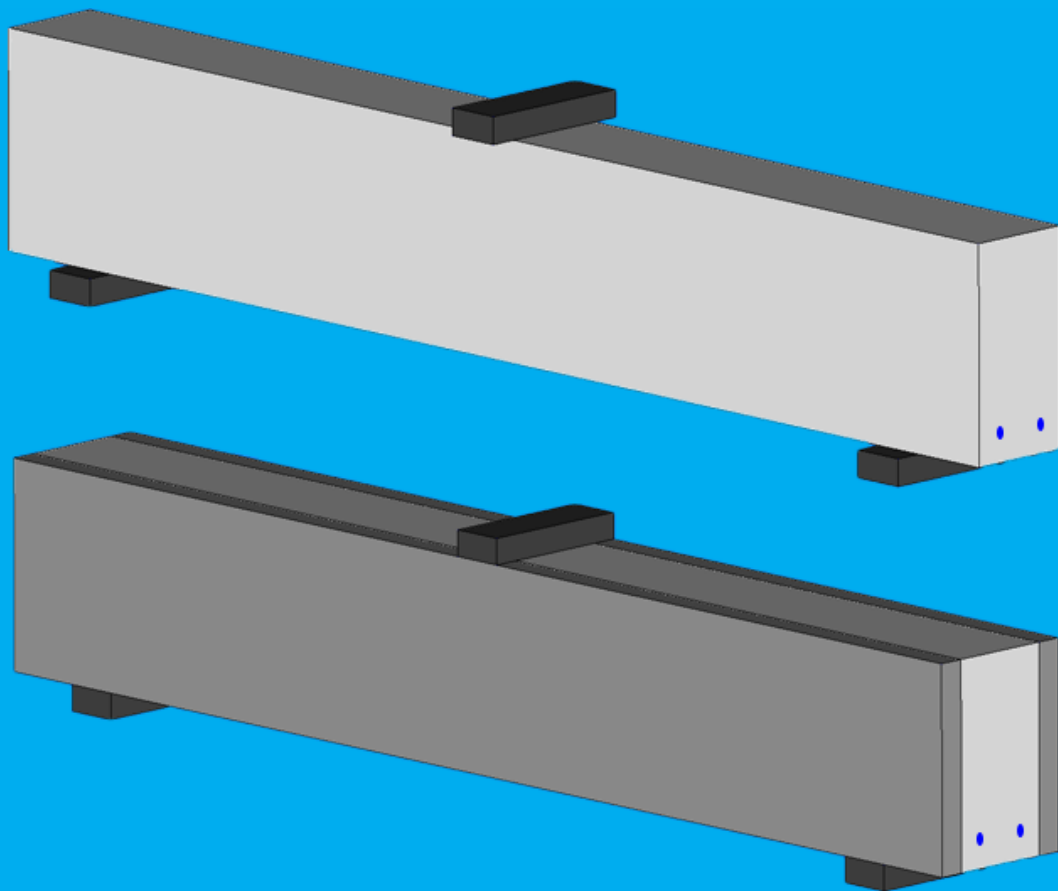


Numerical Study of Shear Strengthening of Reinforced Concrete Beams using Strain-Hardening Cementitious Composites

Ajlal Arif



Numerical Study of Shear Strengthening of Reinforced Concrete Beams using Strain-Hardening Cementitious Composites

by

Ajlal Arif

to obtain the degree of Master of Science
at the Delft University of Technology,
to be defended publicly on Monday November 30, 2020 at 16:00.

Student number: 4808819
Project duration: February 21, 2020 - November 30, 2020
Thesis committee: Dr. ir. M. Luković, TU Delft, Chair and Supervisor
ir. S. Mustafa, TU Delft, Co-supervisor
Prof. dr. ir. E. Schlangen, TU Delft
Dr. ir. C. B. M. Blom, TU Delft
ir. Y. Huang, TU Delft

An electronic version of this thesis is available at <http://repository.tudelft.nl/>.

Abstract

Existing reinforced concrete structures can be strengthened using Strain Hardening Cementitious Composites (SHCC). The ability of SHCC in exhibiting a ductile response under tensile load and high energy absorption capacity due to strain-hardening after crack initiation makes it a viable material to be used in, both, construction and retrofitting of concrete structures. Shear strengthening of concrete beams using SHCC is mostly studied experimentally due to the challenging nature of modelling the shear cracking behaviour and the interface between concrete and SHCC. The main objective of this research is to study the shear behaviour of SHCC-strengthened reinforced concrete (RC) beams using Non-Linear Finite Element Analysis (NLFEA).

Benchmark experimental beams are selected from literature and analysed using different numerical solution strategies in DIANA FEA software package. The selected benchmark beams consist of reinforced concrete beams, reinforced SHCC beam and SHCC-RC hybrid beams. All selected benchmark beams lack the use of transverse reinforcement in the shear span. Total strain-based fixed crack model is used to model both concrete and SHCC. The reinforcement is modelled as embedded reinforcement.

The shear behaviour of benchmark reinforced concrete beams is analysed first using two numerical solution strategies. The main varying parameter in the two solution strategies is the type of shear retention function (SRF) used; Damage-based and Al-Mahaidi. The mesh size is also varied since the numerical response of reinforced concrete beams failing in shear is highly sensitive to the mesh size considered. The numerical results are compared with the experiments to assess how accurately FEA captures the shear behaviour of reinforced concrete beams.

The comparison shows that analysis of the selected reinforced concrete beams analysed using Damage-based shear retention function results in accurate predictions of peak load if a fine mesh size resulting in 30 or more elements in the height of the beam is used. The difference between the numerical and experimental peak loads is observed to be 9% on average. However, the failure type is predicted inaccurately for both coarse and fine mesh sizes due to lack of consideration for aggregate interlock in Damage-based shear retention function. The analysis of the selected reinforced concrete beams using Al-Mahaidi shear retention function results in accurate predictions of peak load if a coarse mesh size resulting in 20 elements in the height of the beam is used. The difference between the numerical and experimental peak loads is observed to be 9.2% on average. The failure type is also predicted accurately using Al-Mahaidi shear retention function with the stated mesh size. The consideration for aggregate interlock implicitly in Al-Mahaidi shear retention function in the form of shear retention factor β allows for accurate prediction of both peak load and failure type. Therefore, the numerical results of reinforced concrete beams modelled using both types of shear retention functions are mesh size-dependent, and improper inputs can lead to unreliable results.

After analysing the shear behaviour of reinforced concrete beams, the shear behaviour of a reinforced SHCC beam is analysed. The numerical solution strategy consisting of Al-Mahaidi shear retention function is selected to model the shear behaviour of a reinforced SHCC beam since it can predict both failure load and failure type accurately for reinforced concrete beams. In comparison with experiment, the peak load for the reinforced SHCC beam is underestimated by 27% and the failure type is also incorrectly modelled. Use of embedded reinforcement results in excessive cracking along the reinforcement, causing convergence issues at a load lower than the experimental peak load. Such excessive cracking is not observed in reinforced concrete beams since cracks are less and more localized in concrete as compared to SHCC, which exhibits multi-cracking behaviour. Therefore, the shear behaviour of selected reinforced SHCC beam using Al-Mahaidi shear retention function is not accurately modelled. However, since reinforcement is in concrete in hybrid beams, therefore, the hybrid beams are continued to be analysed with embedded reinforcements.

After the analysis of shear behaviour of concrete and SHCC separately, their behaviour is studied in the form of SHCC-RC hybrid beams. The numerical solution strategy consisting of Al-Mahaidi shear retention function is used as well, and different types of hybrid interface are modelled. The comparison with experiments shows that the peak load and failure type are accurately predicted when a numerically perfect bond condition is modelled at the hybrid interface for hybrid beams exhibiting no debonding during experimentation. The difference between the numerical and experimental peak loads is approximately 6% on average. This is in case of a mesh size resulting in 20 elements in the height of beam used. The peak load and failure type, however, are inaccurately predicted when delamination is modelled at the hybrid interface for hybrid beams failing due to delamination during experimentation, irrespective of the mesh size considered. This is due to the inability of the Coulomb friction interface model in DIANA in recognising significant delamination at the hybrid interface as a reason for the failure of the hybrid beam. Due to this limitation, the numerical model inaccurately predicts the peak load if the thickness of SHCC is varied as well.

Therefore, the shear behaviour of hybrid beams can only be modelled with reliability using Al-Mahaidi shear retention function if delamination is not considered and a mesh size resulting in 20 elements in the height of the beam is used. If delamination at the hybrid interface is modelled in the hybrid beams, the numerical results are not reliable.

Contents

List of Figures	ix
List of Tables	xv
1 Introduction	1
1.1 Background and Motivation	2
1.2 Problem Statement	3
1.3 Research Scope and Objectives.	3
1.4 Research Hypothesis.	3
1.4.1 Research Questions	3
1.5 Research Approach	4
1.6 Report Outline	5
2 Literature Study	7
2.1 Shear Failure of Concrete Beams	8
2.2 Shear Strengthening of Concrete Beams	10
2.2.1 Common Strengthening Techniques.	10
2.2.2 Strengthening using SHCC	12
2.3 Numerical Analysis	16
2.3.1 Analysis of Reinforced Concrete Beam	16
2.3.2 Analysis of Strengthened Reinforced Concrete Beam	18
3 Benchmark Studies	23
3.1 Study 1 - Guan Wang et al. (2019) [57]	25
3.2 Study 2 - Yongxing Zhang et al. (2015) [61]	27
3.3 Study 3 - Vu Hong Nghiep (2011) [44].	30
3.4 Study 4 - Yongxing Zhang et al. (2011) [64].	32

4	Methodology	35
4.1	Idealisation of Physical Problems	37
4.1.1	Geometry of the Model	38
4.1.2	Loading Conditions and Support Conditions	39
4.2	Numerical Solution Strategy	41
4.2.1	Considerations for Constitutive Model	41
4.2.2	Assumptions around Kinematic Compatibility	45
4.2.3	Equilibrium Conditions	50
4.2.4	Developed Numerical Solution Strategies	51
4.2.5	Judgement of Numerical Solution Strategies	52
4.3	Analysis-Stop Criteria	52
4.4	Material Properties of Benchmark Studies	54
4.4.1	Concrete	54
4.4.2	SHCC	55
4.4.3	Reinforcement	55
4.4.4	Load and Support Plates	56
4.5	Numerical Models	56
5	Results & Conclusions	57
5.1	Modelling Phase I	58
5.1.1	Results Modelling Phase I	58
5.1.2	Discussion Modelling Phase I	65
5.1.3	Conclusions Modelling Phase I	72
5.2	Modelling Phase II	73
5.2.1	Results Modelling Phase II	73
5.2.2	Discussion Modelling Phase II	77
5.2.3	Conclusions Modelling Phase II	79
5.3	Modelling Phase III	79
5.3.1	Results Modelling Phase III	80
5.3.2	Discussion Modelling Phase III	93
5.3.3	Conclusions Modelling Phase III	106
5.4	Conclusions	107

6 Recommendations	109
Appendices	113
A Convergences of the Numerical Models	113
B Poisson Ratio and Compressive Strength of SHCC	121
C Self-weight of SHCC	127
D Hybrid Interface Behaviour in Tension	129
E Numerical Validation of Flexural Behaviour of SHCC	133
F Analytical Calculations for Design of Hybrid Beams	139
G Casting of Concrete Beam in a U-shaped SHCC Jacket Mould	145
Bibliography	147

List of Figures

2.1	Types of shear failure in concrete [49]	8
2.2	Shear-compression vs diagonal-tension failure concrete beams [59]	8
2.3	Types of shear failure in reinforced concrete beam based on the location of the diagonal crack [50]	9
2.4	Shear-resisting mechanisms on a crack [1]	10
2.5	Different techniques of strengthening of concrete beams	11
2.6	Change in mid-span deflection of structures strengthened with FRP laminates and exposed to fire for prolonged periods [26]	11
2.7	Near Surface Mounted FRP laminate configuration for shear strengthening of concrete beams [7]	11
2.8	Schematic illustration of uniaxial stress-strain curves for brittle, quasi-brittle (strain-softening), and strain-hardening cementitious materials [7]	12
2.9	Dam in Japan strengthened using SHCC [36]	12
2.10	Ismail experimental test results [31]	13
2.11	Various cross-section profiles of reinforced concrete beams strengthened using EBR technique with SHCC	14
2.12	Martinola experimental test results; (left) load-displacement curves, (right) failure crack pattern [40]	14
2.13	Various configurations of strengthening of RC beam using FRC, (left) 3-point bend test specimens, (right) 4-point bend test specimens) [3]	15
2.14	Kim experimental test specimens and delamination result [35]	15
2.15	Comparison of numerical results obtained using different crack orientation models with experiment [53]	17
2.16	Comparison of numerical failure modes obtained using different shear retention functions with experiment [53]	17
2.17	Various geometrical configurations of reinforced concrete beams strengthened using UHPFRC [37]	19
2.18	Load-deflection response obtained for hybrid beams [37]	19
2.19	Geometry of strengthened beams with SHCC patches [58]	20
2.20	Comparison of experimental load-deflection response of reference reinforced concrete beams (black lines) with strengthened beams (blue and red lines) [58]	20

2.21 Comparison between numerical and experimental results of reference and strengthened beams [58]	21
2.22 Geometry of strengthened beams with UHPFRC on sides of reinforced concrete beam [63]	21
2.23 Load-deflection response SHCC-strengthened reinforced concrete beam [63]	22
2.24 Numerical crack pattern of strengthened beam; (top) below peak load, (bottom) at peak load [63]	22
3.1 Sketch of specimens of benchmark study 1 (mm) (not to scale)	25
3.2 Uniaxial tensile stress-strain curves of SHCC in benchmark study 1 [57]	26
3.3 Typical experimental plots for control beams in benchmark study 1	27
3.4 Sketch of specimens in benchmark study 2 (mm) (not to scale)	28
3.5 Uniaxial tensile stress-strain curves of SHCC in benchmark study 2	29
3.6 Shear load-displacement curves for beams in benchmark study 2	29
3.7 Typical prismatic and non-prismatic reinforced concrete beams in benchmark study 3 (not to scale)	30
3.8 Geometrical dimensions of test beam 1K1-1K2 in benchmark study 3 (mm) (not to scale)	30
3.9 Uniaxial tensile strength results of rebar in benchmark study 3	31
3.10 Experimental and numerical force-displacement relation for beam 1K1 in benchmark study 3	32
3.11 Sketch of specimen in benchmark study 4 (mm) (not to scale)	33
3.12 Load vs displacement results for "specimen b" in benchmark study 4	33
4.1 Idealised 2D models	38
4.2 Idealised 3D SHCC-RC hybrid model of Study 1 [57]	39
4.3 Tying at load and support plates for 3D quarter model of Study 1	40
4.4 Tying of the symmetry faces of the 3D quarter model of Study 1	41
4.5 Input tensile and compressive behaviour of concrete [28]	44
4.6 Input tensile and compressive behaviour of SHCC [28]	44
4.7 Linear plastic behaviour of reinforcement	45
4.8 Typical mesh of 2D and 3D models of Study 1	47
4.9 Non-linear elastic Coulomb friction model [20]	49
4.10 Secant iteration method [20]	51
4.11 Typical convergence behaviour of reinforced concrete beam without transverse reinforcement	53

4.12 Tensile and compressive inputs for benchmark concrete [28]	54
4.13 Tensile and compressive inputs for benchmark SHCC [28]	55
4.14 Plastic strain-yield stress input for benchmark reinforcements	56
5.1 Load vs mid-span deflection comparison between experimental and numerical results of beam CB1	59
5.2 Load vs number of cracks in numerical model CB1-Damage	59
5.3 Yielding of transverse reinforcement in numerical model CB1-Mahaidi	59
5.4 Experimental failure crack pattern of benchmark beam CB1	60
5.5 Numerical failure crack pattern of beam CB1	60
5.6 Cauchy stresses S2 in numerical models of beam CB1	61
5.7 Failure crack pattern in model CB2-Damage using benchmark reinforcement yield strength	61
5.8 Load vs mid-span deflection comparison between experimental and numerical results of beam CB2	62
5.9 Cracks and Plasticity in numerical models of beam CB2	62
5.10 Experimental failure crack pattern of benchmark beam CB2	63
5.10 Numerical failure crack pattern of beam CB2	63
5.11 Load vs mid-span deflection comparison between experimental and numerical results of beam CB3	64
5.12 Load vs numebr of cracks in numerical models of beam CB3	64
5.13 Experimental failure crack pattern of benchmark beam CB3	65
5.13 Numerical failure crack pattern of beam CB3	65
5.14 Load-deflection response of beams analysed using Al-Mahaidi shear retention function with varying β_{min} values	67
5.15 Mesh size vs peak load comparison of the numerical models	69
5.16 Failure crack pattern for beams modelled using Al-Mahaidi shear retention function and H/20 mesh size	70
5.17 Comparison of experimental and numerical failure crack pattern for beams modelled using Al-Mahaidi shear retention function and H/20 mesh size	71
5.18 Load vs mid-span deflection comparison of model SHCC4-Mahaidi with benchmark experimental beam SHCC4	73
5.19 Stresses in reinforcement in numerical model SHCC4-Mahaidi	74
5.20 Experimental and numerical failure crack pattern of beam SHCC4	74
5.21 Input parameters for lattice modelling of SHCC	75

5.22 Comparison of experimental and DIANA numerical results with numerical results in benchmark study 4	76
5.23 Crack distribution in the numerical models	77
5.24 Strains E1 in numerical model SHCC4-Mahaidi immediately after the last acceptable load step	77
5.25 Cracks and plasticity in numerical model SHCC4-Mahaidi	78
5.26 Types of input tensile curves for SHCC in LECOM model	78
5.27 Different types of input compressive curves for SHCC in numerical models	79
5.28 Various methods of representation of crack patterns in a 3D hybrid beam numerical model	80
5.29 Typical interfacial results of a hybrid beam modelled with Imperfect Bond (IB) hybrid interface	82
5.30 Load vs interface stress STY at point of debonding “A” of numerical model H20Q1-IB .	82
5.31 Load vs mid-span deflection comparison of numerical models H20Q1-PB and H20Q1-IB with benchmark experimental beam H20Q1	83
5.32 Interfacial results of numerical model H20Q1-IB	84
5.33 Reinforcement stresses SXX in numerical models of beam H20Q1	84
5.34 Experimental failure crack pattern of benchmark beam H20Q1	85
5.35 Numerical failure crack pattern of numerical models; (a) H20Q1-PB, and (b) H20Q1-IB .	85
5.36 Load vs mid-span deflection comparison of numerical models H40Q1-PB and H40Q1-IB with benchmark experimental beam H40Q1	86
5.37 Interfacial results of numerical model H40Q1-IB	87
5.38 Experimental failure crack pattern of benchmark beam H40Q1	87
5.39 Numerical failure crack pattern of numerical models; (a) H40Q1-PB, and (b) H40Q1-IB .	88
5.40 Load vs mid-span deflection comparison of numerical models H5Q2-PB and H5Q2-IB with benchmark experimental beam H5Q2	89
5.41 Interfacial results of numerical model H5Q2-IB	89
5.42 Load vs plasticity for numerical models of beam H5Q2	89
5.43 Experimental failure crack pattern of benchmark beam H5Q2	90
5.44 Numerical failure crack pattern of numerical models; (a) H5Q2-PB, and (b) H5Q2-IB . .	90
5.45 Load vs mid-span deflection comparison of numerical models H10Q2-PB and H10Q2-IB with benchmark experimental beam H10Q2	91
5.46 Interfacial results of numerical model H10Q2-IB	92
5.47 Experimental failure crack pattern of benchmark beam H10Q2	92
5.48 Numerical failure crack pattern of numerical models; (a) H10Q2-PB, and (b) H10Q2-IB .	93

5.49	Load vs mid-span deflection comparison of additional numerical models of beam H20Q1	95
5.50	Interface displacement DUY in numerical models of beam H20Q1 with varying interface types (white areas present debonded regions)	96
5.51	Interface displacement DUY of numerical model H20Q1-WB modelled with varying mesh sizes (white areas present debonded regions)	97
5.52	Interface displacement DUY in numerical model H20Q1-HB-20mm at different loads (white areas present debonded regions)	98
5.53	Reinforcement stresses SXX in numerical model H20Q1-HB-20mm	98
5.54	Geometry and mesh configuration of simplified models	99
5.55	Interface displacement DUX vs load factor plot for simplified models of varying SHCC thickness	100
5.56	Deformation and interfacial displacement DUX at 0.025 load factor of simplified models with varying SHCC thickness	100
5.57	Results of simplified model SHCC-WB-20mm	101
5.58	Results for H20Q1-WB-20mm at 44kN load; (a) Crack pattern at localization in SHCC and concrete layers separately (b) Interface displacement (white areas present debonded regions)	102
5.59	Results for H20Q1-WB-20mm at 152kN load; (a) Crack pattern at point of increased delamination (b) Interface displacement (white areas present debonded regions)	103
5.60	Results for H20Q1-WB-20mm at peak load of 195kN load; (a) Crack pattern (b) Interface displacement (white areas present debonded regions)	103
5.61	Different geometries of sample hybrid beam	104
5.62	Load vs mid-span deflection comparison of quarter, half and full-scale models of a sample hybrid beam	105
5.63	Failure crack pattern of different geometries of sample hybrid beam	105
A.1	Convergence plot for model CB1-Damage	113
A.2	Convergence plot for model CB2-Damage	114
A.3	Convergence plot for model CB3-Damage	114
A.4	Convergence plot for model CB1-Mahaidi	115
A.5	Convergence plot for model CB2-Mahaidi	115
A.6	Convergence plot for model CB3-Mahaidi	116
A.7	Convergence plot for model SHCC4-Mahaidi	116
A.8	Convergence plot for model H20Q1-PB	117
A.9	Convergence plot for model H20Q1-IB	117
A.10	Convergence plot for model H40Q1-PB	118

A.11	Convergence plot for model H40Q1-IB	118
A.12	Convergence plot for model H5Q2-PB	119
A.13	Convergence plot for model H5Q2-IB	119
A.14	Convergence plot for model H10Q2-PB	120
A.15	Convergence plot for model H10Q2-IB	120
B.1	Relation between compressive strength vs Poisson ratio of SHCC [66]	121
B.2	Compressive strength of SHCC [66]	122
B.3	Uniaxial compressive strength input for SHCC used in designed experiments	123
B.4	Multi-linear compressive strength input for SHCC of benchmark studies	125
D.1	3D numerical model	129
D.2	Interface displacement DUX at an arbitrary load step	130
D.3	Points A, B and C on interface	130
D.4	Interfacial displacement vs load factor at Points A, B and C	131
D.5	Delaminated interface at the terminated load step	131
E.1	Four-point bending test setup for coupon specimens	133
E.2	Compressive stress-strain curve of SHCC	134
E.3	Experimental tensile and flexural behaviour of SHCC	134
E.4	Numerical model of SHCC coupon	135
E.5	Compressive and tensile input properties of SHCC	136
E.6	Mesh configuration of SHCC coupon	136
E.7	Stress-deflection response from flexural test of SHCC coupon specimen	138
F.1	Concrete cross-section for calculations	140
F.2	SHCC side panel configuration in hybrid beam	142
F.3	Designed beams	144
G.1	Casting of U-shaped SHCC	145
G.2	Casting of Concrete in U-shaped SHCC mould	146

List of Tables

3.1	Material properties of beams in benchmark study 1	26
3.2	Trilinear tensile curve of SHCC in benchmark study 1	26
3.3	Material properties in benchmark study 2	28
3.4	Trilinear tensile curve of SHCC in benchmark study 2	29
3.5	Material properties of benchmark study 3	31
3.6	Material properties in benchmark study 4	33
4.1	Geometrical properties of idealised beams (mm)	38
4.2	Geometrical properties of load and support plates (mm)	39
4.3	Uniform constitutive parameters for “Concrete”	43
4.4	Concrete constitutive properties	43
4.5	SHCC constitutive properties	44
4.6	Reinforcement constitutive properties	45
4.7	Steel plates constitutive properties	45
4.8	Impact on mesh size selection criterion of benchmark studies	46
4.9	Kinematic parameters for concrete, SHCC and steel plates in 2D models [20]	47
4.10	Beam-plate interface parameters for 2D models [19, 20, 43, 53]	48
4.11	Kinematic parameters for concrete, SHCC and steel plates in 3D models [20]	48
4.12	Beam-plate interface parameters for 3D models [20]	48
4.13	Imperfect bond interface properties	49
4.14	Imperfect bond interface kinematic parameters for 3D models [20, 56]	50
4.15	Equilibrium conditions	51
4.16	Numerical solution strategies	51
4.17	Material properties of concrete in benchmark studies [28, 44, 57, 61]	54
4.18	Poisson ratio of SHCC [44, 57, 61, 66]	55
4.19	Numerical models analysed based on the developed modelling strategies	56

5.1	Peak load and failure type comparison between experimental and numerical results of beam CB1	58
5.2	Peak load and failure type comparison between experimental and numerical results of beam CB2	62
5.3	Peak load and failure type comparison between experimental and numerical results of beam CB3	64
5.4	Difference between numerical peak loads of analysed reinforced concrete beams	66
5.5	Summary of numerical peak loads of models analysed	68
5.6	Comparison of experimental and numerical failure type for analysed reinforced concrete beams	68
5.7	Number of elements in height of analysed reinforced concrete beams	68
5.8	Number of elements in height of analysed reinforced concrete beams using different mesh size criterion	69
5.9	Average percentage difference in numerical peak loads of models of varying mesh size	69
5.10	Experimental and numerical diagonal crack angle θ	71
5.11	Peak load and failure type comparison of model SHCC4-Mahaidi with benchmark experimental beam SHCC4	73
5.12	Peak load and failure type comparison between experimental and numerical results of hybrid beam H20Q1	83
5.13	Peak load and failure type comparison between experimental and numerical results of hybrid beam H40Q1	86
5.14	Peak load and failure type comparison between experimental and numerical results of hybrid beam H5Q2	88
5.15	Peak load and failure type comparison between experimental and numerical results of hybrid beam H10Q2	91
5.16	Comparison of experimental peak loads of SHCC-RC hybrid beams with RC beams	94
5.17	Comparison of numerical peak loads of SHCC-RC hybrid beams with RC beams	94
5.18	Comparison of peak loads of numerical SHCC-RC hybrid beams with experimental hybrid beams	94
5.19	Additional analysed hybrid interface types	95
5.20	Additional analyses of beam H20Q1	95
C.1	Material quantities for SHCC	127
C.2	Self-weight calculations for SHCC	127
E.1	Summary of inputs for numerical model of SHCC coupon specimen	137

F.1	Geometrical properties of experimental beams (mm)	139
F.2	Material properties for design of experiments	140
F.3	Trilinear tensile curve of SHCC for design of experiments	141

1

Introduction

This chapter describes the objectives of the research set forth for this thesis and the research approach adopted to address them.

1.1. Background and Motivation

When a reinforced concrete (RC) beam, designed with either inadequate or no transverse reinforcement, is subjected to a combination of bending moment and shear force, a premature shear failure can occur before the beam can reach its design flexural strength. This type of shear failure is sudden and generally catastrophic due to the lack of warning before failing.

In the past, the design of RC beams lacked the use of transverse reinforcement to provide the required shear resistance. Such beams might require shear strengthening for the design capacity to comply with current design codes. A solution to the problem of under-designed existing beams in shear, or even the design of new beams, might be in using different materials with concrete to improve the structural performance without having to over-design the reinforcements, both transverse and longitudinal. These materials can be added in new structures to form better performing concrete structures. An example is the use of steel fibres to form fibre reinforced concrete. For the strengthening of existing structures, however, new concrete (overlay) is cast around the existing old concrete (substrate). The performance of the strengthening concrete layer (overlay), applied to existing concrete (substrate), is dependent on its mechanical properties. Nowadays, engineered cementitious composites that exhibit strain hardening behaviour, called Strain Hardening Cementitious Composites (SHCC), are promising materials that can be used to strengthen existing structures. The benefits of using such an innovative concrete for the strengthening of RC beams, both in shear and flexural, have been explored by researchers in the past. Significant research has been conducted to study shear strengthening of RC beams with externally bonded SHCC layers in the form of plates or sheets. However, most of the research is limited to experimentation, and only a minimal amount of research is available on the numerical modelling of such beams using the Non-linear Finite Element Analysis (NLFEA) method.

Numerical simulations are a useful tool in understanding the structural behaviour of such an innovative concrete used in combination with conventional reinforced concrete structures. Advanced numerical simulations using NLFEA help optimise the design of structures by utilising the non-linear behaviour of concrete. The guidelines for NLFEA provide a starting point for engineers to model the behaviour of concrete structures [28]. However, numerical studies concerning composite materials like SHCC are still ongoing, therefore, no guidelines for design and analysis are defined for them so far. The lack of in-depth finite element studies concerning composite materials is chiefly due to the challenging nature of modelling shear cracking in SHCC-RC hybrid beams and the interface between the substrate (SHCC) and overlay (concrete) materials. Further research needs to be performed to understand the effectiveness of using such composites in design and strengthening of concrete structures in practice.

Existing literature offers significant studies performed to experimentally assess the shear behaviour of conventional concrete beams with various reinforcement configurations and boundary conditions, and using different numerical techniques. These experimental results have been validated to a greater degree. However, the use of SHCC in hybrid with regular concrete is becoming more pronounced in recent years due to its potential to improve the structural performance of regular concrete structures. Several experimental studies in TU Delft have been performed to study the flexural performance of such hybrid beams [30, 51]. However, the validation of such experimental studies numerically using NLFEA is scarcely researched so far. Additionally, the shear behaviour of large-scale reinforced SHCC beams and reinforced SHCC-RC hybrid beams has not been studied significantly, both experimentally and numerically. Using the NLFEA, a robust numerical solution strategy could be developed that can be used in modelling the shear behaviour of such beams. Furthermore, numerical modelling can help develop codes and regulations for the use of composite materials, both separately and in hybrid with regular concrete, in practice as well since these are not yet commonly used in the field.

Therefore, the motivation behind this thesis is to study the shear strengthening effect of Strain Hardening Cementitious Composites (SHCC) on reinforced concrete (RC) beams without transverse reinforcement by modelling the shear behaviour of experimental benchmark concrete and SHCC-RC hybrid beams in finite element software package DIANA.

1.2. Problem Statement

Apart from the tensile properties of SHCC (primarily influenced by the type and percentage of fibres), the main parameter varied in studying the shear strengthening effect of SHCC on reinforced concrete beams in most experimental studies is the geometrical configuration in which SHCC is applied to the RC beam. However, for a specific SHCC geometry, e.g. SHCC layers on the sides of an RC beam, the influence of the varying thickness of SHCC on the shear capacity and failure type of the hybrid beam has been studied scarcely, both experimentally and numerically. Additionally, the influence of the type interface between SHCC and concrete on both the shear capacity and failure type of the hybrid beam has also been studied very limitedly.

Although shear strengthening techniques using SHCC have been reported to be promising in improving the shear behaviour of a hybrid beam, the influence of parameters such as the thickness of SHCC and the type of interface is important to study to conclusively comment about the overall structural performance of using SHCC as a shear strengthening material for RC beams. These parameters are also important to study to optimise the strengthening design used.

1.3. Research Scope and Objectives

This thesis is part of research work at the civil department of TU Delft, investigating the feasibility of utilising SHCC in a hybrid configuration with RC beams to improve their structural performance. Huang [30] assessed the flexural behaviour of SHCC-RC hybrid beams by replacing concrete with SHCC in the tension zone. Additional studies are performed to validate the experimental results of Huang [32], numerically, and to experimentally investigate the influence of the type of interface on the performance of hybrid beams [51].

Developing on the previous research work, this thesis focuses on the study of shear behaviour of SHCC-RC hybrid beams. This thesis aims to evaluate the structural performance of SHCC in improving the shear performance of RC beams when used in a hybrid configuration, using NLFEA method. A numerical solution strategy is required to be developed that can be used to analyse the shear behaviour of SHCC-RC hybrid beams without transverse reinforcement. The scope of this thesis is limited to numerical modelling only, in which the developed numerical solution strategy for modelling simply-supported RC and SHCC-RC hybrid beams in shear is validated using benchmark studies. DIANA FEA software package v10.3 is used.

1.4. Research Hypothesis

Based on the research scope and objectives, the following can be hypothesised,

“A numerical solution strategy that can appropriately model, in terms of the load-deflection response, failure crack pattern and failure mode, the shear behaviour of RC beams without transverse reinforcement in the shear span, can be used to model the shear behaviour of SHCC-RC hybrid beams”

1.4.1. Research Questions

To address the hypothesis mentioned above, the following research questions are formulated,

1. What are the appropriate set of modelling choices that can be used to develop a numerical solution strategy to model the shear behaviour of reinforced concrete (RC) beams without transverse reinforcement in the shear span?

The first step in modelling the shear behaviour of SHCC-RC hybrid beams is to model the shear behaviour of RC beams without transverse reinforcement in the shear span, accurately. Two numerical

solution strategies are used to validate the experimental results of RC beams from different benchmark studies, and the optimal one is selected based on the results obtained. Such validation of the numerical solution strategies on benchmark RC beams helps better model the shear behaviour of benchmark hybrid beams.

2. What are the limitations of the optimal numerical solution strategy in modelling the shear behaviour of reinforced SHCC beam?

The constitutive models that define the tensile and compressive behaviour of SHCC and concrete in the numerical models are different due to their different tensile and compressive behaviours. However, other modelling choices involved in the optimal numerical solution strategy (such as material class, crack model and orientation) need to be kept consistent for both SHCC and concrete for numerical compatibility when hybrid beams are modelled. Therefore, the optimal numerical solution strategy finalised for modelling of shear behaviour of RC beams is tested on reinforced SHCC beam in order to recognise its limitations in modelling the shear behaviour of reinforced SHCC beam.

3. Can the optimal numerical solution strategy, ideal for modelling the shear behaviour of RC beams, be used to model the shear behaviour of SHCC-RC hybrid beams?

The optimal numerical solution strategy developed for modelling of shear behaviour of concrete beams is used to analyse benchmark hybrid beams and based on the results, a conclusion is drawn on the robustness of the finalised numerical solution strategy in being able to model both concrete and hybrid beams in shear.

1.5. Research Approach

This thesis involves numerical validation of benchmark experiments related to shear behaviour of reinforced concrete (RC) beams, reinforced SHCC beam and SHCC-RC hybrid beams. Before modelling the hybrid beams, a numerical study which explores the choices involved in the modelling of shear behaviour of RC beams is performed. The optimal set of modelling choices of the finalised numerical solution strategy are then used to model the shear behaviour of reinforced SHCC beam and hybrid beams. The approach mentioned above is split into three modelling phases in this thesis. Breakdown of the work plan to achieve the set objectives is described below:

- a. Selection of benchmark studies: Different benchmark studies are selected encompassing shear behaviour of RC and SHCC beams, separately, and in a hybrid configuration. Specific selection criteria are defined to select benchmark studies. The selection criteria help introduce some uniformity in the properties of benchmark beams.
- b. Modelling Phase I - Numerical validation of shear behaviour of reinforced concrete (RC) beams without transverse reinforcement: Benchmark RC beams without any transverse reinforcement in the shear span are modelled using different numerical solution strategies, and the numerical results are compared with experiments to finalise a single numerical solution strategy used for subsequent models.
- c. Modelling Phase II - Study of shear behaviour of reinforced SHCC beam without any transverse reinforcement in the shear span: The numerical solution strategy finalised in Modelling Phase I is used to numerically assess the shear behaviour of a reinforced SHCC beam of benchmark study.
- d. Modelling Phase III - Numerical validation of shear behaviour of SHCC-RC hybrid beams without transverse reinforcement: Benchmark SHCC-RC hybrid beams without transverse reinforcement in the shear span are modelled using the optimal numerical solution strategy from Modelling Phase I. Each hybrid beam is modelled using different types of hybrid interface considered in this thesis.

1.6. Report Outline

The report consists of 6 chapters in total, including the introductory Chapter 1 in which background and motivation behind the thesis and the research objectives are discussed. The detailed breakdown of the remaining chapters is as follows:

Chapter 2: Brief review of literature explaining the shear behaviour of RC beams, the mechanisms involved in providing the required shear resistance in RC beams, different strengthening techniques used to improve the structural performance of concrete beams including use of SHCC, the shear behaviour of SHCC beams, different types of hybrid beams experimentally tested for shear and use of non-linear finite element techniques to validate the experimental behaviour of RC beams and hybrid beams.

Chapter 3: Details about the selection criteria for the benchmarks studies and the benchmark studies selected for validation in this thesis.

Chapter 4: Details about the idealised physical problems from benchmarks, the numerical solution strategies used to model them, their input material properties and the criteria for judging the numerical results in this thesis.

Chapter 5: Phase-by-phase presentation of numerical results, their discussion and conclusions. In the end, the overall conclusions of the thesis are discussed.

Chapter 6: Recommendations for future research.

2

Literature Study

The chapter includes a review of the types of shear failure in concrete beams, the strengthening techniques used to improve their structural performance and the numerical analysis performed to validate experimental results of such beams.

2.1. Shear Failure of Concrete Beams

Reinforced concrete (RC) beams fail in shear due to large shearing forces, especially in beams without transverse reinforcement. It is observed that the characteristic shear failure of an RC beam is influenced by the shear span-to-effective depth ratio (a/d). Sinha [52] observes that a shear compression/tension failure occurs when a/d of a beam is between 1 to 2.5. Under loads causing a shear compression/tension failure, flexural cracks develop in the tensile region and propagate into the compression zone. The eventual failure is shear-tension if cracks extend to the longitudinal reinforcement and propagate along, resulting in anchorage failure. If crushing of the concrete in the compression zone adjacent to the point of application of load occurs, it is a shear-compression failure. A diagonal-tension failure occurs if a/d is between 2.5 to 6. Flexural cracks develop, which are followed by diagonal flexural cracks propagating towards the compression zone as loads increase until a sudden diagonal tension failure occurs. A diagonal crack is formed along the shear span due to the tension component of the principal stress [49]. Figure 2.1 shows the different types of shear failures in concrete.

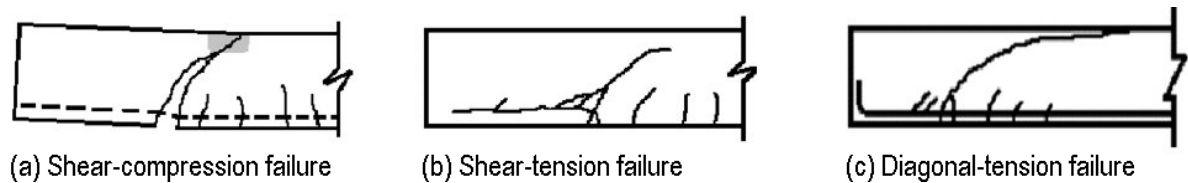


Figure 2.1: Types of shear failure in concrete [49]

Yang [59] observes inclination of flexural cracks during loading as the shear force increases and principal stresses rotate, eventually forming a diagonal crack. This failure results in a sudden drop in the load-bearing capacity due to formation of secondary horizontal cracks. These secondary horizontal cracks allow further rotation of the structure, causing already developed inclined cracks to open further resulting in loss of shear retention in the crack plane. This loss of shear retention results in possible arch action. Whether a beam fails in shear-compression or diagonal-tension (shear-flexure) is based on the residual capacity provided by the arch action. Beam fails in shear-compression if the arch can withstand the load at which the inclined crack forms, as shown in Figure 2.2(a). If the residual arch capacity is insufficient, then a diagonal-tension failure occurs, as shown in Figure 2.2(b). Therefore, the location of the inclined crack is of great importance to the type of failure mechanism and the capacity of the beam. Especially beams without shear reinforcement are highly susceptible to such unstable and brittle failure modes.

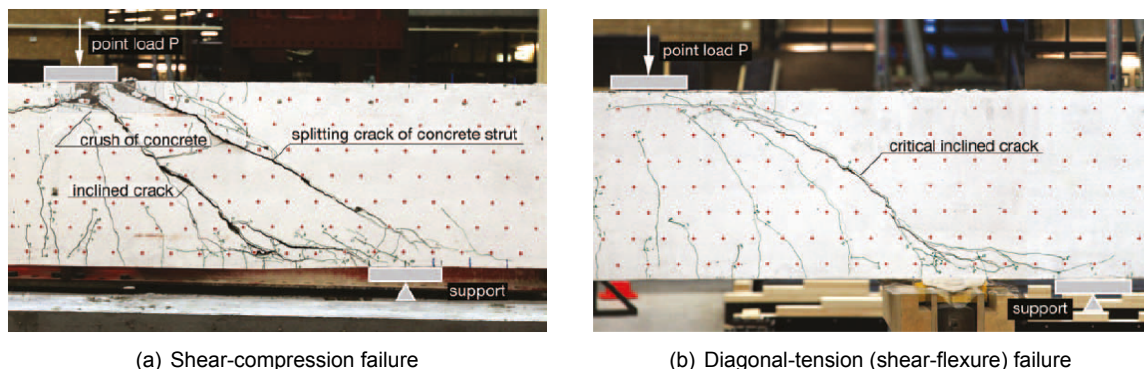


Figure 2.2: Shear-compression vs diagonal-tension failure concrete beams [59]

Sarkhosh [50] describes fracture mechanics behind the shear failure of RC beams without transverse reinforcement and how the location of the diagonal crack influences the types of failure observed. Shear failure is identified if; (a) a diagonal shear crack originating from the flexural cracks occurs, (b) there is anchorage or bond failure along the longitudinal reinforcement, and (c) crushing of concrete in the compression zone near the point load occurs. These aspects are illustrated in Figure 2.3. The location of cracks in the beam influence which of the aspects described above are observed.

One of the possibilities is the occurrence of a diagonal shear crack across the possible compression strut between loading and support plate, as shown in Figure 2.3(a). This mechanism instigates once inclined tensile stress reaches the tensile strength of the concrete, causing diagonal tension cracking. When the shear crack reaches the neutral axis, it does not propagate any further towards the top. Eventually, fracture occurs along the bottom longitudinal reinforcement towards the anchorage, possibly splitting the beam into two. Additionally, the concrete in the compression zone fails at the top in the absence of compression reinforcement. Another possibility is the occurrence of a diagonal shear crack below the possible compression strut between loading and support plate, as shown in Figure 2.3(b). As before, the diagonal shear crack is initiated by a flexural crack from the tensile region and propagates under the compression strut towards the top of the beam, however, the shear crack is only able to grow till the neutral axis under the loading plate and cannot propagate any further towards the top. After reaching the neutral axis, fracture processes in front of the crack tip get confined by compressive stresses due to flexure and the effect of the loading plate. Therefore, higher stresses are required to obtain the crushing of the beam as a consequence of the shear crack. Therefore, such failure results in a relatively higher capacity.

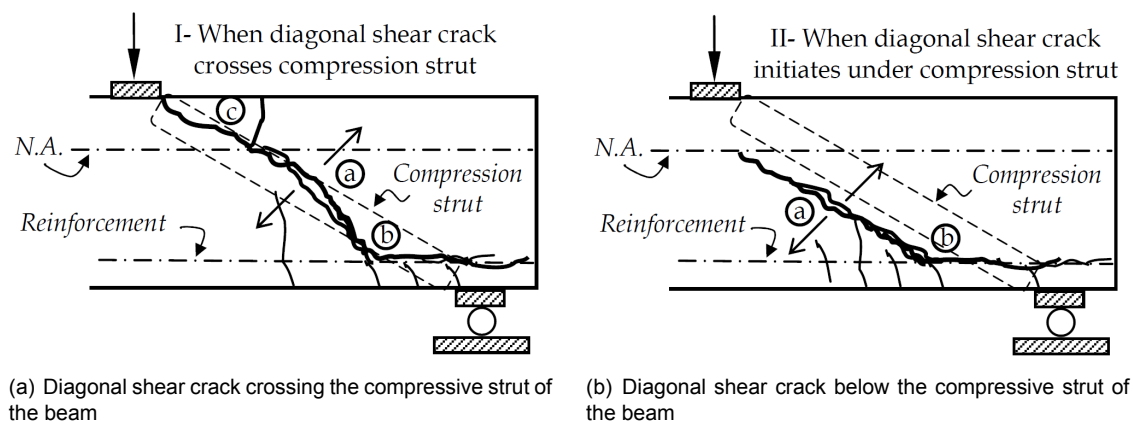


Figure 2.3: Types of shear failure in reinforced concrete beam based on the location of the diagonal crack [50]

In the absence of transverse reinforcement, the widely accepted four types of mechanisms responsible for shear force transfer in a cracked concrete beam since the 1970s (ACI-ASCE Committee 426 1973, ACI-ASCE Committee 445 1998) are [59]:

1. Shear stress in the un-cracked concrete zone,
2. Aggregate interlock due to tangential displacement of the crack faces,
3. Residual tensile stress occurring at limited normal opening of the cracks, and
4. Dowel action due to the longitudinal reinforcement.

The above phenomena are illustrated in Figure 2.4. In modelling the shear behaviour of RC beams, the following phenomena must be modelled to provide the required shear resistance.

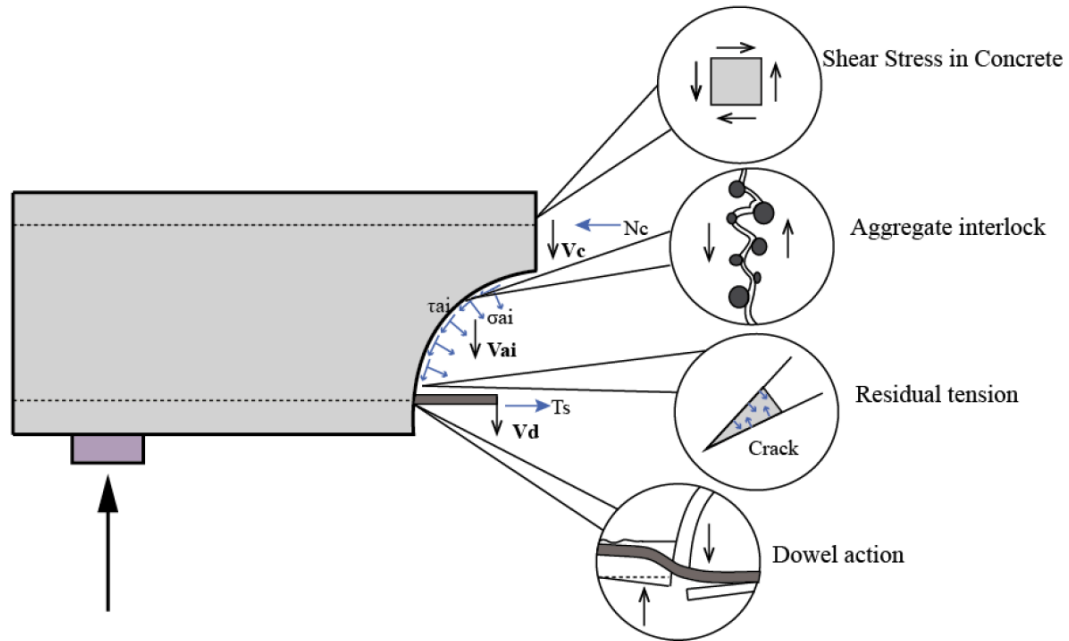


Figure 2.4: Shear-resisting mechanisms on a crack [1]

2.2. Shear Strengthening of Concrete Beams

Reinforced concrete (RC) beams are designed to fail in flexure instead of shear, as latter involves failure without any warning. Typically, adequate amounts of transverse reinforcement are provided to ensure that a ductile flexural failure occurs. However, several RC beams constructed in the early 20th century, that are still in service, were cast without any transverse reinforcement and concrete provided the entire shear resistance. However, over time, these beams are found to be deficient in shear strength due to increased service loads, concrete degradation, reduction in longitudinal reinforcement area because of corrosion and construction defects. Given the extent of concrete infrastructure requiring rehabilitation globally, strengthening is an attractive solution than demolishing and rebuilding in the present economic climate [33, 65].

2.2.1. Common Strengthening Techniques

Different types of strengthening methods have been used in the past to increase the capacity of concrete beams. Steel plates bonded externally to tensile or shear regions of the RC beams using an adhesive/anchor is the most commonly used technique, as illustrated in Figure 2.5(a). This type of strengthening technique is termed as Externally Bonded Reinforcement (EBR). However, the susceptibility of the steel plates to corrosion presents a significant problem [2, 48]. With the advancement in material sciences, laminates made of composites like Fibre Reinforced Polymer (FRP) have been tested to evaluate their efficiency in increasing the flexural and shear strength of RC beams, as illustrated in Figure 2.5(b) [2, 34]. However, issues like debonding of the FRP and poor performance in case of exposure to fire pose a significant problem. Figure 2.6 show the increase in deflection of beams strengthened using FRP laminates in comparison to regular concrete beam strengthened using concrete. The Near Surface Mounted (NSM) Carbon Fibre Reinforced Polymer (CFRP) laminates/rods is another technique used to increase the shear capacity of RC beams, as shown in Figure 2.7 [21, 45]. It involves embedding of CFRP laminates/rods into grooves open on the concrete cover on the tension side and application of CFRP laminate on the sides for shear. However, debonding of CFRP laminates/rods or fracture of concrete surrounding them limits their strengthening potential as well.



(a) L-shaped steel strips for shear strengthening of concrete beams [42]



(b) U-shaped FRP laminate applied on concrete beam [4]

Figure 2.5: Different techniques of strengthening of concrete beams

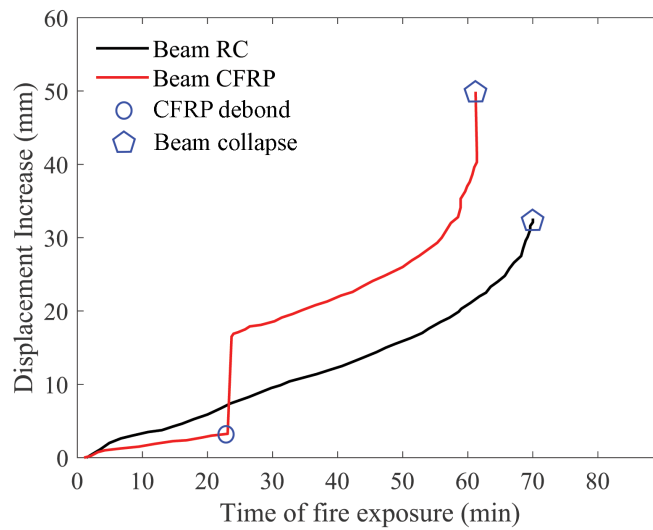


Figure 2.6: Change in mid-span deflection of structures strengthened with FRP laminates and exposed to fire for prolonged periods [26]

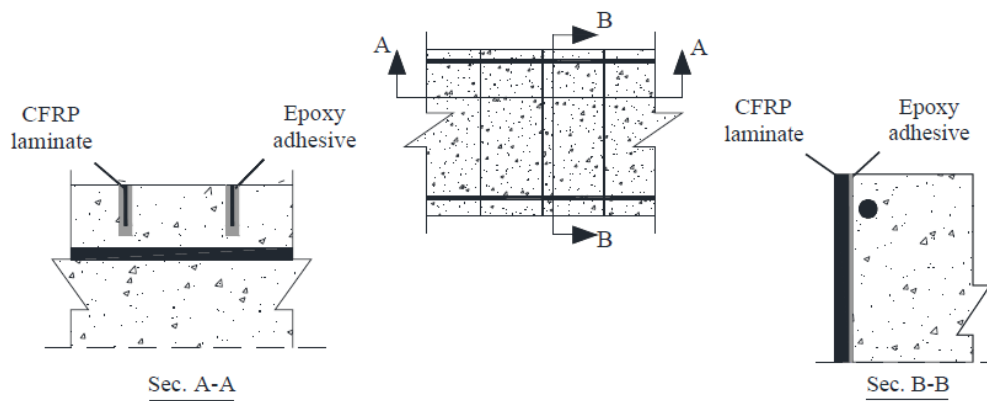


Figure 2.7: Near Surface Mounted FRP laminate configuration for shear strengthening of concrete beams [7]

2.2.2. Strengthening using SHCC

Another class of materials that have become popular in recent years in new construction and rehabilitation of existing structures are engineered cementitious composites exhibiting strain-hardening behaviour, called Strain-Hardening Cementitious Composites (SHCC). SHCC is a class of Fibre Reinforced Cement Composites (FRCC) that exhibits ductile response under tensile load and high energy absorption capacity due to a strain-hardening response rather than strain-softening (quasi-brittle) after crack initiation [24, 38]. This behaviour is illustrated in Figure 2.8. SHCC has been successfully used as, both construction and retrofitting materials, e.g. construction of composite deck for a cable-stayed bridge, retrofitting of a bridge deck, repair of a dam in Japan (Figure 2.9), and as a retrofitting layer for masonry structures [24, 36].

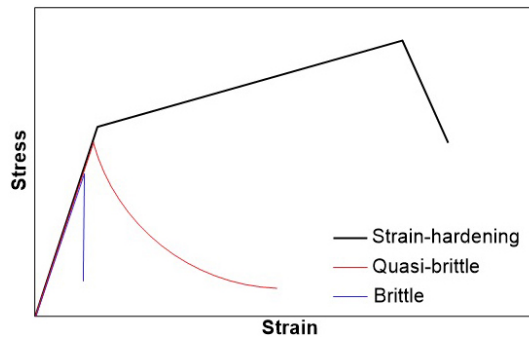


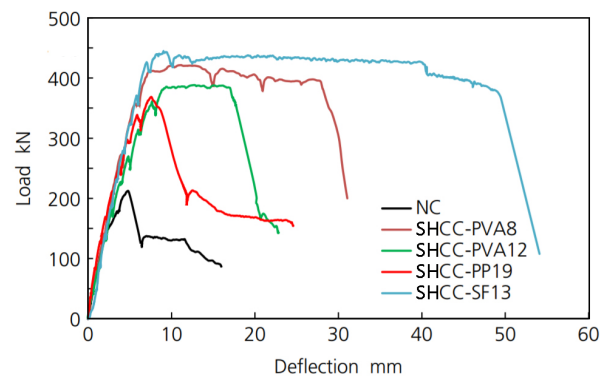
Figure 2.8: Schematic illustration of uniaxial stress-strain curves for brittle, quasi-brittle (strain-softening), and strain-hardening cementitious materials [7]



Figure 2.9: Dam in Japan strengthened using SHCC [36]

Ismail [31] assess the shear behaviour of large-scale Strain-Hardening Cementitious Composite (SHCC) beams reinforced with different types of fibres and without transverse reinforcement. Types of fibre include 8 and 12mm long Polyvinyl Alcohol fibres (PVA8 and PVA12), 19mm long Polypropylene fibres (PP19) and 13mm long Steel Fibres (SF13). The results of SHCC beams are compared with a reference beam made of regular concrete of comparable compressive strength. As shown in Figure 2.10(a), in comparison to NC beam, all the SHCC beams showed better performance in terms of cracking behaviour, shear capacity, ductility and energy absorption. A comparison of the crack pattern at the ultimate failure of NC beam with SHCC-PVA8 beam is shown in Figure 2.10(b). The SHCC beam reinforced with PVA8 fibres showed the highest shear strength and ductility of all the SHCC beams with other polymeric fibres while the use of SF13 proved to be the most effective in improving the

first crack load, ultimate load, ductility and energy absorption capacity. The use of PVA8 and SF13 in SHCC not only improved the capacity in comparison to NC beam, but the SHCC composition (i.e. mix design and type of fibre) is good enough to compensate for the absence of shear reinforcement in the test beams. The beams containing these fibres exhibited a ductile flexural failure mode, unlike the comparable-strength NC beam which failed in shear. Failure of the SHCC beams is generally characterised by the formation of a larger number of narrow cracks compared with what is observed in the regular concrete beam. At the service load level, the crack-width in all SHCC beams is limited till the maximum permissible crack-width recommended by various design codes (ACI 318 2008, BSI 1997, and Model Code 1990). Therefore, SHCCs have a promising potential to be utilised safely in exterior exposed structures.



(a) Load-deflection response of reference beam (NC) and fibre-reinforced concrete beams



(b) Failure cracking pattern of the test beam with of normal concrete (above), and SHCC-PVA8 beam (below)

Figure 2.10: Ismail experimental test results [31]

At TU Delft, Huang [30] performed experimentation to assess the flexure behaviour of reinforced concrete beams when a layer of SHCC is applied in the tension zone. A controlled microcracking behaviour of reinforced SHCC layer under tensile stresses is observed. It was concluded that a hybrid configuration of SHCC and regular concrete could give an optimal flexural design of beams, eliminating serviceability limit state (SLS) as a governing parameter. The use of SHCC was also reported to reduce the amount of longitudinal reinforcement required for crack-width control as well.

Using Externally Bonded Reinforcement (EBR) strengthening technique, composite materials like SHCC can be applied in different geometrical configurations to a concrete beam, resulting in different profiles. For shear strengthening, typical profiles using EBR technique include side bonding, U-wrapping (jacketing), and fully wrapping, as illustrated in Figure 2.11 [7]. Like steel, panels of SHCC can also be applied to existing members to provide additional capacity [37].

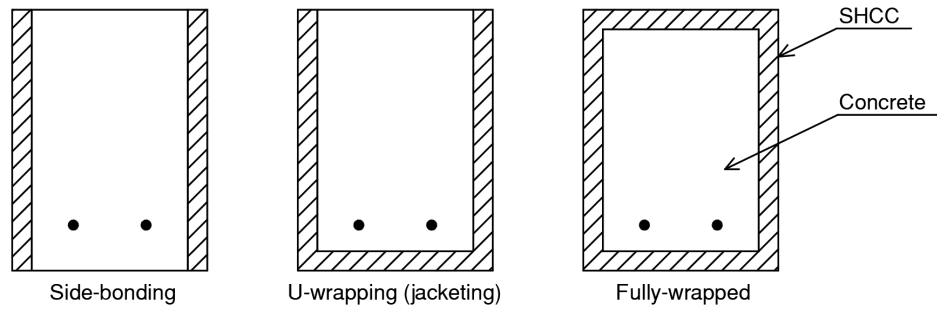


Figure 2.11: Various cross-section profiles of reinforced concrete beams strengthened using EBR technique with SHCC

Literature shows several experimental studies performed to assess the behaviour of using a hybrid configuration of regular concrete-composite material for the strengthening of structural members. Martinola [40] uses a 3-sided jacket made of Fibre Reinforced Concrete (FRC) for strengthening of RC beams. A 40mm thick jacket is directly applied to the beam surface. Both experimental and numerical results show the effectiveness of the proposed technique in increasing the load capacity. The jacketed beam shows increased peak load and softening behaviour in comparison to the control beam, as shown in Figure 2.12 (left). However, the cracks are not well distributed, as shown in Figure 2.12 (right) and collapse occurred due to the rupture of the longitudinal reinforcement.

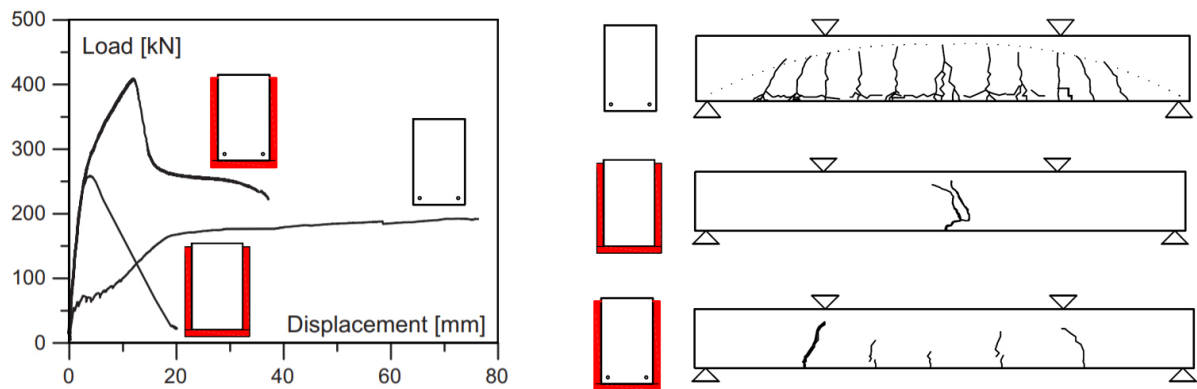


Figure 2.12: Martinola experimental test results; (left) load-displacement curves, (right) failure crack pattern [40]

Alaee [3] assessed the capacity of hybrid beams by combining regular concrete with high-performance FRC (or CARDIFRC – named after Cardiff University). It is observed that damaged RC beams can be successfully strengthened and rehabilitated in a variety of different retrofit configurations using precast CARDIFRC strips adhesively bonded to the prepared surfaces of the damaged beams, as shown in Figure 2.13. It is concluded that CARDIFRC strip bonding system is a promising method for improving the flexural and shear behaviour, as well as the serviceability of damaged concrete beams. An increase of 2-102% in the peak load is recorded by applying CARDIFRC in various geometrical configurations. Three of the four reference beams tested in 3-point setup failed in shear. The application of CARDIFRC to reference beams in a jacketed configuration resulted in all beams failing in flexure instead of shear. The advantage of using FRC over steel plates/strips is that FRC does not suffer from drawbacks such as mismatch of Young's Modulus between the concrete and the repair material, which can affect the long-term performance of the repair applied.

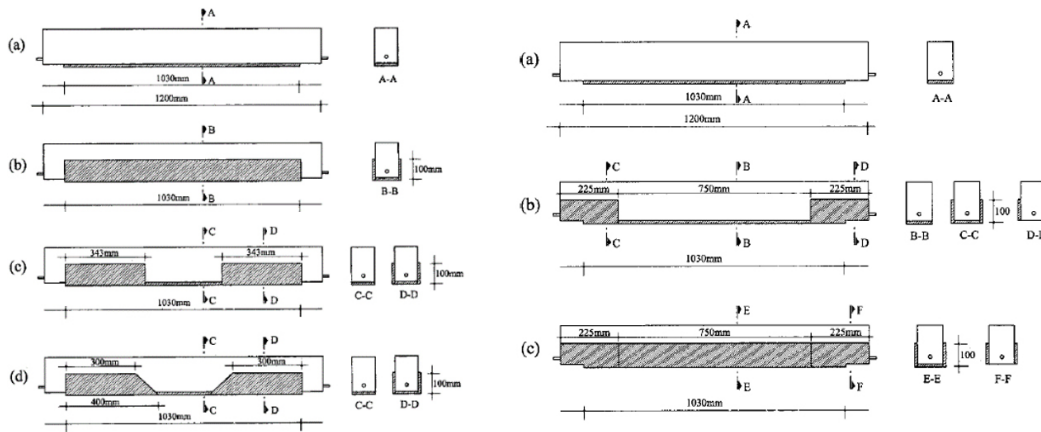


Figure 2.13: Various configurations of strengthening of RC beam using FRC, (left) 3-point bend test specimens, (right) 4-point bend test specimens [3]

Kim [35] experimentally assesses the crack damage mitigation and shear behaviour of RC beams repaired using SHCC. Two types of repairs, based on fully-wrapped profile, are assessed; repair applied by chipping off the cover of the concrete beam, and repair by applying a wrap around the existing concrete beam, as shown in Figure 2.14(a). The experimental results show that the use of SHCC in a wrapping profile increases the peak load by 3-37% as compared to the reference concrete beam. A small increase in shear capacity was in the case when SHCC repaired beams show delamination along the interface between the concrete and SHCC, as shown in Figure 2.14(b). This delamination indicates that the compressive or tensile stresses are transferred along the interface between the bi-materials. Therefore, the final failure of a strengthened beam may be governed by delamination at the interface. This delamination can be minimised by improving interface roughness or by applying different adhesive solutions like epoxy.

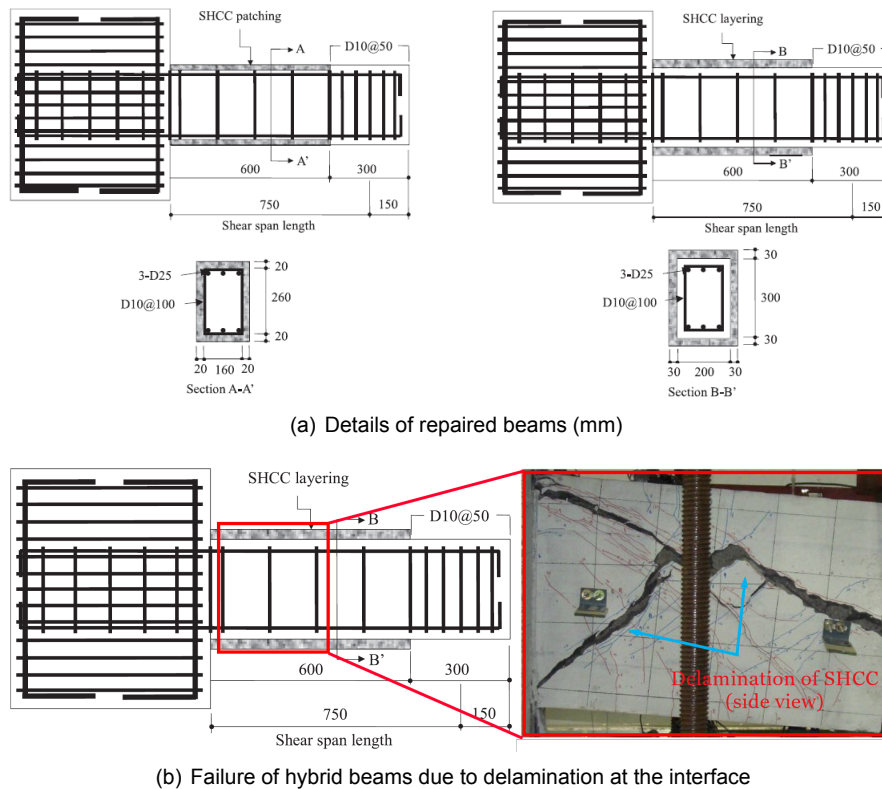


Figure 2.14: Kim experimental test specimens and delamination result [35]

2.3. Numerical Analysis

Non-linear finite element analysis (NLFEA) of reinforced concrete is an advanced numerical analysis tool for predicting the capacity and behaviour of reinforced concrete structures. It is heavily used to design modern structures as well as analysis of existing aged structures. Non-linear design methodologies are applied to analyse concrete structures to optimise the design amidst depleting construction resources globally and increasing complexity of structures. The non-linear analysis accounts for the non-linear response of structures, thereby allowing for better use of construction materials. The accuracy of the numerical predictions using NLFEA, however, is heavily influenced by the choices made by the design engineer to model the structure, and even the type of FEA software package used. Comparison of results obtained using numerical analysis with the experimental ones helps better understand the choices need to be made to model specific types of structures with certain accuracy. This comparison helps improve our engineering judgment regarding the choices for selecting the type of kinematic compatibility, constitutive models and equilibrium conditions in numerical simulation of reinforced concrete.

Most research work on studying the strengthening of reinforced concrete (RC) beams has been limited to experimentation. Numerical modelling of strengthened hybrid beams using the finite element method is studied scarcely due to the challenging nature of modelling shear cracking in RC beams and the interface between different materials. The crack pattern of a strengthened shear-critical RC beam typically consists of several diagonal cracks, with highly localised cracks in concrete. Such localised cracking must be accurately modelled to model the debonding failure of RC beams shear-strengthened with overlay materials like SHCC or FRP. This is because the interfacial slip between concrete and overlay is directly caused by the localised cracking of concrete [13]. So far, very few studies have been successful in modelling such localised cracking of concrete. Studies which define the bond-slip behaviour between the overlay and concrete result in poor agreement with test results as well. This may be due to inaccurate modelling of the crack pattern, and the localised cracking behaviour of concrete [12].

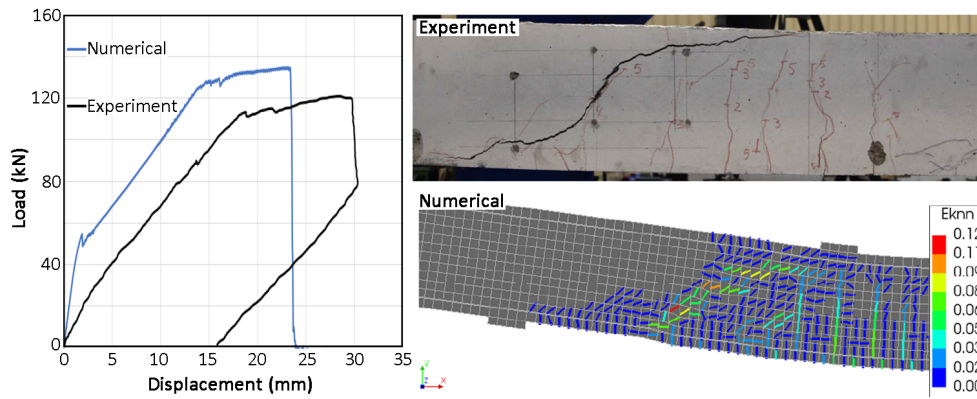
In this thesis, finite element modelling of both un-strengthened and strengthened RC beams is performed. Un-strengthened RC beams are modelled first and based on the results obtained, the strengthened beams are modelled. Following sections describe different numerical studies performed to model such beams.

2.3.1. Analysis of Reinforced Concrete Beam

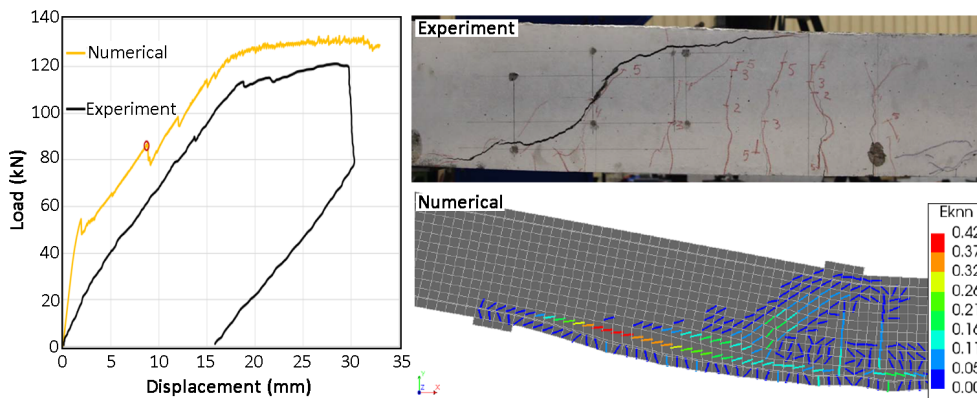
Recent studies on numerical modelling of shear behaviour of reinforced concrete (RC) beams without transverse reinforcement at TU Delft are referenced in this thesis to model RC beams. These are briefly discussed here.

T. Teshome [53]

Teshome [53] defined eight modelling strategies, categorised into three groups to model a set of sixty-seven benchmark experiments on reinforced concrete beams without shear reinforcement of Yang [59]. These beams vary in terms of the reinforcement ratio, concrete compressive strength, beam depth, failure mode and the shear span-to-effective depth ratio. Fixed and rotating crack orientation models with embedded reinforcement are used to model shear-critical RC beams. Based on the results shown in Figure 2.15, it is concluded that fixed-crack orientation model can replicate the flexure-shear (mixed) mode of failure as in experiments to a certain degree, while rotating-crack orientation model demonstrates delamination of the concrete cover unlike in experiments. Due to the higher initial stiffness in the numerical model, the predicted ultimate load is high for both models.



(a) Fixed-crack model results



(b) Rotating-crack model results

Figure 2.15: Comparison of numerical results obtained using different crack orientation models with experiment [53]

Teshome [53] also compared the effect of the shear retention function (SRF) used in case of the fixed-crack orientation model. Between Damage-based and Aggregate-based SRF, predicted ultimate load is higher than experiments for both functions, however, Damage-based SRF can predict the failure mode with relatively more accuracy. The predicted failure modes from the numerical models are illustrated in Figure 2.16.

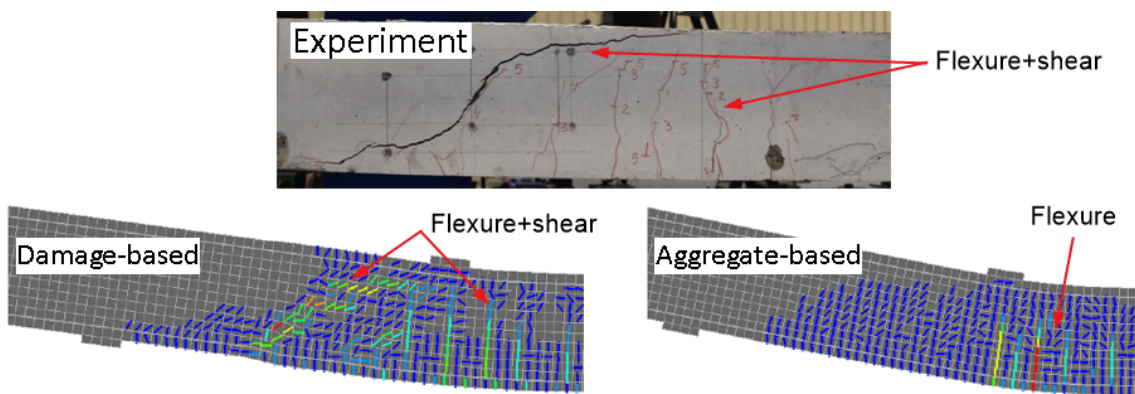


Figure 2.16: Comparison of numerical failure modes obtained using different shear retention functions with experiment [53]

If the rotating-crack model is used in combination with the bond-slip reinforcement type, a lower model uncertainty than the fixed crack model in combination with embedded reinforcement is obtained on average. However, mesh size smaller than one-sixth and one-tenth of the cross-sectional height

must be used for comparable numerical predictions in both cases.

A. de Putter [19]

de Putter [19] tested 119 solution strategies with different choices regarding the constitutive model, the finite element discretization, type of reinforcement and the iterative procedure to model concrete beams. The strategies are benchmarked with 101 experiments on reinforced concrete beams selected from the literature. These beams cover a broad range of design aspects, failing both in shear and flexure, reinforcement configurations and beam depth. The combination of solution strategies and benchmark beams resulted in 1919 NLFEAs which are performed using the DIANA finite element software package.

For beams without transverse reinforcement, the numerical results are significantly influenced by any change of modelling choices in a numerical solution strategy, i.e. the constitutive model, mesh size, reinforcement type, convergence criteria and the maximum number of iterations per load step. Reinforced concrete (RC) beams without transverse reinforcement, having a height less than 600mm, are reliably modelled using a numerical solution strategy consisting of; total-strain based fixed-crack model, Damage-based shear retention function (SRF), a mesh size of (*Height of beam*)/20, the reinforcement modelled with beam elements with unconfined *fib* bond-slip model, Full Newton-Raphson method of iteration and 100 iterations per load step. For a total of 44 beams without transverse reinforcement, this solution strategy results in a mean uncertainty of 1.05 with a coefficient of variation of 0.108. All results are within $\pm 20\%$ of the experimental failure load. The failure mode of a beam without transverse reinforcement is predicted correctly in 33 out of 44 beams considered, resulting in a 75% accuracy. In general, it is concluded that beams with transverse reinforcement can be modelled effectively using a rotating crack model, while beams without transverse reinforcement are better approximated using a fixed crack approach. There are, however, specific choices regarding reinforcement modelling and equilibrium conditions to model both types of beams appropriately.

In both studies described here, it is concluded that for shear critical RC beams, the recommended mesh size from the NLFEA guidelines for the design of concrete structures [28] does not produce the best results, especially for beams without transverse reinforcement. The choice of mesh size significantly influences the accuracy of the numerical results obtained.

2.3.2. Analysis of Strengthened Reinforced Concrete Beam

In addition to concrete beams, many studies have been performed to validate the experimental behaviour of SHCC-RC hybrid beams numerically. A few of these studies are discussed here.

Lampropoulos [37] studied the efficiency of ultra-high performance fibre reinforced concrete (UH-PFRC) for the strengthening of reinforced concrete (RC) beams. A numerical study is conducted on full-scale beams strengthened with UHPFRC applied in the tension zone, compression zone and as a 3-sided jacket, as illustrated in Figure 2.17. The numerical results are compared to experimental beams strengthened with conventional RC layers. The 3-sided jacketed beam is not evaluated experimentally. The interface between concrete and the UHPFRC in the numerical model is defined as a well-roughened interface, with a coefficient of friction equal to 1.5 and cohesion equal to 1.9 MPa. The value for the coefficient of friction is close to the ultimate value recommended by the Model Code 2010 for very well roughened interfaces [22]. Figure 2.18 shows a comparison of experimental and numerical results. Superior performance is observed for beams strengthened with UHPFRC jackets, with a maximum increase of 53% reported in the capacity in comparison to strengthening using regular concrete. In addition to the increased capacity, the slip at the interface for a 3-sided jacket considerably reduced as compared to the respective values of beams strengthened only in the compressive or tensile side.

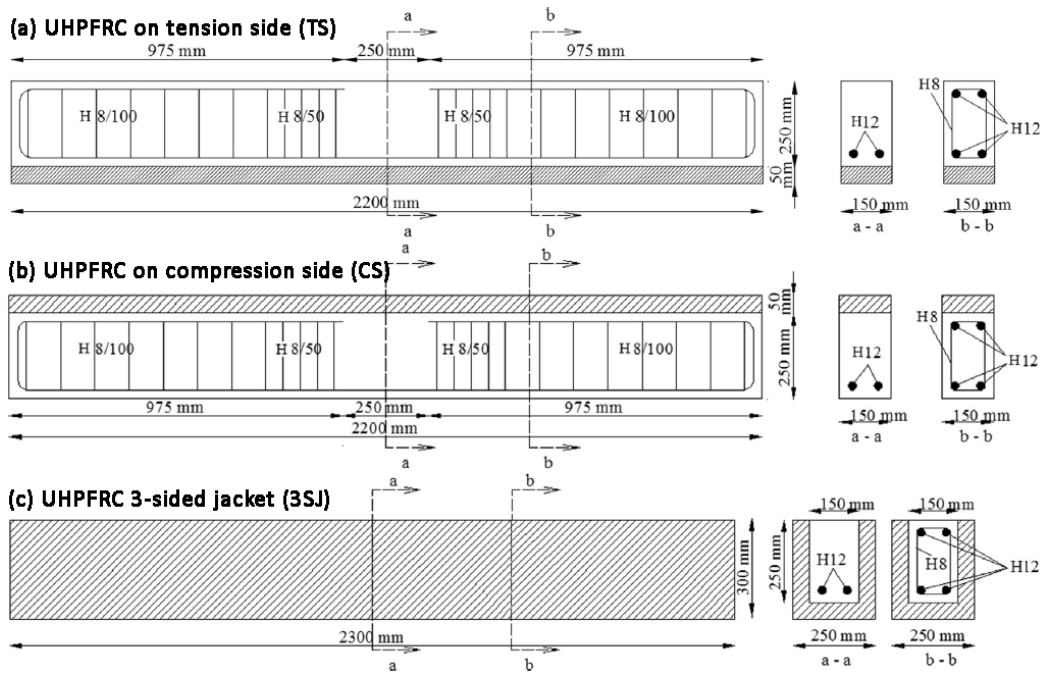


Figure 2.17: Various geometrical configurations of reinforced concrete beams strengthened using UHPFRC [37]

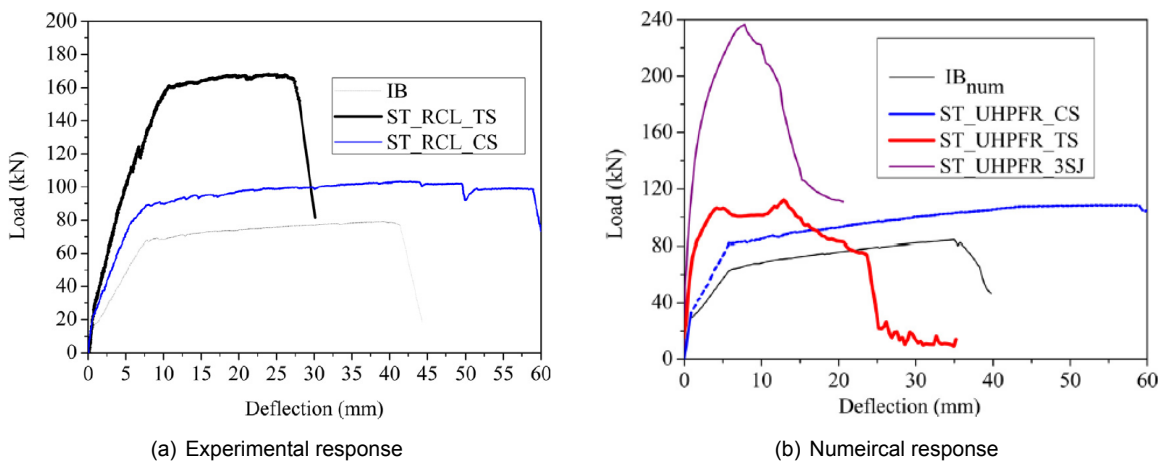


Figure 2.18: Load-deflection response obtained for hybrid beams [37]

Wei [58] investigated, experimentally and numerically, the strengthening effect of high-strength SHCC (HS-SHCC) patch applied to conventional reinforced concrete (RC) beams failing in shear. HS-SHCC patch is applied on the sides of an RC beam, with only half the length of the beam strengthened using HS-SHCC, while the other half is over-designed with closely spaced stirrups. A typical specimen configuration is illustrated in Figure 2.19. Two different shear span-to-effective depth ratios are studied. RC beams are cast first, while high-strength SHCC is then cast as thin patches on lateral surfaces of the RC beams to serve as the strengthening layers. The experimental load-deflection response obtained is illustrated in Figure 2.20.

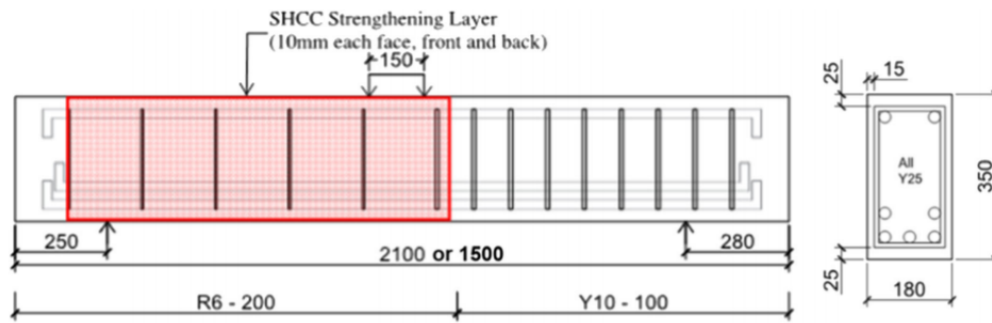


Figure 2.19: Geometry of strengthened beams with SHCC patches [58]

Based on the test results shown in Figure 2.20, it is observed that the ultimate shear capacity of strengthened RC beams increases by 14–19% compared to the reference beams. For the strengthened beams, the shear failure mode is considerably improved compared to the reference beams. Typically, the shear failure of RC beams is brittle, accompanied with large cracks and eventual collapse of crushed concrete. However, for the strengthened beams, cracks on SHCC patches are restrained to fine width, which is the material characteristic of SHCC. Upon ultimate shear failure, no spalling of surface concrete occurred. This is because the concrete-SHCC cement-based bonding system is effective in preventing debonding between the two materials until the ultimate load capacity is reached.

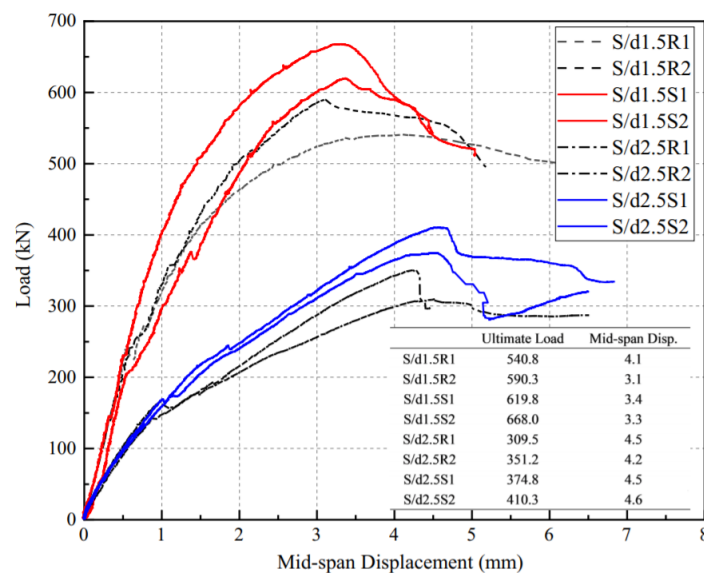


Figure 2.20: Comparison of experimental load-deflection response of reference reinforced concrete beams (black lines) with strengthened beams (blue and red lines) [58]

The experimental results are simulated numerically using a finite element model on ABAQUS software package. The behaviour of the interface between concrete and HS-SHCC patch significantly influences the effectiveness of strengthening applied. A weak interfacial bond is not able to take full advantage of the high performance of the tensile behaviour of SHCC because of premature failure due to delamination. However, the experimental results of strengthened beams in this study indicate that there is negligible debonding between the concrete beam and HS-SHCC before the maximum load capacity of the beams is reached, and the maximum load capacity of the strengthened beams is not affected by delamination at the interface. Therefore, a perfect bond between the concrete substrate and HS-SHCC overlay is assumed in the model for simplicity. The comparison of the numerical load-deflection response with experiments is illustrated in Figure 2.21. The results of finite element analysis correlated well with experimental results.

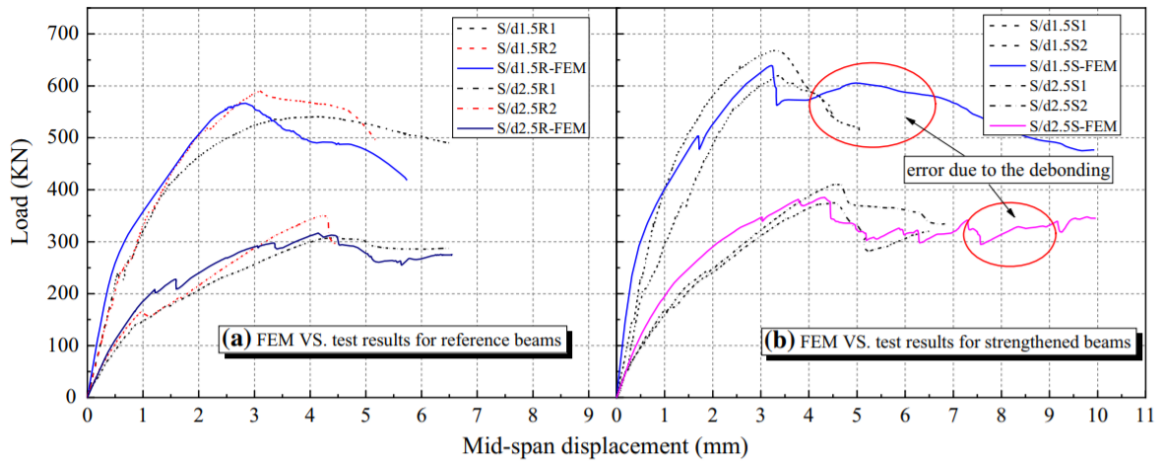


Figure 2.21: Comparison between numerical and experimental results of reference and strengthened beams [58]

Zhang [63] proposed a numerical shear stress transfer model for evaluating the shear fracture behaviour of SHCC for strengthening of reinforced concrete (RC) beams. The shear stress transfer model takes account of contributions from both the contact stress of the matrix and the bridging stress of the fibres by defining inputs such as crack angle θ and asperity height. The proposed shear stress transfer model is evaluated by numerical investigation of an experimental case of SHCC used for shear-strengthening of an RC beam. SHCC is applied on the sides of the beam, as shown in Figure 2.22.

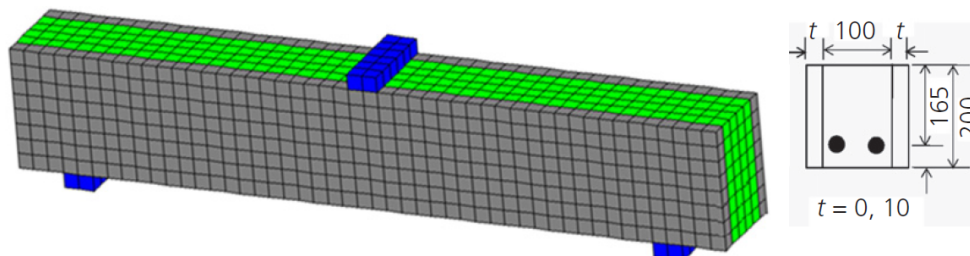


Figure 2.22: Geometry of strengthened beams with UHPFRC on sides of reinforced concrete beam [63]

Based on the load-deflection response illustrated in Figure 2.23(a), it is concluded that the use of SHCC significantly increases the capacity of strengthened beams as compared to reference beams. The numerical model based on the proposed shear transfer model can replicate the experimental behaviour of the strengthened beam, as illustrated in Figure 2.23(b). Numerical evaluation of experimental specimens revealed that the SHCC strengthening layer first experienced the multi-cracking process and finally failed with the localization of some multiple fine cracks at a capacity higher than the reference beams, like in experiments, as illustrated in Figure 2.24.

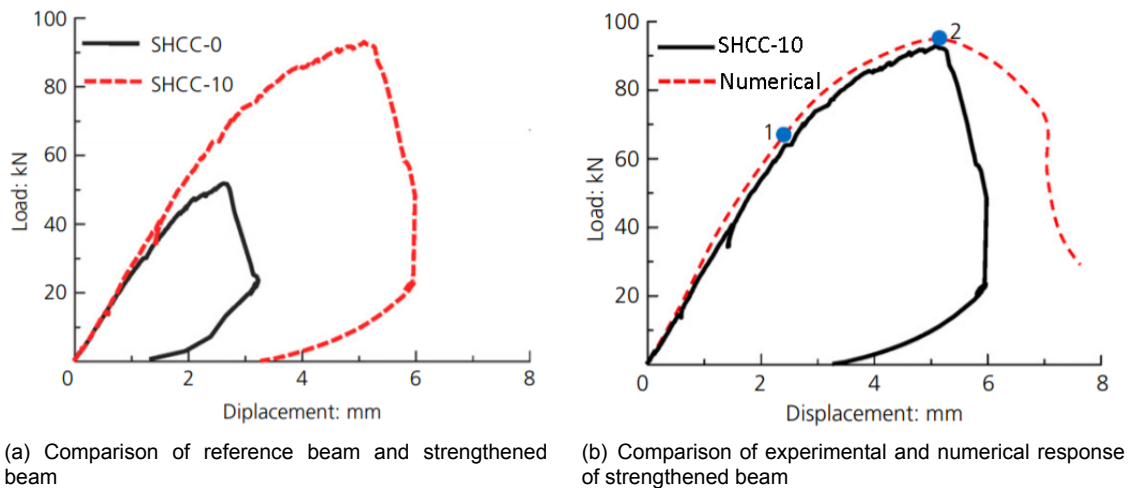


Figure 2.23: Load-deflection response SHCC-strengthened reinforced concrete beam [63]

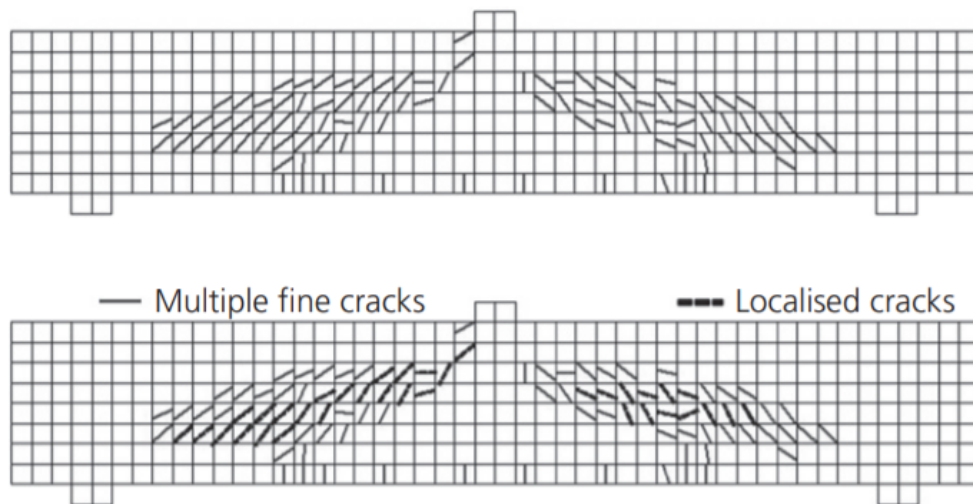


Figure 2.24: Numerical crack pattern of strengthened beam; (top) below peak load, (bottom) at peak load [63]

The above-discussed review of past literature helps outline the important aspects that need to be addressed while modelling of SHCC-strengthened reinforced concrete (RC) beams, termed as hybrid beams in this thesis. The overview of experiments suggests that the most common geometries of application of SHCC as a repair/strengthening is the application in layers, either in the tensile region for flexural strengthening, or on the sides for shear strengthening. SHCC can be applied either along the full length of the beam or in patches. The interface between SHCC and concrete is an important parameter that can govern the final failure load and failure mode of the hybrid beam. In most cases, no delamination at the interface is observed during experimentation. However, in the case of delamination, the shear capacity is decreased. Study of numerical studies performed suggests that the accuracy of replication of the experimental shear behaviour of hybrid beams depends mainly on the modelling choices used, such as shear transfer model, crack orientation type, reinforcement type and others. For the interface, perfect bond conditions were assumed mostly due to lack of delamination in experiments. However, in the case of delamination, the assumption of perfect bond in the numerical model might be incorrect.

3

Benchmark Studies

This chapter summarises the benchmark studies for numerical validation using the finite element analysis (FEA). For details, the reader can reference the published studies.

As stated in Chapter 1, the experimental shear behaviour of SHCC-strengthened RC beams, called hybrid beams in this thesis, is validated numerically by selecting different benchmark studies. Different types of beams are modelled numerically in this thesis, which are classified into three modelling phases. Modelling Phase I involves modelling of shear behaviour of reinforced concrete (RC) beam without transverse reinforcement. Modelling Phase II involves modelling of shear behaviour of SHCC beam without transverse reinforcement. Once the shear behaviour of both RC beam and reinforced SHCC beam is modelled separately, the finalised numerical solution strategy is used to model the shear behaviour of SHCC-RC hybrid beams in Modelling Phase III. RC beams strengthened with SHCC applied on sides are only considered in this thesis.

The benchmark studies, collectively, must have the aforementioned types of beams for numerical modelling in this thesis. Additionally, there are other criteria that the benchmarks must follow. Selection criteria are developed according to which the benchmark studies are selected. The benchmark study must,

- have a beam with a shear span-to-effective depth ratio (a/d) of 3 to obtain shear failure in concrete beams,
- have shear as the governing experimental failure type in all types of beams,
- not have high strength concrete, and
- not have transverse reinforcement at least in the shear span of the beam.

In addition to the above-mentioned mandatory requirements, a non-mandatory requirement is to have a common benchmark study for RC and hybrid beams so that the same study can be used in Modelling Phase I and III.

Based on the aforementioned criteria, the following four benchmark studies are selected;

1. Shear behaviour of RC beams externally strengthened with engineered cementitious composite (ECC) layers, by Guan Wang et al. 2019, referred to as Study 1 in the report [57]
2. Failure behaviour of strain-hardening cementitious composites (SHCC) for shear strengthening RC member, by Yongxing Zhang et al. 2015, referred to as Study 2 in the report [61]
3. Shear design of straight and haunched concrete beams without stirrups, by Vu Hong Nghiep 2011, referred to as Study 3 in the report [44]
4. Evaluation of shear failure of strain-hardening cementitious composite beams, by Yongxing Zhang et al. 2011, referred to as Study 4 in the report [64]

The benchmark studies selected are such that the selection criteria are satisfied. Studies 1-3 are used in Modelling Phase I, Study 4 is used in Modelling Phase II and Studies 1 and 2 are used in Modelling Phase III.

Experimentally reported values of material properties of concrete, SHCC and reinforcements of each benchmark study are used in the numerical models. However, there are additional properties required which are not provided in each study, e.g. compressive and tensile fracture energy of concrete, the tensile strength of concrete (in some cases) and uniaxial compressive strength curve of SHCC. To determine the unknown concrete properties, the NLFEA guidelines RTD:1016-1:2017 [28] are used. The material properties calculated using the guidelines are described in Chapter 4. For SHCC, additional experimental and analytical studies from the literature are referenced to obtain the material properties missing from the selected benchmark studies. These are also discussed in Chapter 4. In this chapter, the description of benchmark studies is based on the data provided in the respective papers, unless otherwise stated.

3.1. Study 1 - Guan Wang et al. (2019) [57]

The first benchmark includes the study of reinforced concrete (RC) beams externally strengthened using engineered cementitious composite (ECC). The beams are designed without any transverse reinforcement in shear spans of the beam and ECC is sprayed onto the sides of beams. Parameters such as ECC thickness, shear span-to-depth ratio and reinforcement ratio are varied in the study to assess their influence on the strengthening effect. Two different reinforcement ratios (ρ_l) of 0.89% and 2.12% with respect to concrete cross-section are tested. These are termed as beam types A and B, respectively. For each beam type, the ECC thickness of 20 mm and 40 mm is tested. And for each beam type and ECC thickness, two different shear span-to-effective depth ratios (a/d) of 2 and 3 are also tested. The results of the hybrid beams are compared with the un-strengthened RC beam.

Based on the criteria defined for selecting the type of hybrid beams to be modelled in this thesis, beam-type B with a reinforcement ratio of 2.12% and a/d of 3 is selected for modelling. Higher reinforcement ratio is selected to ensure that the beam fails in shear to maximum utilize the capacity of ECC in a hybrid configuration. Also, the term "ECC" is replaced by "SHCC" in this thesis for uniformity in the reporting terminology used for the materials.

Geometry

The sketch of the beam and the loading setup is shown in Figure 3.1. The beam is loaded in a four-point bending configuration and a load-controlled test is performed until final failure occurs. Shear strain is recorded on each side of the beam using strain rosettes formed with three Fibre Bragg Grating (FBG) sensors with a gauge length of 15 cm each. Three LVDTs are used to measure the deflections at the mid-span and the two loading points. Two $\phi 25$ mm longitudinal bars are provided at the bottom ($\rho_l = 2.12\%$). Four $\phi 10$ mm steel stirrups with 50mm spacing are placed at each end of the beams beyond the shear spans to avoid fracture due to stress concentration at the supports.

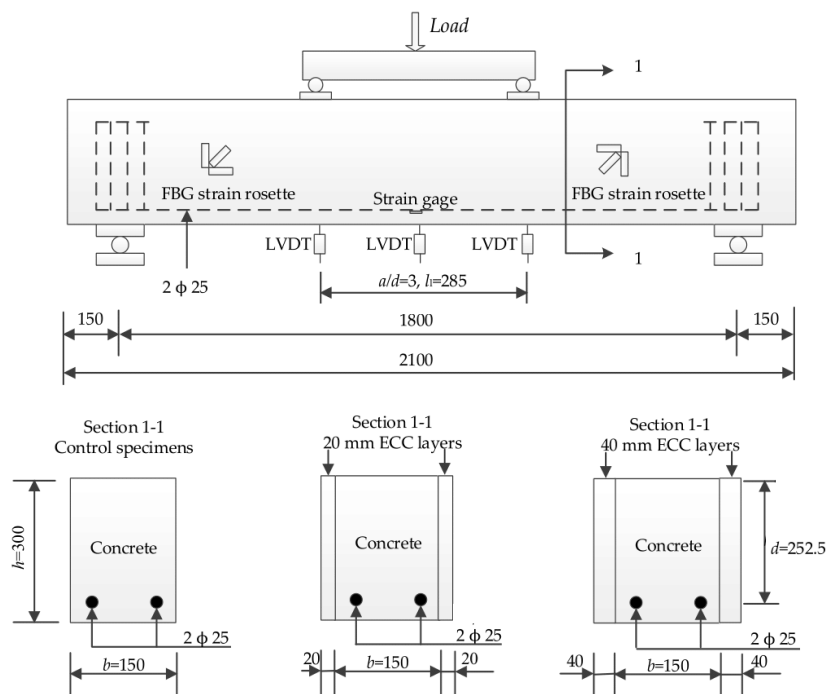


Figure 3.1: Sketch of specimens of benchmark study 1 (mm) (not to scale)

Material Properties

The properties of concrete, SHCC and steel rebar used in the experiments are shown in Table 3.1.

Table 3.1: Material properties of beams in benchmark study 1

Type	Dia. (mm)	Net Area (mm ²)	f_c (MPa)	f_t (MPa)	f_y (MPa)	ε_y	f_u (MPa)	ε_u	E (GPa)
Concrete	-	-	32	2.6	-	-	-	-	30.0
SHCC	-	-	56	4.05	-	-	-	-	24.9
Stirrups	10	50.2655	-	-	259	0.00122	329	0.012	212.3
Rebar	25	490.8738	-	-	374	0.00186	439	0.011	201.6

In order to calculate the fracture energies using the NLFEA guidelines [28], the characteristic cylindrical compressive strength of concrete is required. The value reported in Table 3.1 is the mean cubic strength of concrete (f_c), which is 32MPa. From this value, the characteristic cubic strength ($f_{ck,cube}$) can be calculated, which is 24MPa. Based on this value, the concrete can be classified as approximately C20/25 as per Eurocode 2 [15], with $f_{ck,cube}$ of 25MPa. Therefore, the characteristic cylindrical compressive strength $f_{ck,cyl}$ is 20MPa.

SHCC consists of 1.5% Polyvinyl Alcohol (PVA) Fibres. The tensile strength, reported in Table 3.1, is determined by performing a direct tensile strength test on three dog-bone specimens, the results of which are shown in Figure 3.2. The cracking tensile strength is reported to be 4.05MPa and the maximum tensile strength is 4.84MPa. For input in the numerical model, the experimental results are transformed into a trilinear curve illustrated by the dashed orange line in Figure 3.2. The input data for SHCC is summarized in Table 3.2.

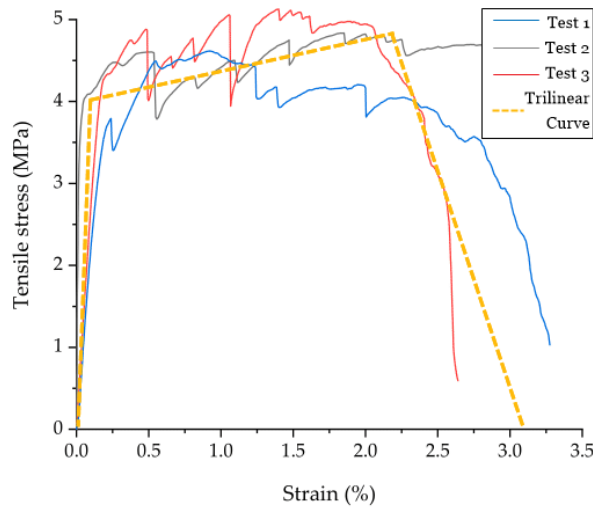


Figure 3.2: Uniaxial tensile stress-strain curves of SHCC in benchmark study 1 [57]

Table 3.2: Trilinear tensile curve of SHCC in benchmark study 1

	σ_{cr} (MPa)	ε_{cr} (%)	σ_{max} (MPa)	ε_{max} (%)	ε_u (%)
Average	4.05	0.016	4.84	2.27	3.12

The hybrid interface between SHCC and concrete is also prepared before casting the SHCC

layers on the sides. First, both sides of the RC beam are chiselled, cleaned and wet to a standard dry surface condition. Then, an interface agent (constituents: 0.85 cement + 0.05 silica fume + 0.1 expansive agent + 0.3 water, by mass) is applied and SHCC is sprayed to the designed thickness.

Experimental Results

The experimental results reported include the graphs for load vs mid-span deflection and load vs shear strain. Based on the selection criteria, results of beam specimens with an a/d of 3 and ρ_l of 2.12% are only reported and discussed in this thesis. These specimens include control beam "CB3", hybrid beams with 20mm SHCC thickness "SB-20-3" and 40mm SHCC thickness "SB-40-2". Typical plots for the graph mentioned above are shown in Figure 3.3. Note that the results in magenta colour are relevant for this thesis only.

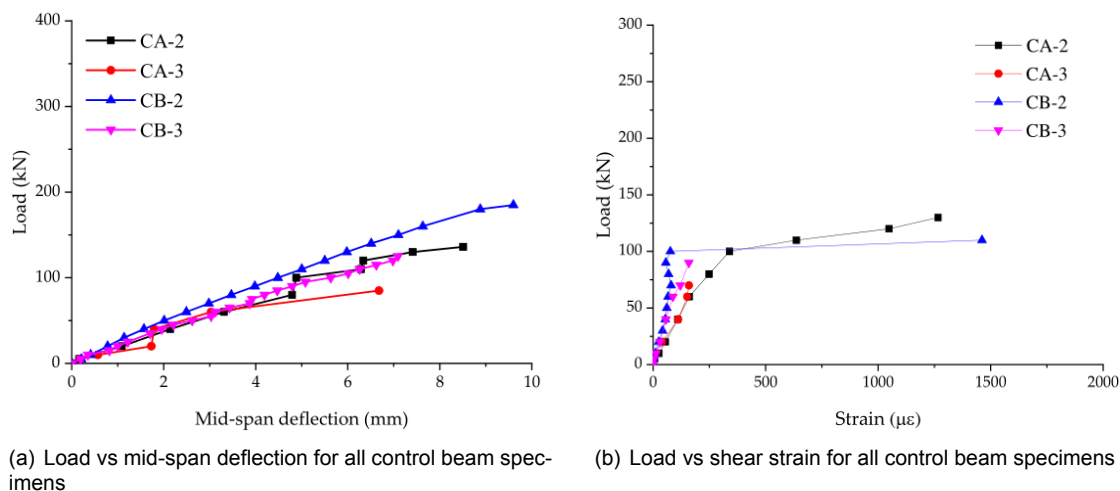


Figure 3.3: Typical experimental plots for control beams in benchmark study 1

The study also contains images related to the final condition of beams once ultimate failure occurs. Comment regarding the behaviour of hybrid beams during testing and after the ultimate failure is also provided. These aspects are discussed in detail with the numerical results in Chapter 5.

3.2. Study 2 - Yongxing Zhang et al. (2015) [61]

The second benchmark presents an experimental investigation into the advantage of shear strengthening of reinforced concrete (RC) member using strain-hardening cementitious composite (SHCC). The study is focused on the final crack pattern of SHCC strengthening layer at failure and the resultant increase in shear load-carrying capacity of the strengthened member. The beams are designed without any transverse reinforcement, and the SHCC layer is cast on the sides of beams. Unlike Study 1, only the thickness of SHCC is varied here (5mm and 10mm). The shear span-to-effective depth ratio (a/d) is 3, and the reinforcement ratio ρ_l is 0.95%. The results of the hybrid beams are compared with the un-strengthened RC beam.

Geometry

The sketch of the beam is shown in Figure 3.4. The beam is loaded in a three-point bending configuration and a load-controlled test is performed until final failure occurs. Two SHCC thicknesses of 5mm and 10mm are tested for strengthening of RC beam. Displacement transducers are used to measure displacements at loading, support and mid-points, whereas a load-cell measures the load.

Two $\varnothing 10\text{mm}$ deformed longitudinal bars are provided at the bottom ($\rho = 0.95\%$), and no transverse reinforcement is provided throughout the member.

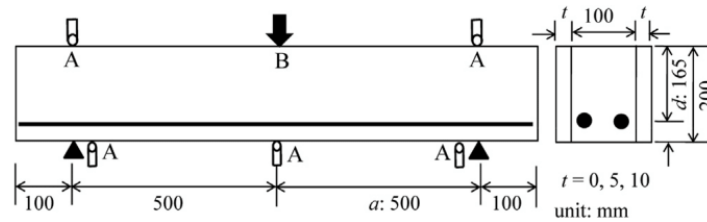


Figure 3.4: Sketch of specimens in benchmark study 2 (mm) (not to scale)

Material Properties

The properties of concrete, SHCC and steel rebar used in the experiments are shown in Table 3.3.

Table 3.3: Material properties in benchmark study 2

Type	Dia. (mm)	Net Area (mm ²)	f_c (MPa)	f_t (MPa)	f_y (MPa)	ε_y	f_u (MPa)	ε_u	E (GPa)
Concrete	-	-	27	-	-	-	-	-	23.5
SHCC	-	-	91	4.6	-	-	-	-	29
Rebar	10	50.2655	-	-	345	0.00173	432	0.045	200

In Table 3.3, the compressive strength reported for concrete is the mean cylindrical strength ($f_{cm,cyl}$) of 27MPa. For the calculation of fracture energies using NLFEA guidelines [28], this value is used directly. For the calculation of the tensile strength of concrete, the characteristic cylindrical compressive strength ($f_{ck,cyl}$) is used, which is approximately 19MPa.

For rebar, the ultimate strain ε_u is 0.045, as that of the standard value for B500 rebar, as it is not provided in the study. The yield strength f_u is referenced from [62], which is a study related to the strengthening of flexural members using SHCC of the same authors.

SHCC consists of 1.5% Polyvinyl Alcohol (PVA) Fibres. The tensile strength, reported in Table 3.3, is determined by performing a uniaxial tensile strength test on five dumbbell specimens, the results of which are shown in Figure 3.5. For input in the numerical model, the experimental results are transformed into a trilinear curve indicated by the solid red line in Figure 3.5. The input data is summarized in Table 3.4.

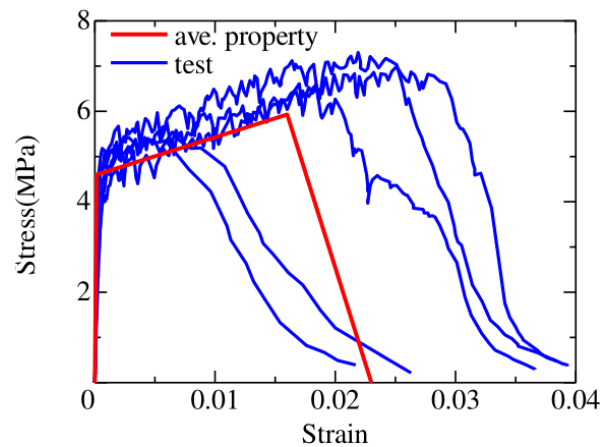


Figure 3.5: Uniaxial tensile stress-strain curves of SHCC in benchmark study 2

Table 3.4: Trilinear tensile curve of SHCC in benchmark study 2

	σ_{cr} (MPa)	ε_{cr} (%)	σ_{max} (MPa)	ε_{max} (%)	ε_u (%)
Average	4.6	0.016	5.8	1.6	2.35

The hybrid interface between SHCC and concrete is prepared by washing out the sides of the RC beam using a retarder to obtain roughed surfaces. The SHCC is then cast to desired thickness.

Experimental Results

The shear load vs displacement at the mid-span is reported for the three beam specimens tested in this study, as shown in Figure 3.6. Note here that SHCC-0 is the control specimen, i.e. RC beam without any SHCC.

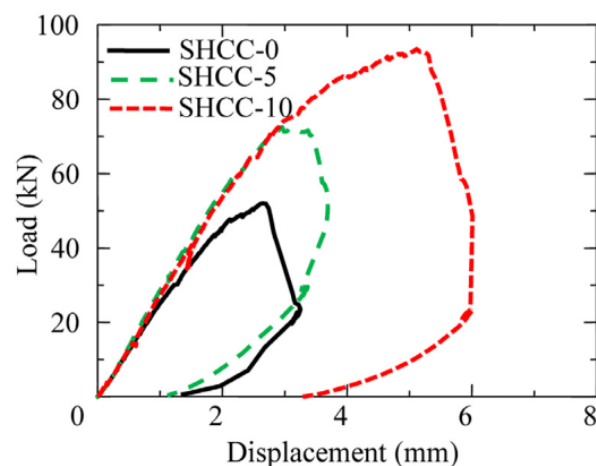


Figure 3.6: Shear load-displacement curves for beams in benchmark study 2

In addition to the results mentioned above, images of the specimens after the ultimate failure are also provided. These are discussed in detail with the numerical results in Chapter 5.

3.3. Study 3 - Vu Hong Nghiep (2011) [44]

The third benchmark aims to study the differences of shear behaviour between prismatic and non-prismatic (tapered i.e. different inclinations of the compression chord) reinforced concrete (RC) beams without transverse reinforcement in the shear span, as shown in Figure 3.7. An experimental program of testing of 18 reinforced concrete beams without transverse reinforcement of varying shear slenderness and inclination of compression chord is developed. The obtained experimental results are validated using finite element analysis (FEA) on ABAQUS software. Based on the experimental and numerical results, an analytical shear design model for practical use valid for prismatic and non-prismatic concrete beams without transverse reinforcement is developed.

Unlike in the first two studies, this thesis does not contain an SHCC-RC hybrid beam. The purpose of this study is to have an additional benchmark in Modelling Phase I to assess different numerical solution strategies.

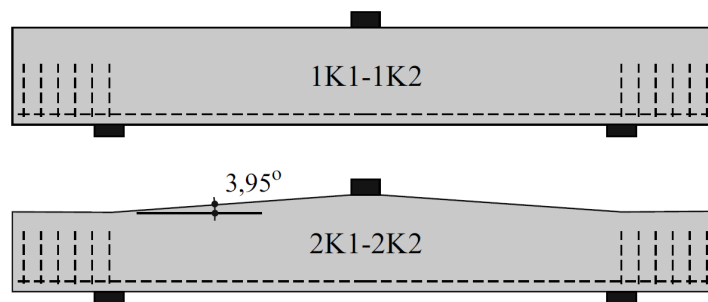


Figure 3.7: Typical prismatic and non-prismatic reinforced concrete beams in benchmark study 3 (not to scale)

Geometry

A total of 9 RC beams are tested in the study. Each beam type is tested twice for increased reliability. Therefore the total number of beams are 18. Out of 18 benchmark beams, specimen “1K1-1K2” are selected as they satisfy the defined selection criteria in this thesis. The longitudinal section and cross-section of the selected beam are shown in Figure 3.8. Three $\text{\O}20\text{mm}$ bars are provided at the bottom to ensure shear failure to occur in the test beams. The length from support to the end of the beam contains transverse reinforcement to increase the shear resistance of this region. A hydraulic jack attached at a testing steel frame is used to load the test beams at the mid-span through two thick steel plates adhered to the test beams. The contact area between the steel pad and concrete beams is $100\text{mm} \times 200\text{mm}$. The test beam was supported by two steel-box bearings $100\text{mm} \times 200\text{mm}$ located on steel pins. These two steel-box bearings are later adjusted to be fixed or moveable during the test to ensure the boundary conditions of the system. Strain gauges are used to measure the deflection and crack-widths at the mid-span of the beam.

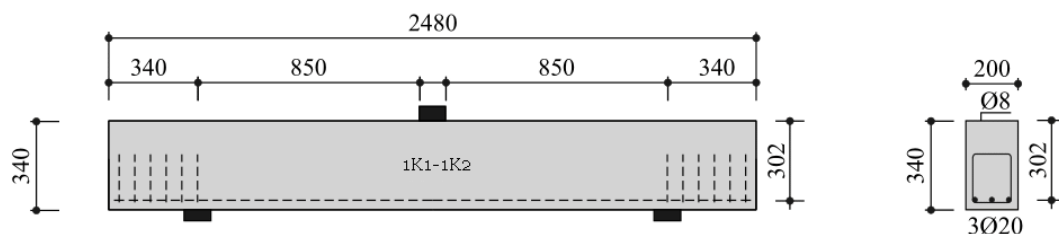


Figure 3.8: Geometrical dimensions of test beam 1K1-1K2 in benchmark study 3 (mm) (not to scale)

Material Properties

The concrete mix design corresponded to type C30/37 with a maximum aggregate size of 16 mm, however, the measured compressive strength corresponds to a higher strength class. Therefore, the experimentally tested compressive strength is used in the numerical models. The properties of concrete and steel rebar used in the experiments are shown in Table 3.5. The compressive strength reported here is the mean cylindrical compressive strength.

Table 3.5: Material properties of benchmark study 3

Type	Dia. (mm)	Net Area (mm ²)	f_c (MPa)	f_t (MPa)	f_y (MPa)	ε_y	f_u (MPa)	ε_u	E (GPa)
Concrete	-	-	53.57	-	-	-	-	-	31.3
Rebar	20	942.48	-	-	550	0.0035	610	0.04	157

Reinforcement BSt500s of $\varnothing 20$ mm diameter is used in the experiments. Three samples are tested for uniaxial strength, and the corresponding stress-strain curves are shown in Figure 3.9. From this, the value of effective yield strength of 550MPa and the ultimate strength of 610MPa is used. Properties of transverse reinforcement are not mentioned, hence are assumed to be the same as the longitudinal rebar.

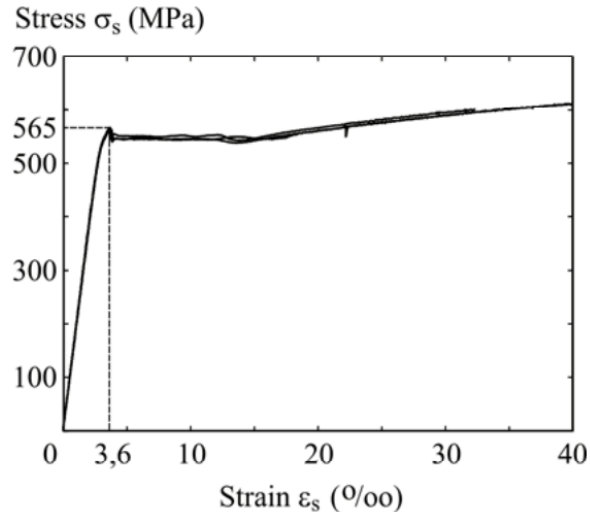


Figure 3.9: Uniaxial tensile strength results of rebar in benchmark study 3

Experimental Results

For simplicity, the results of beam “1K1” are reported in this thesis due to negligible differences in results between beams 1K1 and 1K2. The experimentally and numerically obtained load vs mid-span deflection graph is shown in Figure 3.10.

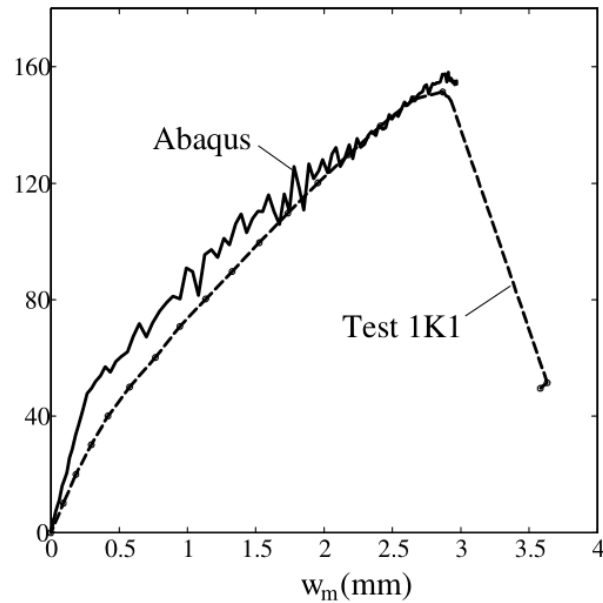


Figure 3.10: Experimental and numerical force-displacement relation for beam 1K1 in benchmark study 3

In addition to the aforementioned results, images of the beams at different loading intervals until the ultimate failure load are also provided to observe the development and progression of the cracks. These are discussed in Chapter 5.

3.4. Study 4 - Yongxing Zhang et al. (2011) [64]

The fourth benchmark presents an experimental investigation into the mechanical behaviour and fracture mechanisms of SHCC member failed in diagonal shear. This study is a continuation of the study performed by the authors of Study 1. The SHCC member is designed without any transverse reinforcement, and the thickness of SHCC member is 50mm. The only varying parameter is the shear span-to-effective depth ratio (a/d), which is kept as 2 and 3. These member types are termed as specimens “a” and “b”, respectively. In this thesis, only specimen “b” is considered. Single $\text{Ø}25\text{mm}$ longitudinal rebar is provided to ensure the shear failure of the member. A numerical shear transfer model based on Lattice Equivalent Continuum Model (LECOM) for SHCC is then proposed, which is based on SHCC’s characteristics of multiple fine cracking and eventual localization into one crack during strain softening. The experimental results are validated using the proposed numerical model in the study as well.

Geometry

The sketch of the beam is shown in Figure 3.11. The beam is loaded in a three-point bending configuration and a load-controlled test is performed until final failure occurs. Displacement transducers are used to measure displacements at the loading point. A single $\text{Ø}25\text{mm}$ deformed longitudinal bar is provided at the bottom and no transverse reinforcement is provided in the member.

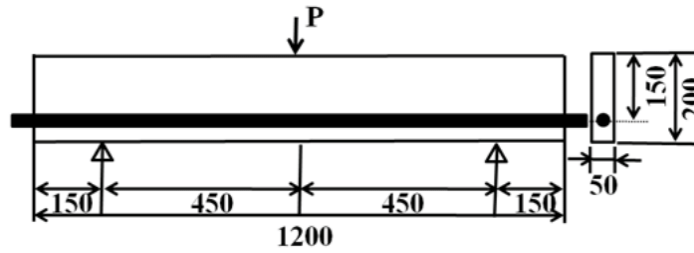


Figure 3.11: Sketch of specimen in benchmark study 4 (mm) (not to scale)

Material Properties

The properties of SHCC and steel rebar used in the experiment are shown in Table 3.6.

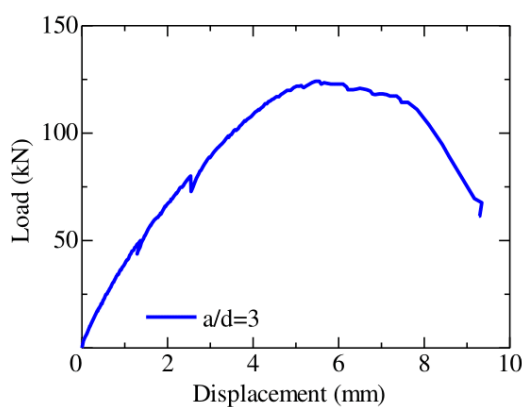
Table 3.6: Material properties in benchmark study 4

Type	Dia. (mm)	Net Area (mm ²)	f_c (MPa)	f_t (MPa)	f_y (MPa)	ϵ_y	f_u (MPa)	ϵ_u	E (GPa)
SHCC	-	-	91	4.6	-	-	-	-	29
Rebar	25	490.87	-	-	1050	0.0053	1050	0.045	200

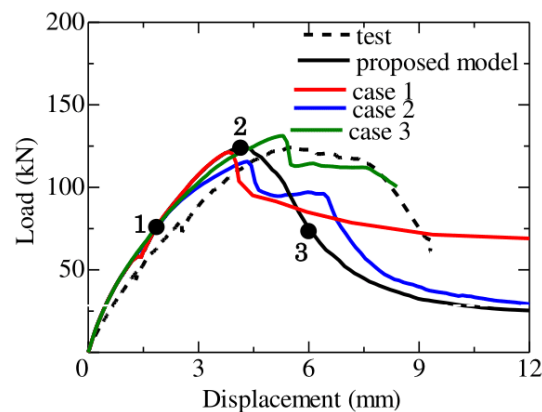
In Table 3.3, the compressive strength reported for SHCC is the mean cylindrical strength ($f_{cm,cyl}$) of 91 MPa as the material is classified as ultra-high performance SHCC (UHP-SHCC). The SHCC used here is the same as that in Study 1. The experimental tensile properties and the equivalent trilinear tensile curve used for input in the numerical models can be referenced from Figure 3.5 and Table 3.4. For rebar, the ultimate strain ϵ_u is 0.045, as that of the standard value for B500 rebar, as it is not provided in the study.

Experimental Results

The experimental load vs displacement at the mid-span for “specimen b” is shown in Figure 3.12(a).



(a) Experimental load vs mid-span deflection beam specimen b



(b) Numerical load vs shear strain for all test cases of specimen b

Figure 3.12: Load vs displacement results for “specimen b” in benchmark study 4

In LECOM numerical model, the parameters which define the shape of the shear crack include the crack angle (θ) and asperity height. The asperity height is input as a function of the maximum aggregate size in the mix for SHCC. These two parameters are varied to assess their influence on the shear behaviour of reinforced SHCC member. Three different cases are numerically tested, as shown in Figure 3.12(b). Corresponding to points 1-3, the localised crack distribution pattern is also provided. These aspects are discussed in detail in Chapter 5.

The influence of shrinkage strain modelled as an initial strain before loading is also tested numerically in this study, but the results are not used in this thesis. The input for the trilinear tensile behaviour of SHCC is also varied (minimum, maximum and average). But for this thesis, only the average input is considered, as shown in Figure 3.5.

4

Methodology

This chapter describes the set of modelling choices for finite element analysis (FEA) of the idealised physical problems. The set of idealisations are based on benchmark studies described in Chapter 3. Different numerical solution strategies to model the idealised physical problems are discussed.

Set of modelling choices can be called as a “modelling strategy”, which includes choices regarding the idealisation, constitutive properties, discretization and analysis procedure of a physical problem [53]. Choices regarding constitutive properties, discretization and analysis procedure can also be classified as a “solution strategy” [19]. In this thesis, both these terminologies are used to outline the methodology of the numerical modelling performed.

A modelling strategy is split into two main parts; idealisation of the physical problem, and numerical solution strategy.

1. Idealisation of the Physical Problem: This includes a reasonable idealisation of the geometry of the structure, boundary conditions and type of load applied [53]. In this thesis, results from finite element analysis (FEA) are compared with respective benchmark experimental results. Therefore, it is important to construct geometry and impose boundary conditions that are representative of the physical problem. Symmetry can also be used to reduce the computational time of the model. Loading can be applied by either directly applying a force (force-controlled) or forcing a displacement (displacement-control). The latter option is often chosen in FEA because it is easier to find equilibrium. However, the ultimate choice is based on what is applied during the experiments.

2. Numerical Solution Strategy: This includes considerations for the constitutive properties, assumptions around kinematic compatibility (called discretization in [53]) and equilibrium conditions (called analysis procedure in [53]) to model an idealised physical problem [19]. Details regarding aspects of a numerical solution strategy are elucidated below:

a. Considerations for the Constitutive Properties

The relation that links the finite element strains to stresses is called a constitutive relation. A finite element software package like DIANA provides numerous constitutive relations to model the linear and non-linear behaviour of different materials. For modelling concrete and SHCC, accurate definition of the tensile cracking and compressive behaviour is important. Other parameters related to confinement effect, reduction of compressive strength due to lateral cracking and Poisson ratio reduction can also be considered. Modelling confinement increases and lateral cracking reduces the compressive strength of concrete. For the non-linear modelling of the reinforcement, accurate definition of the yielding behaviour is important.

b. Assumptions around Kinematic Compatibility

For kinematic compatibility, the finite element type, mesh (element) size and condition of interface between materials need to be specified. The choice for element types is based on the type of material and geometry of the model (2D or 3D). Other choices related to kinematic compatibility include analytical versus numerical integration, Gaussian versus Newton-Cotes numerical integration and regular versus high integration scheme [20]. de Putter [19] also includes details about the boundary conditions while describing assumptions for kinematic compatibility, however, these are described during idealisation in this thesis, as in [53].

c. Equilibrium Conditions

These consist of choices regarding analysis control, load step and increment, iteration scheme, maximum permissible iterations and convergence criteria. Analysis control options such as an arc-length algorithm and linesearch can be used to search for equilibrium if softening behaviour is required to be captured in the force-controlled analysis [19]. In a non-linear analysis, an iterative procedure for solving the system of equations in each load step to obtain equilibrium between internal and external forces needs to be defined. This iterative procedure takes into account the varying stiffness of the structure as loading progresses, which is important to follow the equilibrium path accurately. For each load step, the iterative process concludes once the convergence criterion is satisfied or the maximum number of permissible iterations for each load step is reached. The number of iterations is specified to prevent excessive computation due to non-convergence, which takes significant computation time. Mechanism of application of load is also described in this section by de Putter [19], however, it is discussed in idealisation in this thesis, as in [53].

Note that a numerical solution strategy is always specific for the physical problem under consid-

eration. A single solution strategy can be used to model different physical problems from different studies, provided the idealisations among them are similar. The non-linear finite element analysis (NLFEA) guidelines for concrete structures [28] serve as a starting point to develop a numerical solution strategy that can accurately model concrete structures.

This chapter is divided into two main sections based on the two main aspects in a modelling strategy; Idealisation of Physical Problems, and Numerical Solution Strategy. Section 4.4 describes material properties from each benchmark study required as inputs in a modelling strategy and Section 4.5 outlines the analyses performed based on the modelling phases described in Chapter 1.

4.1. Idealisation of Physical Problems

As stated Chapter 1, the numerical analyses are divided into three modelling phases. Within each phase, different benchmark studies are used to model different types of beams. Therefore, the idealised physical problems are described in terms of modelling phases and the respective benchmark beams modelled. All benchmark beams have a shear span-to-effective depth ratio (a/d) of 3. The following idealised models are produced in total;

Modelling Phase I:

1. Model **CB1** (Reinforced Concrete Beam of Study 1), which is representative of the experimental beam “CB-3” of Study 1. It is a reference/control reinforced concrete beam without any transverse reinforcement in the shear span.
2. Model **CB2** (Reinforced Concrete Beam of Study 2), which is representative of the experimental beam “SHCC-0” of Study 2. It is a reference/control reinforced concrete beam without any transverse reinforcement.
3. Model **CB3** (Reinforced Concrete Beam of Study 3), which is representative of the experimental beam “1K1” of Study 3. It is a reference/control reinforced concrete beam without any transverse reinforcement in the shear span.

Modelling Phase II:

Model **SHCC4** (Reinforced SHCC Beam of Study 4), which is representative of the experimental beam specimen “b” of Study 4. It is a reinforced SHCC beam without any transverse reinforcement.

Modelling Phase III:

1. Model **H20Q1** (SHCC-RC Hybrid Quarter beam model of Study 1), which is representative of the experimental beam “SB-20-3” of Study 1. It is a 3D quarter model of SHCC-RC hybrid beam without any transverse reinforcement in the shear span with 20mm thick SHCC applied on each side of the reinforced concrete beam CB1.
2. Model **H40Q1** (SHCC-RC Hybrid Quarter beam model of Study 1), which is representative of the experimental beam “SB-40-3” of Study 1. It is a 3D quarter model of SHCC-RC hybrid beam without any transverse reinforcement in the shear span with 40mm thick SHCC applied on each side of the reinforced concrete beam CB1.
3. Model **H5Q2** (SHCC-RC Hybrid Quarter beam model of Study 2), which is representative of the experimental beam “SHCC-5” of Study 2. It is a 3D quarter model of SHCC-RC hybrid beam without any transverse reinforcement with 5mm thick SHCC applied on each side of the reinforced concrete beam CB2.
4. Model **H10Q2** (SHCC-RC Hybrid Quarter beam model of Study 2), which is representative of the experimental beam “SHCC-10” of Study 2. It is a 3D quarter model of SHCC-RC hybrid beam without any transverse reinforcement with 10mm thick SHCC applied on each side of the reinforced concrete beam CB2.

Note that all hybrid beam models in Modelling Phase III are in 3D. As discussed in Section 4.2.2, a very small mesh size is selected for modelling of these beams. For 2D models in Modelling Phase I and II, the computational time is a few hours, but 3D models are estimated to take several days to run. Due to a computational time restraint, only a quarter of the 3D beams is modelled using both longitudinal and cross-section symmetry in Modelling Phase III. In the following subsections, the details about the numerical models are discussed, which are classified based on the type of geometry i.e. 2D or 3D.

4.1.1. Geometry of the Model

2D Models - Phase I & II

2D models are produced using regular plane stress elements. The geometry of the models represents the experimental configuration. The idealised geometry of the models is illustrated in Figure 4.1 and geometric properties are listed in Table 4.1.

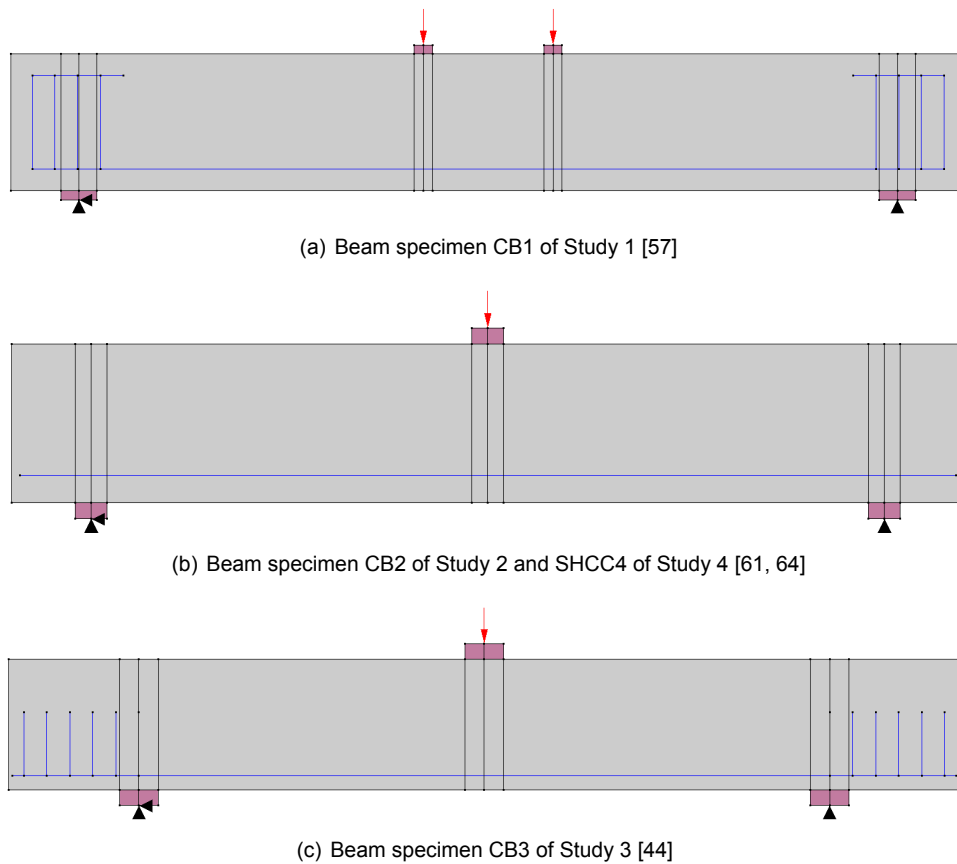


Figure 4.1: Idealised 2D models

Table 4.1: Geometrical properties of idealised beams (mm)

Dimension	Study 1	Study 2 and 4	Study 3
Length	2100	1200	2480
Height	300	200	340
Width	150	100	200
a/d	3	3	3

3D Models - Phase III

3D models are produced using solid brick elements. The geometry of the models represents a quarter of the experimental configuration. The geometric properties of the beam models are the same as listed in Table 4.1 and Figure 4.2 shows a typical idealised 3D model.

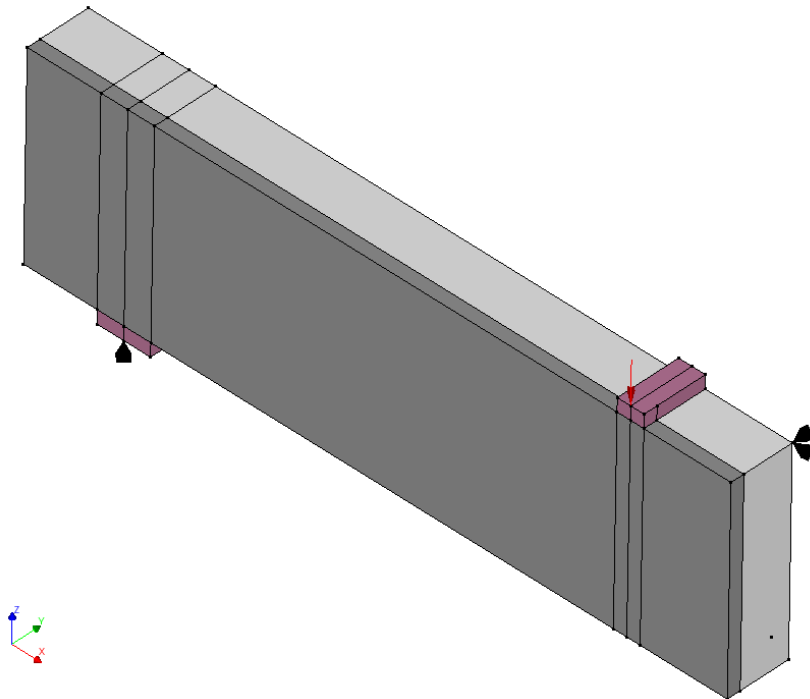


Figure 4.2: Idealised 3D SHCC-RC hybrid model of Study 1 [57]

4.1.2. Loading Conditions and Support Conditions

2D Models - Phase I & II

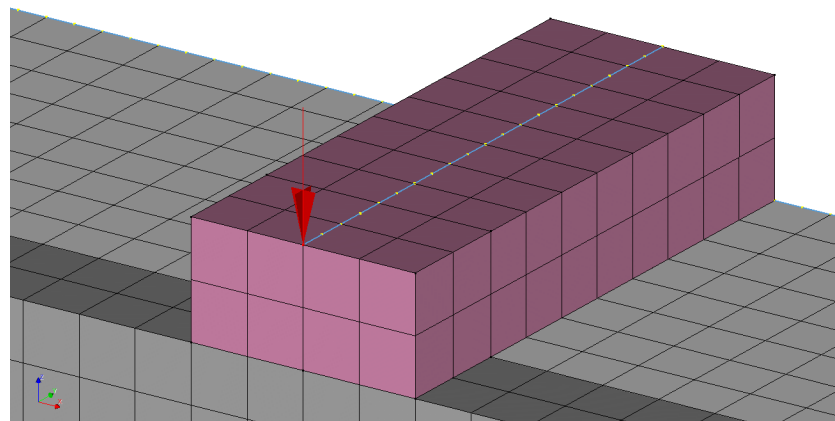
Load and support conditions are modelled to mimic the experiments. A pin-hinge configuration is used. Vertex loads and supports are provided at the centre of steel plates in 2D models, as shown in Figure 4.1. The geometric properties of the plates in each model are listed in Table 4.2.

Table 4.2: Geometrical properties of load and support plates (mm)

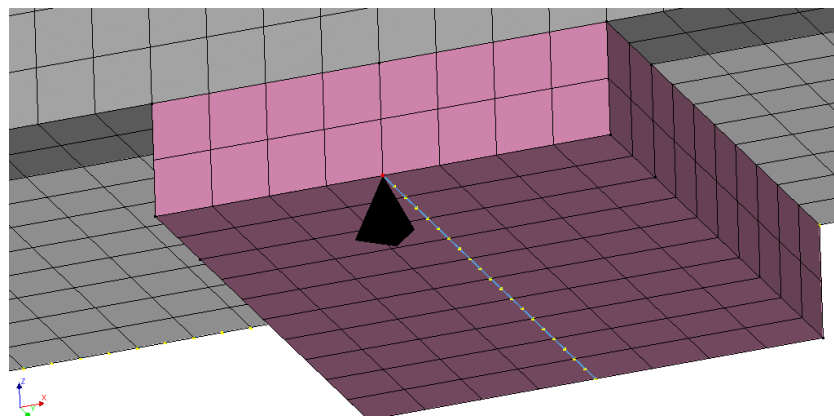
Dimension	Study 1	Study 2 and 4	Study 3
Load Plates			
Length	80	80	100
Height	20	20	20
Width	150	100	200
Support Plates			
Length	100	80	100
Height	20	20	20
Width	150	100	200

3D Models - Phase III

In 3D models, load and supports are modelled using "tying" option. The nodal deformations of the vertices along the centreline of the loading plate are tied to the centre-edge node on top of the loading plate, as shown in Figure 4.3(a). This helps in applying line load as a concentrated force. Similarly, the line supports are converted into vertex supports by tying the nodal deformations along the centre line of the support plates to the centre-corner node at the bottom of the support plate, as shown in Figure 4.3(b). This helps in obtaining the reaction forces as a concentrated force as well.



(a) Tying at the load plate



(b) Tying at the support plate

Figure 4.3: Tying at load and support plates for 3D quarter model of Study 1

To prevent rigid body rotation and simulate symmetry in 3D quarter models, restraint at the cross-sectional (abbreviated as X-S) edge face and longitudinal-section (abbreviated as L-S) edge face is provided. In the numerical model, the deformation occurs in the Z direction while the X-S edge face is restrained in the X direction, and L-S edge face is restrained in the Y direction. The restraints mentioned above are also modelled using tying. The deformations of these edge faces are tied to the same top corner node, as shown in Figure 4.4.

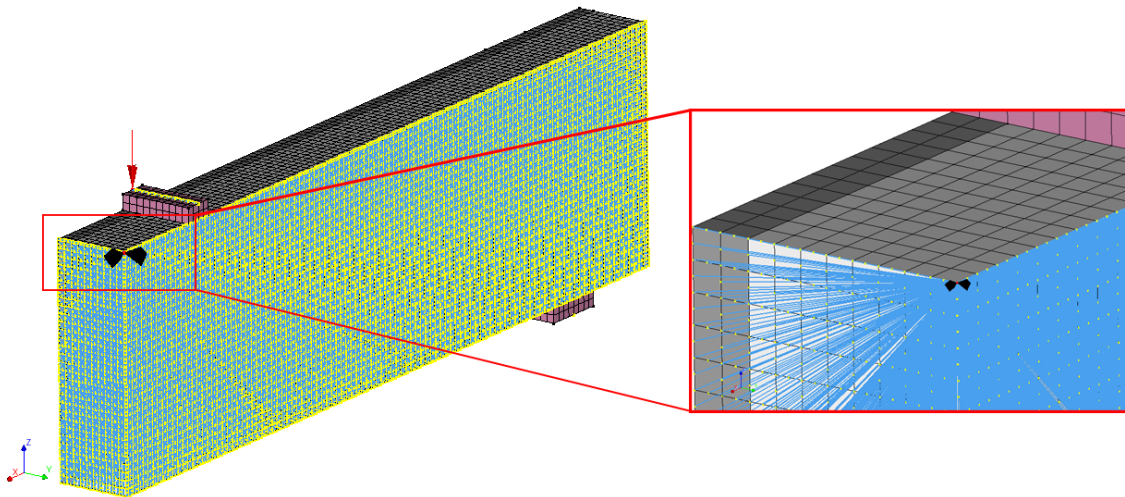


Figure 4.4: Tying of the symmetry faces of the 3D quarter model of Study 1

4.2. Numerical Solution Strategy

A numerical solution strategy consists of three components; considerations for the constitutive model, the assumptions around the kinematic compatibility and the equilibrium conditions [19]. These are discussed in detail in subsections below:

4.2.1. Considerations for Constitutive Model

The constitutive considerations are based on the type of material to be modelled. There are four types of materials considered in this thesis, concrete, SHCC, reinforcement and steel plates. Although the tensile and compressive behaviour of concrete and SHCC differs, they both can be classified as concrete for certain considerations in the constitutive model. These uniform constitutive considerations for SHCC and concrete include; material class, material crack model and crack orientation. As stated in Chapter 1, uniformity is necessary for certain modelling choices to ensure numerical compatibility when both concrete and SHCC materials are modelled together in a hybrid configuration. The term “concrete” in quotations is used when mentioning both concrete and SHCC collectively, and their uniform modelling choices are discussed in subsection below. Without the quotations, it is just regular concrete unless otherwise stated.

Uniform considerations for “Concrete”

Cracking behaviour of any material can be modelled using two main approaches; discrete cracking and smeared cracking. Discrete cracking involves introducing discontinuity between elements that replicate cracking by assigning a non-linear interface. However, prior knowledge regarding the location and orientation of the cracks in a member is needed. Possible heterogeneity in the composition of materials like concrete renders this approach ineffective as it is difficult to pre-determine the location and orientation of cracks. A more realistic approach is smeared cracking, in which cracks are smeared throughout the continuum elements.

Modelling of shear behaviour of concrete is intricate due to the unpredictable behaviour of shear cracks, especially in the absence of transverse reinforcement [53]. Furthermore, the cracking behaviour of SHCC is different from concrete. SHCC exhibits multi-cracking behaviour due to relatively higher ductility than concrete [30]. Therefore, a smeared crack approach is adopted to model “concrete” in this thesis.

Total strain-based crack model is used to model cracks using the smeared crack approach for “concrete”. There are two main choices regarding crack orientation in this model; rotating and fixed. The rotating crack orientation model allows for the rotation of the axis of application of the stress-strain constitutive relation with the direction of the principle strain vector, i.e. the constitutive relation is applied in principle strain direction. The fixed crack orientation model has a fixed direction of the stress-strain relation upon the formation of cracks, and the crack plane is used as the axis for a constitutive coordinate system. In simple words, both crack concepts calculate stresses in the direction of the crack, but the transformation matrix (used to transform local strains into crack plane direction) in case of rotating crack orientation is continually calculated based on the direction of the principle strain vector (since it is the assumed crack plane), while it is fixed upon crack initiation for the fixed crack orientation [53]. Another option is to use rotating-to-fixed model, however, a critical threshold needs to be defined according to which the crack orientation type switches from rotating to fixed.

The most significant difference between the two main crack orientation approaches is how shear strains are treated. Shear stresses in a rotating model cannot develop since the crack follows the principle strain. Therefore, an implicit shear modulus is needed for coaxiality between rotating principle stress and strain [47]. This problem does not exist for fixed crack orientation, and the inherent Shear Retention Function (SRF) serves as means of reducing the shear modulus with increasing strains, which replicates reduction of shear stiffness due to cracking [39].

Both types of crack orientation models are used to model reinforced concrete structures. However, a fixed crack model is known to better mimic the physical nature of cracks. Teshome [53] reports not to use rotating crack orientation to model concrete beams without transverse reinforcement as delamination-like behaviour is observed along the longitudinal reinforcement, predicting the wrong failure type [19]. Therefore in this thesis, the fixed crack orientation model is used to model “concrete”. It is worth mentioning here that the fixed crack model performs better in terms of predicting the correct failure type and the peak load of beams when a fine mesh size is used. This aspect is duly considered in deciding for the mesh size for all the numerical models in this thesis.

The shear stiffness of a cracked section is believed to deteriorate based on the crack opening width, which is governed by different factors. Different types of SRFs based on different factors are available in DIANA to model shear stiffness accurately. The NLFEA guidelines [28] recommend verification of the shear retention function used for modelling of reinforced concrete beams without transverse reinforcement when fixed-crack orientation is used. Therefore, Teshome [53] tested two types of functions; damage-based and aggregate-based. It is concluded that damage-based function performs better than the aggregate-based one. This conclusion is consistent with findings in other research work as well [19]. Based on this reasoning, the damage-based function could be directly used in this thesis. However, it is also stated that the set of modelling choices are always tailored to model specific failures, and a single set of modelling choices cannot be generalised for all cases [53]. Therefore, in this thesis, two types of SRFs are considered in Modelling Phase I. These include (a) Damage-based and, (b) Al-Mahaidi. Based on the results of Modelling Phase I, one SRF is finalised, which is then used to model the hybrid beams in shear. The aggregate-based function is not used since it requires input for mean aggregate size, which is not provided in the benchmark studies [20, 53]. The selected functions are briefly described below.

A. Damage-based Shear Retention Function

Damage-based shear retention function involves a reduction of shear stiffness of the crack plane at the same rate as the normal stiffness. The updated shear stiffness after cracking is calculated as,

$$G_{cr} = \frac{\mu E}{2(1 + \nu)} \quad (4.1)$$

Where, G_{cr} is the shear stiffness of the cracked surface, μ is the reduction factor for Young's Modulus E of the material and ν is the Poisson ratio. The damage-based model does not take aggregate interlock into account [59].

B. Al-Mahaidi Shear Retention Function

Al-Mahaidi shear retention function involves a reduction of shear stiffness of the crack plane as a function of normal total strain according to,

$$\beta = 0.4 \frac{f_t}{E \varepsilon_{nn}} \quad (4.2)$$

Where, β is the shear retention factor, f_t is the tensile strength of the material, E is Young's Modulus of the material and ε_{nn} is the normal total strain. The shear retention factor β is required as input for this model. β can be considered as a parameter that provides roughness to the cracked faces, mimicking aggregate interlock, which is among the main phenomena that provide shear resistance in concrete [14, 39]. The minimum value for shear retention factor β_{min} is kept constant at 0.01 in Modelling Phase I [20]. However, a sensitivity study for the input value of β_{min} is performed to assess its influence on the capacity of the models.

Table 4.3 summarises the constitutive inputs finalised for modelling of "concrete" in this thesis.

Table 4.3: Uniform constitutive parameters for "Concrete"

Material class	Concrete and Masonry
Crack model	Total strain-based
Crack orientation	Fixed
Shear retention functions	Damage, Al-Mahaidi
Compressive strength reduction model	Vecchio & Collins 1993 [55]
Compressive strength reduction factor	0.4
Confinement model	Vecchio & Selby
Poisson Reduction	Damage-based

There are additional parameters that are uniform in both concrete and SHCC materials. The reduction in compressive strength due to lateral cracking of "concrete" is modelled according to the reduction model proposed by Vecchio & Collins [55]. A reduction factor of 0.4 is taken for concrete [28]. The same is used for SHCC as well. A factor of 0.4 means that only 40% of the original compressive strength at any integration point with a big crack is retained. Confinement of "concrete" is taken into account using the relation proposed by Vecchio & Selby. Damage-based Poisson ratio reduction is also considered.

In the following subsections, choices for modelling the tensile and compressive behaviour of SHCC and concrete, and modelling of reinforcement and steel plates are discussed.

Concrete

The constitutive properties to model tensile and compressive behaviour of concrete are listed in Table 4.4.

Table 4.4: Concrete constitutive properties

Tensile curve	Hordijk
Crack bandwidth estimator	Govindjee
Compression curve	Parabolic

The tensile behaviour of concrete is defined using the Hordijk tension softening curve, as suggested in the NLFEA guidelines [28]. The Govindjee crack-bandwidth [27] is used as it bases the bandwidth on the shape and other properties of the element and also takes into account the direction of the crack [19]. Parabolic compressive behaviour is used for modelling more realistic compression failure of concrete, also suggested in the guidelines [28].

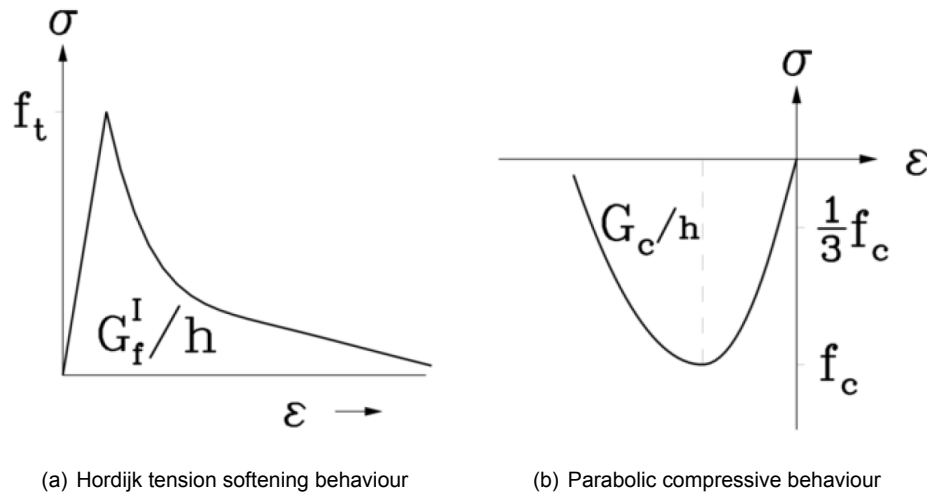


Figure 4.5: Input tensile and compressive behaviour of concrete [28]

SHCC

The tensile behaviour of SHCC is modelled using *fib* fibre reinforced concrete (FRC) tensile curve to replicate its hardening behaviour [51]. The compressive behaviour is modelled using a multi-linear curve. The constitutive properties are listed in Table 4.5.

Table 4.5: SHCC constitutive properties

Tensile curve	<i>fib</i> Fibre-reinforced concrete
Compression curve	Multi-linear

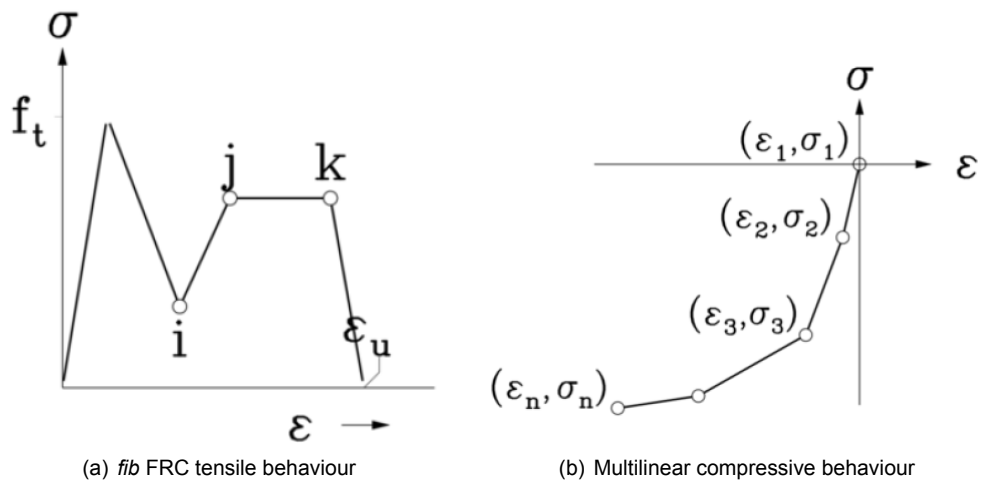


Figure 4.6: Input tensile and compressive behaviour of SHCC [28]

Reinforcement

Teshome [53] recommends using embedded reinforcement when fixed crack orientation is used to model beams in shear, simulating perfect bond between concrete and reinforcement, i.e. no slip. The embedded reinforcement follows the displacement and strains of the so-called “Mother” elements that it is embedded in. Bi-linear constitutive relation is used to model the reinforcements. Plastic strain-yield stress hardening function is used for embedded reinforcements [19]. The constitutive properties are listed in Table 4.6.

Table 4.6: Reinforcement constitutive properties

Reinforcement type	Smearred
Plasticity model	Von Mises
Plastic hardening function	Plastic strain-yield stress

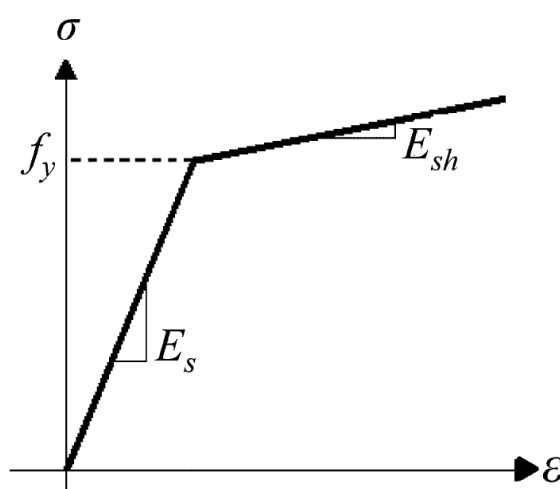


Figure 4.7: Linear plastic behaviour of reinforcement

Steel Plates

The load and support plates are modelled as steel, ignoring their self-weight. Additionally, a linear elastic 2D line interface is modelled between the beam and the plates to avoid localization of stresses and any contribution from the stiffness of the steel plates to the stiffness of the beams [43, 53]. Further details are discussed in Section 4.2.2. The constitutive parameters for modelling steel plates are listed in Table 4.7.

Table 4.7: Steel plates constitutive properties

Class	Steel
Material model	Linear elastic isotropic

4.2.2. Assumptions around Kinematic Compatibility

This section contains details about the mesh size for all numerical models in this thesis. Subsequently, the details about the finite element types, integration scheme and hybrid interface are discussed based on the geometry of the model (2D or 3D).

Mesh

The choice of mesh size can be made from either of the following selection criterion:

1. NLFEA guidelines [28]
2. 20 elements in the height of the beam based on the conclusions in a recent study performed at TU Delft [19]. This criterion is termed as “H/20” in this thesis
3. Based on the thickness of SHCC in the hybrid beams

The NLFEA guidelines [28] consist of guidelines to model the non-linear behaviour of concrete structures using finite element analysis (FEA). In the guidelines, formulas to calculate the mesh size for 2D or 3D modelling of beams and slabs is provided. These guidelines are used in numerous studies to model concrete beams. However, recent studies at TU Delft on the modelling of shear behaviour of reinforced concrete beams show that the mesh size calculated using the guidelines is not able to produce the best results [19, 53]. de Putter [19] concluded to provide 20 elements in the height of the beam for beams with 600mm or less height to obtain good results. Therefore, this criterion can be used to define the mesh size. But an additional aspect unique to this thesis is the fact that SHCC is modelled in hybrid with concrete, and typically, the thickness of SHCC is very small as compared to the dimensions of the concrete beam. Therefore, to obtain a good quality mesh, the SHCC thickness might be the governing factor.

Additionally, the mesh size influences the results for beams without shear reinforcement [11, 19]. The numerical failure loads increase with reducing mesh size, and this dependency is severe for deep beams, especially. These over-predictions can be attributed to a deficiency in the finite element model [19]. Therefore, choice for the mesh size will influence the results obtained. The dimensions of beams and SHCC thickness vary within each benchmark beam considered in this thesis. This is indicated in Table 4.8.

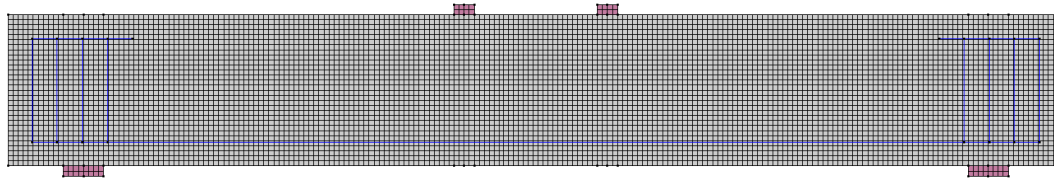
Table 4.8: Impact on mesh size selection criterion of benchmark studies

Criterion	Mesh Size in 2D Models (mm)				
	Study 1	Study 2	Study 3	Study 4	
Guidelines [28]	42	24	50	24	
H/20 [19]	15	10	17	10	
Smallest modelled SHCC thickness	20	10	-	50	
Criterion	Mesh Size in 3D Models (mm)				
	Guidelines [28]	32	20	-	-
	H/20 [19]	15	10	-	-
	Smallest modelled SHCC thickness	20	10	-	-

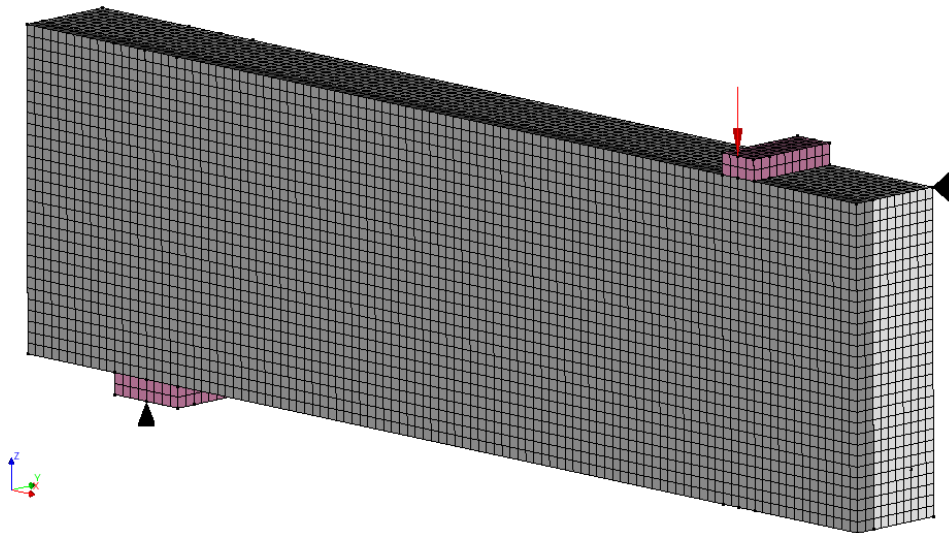
Note that in benchmark study 2, the smallest SHCC thickness is 5mm, but this is extremely small and computationally time-consuming to model, especially in 3D. Therefore, 5mm SHCC thickness as possible mesh size is not being considered. A consequence of this would be that the element shape of 5mm thick SHCC layers in hybrid beams are slender rectangular solids or cuboids. According to the DIANA manual [20], if the element shape parameters (length, width and height) are such that the aspect ratio of the element is higher than the default eigenvalue tolerance, a warning message is generated. During modelling of all hybrid beams with slender cuboidal elements of SHCC (e.g. hybrid beam with 5mm thick SHCC layer) in this thesis, such a warning is not obtained. This indicates that the aspect ratio distortion of the element is within permissible tolerance. Although not the case for this thesis, if a warning message is obtained, then the permissible tolerances for aspect ratio distortion of the elements can be user-specified [20].

Table 4.8 suggests that if the criteria mentioned above are used, the mesh size in each study will be different. Because of these differences, the numerical results cannot be compared between different studies and modelling phases. Therefore, for uniformity in the complete thesis, a single mesh size is used.

The thinnest SHCC layer considered in this thesis (apart from 5mm) is 10mm in benchmark study 2. Therefore, a mesh size of 10mm is selected for numerical modelling in this thesis. As Table 4.8 shows that the mesh sizes from the criteria for each study are either equal to or higher than 10mm, therefore, the selected mesh size is acceptable. Typical 2D and 3D meshed models are shown in Figure 4.8.



(a) Mesh of a 2D model



(b) Mesh of a 3D quarter model

Figure 4.8: Typical mesh of 2D and 3D models of Study 1

2D Models

Every element in 2D models is modelled using quadratic plane stress elements. The mesh size is kept the same in all the material components (concrete, SHCC and steel plates), ensuring an aspect ratio 1:1 where possible. Since models are in 2D, therefore the thickness of each component is incorporated in the respective element geometries. 2D kinematic parameters are listed in Table 4.9.

Table 4.9: Kinematic parameters for concrete, SHCC and steel plates in 2D models [20]

Element type	Plane stress
Element name	CQ16M
Integration scheme	2x2 Gaussian (Default)
Interpolation type	Quadratic

To avoid the development of tensile stresses (due to rotation of the beam over the plate), a 2D line interface is modelled between the beam and steel plates. This requires the input of normal and shear stiffness. The interface parameters are listed in Table 4.10.

Table 4.10: Beam-plate interface parameters for 2D models [19, 20, 43, 53]

Element type	2D line interface
Element name	CL12I
Integration scheme	3-point Newton-Cotes (Default)
Interpolation type	Quadratic
Normal stiffness (N/mm^3)	E
Shear stiffness (N/mm^3)	$E/1000$

Where E is the Young's Modulus of concrete or SHCC.

3D Models

Every element in 3D models is modelled using solid brick elements. The mesh size is kept the same in all the material components (concrete, SHCC and steel plates). 3D kinematic parameters are listed in Table 4.11.

Table 4.11: Kinematic parameters for concrete, SHCC and steel plates in 3D models [20]

Element type	Solid brick
Element name	CHX60
Integration scheme	3x3x3 Gaussian (Default)
Interpolation type	Quadratic

Like 2D models, an interface is provided between the beam and steel plates to avoid the development of tensile stresses. The beam-plate interface parameters are listed in Table 4.12.

Table 4.12: Beam-plate interface parameters for 3D models [20]

Element type	3D surface interface
Element name	CQ481
Integration scheme	3x3 Newton-Cotes (Default)
Interpolation type	Quadratic
Normal stiffness (N/mm^3)	E_s
Shear stiffness (N/mm^3)	$E_s/1000$

Where E_s is the Young's Modulus of steel plates. Typically, modulus of concrete is used instead of steel plates. But in hybrid beams, the steel plates are on both SHCC and concrete, and their Young's Moduli are different. Therefore, for uniformity, the Young's Modulus of steel plates is used as input to calculate the stiffness of the interface between steel plates and hybrid beams. The main purpose is to avoid concentration of stresses and this can be achieved using the Young's Modulus of steel as well.

Hybrid Interface

An interface can be provided between the substrate, i.e. concrete and the overlay, i.e. SHCC in the hybrid beams. It is termed as “hybrid interface” in this thesis. For example, a hybrid interface can be smooth, corrugated or bonded using adhesive, depending on the technique or materials used for its preparation. As stated in Chapter 3, different techniques are used in benchmark studies to form a hybrid interface. The intention for using such techniques is to have a strong interface between concrete and SHCC such that it is not the governing parameter in causing the failure of the beam.

In the numerical models, the perfectly bonded hybrid interface can be easily simulated by defining no interface between concrete and SHCC. The model is constructed such that the nodes of element faces of SHCC are the same as the neighbouring concrete elements at the interface and no additional surface is modelled in between these two materials. This replicates a perfect bond condition in the numerical model. Such a model is described as “Perfect Bond” or **PB** in this thesis.

The reality, however, is that it is almost impossible to develop a completely perfectly bonded interface in the experiments as in the numerical model. Therefore, another type of interface needs to be tested that is not as perfect as the “Perfect Bond” interface. This second interface type is referred to as “Imperfect Bond” or **IB**. Note that the use of imperfect interface type does not necessarily mean that the interface governs the ultimate failure of the hybrid beams. An interface can be imperfect or weak, but still not be the governing factor that causes the failure of the hybrid beam.

Most of the studies performed in studying the interface between substrate and overlays are on old and new concrete. Wagner [56], however, studied the behaviour of the interface between SHCC and concrete. This study is used as a reference in this thesis to obtain the parameters required to model the imperfect bond interface type.

Wagner's failure criterion is based on Coulomb friction [56]. Therefore, the “imperfect” interface is modelled using a Coulomb friction model available in DIANA, as shown in Figure 4.9. The input parameters and respective input values used to define the imperfect bond interface are shown in Table 4.13.

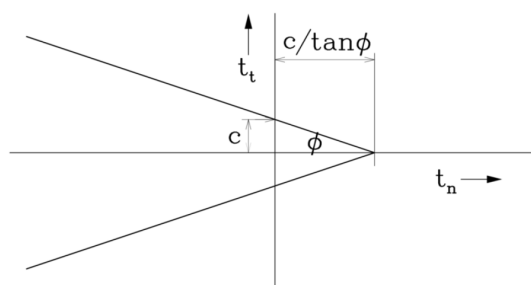


Figure 4.9: Non-linear elastic Coulomb friction model [20]

Table 4.13: Imperfect bond interface properties

Class	Interface elements
Material Model	Coulomb friction
Cohesion (N/mm^2)	2
Friction Angle (rad)	0.61
Dilatancy (rad)	0
Interface opening model	Gapping model
Tensile strength (N/mm^2)	1
Gap model	Brittle

Wagner varied the angle of hybrid interface with respect to loading direction, from 0 to 90 degrees, representing the interface being loaded in pure tension to theoretically pure shear, respectively. The tensile strength in case of pure tension is approximately 1MPa. The cohesion of the interface is assumed to be twice the interface tensile strength [10]. The dilatancy is considered to be 0. And since no chemical, epoxy or any other material or interface preparation technique is used to make the interface, and the two materials are cast next to each other, therefore a smooth interface condition can be considered. According to *fib* Model Code 2010 [22], a smooth interface has a coefficient of friction between 0.5 to 0.7. Austin [6] cites various studies according to which a smooth interface can be described with a coefficient of friction u ranging between 0.7-0.87. Based on this, the coefficient of friction in this thesis to model the imperfect bond interface is 0.7. In DIANA, the actual input is the friction angle ϕ , which is the tangent inverse of u . Based on the value of u , ϕ is approximately 0.61 radians. The kinematic parameters of the interface are listed in Table 4.14.

Table 4.14: Imperfect bond interface kinematic parameters for 3D models [20, 56]

Element type	3D surface interface
Element name	CQ481
Integration scheme	3x3 Newton-Cotes (Default)
Interpolation type	Quadratic
Normal stiffness (N/mm^3)	408
Shear stiffness (N/mm^3)	408

The normal stiffness is calculated based on the linear elastic stiffness of the load-deflection response obtained by Wagner using inverse analysis of slant tension-shear tests (Note: the load-deflection results of interface with 40 degrees inclination are only provided, hence are used to obtain the stiffness). The shear stiffness is considered equal to the normal stiffness [10].

4.2.3. Equilibrium Conditions

The equilibrium conditions consist of choices regarding the iteration scheme, maximum permissible iterations, convergence criteria, load step and analysis control tools. The iteration scheme, maximum permissible iterations and convergence criteria are kept constant in all the numerical solution strategies in this thesis. Load increment is based on the experimental peak load of each benchmark study, and the load steps are so provided to achieve numerical failure of the models, i.e. occurrence of divergence due to failure of the iteration method at the final load step. No analysis control tools such as arc-length or linesearch are used.

The Secant (Quasi-Newton) method of iteration is used to model beams in shear. Evangeliou [25] suggests that the secant iterative method is suitable for reinforced concrete beams without transverse reinforcement as it is computationally less demanding (as compared to Newton-Raphson method) and possess the ability to surpass local deformation effects in the equilibrium path [53]. However, it does require relatively more iterations per load step to satisfy the set convergence norm. In this iteration method, the stiffness matrix is computed only for the first iteration of each load step increment and is not modified for the rest of the iterations of the same load step. Graphical representation of the Secant iterative solution procedure is shown in Figure 4.10.

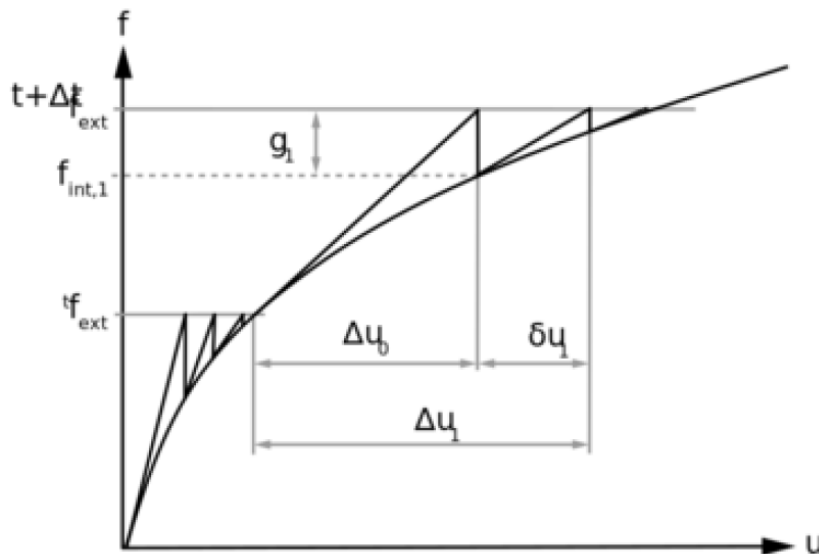


Figure 4.10: Secant iteration method [20]

A maximum of 100 iterations per load step are permitted with the energy convergence norm tolerance of 0.001, as per recommendations in the NLFEA guidelines [28]. In case of no convergence at a load step, the analysis continues. Results are still accepted beyond a load step which breaches the norm tolerance, provided certain conditions are met. These are discussed in detail in Section 4.3. These conditions are kept the same for modelling of SHCC in shear as well. The equilibrium conditions are listed in Table 4.15.

Table 4.15: Equilibrium conditions

Iteration Method	Secant
Max Permissible Iterations	100
Convergence Norm	Energy
Norm Tolerance	0.001
No convergence	Continue analysis

4.2.4. Developed Numerical Solution Strategies

Based on the discussion so far, the types of numerical solution strategies used to model the idealised physical problems vary in terms of the type of shear retention function of “concrete” and the hybrid interface. Based on these parameters, the numerical solution strategies developed are listed in Table 4.16.

Table 4.16: Numerical solution strategies

Model Geometry	Solution Strategy	Shear Retention Function	Hybrid Interface Type	Notation
2D	SS1	Damage -based	-	Damage
	SS2	Al-Mahaidi	-	Mahaidi
3D	SS2a	Al-Mahaidi	Perfect Bond	Mahaidi-PB
	SS2b	Al-Mahaidi	Imperfect Bond	Mahaidi-IB

The ultimate goal of this thesis is to model the shear behaviour of SHCC-RC hybrid beams. But first, the shear behaviour of concrete and SHCC beams separately is modelled using different numerical solution strategies i.e. SS1 and SS2. Based on their results, the hybrid beams are modelled with the optimal numerical solution strategy. Discussed in detail in Chapter 5, but from Table 4.16, it can already be seen that SS2 comes out to be the optimal numerical solution strategy. This is why only the Al-Mahaidi shear retention function is used to model the 3D beams hybrid beams. There are, however, two solution strategies for modelling the 3D hybrid beams which vary in terms of the type hybrid interface.

4.2.5. Judgement of Numerical Solution Strategies

The numerical solution strategies are judged based on the numerical results they produce in each modelling phase. In Modelling Phase I, the solution strategies SS1 and SS2, in which the varying parameter is the shear retention function, are used to model the shear behaviour of benchmark concrete beams described in Chapter 3. From the numerical results of Modelling Phase I, the type of shear retention function (i.e. solution strategy SS1 or SS2) is finalised to be used for the rest of the models in this thesis. The solution strategy is acceptable if,

- The numerical and experiment load vs mid-span deformation curves are qualitatively comparable¹,
- Numerical failure crack pattern and failure mode are representative of the experimental failure of the respective benchmark beam, and
- Consistent satisfaction of the above two criterion in all relevant benchmark studies.

Based on the finalised numerical solution strategy, benchmark SHCC beam in shear is modelled in Modelling Phase II. The same solution strategy is then used to model the benchmark hybrid beams in Modelling Phase III with varying hybrid interface type.

The reliability of a solution strategy can also be assessed by determining the model uncertainty [19]. For this thesis, the solution strategies are assessed by a comparison between numerical and experimental results and calculations for model uncertainty are not performed due to the study of a small number of benchmarks and solution strategies, and a specific type of failure i.e. shear failure.

4.3. Analysis-Stop Criteria

The benchmark beams selected are such that experimental shear failure is observed. This failure is easy to qualitatively assess, experimentally, because; (a) it is a brittle failure and therefore the experiment would most likely immediately stop after the peak load is reached, and (b) diagonal crack in the shear span is observed. But in the numerical models, it could be that the analysis continues to run beyond the point where the experimental failure type is already achieved. Therefore, failure of analysis might be different from the experimental failure.

The equilibrium conditions outlined in this thesis are such that the analyses are allowed to run until a numerical failure is observed, which is the occurrence of divergence. However, it might be that the experimental failure occurs way before such a numerical failure is obtained. Therefore, stop criteria are defined for the failure of analysis, which is used to judge the numerical results. The analysis is stopped if,

¹meaning the general shape, exact load and deformations might be different

- (a) Concrete compressive strain value of 3.5 ‰ is breached [28],
- (b) A fully developed shear crack pattern is obtained, i.e. a major inclined diagonal crack opens either towards the load plate, along the longitudinal reinforcement or both [19],
- (c) Sudden critical loss of load-carrying capacity, i.e. drop of 10-20% of the maximum peak load occurs within a single load step,
- (d) Maximum plastic strains in the reinforcements are developed [19], and
- (e) Poor convergence is observed in successive load steps, i.e. the convergence exceeds 0.01, which is the permissible energy tolerance per load step. The actual tolerance criteria as per NLFEA guidelines is 0.001 [28]. Poor convergence can be a consequence of yielding of reinforcement, sudden change in cracks, sudden change in plasticity or a combination of the three.

If the conventional numerical failure of divergence occurs before either of the criterion mentioned above, then results till that last load steps are considered. Note that a sudden drop in load-deformation curve alone must be accompanied by a large increase in crack-width or plastic deformation [19]. Therefore, an analysis might be stopped if either or a combination of the criterion mentioned above is satisfied.

The last criterion regarding convergence is further explained. The fact that a load step does not converge is not reminiscent of divergence. A non-converged load step can be followed by successive converged steps, completing the desired analysis [19]. Since a total strain crack model is used in this thesis, such a convergence issue is inherent to this material class. Take an example of a typical convergence plot of concrete beam modelled in shear shown in Figure 4.11. This is divided into different zones for a better understanding [19].

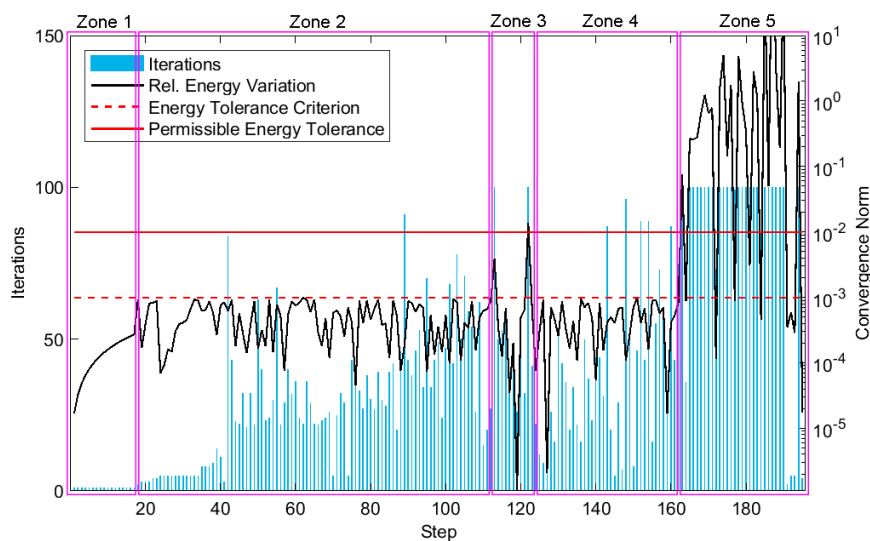


Figure 4.11: Typical convergence behaviour of reinforced concrete beam without transverse reinforcement

Zone 1 reflects linear elastic behaviour and almost negligible iterations are needed to converge as per the energy tolerance criteria. In Zone 2, cracking starts and more iterations are required, but the criteria are still satisfied. Zone 3 reflects localization of cracks or a sudden increase in crack-width of an already localised crack, not satisfying the criteria. Successive converged load steps then follow it in Zone 4 as the cracks are opening stably. Eventually, non-linear effects like yielding of reinforcement and crushing of concrete start occurring in Zone 5, leading to excessive cracking and plasticity, resulting in convergence difficulties [19]. According to guidelines NLFEA [28], a load step is considered converged when the energy tolerance criterion of 0.001 is satisfied. However, the load steps are acceptable if they converge within permissible tolerance of 0.01. As Zone 5 breaches both norms, therefore the analysis must be stopped where Zone 4 ends. If a single load step does breach both norms, like in Zone 3, but is followed by converged load steps, then it is still acceptable but with appropriate explanation.

4.4. Material Properties of Benchmark Studies

4.4.1. Concrete

The mean compressive strength and Young's Modulus of concrete from the benchmark studies are used as input in the models, mentioned in Chapter 3. Additionally, the tensile (G_F^I) and compressive fracture energies (G_C) are required when using Hordijk tensile behaviour and parabolic compressive behaviour, respectively. These parameters are calculated using formulas provided in the guidelines [28], which are based on the mean compressive strength of concrete. The formula for tensile strength of concrete in the guidelines (as per the strength class of concrete) is used to calculate the tensile strength of concrete in case it is not provided in the benchmark study, which is based on the characteristic compressive strength of concrete ($f_{ck} = f_{cm} - 8$). The mass density and initial Poisson ratio for concrete are also taken from the guidelines [28]. The formulas and values for the required additional parameters are listed in Table 4.17.

Table 4.17: Material properties of concrete in benchmark studies [28, 44, 57, 61]

Parameter	Formula	Units	Study 1	Study 2	Study 3
f_{ctm}	Experiment / $0.3f_{ck}^{2/3}$	N/mm ²	2.21	2.14	3.6
G_F^I	$73f_{cm}^{0.18}$	N/mm	0.133	0.132	0.149
G_C	$250G_F^I$	N/mm	33.25	33.03	37.37

The stress-strain relations for concrete elements are shown in Figure 4.12. The tensile fracture energy G_F^I and compressive fracture energy G_C are used as inputs to draw the respective curves. Integrating over the stress-strain relation gives G/h , where h is the mesh size. This means that the value of ultimate strain is dependent on the bandwidth. Therefore, smaller elements result in a smaller bandwidth, showing a more ductile behaviour than elements with a larger bandwidth [19].

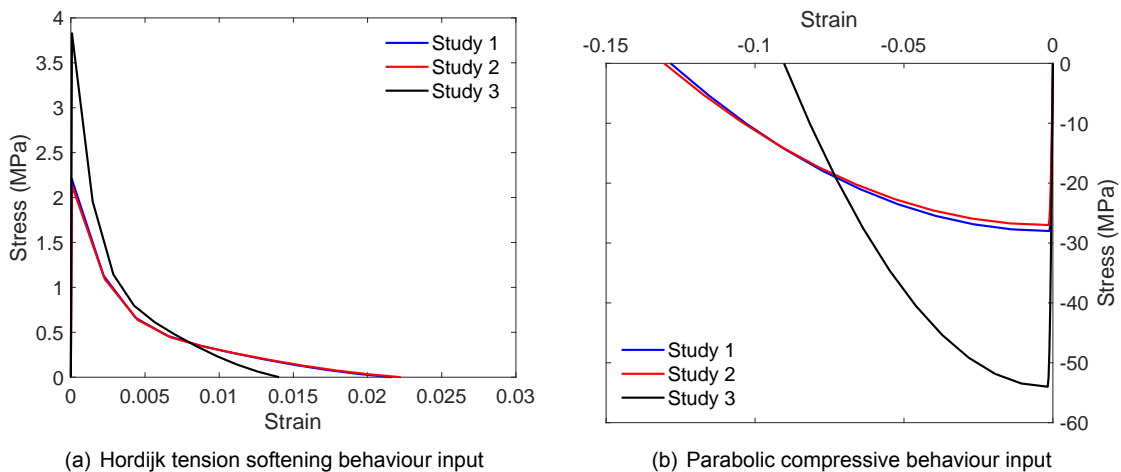


Figure 4.12: Tensile and compressive inputs for benchmark concrete [28]

Note that the plots for compressive and tensile behaviour are created assuming a crack-bandwidth of 10, which is equal to the mesh size considered. However, while discussing the results for models of RC beams in Chapter 5, mesh size study is performed. For models with a mesh size different than 10mm, the input compressive and tensile behaviour is different from the above shown plots.

4.4.2. SHCC

For SHCC, mean compressive strength and Young's Modulus reported in the benchmark studies are used, mentioned in Chapter 3. The mass density of 2034 kg/mm^3 is input (This value is based on calculations performed in Stevin Lab of TU Delft on SHCC samples, described in Appendix C). For *fib* FRC tensile behaviour, data from the trilinear tensile curves obtained from the uniaxial tensile test curves of each benchmark study is used, as shown in Figure 4.13(a).

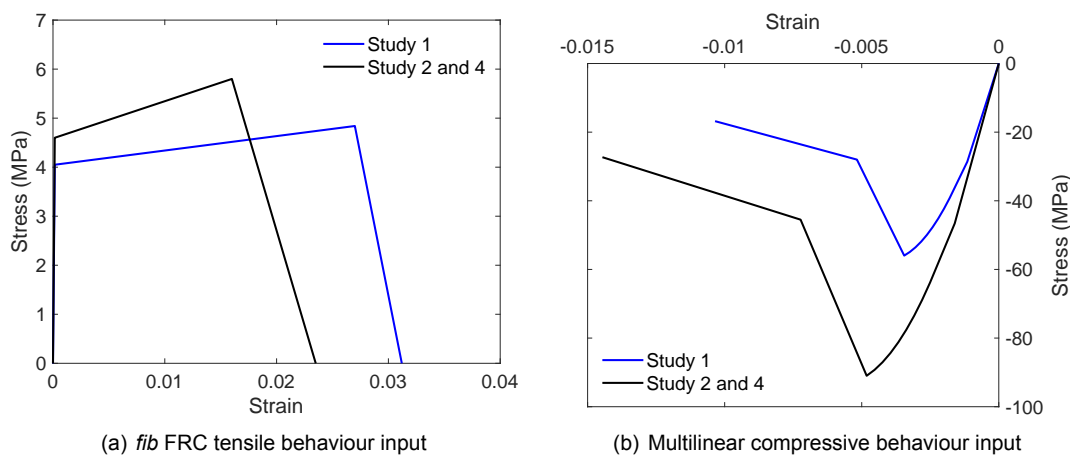


Figure 4.13: Tensile and compressive inputs for benchmark SHCC [28]

As discussed in the constitutive considerations for SHCC, a multi-linear compression curve is used as input to define the compressive behaviour of SHCC in the benchmark studies. This is because the uniaxial compressive behaviour of SHCC does not resemble with the parabolic compressive behaviour for concrete. The benchmark studies, however, do not provide the uniaxial compressive behaviour of SHCC. Therefore, the analytical model proposed by Jiajia Zhou et al. [66] is used to calculate these compressive curves. This study involves assessment of the mechanical behaviour of fibre-reinforced engineered cementitious composites (ECC) (referred to as SHCC in this thesis) in uniaxial compression. First, the SHCC of varying mix designs is tested in compression. Mix design is varied to produce SHCC of strengths between 35-70 MPa. Then, an analytical model is developed which reproduces reasonably accurate curves in comparison to the experimental results. This study is selected since the type of fibre used is the same as in the SHCC of the benchmark studies, i.e. Polyvinyl Alcohol (PVA) fibres. Details about the analytical model, its reliability and the calculations involved in producing the multi-linear compressive curves of each benchmark study are discussed in Appendix B. The obtained compressive curves are shown in Figure 4.13(b). Additionally, the input for the initial Poisson ratio is also obtained from this study, and is also discussed in Appendix B. The values for the Poisson ratio of SHCC for each study are listed in Table 4.18.

Table 4.18: Poisson ratio of SHCC [44, 57, 61, 66]

Parameter	Study 1	Study 2	Study 3	Study 4
ν_{SHCC}	0.17	0.17	-	0.17

4.4.3. Reinforcement

A linear strain hardening constitutive relation for the longitudinal reinforcement is used. For embedded reinforcement, 'plastic strain-yield stress' hardening function is used [19]. Embedded reinforcement type is also used for the transverse reinforcement present outside the effective length of the beams. The input material properties for reinforcements are mentioned in Chapter 3. The linear curves input are shown in Figure 4.14.

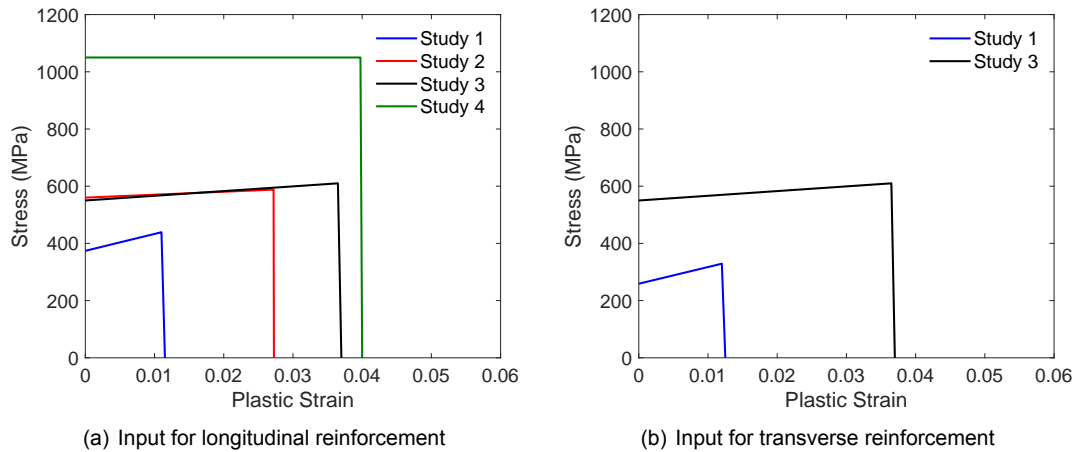


Figure 4.14: Plastic strain-yield stress input for benchmark reinforcements

4.4.4. Load and Support Plates

The load and support plates are modelled as steel, ignoring the self-weight of the plates. These plates are modelled as linear elastic with a Young's Modulus of 210000 MPa and Poisson ratio of 0.2.

4.5. Numerical Models

The modelling strategies are developed based on the types of idealised physical problems and numerical solution strategies. As discussed earlier in this chapter, the idealisations are split into three modelling phases. Each idealisation of each phase is linked with the appropriate solution strategy. As a result, numerical models required to be analysed are developed, which are listed in Table 4.19.

Table 4.19: Numerical models analysed based on the developed modelling strategies

Phase	Study	Idealisation	Solution Strategy	Notation
I-Shear behaviour of concrete beam	1	CB1	SS1	CB1-Damage
			SS2	CB1-Mahaidi
	2	CB2	SS1	CB2-Damage
			SS2	CB2-Mahaidi
	3	CB3	SS1	CB3-Damage
			SS2	CB3-Mahaidi
II-Shear behaviour of SHCC beam	4	SHCC4	SS2	SHCC4-Mahaidi
III-Shear behaviour of hybrid beams	1	H20Q1	SS2a	H20Q1-PB
			SS2b	H20Q1-IB
		H40Q1	SS2a	H40Q1-PB
			SS2b	H40Q1-IB
	2	H10Q2	SS2a	H5Q2-PB
			SS2b	H5Q2-IB
		H10Q2	SS2a	H10Q2-PB
			SS2b	H10Q2-IB

Note that Modelling Phase III beams are all modelled using the AI-Mahaidi shear retention function and notations **PB** and **IB** mean "perfect" and "imperfect" hybrid interface bond type, respectively.

5

Results & Conclusions

The results of NLFEA performed on benchmark experimental beams using different numerical solution strategies are discussed in this chapter. The results are split into three main sections based on three modelling phases defined in this thesis. Each section consists of three sub-sections; the description of numerical and experimental results, discussion section in which results of all beams are described collectively, and conclusions of each modelling phase. At the end of the chapter, conclusions are drawn for the complete thesis. The presented numerical results correspond to the load step before which poor convergence is observed for all analyses, unless otherwise stated. Numerical convergence data is provided for all the numerical models in Appendix A.

5.1. Modelling Phase I

In Modelling Phase I, benchmark reinforced concrete (RC) beams from studies 1, 2 and 3 are analysed using two numerical solution strategies; SS1 and SS2. These numerical solution strategies differ in the type of shear retention function (SRF) used. For this thesis, only two shear retention functions are assessed; Damage-based and Al-Mahaidi.

5.1.1. Results Modelling Phase I

The results are split into three sub-sections based on the benchmark RC beam analysed. Each beam is analysed using numerical solution strategies SS1 and SS2, consisting of Damage-based and Al-Mahaidi SRF, respectively. As discussed in Chapter 4, an input for the minimum shear retention factor β_{min} is required for the Al-Mahaidi SRF. For all beams modelled in this thesis, a value of 0.01 for β_{min} is used [20]. However, in the discussion section, a sensitivity study on β_{min} is performed to assess its influence on the numerical peak load of benchmark RC beams.

Beam CB1

The experimental and numerical peak loads and failure type are listed in Table 5.1. The experimental and numerical load-deflection response of beam CB1 is shown in Figure 5.1. The initial numerical stiffness for both models is higher as compared to experiment. Inaccurate prediction of initial numerical stiffness in the FE models suggests that the elastic constants and boundary conditions are possibly inaccurate in the numerical models. High initial elastic stiffness can be attributed to inconsideration of factors such as shrinkage of the beam or support settlement as no information is provided in the benchmark study about them. Furthermore, the mid-span deflection in experiments is recorded using physical instruments (like LVDTs), which can result in inaccurate deflection readings as well. Once cracks localize at around 48kN in the numerical models, the global stiffness reduces slightly. The numerical peak load for CB1-Damage model is approximately 13% lower as compared to experiment, while the numerical peak load for CB1-Mahaidi model is approximately 33% higher as compared to experiment. Neither numerical models, are able to predict the experimental peak load accurately. Higher capacity in CB1-Mahaidi model as compared to CB1-Damage model is possibly due to the shear retention factor β considered in Al-Mahaidi SRF. Furthermore, numerical peak loads are also reported to be mesh size dependent [19, 53]. Possible influence of these aspects is elaborated in the discussion section. The numerical peak load in CB1-Damage model is limited by poor convergence due sudden increase in cracks, as shown in Figure 5.2. The numerical peak load of CB1-Mahaidi model is also limited by poor convergence, but due to yielding of transverse reinforcement instead, as shown in Figure 5.3.

Table 5.1: Peak load and failure type comparison between experimental and numerical results of beam CB1

R_{exp} (kN)	R_{Damage} (kN)	$R_{Mahaidi}$ (kN)	Failure _{exp}	Failure _{Damage}	Failure _{Mahaidi}
121.7	105.9	161.9	Shear compression	Shear flexure	Shear flexure

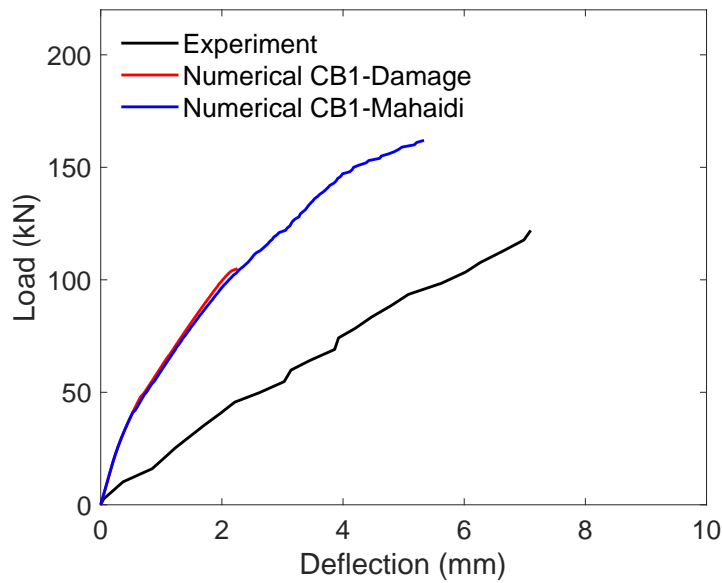


Figure 5.1: Load vs mid-span deflection comparison between experimental and numerical results of beam CB1

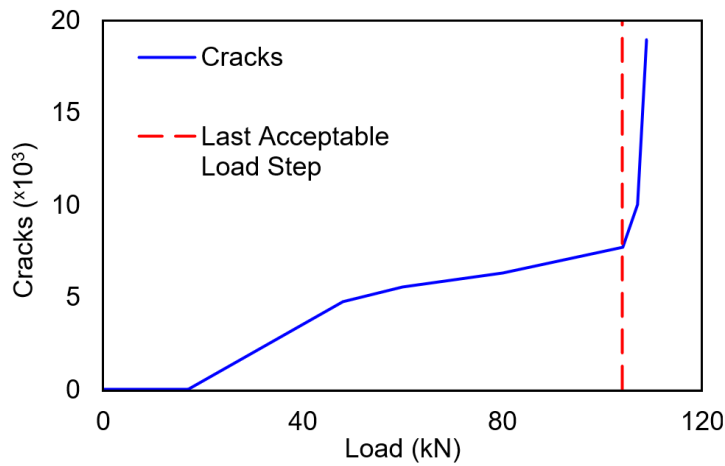


Figure 5.2: Load vs number of cracks in numerical model CB1-Damage

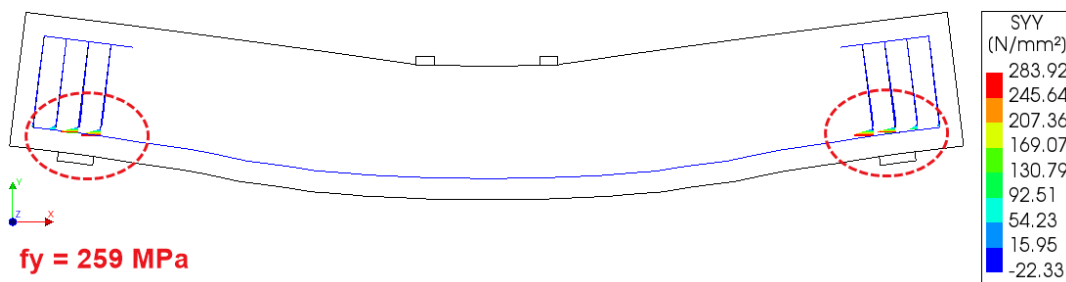


Figure 5.3: Yielding of transverse reinforcement in numerical model CB1-Mahaidi

A brittle shear failure is observed in experiment for beam CB1, as shown in Figure 5.4. The authors, however, have not described whether the failure is shear-compression or shear-tension. From the figure, it is observed that the concrete crushes at the top near the load plate, indicating shear-compression failure. However, the beam also appears to suffer from splitting failure, which can be a

consequence of a shear-tension failure. It is unclear whether there is any anchorage failure from the provided figure, therefore, the experimental failure is characterised as shear-compression. In comparison, the failure type in both numerical models is not as brittle as in experiment and a relatively ductile shear flexure failure is observed, as shown in Figure 5.5. A possible reason for ductile failure in the numerical models could be the mesh size considered. RC beams without shear reinforcement show severe dependence on mesh size in order to produce accurate peak loads and failure types [19]. This aspect is investigated in the discussion section. The numerical models show almost negligible crushing of concrete close to the loading plates as well, as shown in Figure 5.6. Crushing in the numerical model is identified by the white colour in the contour region, where the stresses exceed the concrete compressive strength of 27MPa. Negative stress values on the contour scale represent compressive stresses.



Figure 5.4: Experimental failure crack pattern of benchmark beam CB1

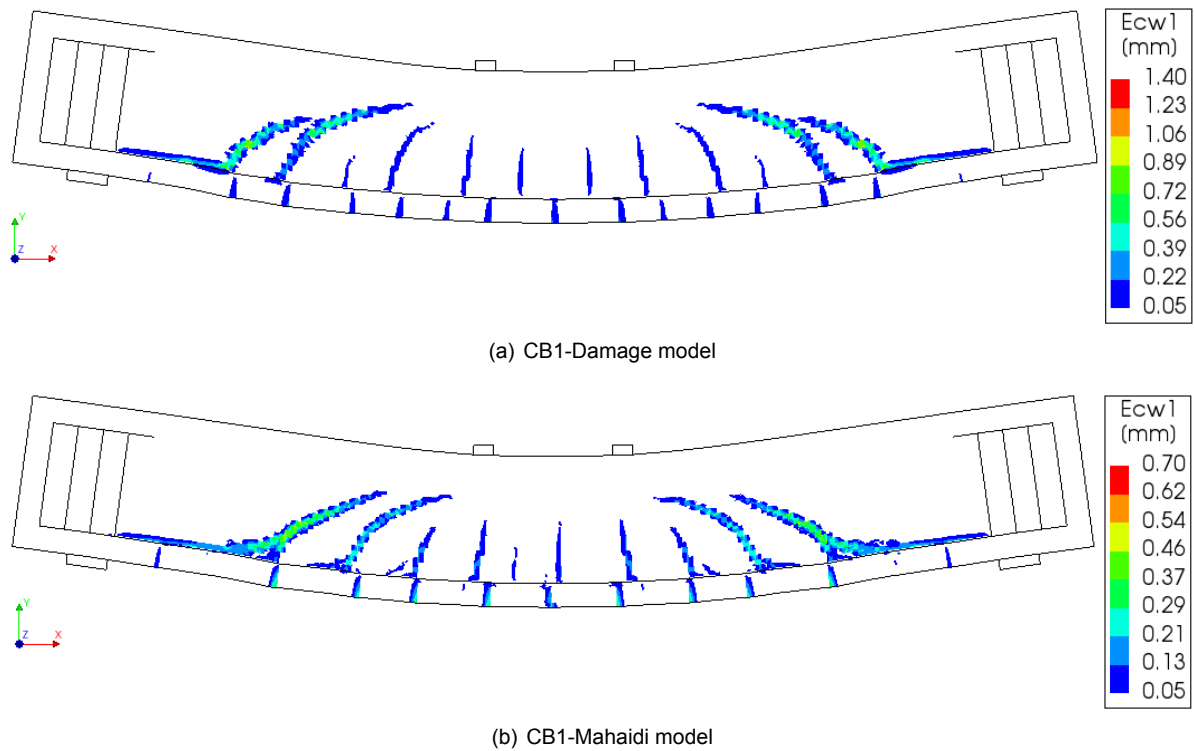


Figure 5.5: Numerical failure crack pattern of beam CB1

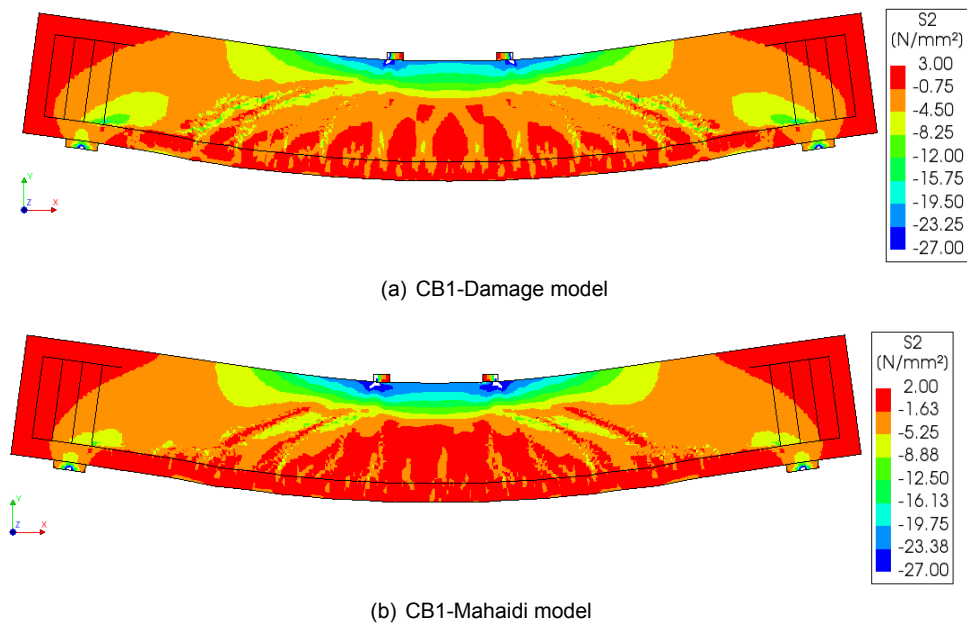


Figure 5.6: Cauchy stresses S_2 in numerical models of beam CB1

Beam CB2

During modelling of beam CB2 of benchmark study 2, it was observed that the numerical model failed in flexure at approximately 38kN in contrast to shear failure reported in the study. Yielding of longitudinal reinforcement at approximately 38kN was observed, which resulted in the localization of flexural cracks, as is illustrated in Figure 5.7, instead of development of a wide diagonal shear crack as seen in the experiments.

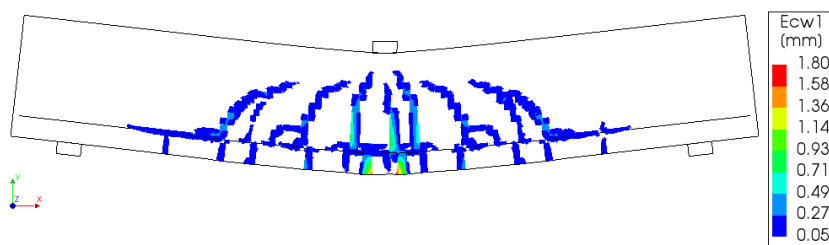


Figure 5.7: Failure crack pattern in model CB2-Damage using benchmark reinforcement yield strength

Appropriate diagnostics on the numerical model were performed to check the reason for this, including checking the diameter of the bars, the yield stress and strain values and several other parameters included in the construction of the numerical model. However, no problem was found. Analytical calculations were also performed to corroborate the results. According to these calculations, the reinforcement should yield at approximately 32kN, which is 63% lower than the peak experimental load at which the beam fails in shear. Therefore, the reported yield strength of reinforcement is taken to be inadequate to instigate shear failure in the beam. Therefore, for further modelling of beam CB2, the reinforcement yielding properties are input as that of B500 steel, as stated in Chapter 4.

The experimental and numerical peak loads and failure type are listed in Table 5.2. The experimental and numerical load-deflection response of beam CB2 is shown in Figure 5.8. Like for beam CB1, the initial numerical stiffness for both models of beam CB2 is also high as compared to experiment. However, the numerical stiffness post crack localization at around 17kN in the numerical models is lower than the experiment. The numerical peak load for CB2-Damage model is approximately 28%

lower, and the numerical peak load for CB2-Mahaidi model is approximately 5% lower, as compared to experiment. Additional capacity in CB2-Mahaidi model as compared to CB2-Damage model can be attributed to the shear retention factor β considered in Al-Mahaidi SRF. Unlike model CB1-Mahaidi, model CB2-Mahaidi can predict the peak load relatively accurately. A possible reason for this could be the fact that a mesh size of 10mm results in 20 elements in the height of beam CB2, which are the recommended number of elements in the height of the beam according to de Putter for accurately analysing shear behaviour of RC beams without transverse reinforcement [19]. In model CB1-Mahaidi, a mesh size of 10mm results in 30 elements in the height of the beam. Use of such a fine mesh size can result in overestimated numerical peak loads. Such a possible influence of mesh size is investigated further in the discussion section. The numerical peak load in CB2-Damage model is corresponding to load step at which poor convergence due to sudden increase in cracks is observed, as shown in Figure 5.9(a). Numerical peak load of CB2-Mahaidi model is limited by poor convergence but due to a sharp increase in plasticity, as shown in Figure 5.9(b).

Table 5.2: Peak load and failure type comparison between experimental and numerical results of beam CB2

R_{exp} (kN)	R_{Damage} (kN)	$R_{Mahaidi}$ (kN)	Failure _{exp}	Failure _{Damage}	Failure _{Mahaidi}
52.5	37.9	50.5	Shear tension	Shear flexure	Shear tension

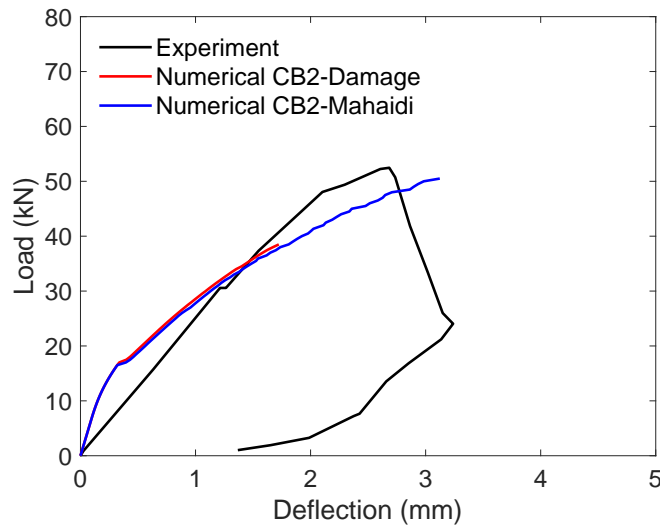
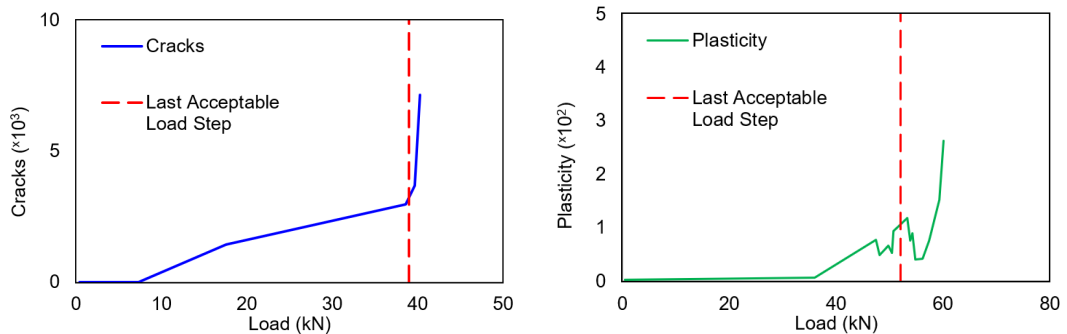


Figure 5.8: Load vs mid-span deflection comparison between experimental and numerical results of beam CB2



(a) Load vs number of cracks in numerical model CB2-Damage

(b) Load vs plasticity in numerical model CB2-Mahaidi

Figure 5.9: Cracks and Plasticity in numerical models of beam CB2

A shear-tension failure is observed in experiment for beam CB2, as shown in Figure 5.10. Unlike shear-tension failure of most concrete beams, the failure for beam CB2 is not relatively brittle. However, it is still characterised as shear-tension in this thesis due to presence of a dominant diagonal shear crack accompanied with diagonal cracking along the longitudinal reinforcement. In comparison, a shear flexure failure is observed in model CB2-Damage, as shown in Figure 5.11(a). However, model CB2-Mahaidi is able to model the shear-tension failure observed in experiment as shown in Figure 5.11(b), unlike model CB1-Mahaidi. Accurate prediction of failure type in model CB2-Mahaidi as compared to model CB1-Mahaidi can, again, be attributed to the difference in the number of elements in the height of each beam. A 10mm mesh size is able to better predict the peak load and failure type for beam CB2 as compared to beam CB1 when AI-Mahaidi SRF is used. The influence of mesh size on peak load and failure type is investigated in the discussion section.



Figure 5.10: Experimental failure crack pattern of benchmark beam CB2

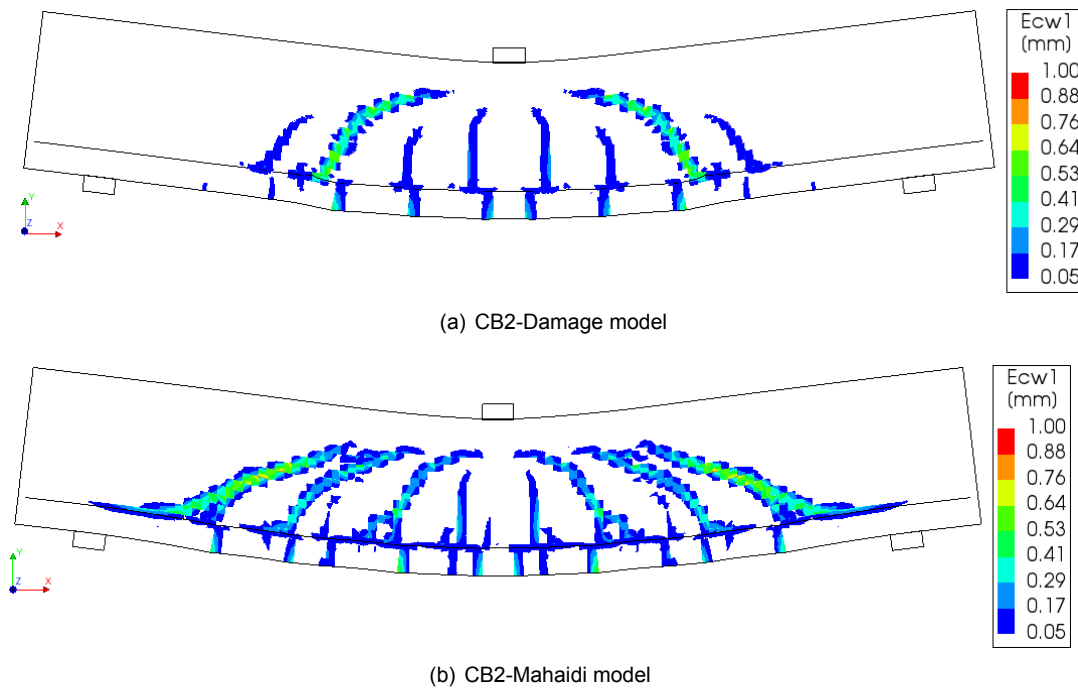


Figure 5.10: Numerical failure crack pattern of beam CB2

Beam CB3

The experimental and numerical peak loads and failure type are listed in Table 5.3. The experimental and numerical load-deflection response of beam CB3 is shown in Figure 5.11. Like previous two beams, the initial numerical stiffness for both models of beam CB3 is higher as compared to experiment. During experimentation, the load on beam CB3 is applied cyclically (cycles up to 40% of peak load) before eventually loading it to its full capacity. This history of cyclic loading is not incorporated in the numerical model, which can result in high initial stiffness as well [53]. The numerical stiffness is almost identical to experiment once cracks localize at approximately 67kN, which is different from the first

two beams. The numerical peak load for CB3-Damage and CB3-Mahaidi models is approximately 5% and 28% higher, respectively, as compared to experiment. As stated earlier, the consideration of shear retention factor β in Al-Mahaidi SRF results in additional capacity in CB3-Mahaidi model as compared to CB3-Damage model. Unlike models CB1-Damage and CB2-Damage, model CB3-Damage is able to predict the peak load relatively accurately. A possible reason for this could be the use of a very fine mesh size of 10mm, resulting in 34 elements in the height of beam CB3. Use of finer mesh size results in increase in peak load [53]. A consequence of such a fine mesh size used in model CB3-Mahaidi is that the peak load is overestimated as Al-Mahaidi SRF consists of shear retention factor β , which also results in additional capacity [14]. The influence of mesh size and behaviour of shear retention factor β is investigated in the discussion section. The numerical peak load in both CB3-Damage model and CB3-Mahaidi models is corresponding to load step at which poor convergence due to sudden increase in cracks is observed, as shown in Figure 5.12.

Table 5.3: Peak load and failure type comparison between experimental and numerical results of beam CB3

R_{exp} (kN)	R_{Damage} (kN)	$R_{Mahaidi}$ (kN)	Failure _{exp}	Failure _{Damage}	Failure _{Mahaidi}
151.3	158.7	185.9	Shear tension	Shear flexure	Shear flexure

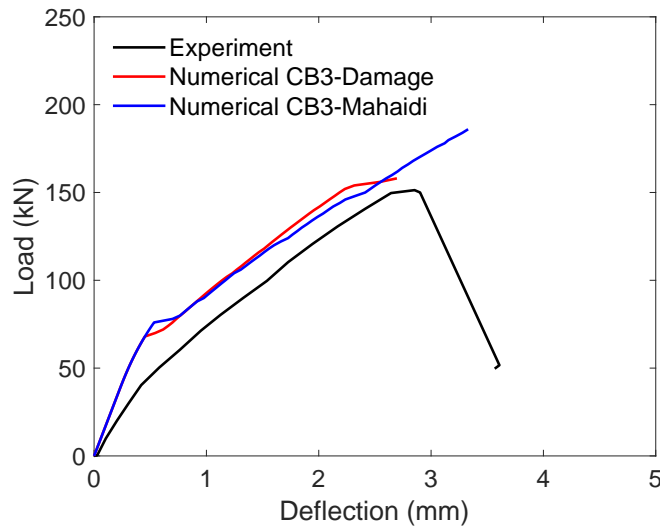


Figure 5.11: Load vs mid-span deflection comparison between experimental and numerical results of beam CB3

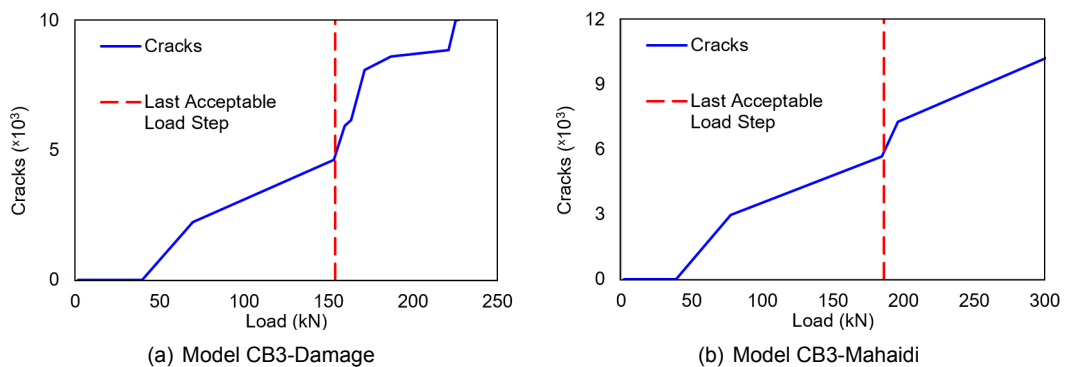


Figure 5.12: Load vs numebr of cracks in numerical models of beam CB3

A typical shear-tension failure is observed in experiment for beam CB3, as shown in Figure 5.13. In comparison, the failure type in both numerical models is a relatively ductile shear flexure failure, as shown in Figure 5.13. A possible reason for ductile failure in the numerical models could be the mesh size considered since the numerical results of RC beams without shear reinforcement are mesh size-dependent [19]. This aspect is investigated in the discussion section.

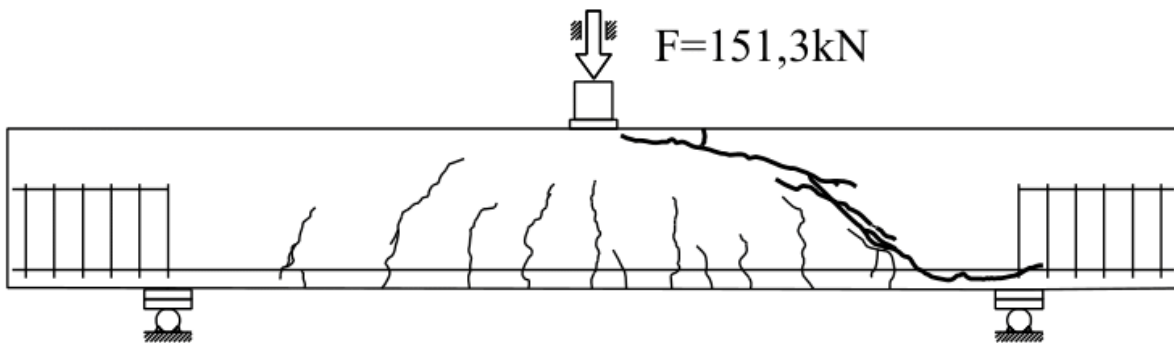


Figure 5.13: Experimental failure crack pattern of benchmark beam CB3

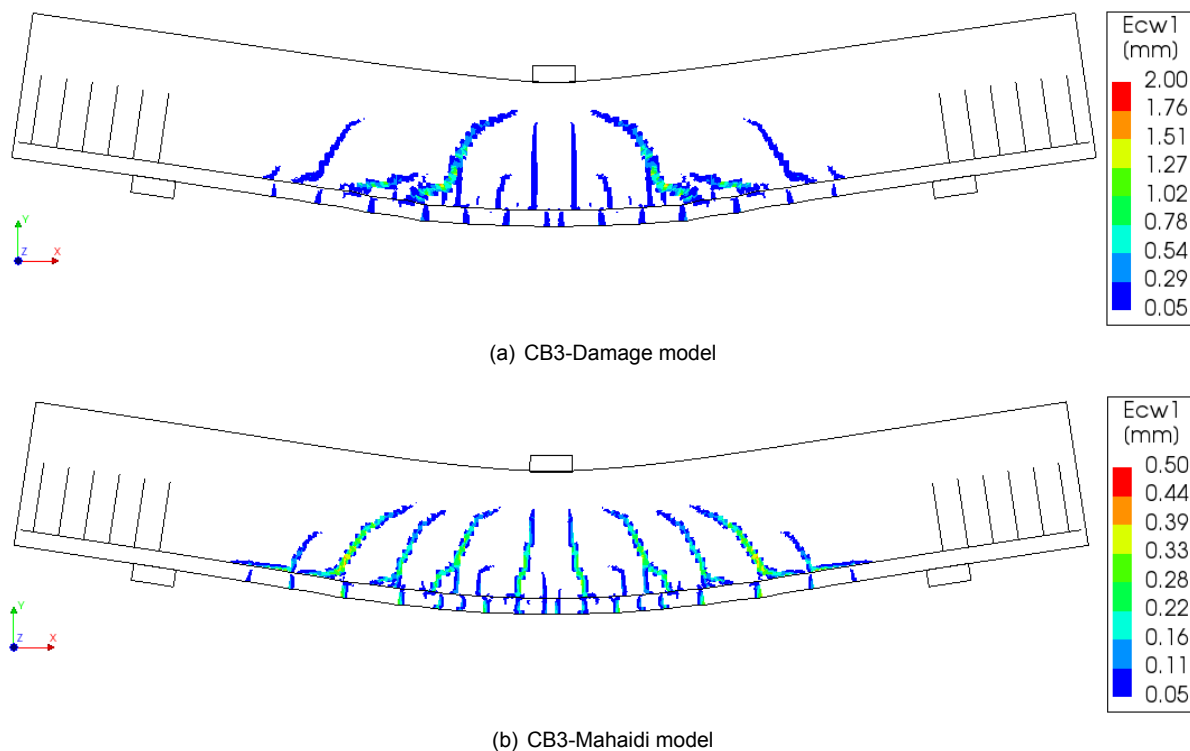


Figure 5.13: Numerical failure crack pattern of beam CB3

5.1.2. Discussion Modelling Phase I

The decision for the solution strategy, specifically, the type of shear retention function (SRF), to be used for further modelling of beams in this thesis is based on the accurate prediction of peak load and failure type. The previous section details results of the numerical analyses and their comparison with the respective experimental tests. As observed, there is inconsistency for both Damage-based and Al-Mahaidi SRFs to predict the peak load accurately and failure type of the three reinforced concrete (RC) beams considered in this thesis. The two main factors that are possibly influencing the numerical

behaviour, mentioned in the results section, are; shear retention factor β in Al-Mahaidi SRF, and mesh size. The influence of these factors is discussed in this section. The influence of the input value of minimum shear retention factor β_{min} is also briefly assessed.

Influence of Shear Retention Factor β

Table 5.4 compares the numerical peak loads of RC beams analysed using both SRFs. The percentage increase is calculated with respect to the peak load values of Damage-based SRF models. Based on the numerical results for all three RC beams, it is observed that in comparison to beams modelled with Damage-based SRF, modelling using Al-Mahaidi SRF results in an increased peak load.

Table 5.4: Difference between numerical peak loads of analysed reinforced concrete beams

Beam	R_{Damage} (kN)	$R_{Mahaidi}$ (kN)	Difference (%)
CB1	105.9	161.9	+53.9
CB2	37.9	50.5	+33.3
CB3	158.7	185.9	+17.1

The reason for an increased peak load in beams analysed using Al-Mahaidi SRF as compared to Damage-based SRF is how the shear stiffness, G , is reduced once the elements crack. Damage-based SRF reduces G as a function of normal stiffness, while Al-Mahaidi SRF reduces G by βG , where β is the shear retention factor. In an analysed beam, if there is a sudden decrease in normal stiffness due to localization of shear cracks, the beam analysed using Damage-based SRF will experience a sudden decrease in shear stiffness as well. Consequently, not only the capacity of the beam will be low, but due to sudden, sharp change in stiffness, there will be numerical instability which leads to convergence issues. However, if the beam is analysed using Al-Mahaidi SRF, the shear stiffness reduces gradually due to consideration of β factor. Such a gradual decrease in shear stiffness leads to higher capacity and better numerical stability. Therefore, it is preferable to use an SRF that results in improved numerical stability to model brittle shear failure of concrete beams.

Consideration of β factor in the shear retention function results in the development of principal tensile stresses at a cracked gauss integration point in an element due to rotation in an inclined direction on further loading [16, 46]. Such stress rebuild results in increased stiffness of the cracked element [46]. This aspect of increased stiffness of elements post-cracking is missing from beams analysed using Damage-based SRF, and therefore, result in relatively lower peak loads.

Due to the nature of stress rebuild in cracked elements when shear retention factor β is considered, researchers attribute this behaviour to the modelling of aggregate interlock [14, 18, 29]. Therefore, it can be said that consideration of shear retention factor β is a consideration of aggregate interlock, which is an important factor that needs to be considered to provide shear resistance, especially for shear-critical RC beams which lack the use of transverse reinforcement. Interpretation of shear retention factor β as modelling of aggregate interlock is, however, implicit because it does not accurately represent the shear dilation [14]. Some researchers even describe consideration of β factor as dowel action, which is another important factor that provides shear resistance for RC beams without transverse reinforcement [18].

Influence of Value of Minimum Shear Retention Factor β_{min}

Use of Al-Mahaidi SRF requires input for the value of the minimum shear retention factor β_{min} . A value of 0 represents no aggregate interlock, whereas 1 represents full aggregate interlock. If a very high value is specified, there is a possibility of stress locking [41]. Researchers have used variable values for the shear retention factor, tailored to the beams specifically being analysed, as the aim is to obtain accurate results. Study to determine the critical β_{min} value for each RC beam considered

in this thesis is not part of the scope of research as each beam needs to be evaluated for several values of β_{min} , which requires several additional analyses. Therefore, β_{min} value of 0.01 is selected [20]. However, it is important to be familiar with the extent of influence of the input β_{min} value on the numerical peak load. The β_{min} value is varied between 0.0, 0.005 and 0.01 for RC beams CB1, CB2 and CB3 to investigate this.

The load-deflection response obtained for Al-Mahaidi models for beams CB1, CB2, and CB3 with varying input value of β_{min} are shown in Figure 5.14. It is observed that with reducing β_{min} , the stiffness and peak load of the numerical model reduces. This means that higher the β value, higher the peak load. This relation is observed for all three types of RC beams analysed in this thesis. However, the magnitude of the difference in peak load with varying β_{min} value in each beam case is different. As it is challenging to decide on beam-specific β_{min} value and is beyond the scope of research of this thesis, therefore, for all the models in this thesis, a value of 0.01 for β_{min} is used.

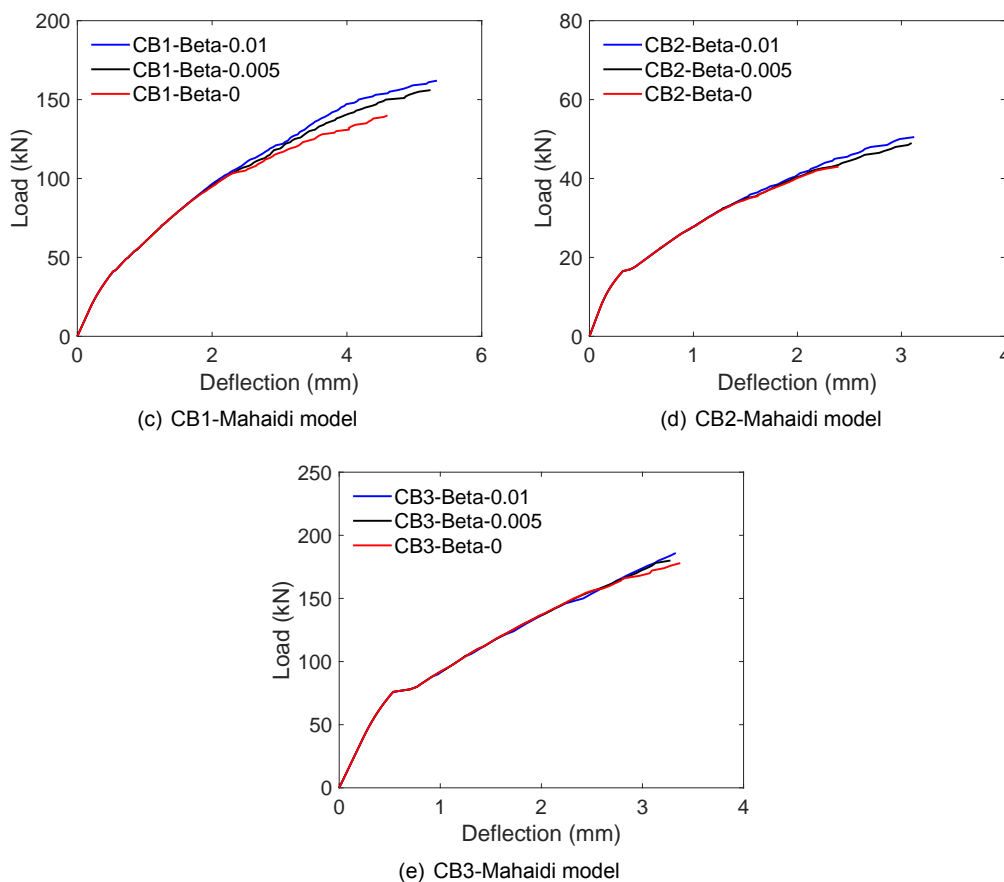


Figure 5.14: Load-deflection response of beams analysed using Al-Mahaidi shear retention function with varying β_{min} values

Influence of Mesh Size

Table 5.5 compares the experimental and numerical peak loads for the reinforced concrete (RC) beams analysed earlier. The percentage difference is calculated with respect to the experimental value. The positive sign indicates an increase and negative sign indicates a decrease with respect to the experimental value. Out of the three RC beams analysed using Damage-based SRF, two beams have a relatively lower peak load (CB1-Damage and CB2-Damage) as compared to experiment, and the peak load of only model CB3-Damage is relatively close to experiment. For beams analysed using Al-Mahaidi SRF, two out of three models have a numerical peak load significantly higher as compared to experiment, and only CB2-Mahaidi model is able to replicate the experimental peak load, approximately.

Table 5.5: Summary of numerical peak loads of models analysed

Model	R_{exp} (kN)	R_{num} (kN)	Difference (%)
CB1-Damage	121.7	105.9	-13
CB1-Mahaidi		161.9	+33
CB2-Damage	52.46	37.9	-28
CB2-Mahaidi		50.5	-4.6
CB3-Damage	151.3	158.7	+4.9
CB3-Mahaidi		185.9	+23

Table 5.6 compares the experimental and numerical failure types for RC beams analysed earlier. Neither of the three RC beams analysed using Damage-based SRF are able to predict the experimental failure type, and only beam CB2 modelled with AI-Mahaidi SRF is able to predict the experimental failure type accurately.

Table 5.6: Comparison of experimental and numerical failure type for analysed reinforced concrete beams

Beam	Failure _{exp}	Failure _{Damage}	Failure _{Mahaidi}
CB1	Shear-compression	Shear-flexure	Shear-flexure
CB2	Shear-tension	Shear-flexure	Shear-tension
CB3	Shear-tension	Shear-flexure	Shear-flexure

The mesh size significantly influences the analysis of RC beams without transverse reinforcement. A recent study at TU Delft recommends using 20 elements in the height of the beam for accurate modelling of shear behaviour of RC beams without transverse reinforcement. This recommendation is one of the criterion described to select the mesh size in this thesis, as described in Chapter 4, and is termed as "H/20". Table 5.7 states the number of elements in the height of the three RC beams modelled in this thesis when 10mm mesh is considered. It is observed that only beam CB2 satisfies the "H/20" criterion, and the mesh size in the remaining two beams is very fine.

Table 5.7: Number of elements in height of analysed reinforced concrete beams

Beam	Mesh size (mm)	Number of elements in height H
CB1		30
CB2	10	20
CB3		34

A constant mesh size of 10mm is kept in all beams analysed in this thesis to be able to compare the results of RC beams with hybrid beams. However, a consequence of this is that the mesh configuration between the three types of RC beams analysed in this thesis is different. However, this difference in mesh configuration can explain the difference in peak loads and failure types predicted in the analysed RC beams.

The three RC beams analysed using 10mm mesh size for both SRFs are also modelled using the first two criteria of selecting the mesh size, described in Chapter 4; NLFEA guidelines (*length of beam L*)/50, and "H/20". The resulting number of elements in the height of the beam are listed in Table 5.8. Figure 5.15 shows a comparison of peak loads obtained for RC beams analysed using the selected SRFs with mesh sizes listed in Table 5.8. It is observed that as the number of elements in the height of beam increase i.e. with increased refinement in mesh size, the peak loads increase as well.

Table 5.8: Number of elements in height of analysed reinforced concrete beams using different mesh size criterion

Beam	10mm Mesh Size	H/20	NLFEA Guidelines (L/50)
CB1	30	20	7
CB2	20	20	8
CB3	34	20	7

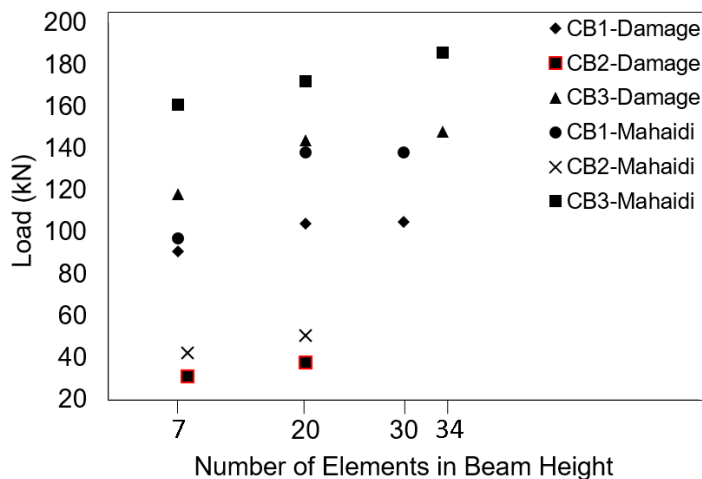
**Figure 5.15:** Mesh size vs peak load comparison of the numerical models

Table 5.9 compares the experimental peak loads of RC beams with respective numerical peak loads modelled using 10mm mesh size and “H/20” mesh criterion with both SRFs considered. It is observed that if beams CB1 and CB3 are also modelled with 20 elements in the height of the beam, then the percentage difference of numerical peak load in comparison to experiment reduces significantly for both SRFs. This reduction leads to better performance of beams analysed using AI-Mahaidi SRF such that the predicted numerical peak loads are -4.6% to +13.7% different from experiments, as compared to beams analysed using Damage-based SRF where the difference is between -27.8% to -4.8%. A solution strategy with a peak load difference of $\pm 20\%$ with respect to experiment for such RC beams is acceptable (the reported mean uncertainty for such beams lies between 1.01 to 1.05, which is okay) [19, 53]. Therefore, solution strategy SS2 with AI-Mahaidi SRF performs better in terms of predicting the peak load with greater accuracy for “H/20” mesh size configuration. However, if a very fine mesh size is used, Damage-based SRF predicts the peak load with greater accuracy.

Table 5.9: Average percentage difference in numerical peak loads of models of varying mesh size

Model	R_{exp} (kN)	R_{num} (kN) Diff. (%)	
		10mm Mesh Size	H/20
CB1-Damage	121.7	105.9	-13
CB1-Mahaidi		161.9	33
CB2-Damage	52.46	37.9	-27.8
CB2-Mahaidi		50.5	-4.6
CB3-Damage	151.3	158.7	4.9
CB3-Mahaidi		185.9	23

The drawback of analysing selected RC beams with Damage-based SRF is the incorrect prediction of failure type. A fine mesh size does lead to accurate prediction of peak loads, but as described in Table 5.6, the predicted failure type is not accurate. However, beam CB2 modelled with Al-Mahaidi SRF accurately predicts the failure type as well in addition to peak load for “H/20” mesh configuration. Therefore, the failure crack pattern of beams CB1 and CB3 is analysed for “H/20” mesh configuration and Al-Mahaidi SRF as well and the result is shown Figure 5.16. It is observed that with “H/20” mesh configuration, a shear-tension failure is obtained for beam CB3 as well. For the model of beam CB1, failure is not shear-compression as classified in the experiment but is shear-tension, but since a localised diagonal shear crack is obtained, the result is acceptable.

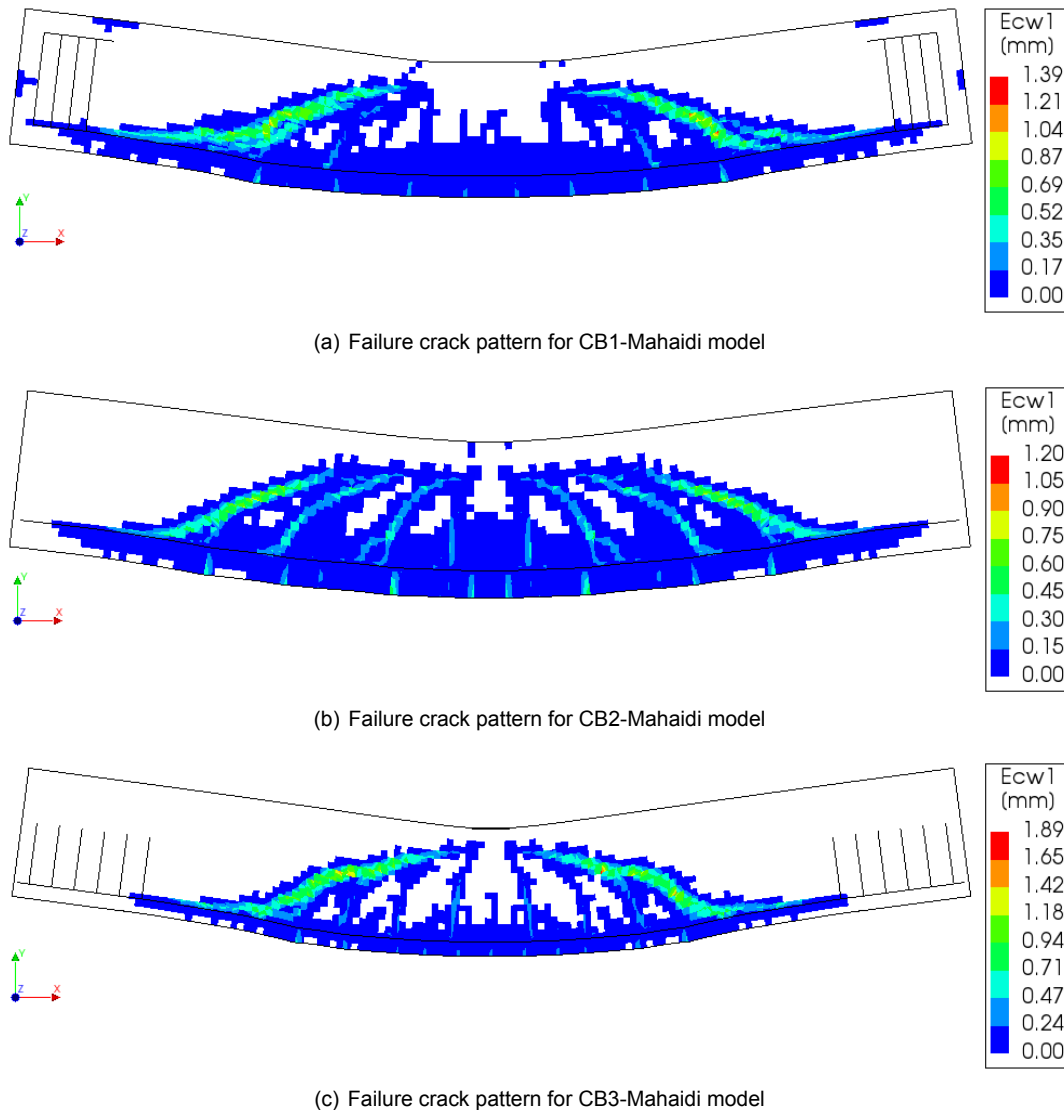
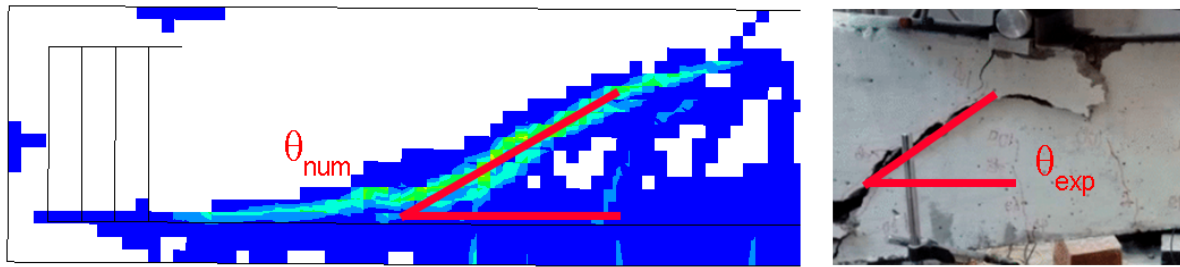
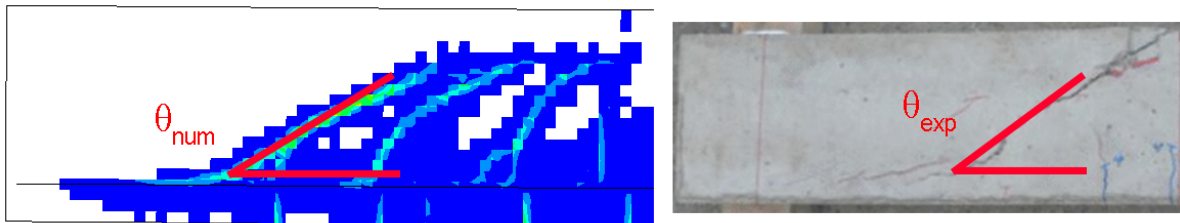


Figure 5.16: Failure crack pattern for beams modelled using Al-Mahaidi shear retention function and H/20 mesh size

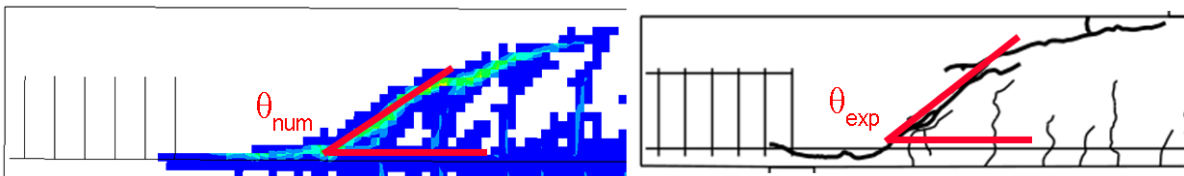
Figure 5.17 shows the measurement of the main diagonal crack angle of the RC beams analysed using “H/20” mesh configuration and Al-Mahaidi SRF and the respective experimental crack angle. Table 5.10 lists the values obtained from Figure 5.17. θ values for diagonal cracks obtained in RC beams analysed using “H/20” mesh configuration and Damage-based SRF are also listed for comparison, but not graphically presented. These results show that the crack angle in case of beams analysed using Al-Mahaidi SRF is closer to experiments as compared to Damage-based SRF.



(a) Experimental vs numerical diagonal crack pattern for CB1-Mahaidi model



(b) Experimental vs numerical diagonal crack pattern for CB2-Mahaidi model



(c) Experimental vs numerical diagonal crack pattern for CB3-Mahaidi model

Figure 5.17: Comparison of experimental and numerical failure crack pattern for beams modelled using Al-Mahaidi shear retention function and H/20 mesh size

Table 5.10: Experimental and numerical diagonal crack angle θ

Beam	θ_{exp}°	Shear Type	
		Damage	Al-Mahaidi
		θ_{num}°	
CB1	31.1	44.5	34.9
CB2	29.6	51.3	30.1
CB3	32.6	52.3	34.3

Remarks

From the above discussion, it is clear that mesh size has a significant influence on the numerical results obtained for RC beams failing in shear. It can be concluded with certainty that irrespective of the SRF used, increased refinement in mesh leads to increased peak loads. There, however, is an optimum mesh size beyond which it's influence is negligible [17], but this is not determined in this thesis.

When a relatively coarse mesh size is used (less than 10 elements in the height of the beam), then at a particular load level "A" for an RC beam model, a large volume of concrete is cracked due to which the contribution of cracked concrete in providing additional stiffness is low. This results in conservative predictions of peak loads in the numerical model. In case of relatively fine mesh size

(more than 20 elements in the height of the beam), then at the same load level, “A”, a relatively small volume of concrete is cracked due to which the contribution of cracked concrete in providing additional stiffness is high. This results in an overestimation of peak loads in the numerical model [11]. Increased refinement of mesh size results in increased ductility [19], and consequently, the cracks propagate in a relatively ductile manner - this is not accurate modelling of RC beams exhibiting brittle shear behaviour. Excessive ductility due to a very fine mesh size results in a ductile shear flexure failure, which is incorrect for the RC beams analysed in this thesis. Therefore, the mesh should not be too coarse such that it leads to conservative predictions, but it should also not be too fine as it would make the behaviour more ductile, which is wrong if a relatively brittle behaviour is desired to be modelled.

As the behaviour of both the shear retention factor β and mesh size is now understood, their effect on the SRF for accurate modelling of shear-critical RC beams is explainable now. RC beams analysed using Damage-based SRF result in relatively lower peak loads as compared to Al-Mahaidi SRF due to absence of β factor. However, this can be compensated by using a very fine mesh size which results in increased accuracy of the predicted peak load. The result is that peak load is accurately predicted, however, the failure type is wrongly predicted due to increased ductility, and due to a very fine mesh, a high computational time is also required.

If RC beams are analysed using Al-Mahaidi SRF, relatively coarser mesh size can be used to predict the peak load and failure type accurately, while also being computationally less time-consuming. β factor provides the additional capacity due to which a coarser mesh size can be used. A combination of Al-Mahaidi SRF with a relatively coarse mesh size can model the brittle shear cracking in the selected type of RC beams accurately, again, because of the consideration of β factor which results in higher numerical stability. Furthermore, in beams analysed using Al-Mahaidi SRF, the peak load accuracy can be further increased by changing the input value for the minimum shear retention factor β_{min} .

5.1.3. Conclusions Modelling Phase I

In Modelling Phase I, the shear behaviour of reinforced concrete (RC) beams is modelled. Two numerical solution strategies, varying in type of shear retention function (SRF) considered, are used to model RC beams. The selected SRFs vary in consideration of aggregate interlock in the form of a shear retention factor β . The influence of this β factor and mesh size on accurate prediction of peak load and failure type is investigated.

- Modelling of shear behaviour of RC beams without transverse reinforcement using solution strategy SS1, specifically Damage-based SRF, can predict the experimental peak load with a difference ranging between -13% to +4.9% when a very fine mesh size resulting in 30 or more elements in the height of the beam is considered. However, the predicted failure type is wrong, and ductile shear flexure failure is obtained instead of brittle shear-tension/compression. Finer mesh size compensates for the lack of consideration of aggregate interlock implicitly in the form of shear retention factor β due to increased stiffness of cracked concrete. If a coarser mesh size is used, then both the predicted peak load and failure type are inaccurate.
- Modelling of shear behaviour of RC beams without transverse reinforcement using solution strategy SS2, specifically Al-Mahaidi SRF, can predict the experimental peak load with a difference ranging between -4.6% to +13.7% when a relatively coarse mesh size resulting in 20 elements in the height of the beam is considered, as per de Putter’s recommendation [19]. The predicted failure type is also accurate for a relatively coarse mesh, with a brittle shear-tension failure observed. Consideration of aggregate interlock implicitly in the form of shear retention factor β allows beams analysed using Al-Mahaidi SRF to be accurately modelled using a relatively coarser mesh size. If a finer mesh size is used, then both the predicted peak load and failure type are inaccurate.

5.2. Modelling Phase II

The analyses performed in Modelling Phase I indicate that the numerical solution strategy SS2 with Al-Mahaidi shear retention function (SRF) can predict the failure load and failure type of the benchmark reinforced concrete (RC) beams relatively better as compared to SS1 with Damage-based SRF. Consequently, SS2 is used to model reinforced SHCC beam of benchmark study 4 in Modelling Phase II. However, a mesh sensitivity study is not performed, and the SHCC beam is modelled using a defined mesh size of 10mm. The benchmark study includes a 3-point bend test of reinforced SHCC beam as well as numerical evaluation of the test results using finite element analysis (FEA). Both experimental and numerical benchmark results are compared with the numerical results obtained using DIANA in the following sections.

5.2.1. Results Modelling Phase II

Comparison of Benchmark Experimental vs DIANA Numerical Results

This section compares the benchmark experimental results of reinforced SHCC beam with numerical model SHCC4-Mahaidi modelled using numerical solution strategy SS2 consisting of Al-Mahaidi SRF. The peak load and failure type observed in the experiment and the numerical model for beam SHCC4 are listed in Table 5.11. A comparison between experimental and numerical load-deflection curves for beam SHCC4 is shown in Figure 5.18. The predicted numerical peak load is approximately 27% less than the experimental peak load. The numerical peak load is limited to the load step beyond which poor numerical convergence is observed. During the analyses of RC beams in Modelling Phase I, the numerical peak load is limited by increased plasticity, yielding of reinforcement or a sudden increase in cracks, specifically development of new shear cracks. These phenomena cause numerical instability, resulting in poor convergence. For the SHCC beam, it is observed that the longitudinal reinforcement in the numerical model is not close to the input yield strength of 1050MPa, as shown in Figure 5.19. Also, based on the comparison of the experimental and numerical failure crack patterns illustrated in Figure 5.20, no diagonal shear crack is observed in the numerical model as well. Therefore, for the numerical model of the reinforced SHCC beam, neither of the two reasons mentioned above describes why poor numerical convergence is observed in the SHCC beam. The reason for such behaviour is investigated in the discussion section.

Table 5.11: Peak load and failure type comparison of model SHCC4-Mahaidi with benchmark experimental beam SHCC4

R_{exp} (kN)	R_{num} (kN)	Failure _{exp}	Failure _{num}
124.17	90.02	Diagonal shear crack	Cracking along reinforcement

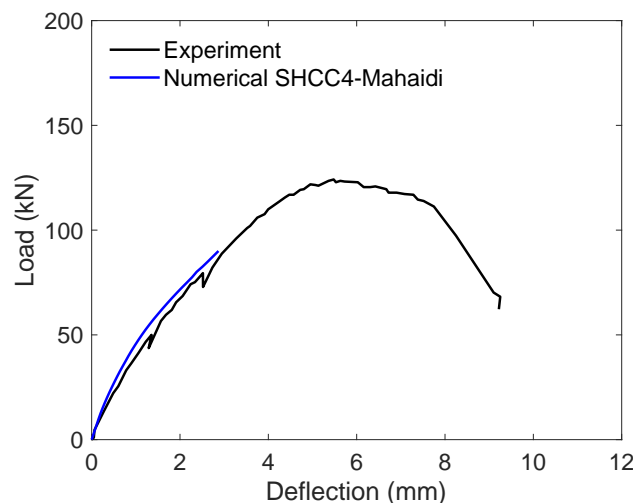


Figure 5.18: Load vs mid-span deflection comparison of model SHCC4-Mahaidi with benchmark experimental beam SHCC4

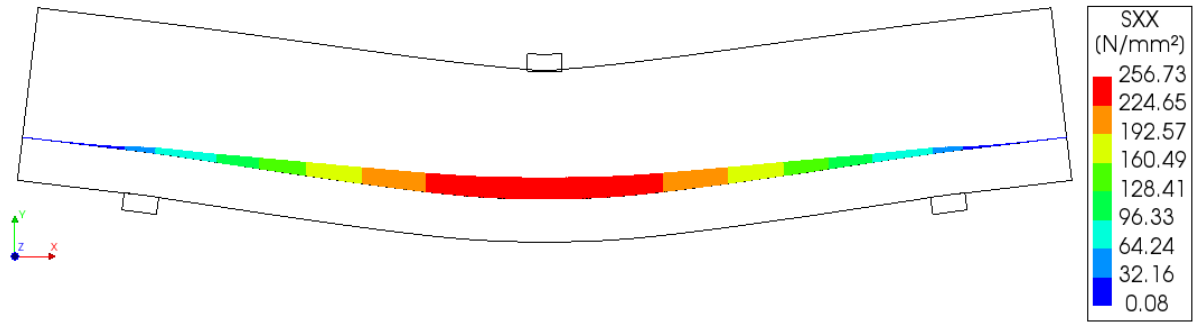
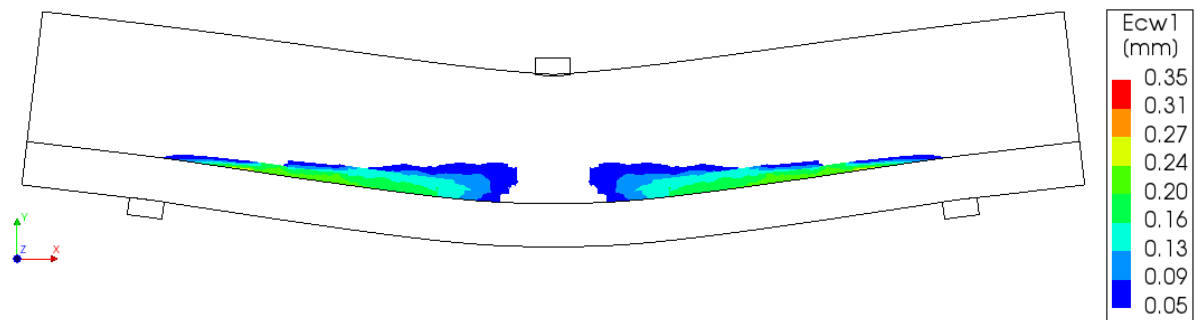


Figure 5.19: Stresses in reinforcement in numerical model SHCC4-Mahaidi

The numerical failure crack pattern is shown in Figure 5.20(b). In comparison with experimental failure, shown in Figure 5.20(a), a localized diagonal shear crack is not observed in the numerical model. The numerical crack pattern, however, might not be comparable with the experiment because the latter can capture the post-peak behaviour and the failure pattern is corresponding to approximately 60kN load and 9.2mm mid-span deflection. Such a post-peak behaviour is not captured in the numerical model due to load-controlled analysis performed without arc-length control [19].



(a) Experimental failure crack pattern



(b) Numerical failure crack pattern

Figure 5.20: Experimental and numerical failure crack pattern of beam SHCC4

Comparison of Benchmark Numerical vs DIANA Numerical Results

In the benchmark study, the authors evaluate the experimental results using finite element analysis (FEA) as well. The constitutive model used in the analysis is the Lattice Equivalent Continuum Model (LECOM). It is based on a fixed smeared crack model and consists of a combination of tension, compression and shear lattices. A trilinear curve is used as input for defining the tensile behaviour of SHCC, as shown in Figure 5.21(a). The compressive behaviour is split into two parts; Saenz equation is used up to the compressive strength, and a linear softening branch is assumed which is defined by considering the compressive fracture energy, as shown in Figure 5.21(b). The reinforcement is modelled as embedded reinforcement using truss elements, and the material property is assumed to be

linear elastic. The shear transfer model is developed considering the mechanisms involved in shear stress transfer, such as shear deformation and aggregate interlocking action on the crack surface. The parameters that help define the shear shape of the crack surface in the shear transfer model include angle θ , asperity height and contact coefficient. Usually, half of the maximum coarse aggregate size is taken as the asperity height for normal strength concrete.

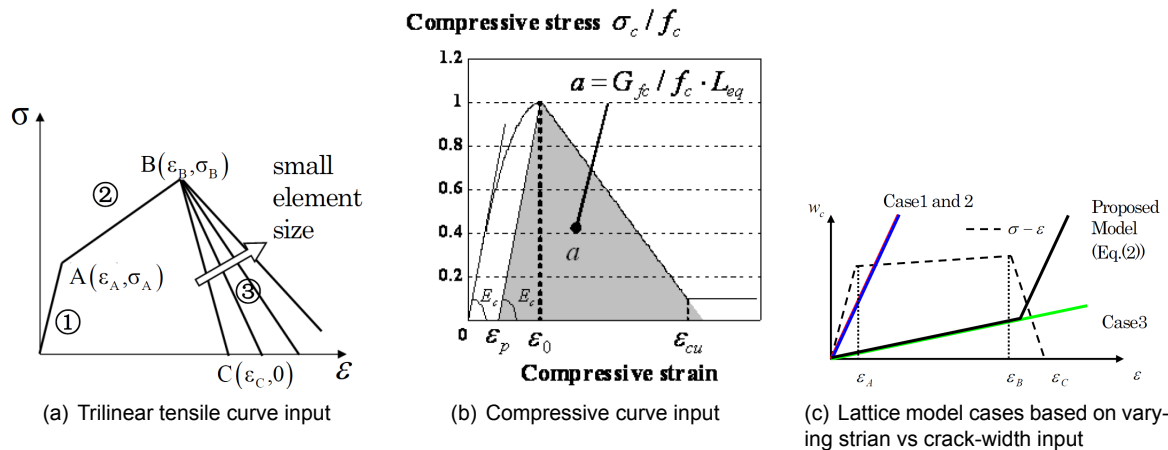


Figure 5.21: Input parameters for lattice modelling of SHCC

In the lattice model, the possible variations in inputs are the angle θ , asperity height and the trilinear tensile curve. The authors vary these parameters to perform a sensitivity study, understanding which of these factors influence the numerical results. The load-deflection curves are shown in Figure 5.22. These numerical results are compared with the experimental and the numerical results obtained in DIANA for model SHCC4-Mahaidi.

Figure 5.22(a) compares the experimental and numerical results of model SHCC4-Mahaidi with four variations of the lattice model of the same beam. In the lattice models, the parameters varied include θ and asperity height. The parameters are varied as such to obtain a different relationship between crack width and strain, as illustrated in Figure 5.21(c). These relationships are defined to replicate the experimental cracking behaviour of the SHCC beam, i.e. initial multiple fine cracking followed by eventual localization of one of the fine cracks. The comparison of these numerical results with results obtained from DIANA for model SHCC4-Mahaidi shows that the LECOM model can better replicate the experimental load-deflection response.

Similarly, Figures 5.22(b) and 5.22(d) compare the results of beam model SHCC4-Mahaidi with lattice models of varying asperity height and tensile behaviour input of SHCC, respectively. The three variations of SHCC tensile curve input are illustrated in Figure 5.22(c). Again, the comparison of these numerical results with results obtained from DIANA for model SHCC4-Mahaidi shows that the LECOM model can better replicate the experimental load-deflection response.

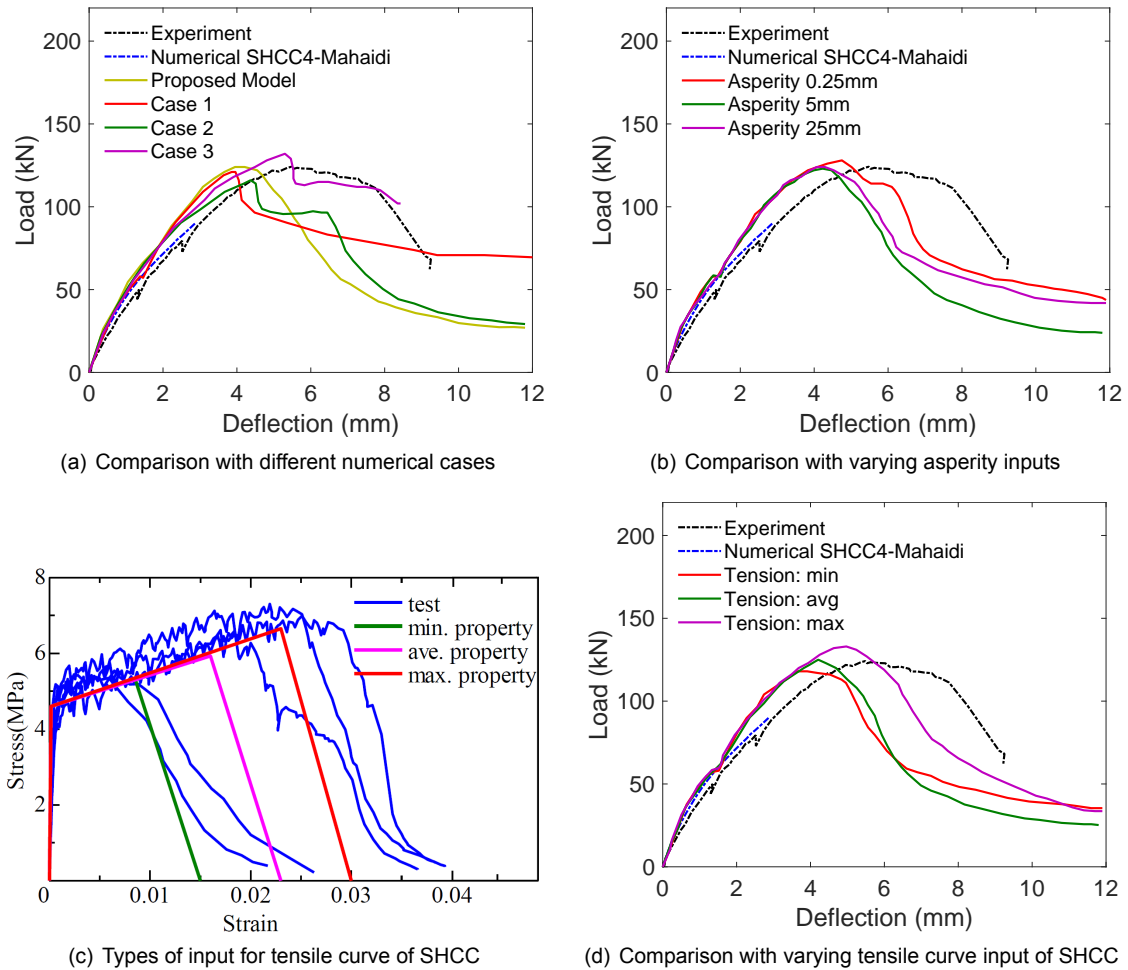


Figure 5.22: Comparison of experimental and DIANA numerical results with numerical results in benchmark study 4

Figure 5.23 compares the localized crack pattern at the peak load of the “proposed” model and SHCC4-Mahaidi model. It is observed that at the peak load, the crack pattern for both models is similar, i.e. cracking along the embedded reinforcement. Furthermore, as the lattice model runs beyond the peak load capturing the post-peak behaviour, the crack pattern in this region resembles the experimental crack pattern shown in Figure 5.20(a). Therefore, simulating the beam with displacement-controlled analysis to capture the post-peak response in DIANA might further improve the numerical crack pattern when compared with experimental observation.

The comparison of the numerical crack pattern of DIANA with LECOM shows the possible potential of the DIANA model in replicating the experimental crack pattern. However, the peak load obtained in DIANA model is still significantly lower from the numerical response obtained using lattice modelling by the authors. The resin for such behaviour is investigated in the discussion section.

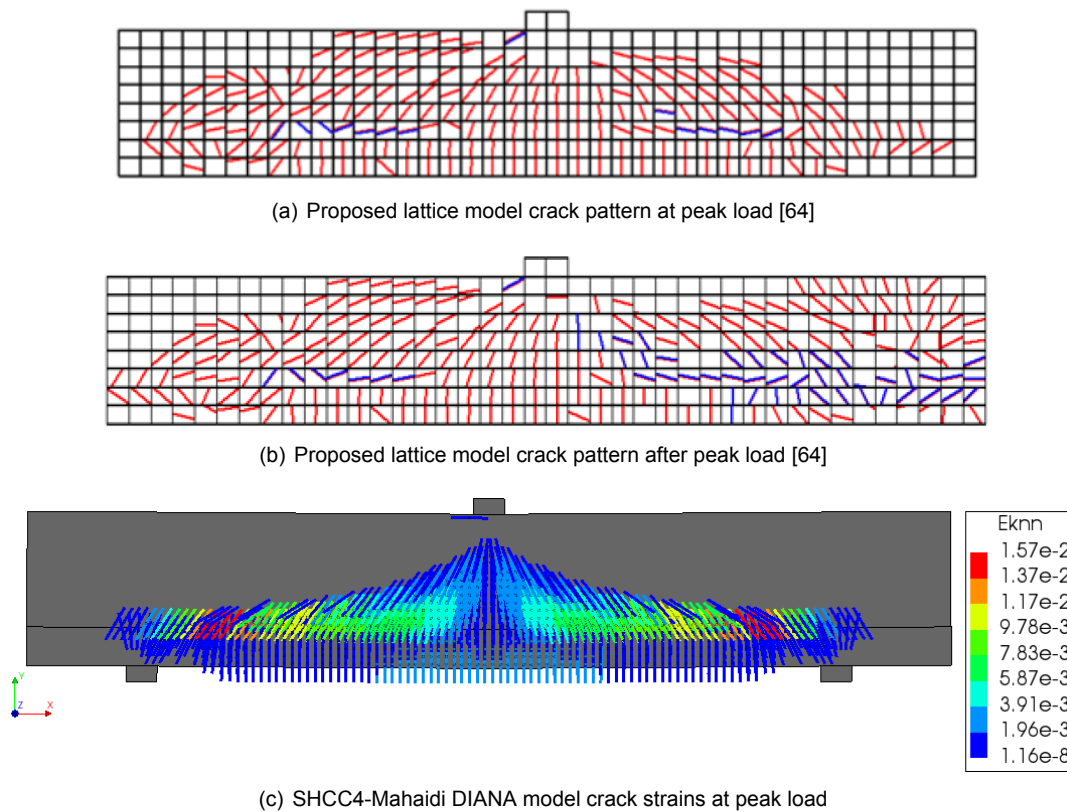


Figure 5.23: Crack distribution in the numerical models

5.2.2. Discussion Modelling Phase II

Cause of numerical failure in DIANA model

As described earlier, the numerical peak load in model SHCC4-Mahaidi is limited due to poor convergence, however, this is not because of yielding of reinforcement or sudden localization of diagonal shear cracks. In the numerical model, after reaching the peak load, a sudden increase in cracked elements along the longitudinal reinforcement is observed, as shown in Figure 5.24. These elements crack once they exceed the tensile strain capacity of SHCC. A possible reason for excessive cracking along the reinforcement might be the inconsideration of bond-slip between reinforcement and SHCC. Such a sudden increase in cracks results in poor convergence, causing the numerical model to fail at a lower peak load as compared to experiments. Figure 5.25 shows the trend for an increase in cracks and plasticity corresponding to the load steps in model SHCC4-Mahaidi. The peak load is corresponding to the last acceptable load step indicated by the vertical blue line.

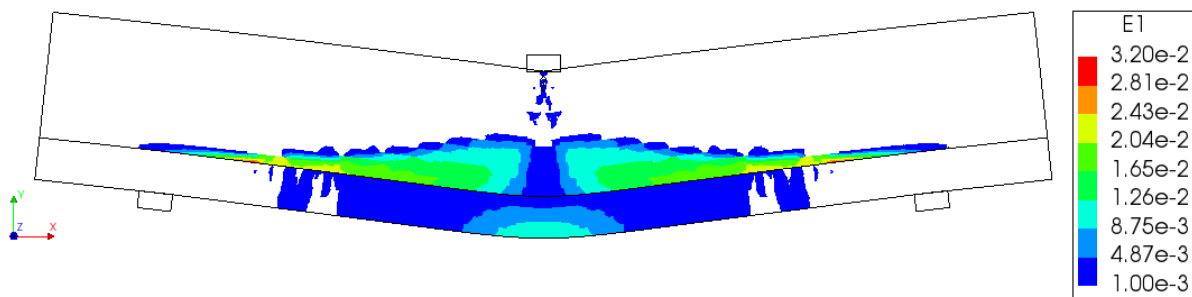


Figure 5.24: Strains E1 in numerical model SHCC4-Mahaidi immediately after the last acceptable load step

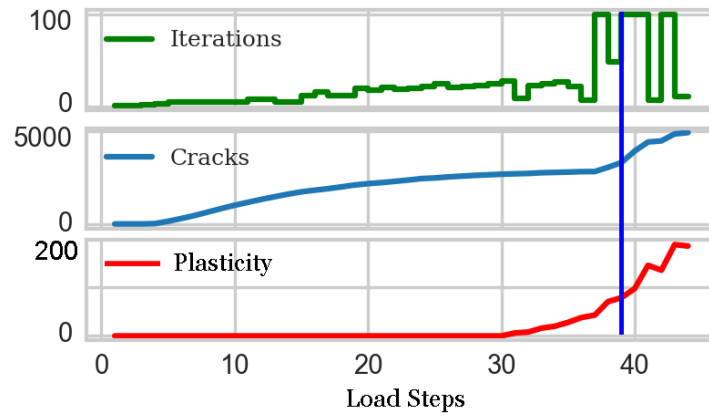


Figure 5.25: Cracks and plasticity in numerical model SHCC4-Mahaidi

The ultimate stress-strain values used to define the trilinear tensile behaviour of SHCC can also affect the numerical peak load. Beam SHCC4 is modelled in DIANA using the average tensile input of SHCC, shown in Figure 5.26. However, the ultimate tensile stress-strain values during experimentation may be higher than the averaged values used in the numerical model. This underestimation is critical for the numerical peak load for SHCC beam since the peak load is limited by the ultimate tensile strain capacity of SHCC in the numerical model. If a strain capacity lower than experiment is used as input in the numerical model, then SHCC cracks at a lower peak load as well.

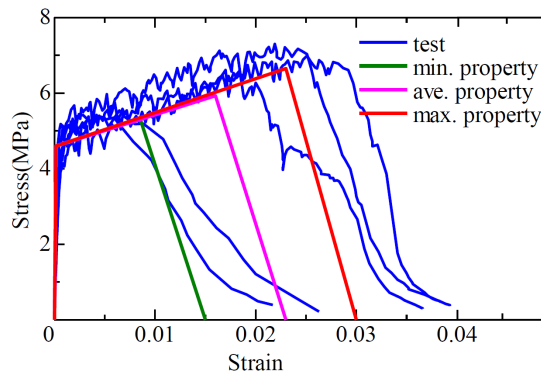


Figure 5.26: Types of input tensile curves for SHCC in LECOM model

Higher numerical peak load in LECOM model compared to DIANA model

A possible reason for the higher peak load in LECOM models as compared to DIANA model might be due to the constitutive relation selected to define the compressive behaviour of SHCC. NLFEA guidelines [28] recommend using parabolic compressive behaviour for normal concrete, but the uniaxial compressive behaviour of SHCC is different from concrete, as shown in Figure 5.27. However, as indicated in Figure 5.27(c), the compressive curve input in the lattice models resembles a parabolic curve as compared to the actual uniaxial compressive behaviour of SHCC. Therefore, the modelled compressive behaviour in LECOM models is different from DIANA model. Unlike parabolic compression, the input multi-linear compressive curve in DIANA includes a sudden, steep drop in strength after the peak strength, which can cause convergence problems in analysis. Nevertheless, the parabolic compressive behaviour is not considered for SHCC since it differs from the actual uniaxial compressive behaviour of SHCC.

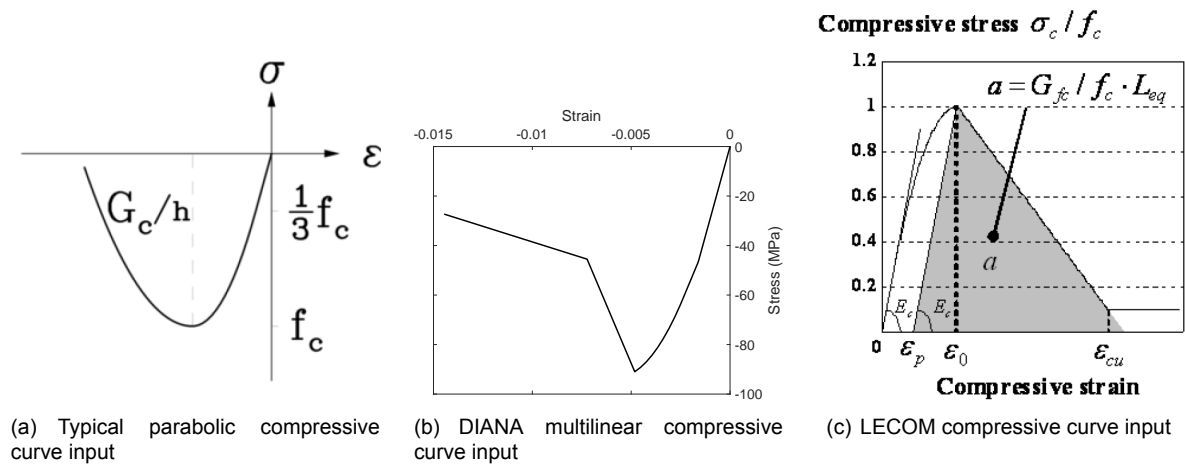


Figure 5.27: Different types of input compressive curves for SHCC in numerical models

5.2.3. Conclusions Modelling Phase II

- The tensile behaviour of SHCC modelled using *fib* FRC tensile curve can model cracking in SHCC. However, the use of embedded reinforcement can cause excessive cracking due to lack of bond-slip considered, causing convergence issues.
- The peak load is limited by the ultimate tensile strain value input in the numerical model and possible underestimation in the ultimate tensile strain value, as compared to experiments, can result in lower peak loads.
- The modelling shear behaviour of reinforced SHCC beam using Al-Mahaidi shear retention function is not feasible for the considered beam because of failure due to excessive cracking along the reinforcement instead of diagonal shear cracking as observed in the experiment.
- The comparison of numerical failure crack pattern with experiment for the considered beam remains inconclusive as it does not represent the ultimate crack pattern observed in the experiment. This is due to the lack of post-peak behaviour in the numerical model. The equilibrium conditions considered in the solution strategy SS2 are not able to capture the post-peak behaviour.

5.3. Modelling Phase III

In Modelling Phase III, benchmark SHCC-RC hybrid beams are analysed. The results are split into four sub-sections based on the benchmark hybrid beam analysed. SHCC is applied to reinforced concrete (RC) beams of benchmark studies 1 and 2. Each study consists of two hybrid beams of varying SHCC thickness applied on the sides. Solution strategy SS2, consisting of Al-Mahaidi shear retention function (SRF), is used to model the benchmark hybrid beams. An interface is defined between concrete and SHCC, termed as “hybrid interface” in this thesis. The results presented for hybrid beams in the result section consist of analyses of all hybrid beams using two types of hybrid interface, as described in Chapter 4, namely Perfect Bond (PB) and Imperfect Bond (IB). However, in the discussion section, two additional types of interface, namely Weak Bond (WB) and Hypothetical Bond (HB) are also tested for beam H20Q1. Their properties are described in the discussion section. From the discussion of results in Modelling Phase I, it is evident that a mesh size of 10mm can be too fine and can result in the inaccurate prediction of peak loads and failure type when RC beams are modelled using Al-Mahaidi SRF. Still, the hybrid beams are modelled with a 10mm mesh size due to limitation by the SHCC thicknesses considered. However, in the discussion section, the influence of mesh size on peak load and failure type is investigated, but for a single hybrid beam, H20Q1 only, as the hybrid beams modelled in 3D are computationally time-consuming even at relatively coarser mesh sizes. The hybrid

beams are continued to be modelled using embedded reinforcement, despite the premature failure of reinforced SHCC beam discussed in Modelling Phase II, because reinforcement in hybrid beams is in concrete. Failure due to excessive cracking along the longitudinal, like in reinforced SHCC beam, is not observed in RC beams probably because of localized cracking behaviour in concrete as compared to multi-cracking behaviour of SHCC.

5.3.1. Results Modelling Phase III

Before presenting the detailed results of hybrid beams, the format in which numerical results for crack pattern and interface delamination are presented for the hybrid beams are elaborated in the following paragraphs.

During experimentation, the failure crack pattern presented for the hybrid beams is the crack pattern on the SHCC layer since concrete is covered with SHCC from both sides. Therefore, the crack pattern of concrete at the time of failure cannot be observed, experimentally. In the benchmark studies, no remarks regarding the condition of the concrete part of the hybrid beam are provided as well. In the numerical model, however, it is possible to toggle SHCC and concrete layers “on” and “off” to view the crack pattern in the desired layer. For a hybrid beam, cracks on concrete and SHCC layers can be observed, both separately and combined. This is illustrated in Figure 5.28, which shows crack-width in model H20Q1-PB at an arbitrary load step before failure.

For consistency between experimental and numerical results, the crack pattern in the numerical model with only SHCC layer toggled on is observed, as illustrated in Figure 5.28(b). However, it does not imply that the contribution of concrete, reinforcement and hybrid interface in the formation of the crack pattern on the SHCC layer is neglected. The analysis simulates the beam as a hybrid and the crack pattern developed on the SHCC layer is influenced by concrete, reinforcement and hybrid interface. Similarly, the developed failure crack pattern on the concrete layer is also influenced by SHCC, reinforcement and hybrid interface, as illustrated in 5.28(c). If the cracks are observed by toggling both concrete and SHCC layers “on”, as shown in Figure 5.28a, a superimposed crack pattern is obtained, which gives a wrong impression of the numerical failure crack pattern. Therefore, the numerical failure crack patterns presented in the following sub-sections for hybrid beams are with SHCC layer toggled on only, unless otherwise stated.

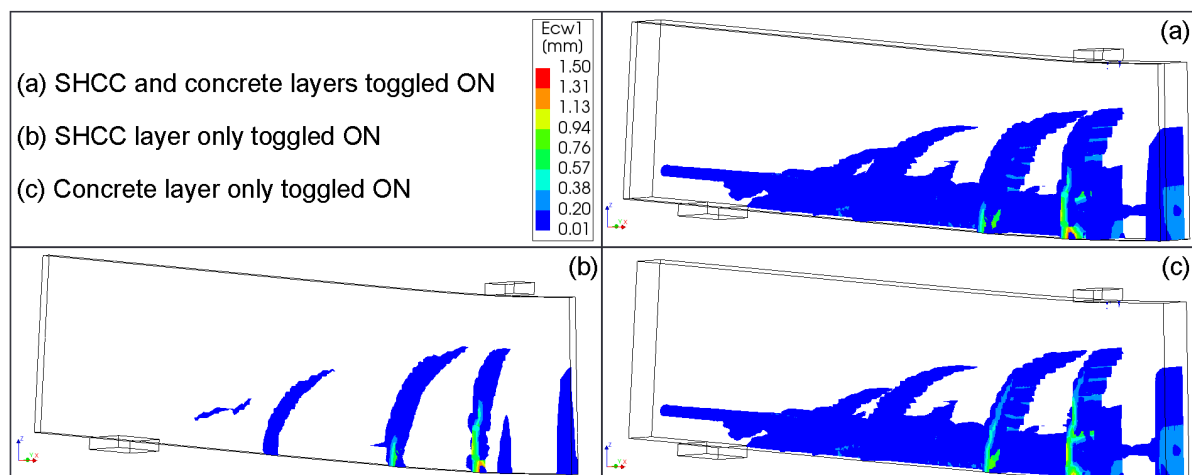


Figure 5.28: Various methods of representation of crack patterns in a 3D hybrid beam numerical model

As the interface is modelled between concrete and SHCC in hybrid beams as well, the relevant results are also studied. As described earlier, each hybrid beam presented in the result section is analysed using Perfect Bond (PB) and Imperfect Bond (IB) interfaces. Numerically, the PB interface means no delamination possible at the interface. Therefore, output results, such as interfacial displacement or stresses, are not needed. However, for the IB interface, the outputs mentioned above are included in order to assess if and where delamination of the interface occurs.

The format of presentation interfacial results in this thesis is discussed here. Consider Figure 5.29, which is an example of interfacial displacement and stresses normal to the interface surface. For all 3D hybrid beam models analysed in this thesis, the interface surface is defined in the global X-Z plane, and the axis normal to the interface surface is global Y-axis. Therefore, interfacial displacement or stresses are read in the global X-Z plane, for global Y-axis. While defining a surface interface in DIANA, a “source” and a “target” face is selected and the displacements and stresses shown in Figure 5.29 are the relative displacements and stresses between the “source” face and the “target” face. In all 3D models in this thesis, concrete is the source face, and SHCC is the target face. Sign convention for interfacial results are with respect to source and target face, and not the global axis. Further details on sign conventions are discussed by considering a simple example of interface loaded in tension in Appendix D.

For displacement of the interface, as illustrated in Figure 5.29(a), positive values indicate that concrete moves into SHCC. Negative values for the displacement of interface indicate debonding of SHCC and concrete layers due to delamination at the interface. The critical displacement value for IB interface beyond which the layers debond is 0.00245mm. In other words, if the relative interfacial displacement exceeds 0.00245mm in the negative, then debonding occurs. The debonded parts are presented with white colour in the contour plot. Note that such presentation of debonded regions is opposite of how cracks are presented. Non-white parts of crack plots show parts of the beam that are cracked and the white coloured region indicates uncracked parts of the beam. In contrast, white colour regions in interface displacement plots indicate debonded part, and non-white parts indicate bonded parts. This is highlighted in Figure 5.29.

For stresses at the interface, as illustrated in Figure 5.29(b), positive values indicate that the interface is under compression and negative values indicate that the interface is in tension. As described in Chapter 4, the tensile strength of IB interface is 1MPa and if the interfacial stresses exceed 1MPa in the negative, then the interface delaminates, causing debonding of SHCC and concrete layers. However, unlike displacements, parts of the interface which have exceeded the tensile strength are represented as regions of 0MPa stresses instead of white coloured regions. According to Figure 5.29(a), the delamination of the interface occurs at Point A such that the SHCC and concrete layers have debonded at this point. But correspondingly in Figure 5.29(b), the tensile stress is approximately 0MPa. This 0 MPa is due to debonding and not because the interface at Point A is not stressed. This is illustrated by looking at the stresses at Point A with respect to increasing load in Figure 5.30. At 150kN load, the interface reaches the tensile strength of 1MPa, and afterwards, it goes back to 0MPa due to delamination. Therefore, while studying delamination at the interface using stress contour plots, the interfacial displacement plots are also needed. Both these results are discussed together for each hybrid beam in the following subsections.

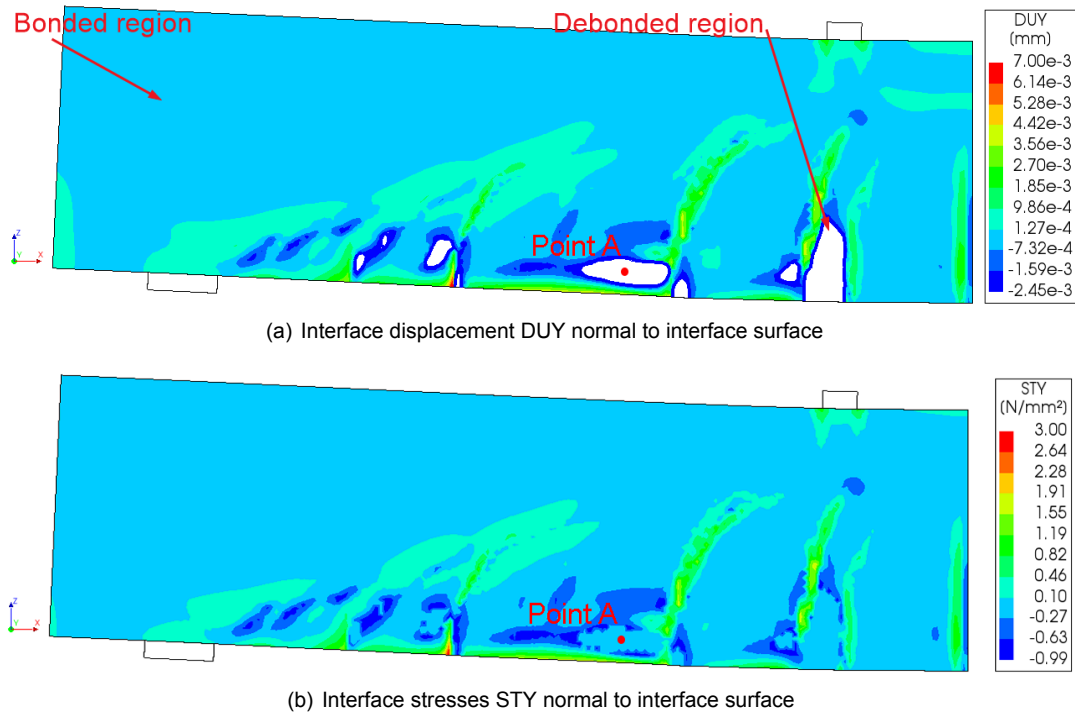


Figure 5.29: Typical interfacial results of a hybrid beam modelled with Imperfect Bond (IB) hybrid interface

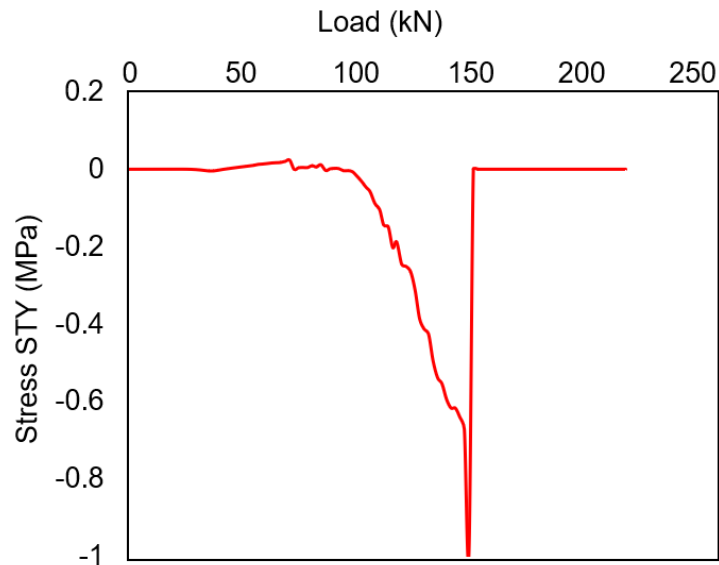


Figure 5.30: Load vs interface stress STY at point of debonding "A" of numerical model H20Q1-IB

Beam H20Q1

Figure 5.31 shows the comparison of the load-deflection response of experimental beam H20Q1 with respective numerical models modelled using Perfect Bond (PB) and Imperfect Bond (IB) hybrid interface types. The experimental load-shear strain response at the interface is also recorded during the experiment using strain gauges, which is illustrated using dash lines in Figure 5.31. The authors of the benchmark study report that for beam H20Q1, the SHCC layers peel off of concrete after the beam fails at the ultimate load, indicating complete debonding. However, the experimental load-deflection curve indicates a change in the stiffness at around 118kN, suggesting possible localized partial debond-

ing. Therefore, the interface delamination is gradual in the experiment. From approximately 138kN onwards, no further shear strains are recorded, which suggests complete debonding at the location where strain gauges are installed. Therefore, localized debonding occurs in during testing before reaching the peak load. (Note: The term “localized” debonding is used since the interface may debond locally where the strain gauges are installed, and complete debonding of SHCC layers does not occur. The term “partial” debonding means that the SHCC and concrete layers start to separate, but the tensile strength of interface is not breached)

Comparison of the experimental load-deflection response with the numerical response of model H20Q1-PB indicates that the numerical stiffness is comparable to experiment once cracks localize at approximately 75kN. For model H20Q1-PB, the hybrid interface has a perfect bond condition i.e. no debonding of SHCC and concrete layers is modelled, contrary to experimentation in which debonding of SHCC is observed. Hence, the numerical peak load is approximately 43% higher as compared to experiment, and no change in stiffness is recorded at 118kN as well.

Unlike model H20Q1-PB, the interface is modelled in model H20Q1-IB to allow for delamination. However, the numerical load-deflection response of model H20Q1-IB is almost identical to model H20Q1-PB. This suggests that IB interface is not modelled appropriately such that sufficient debonding can occur which can result in a comparable peak load and stiffness as observed in the experiment. The behaviour of debonding of SHCC due to delamination at the interface is investigated in the discussion section. Figure 5.32(a) shows that parts of the shear span in the bottom half of the beam have debonded only, and no significant debonding is observed elsewhere. As illustrated in Figure 5.32(b), the elements in the vicinity of the debonded parts are close to the tensile strength of the interface, however, before they could exceed the interfacial tensile strength, the longitudinal reinforcement yields and the numerical analysis stops due to poor convergence. For both numerical models, the peak load is limited by poor convergence due to the yielding of longitudinal reinforcement ($f_y = 374\text{MPa}$), as shown in Figure 5.33.

Table 5.12: Peak load and failure type comparison between experimental and numerical results of hybrid beam H20Q1

R_{exp} (kN)	R_{PB} (kN)	R_{IB} (kN)	Failure _{exp}	Failure _{PB}	Failure _{IB}
148	212	216	Shear flexure	Shear flexure	Shear flexure

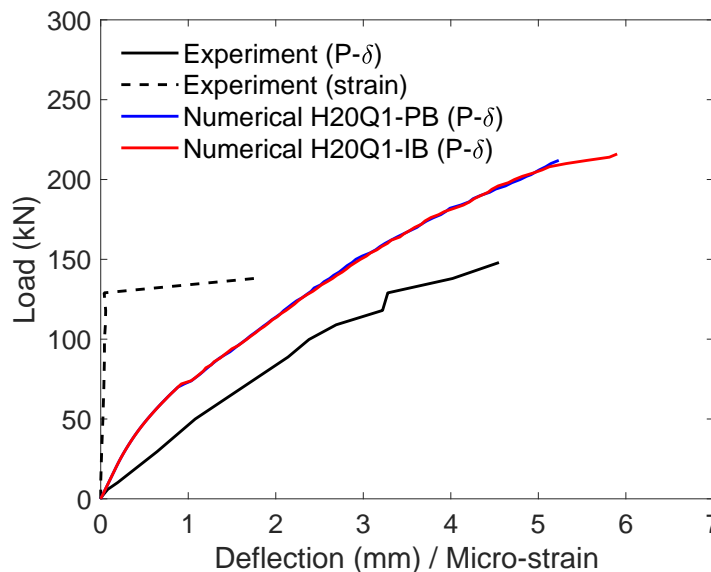


Figure 5.31: Load vs mid-span deflection comparison of numerical models H20Q1-PB and H20Q1-IB with benchmark experimental beam H20Q1

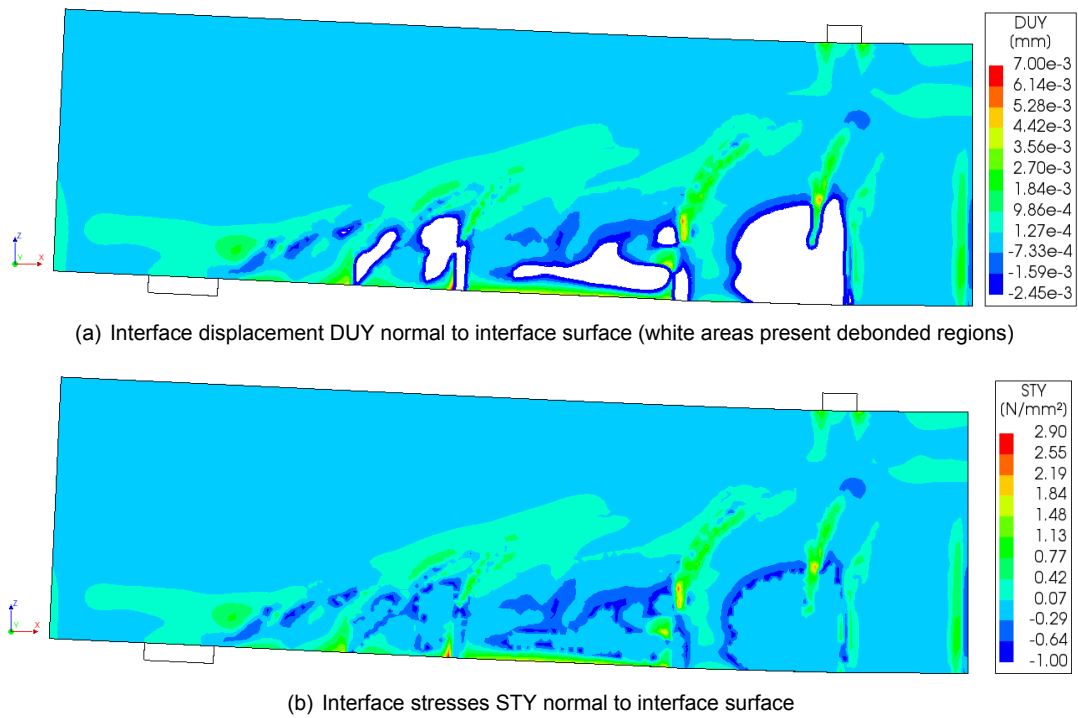


Figure 5.32: Interfacial results of numerical model H20Q1-IB

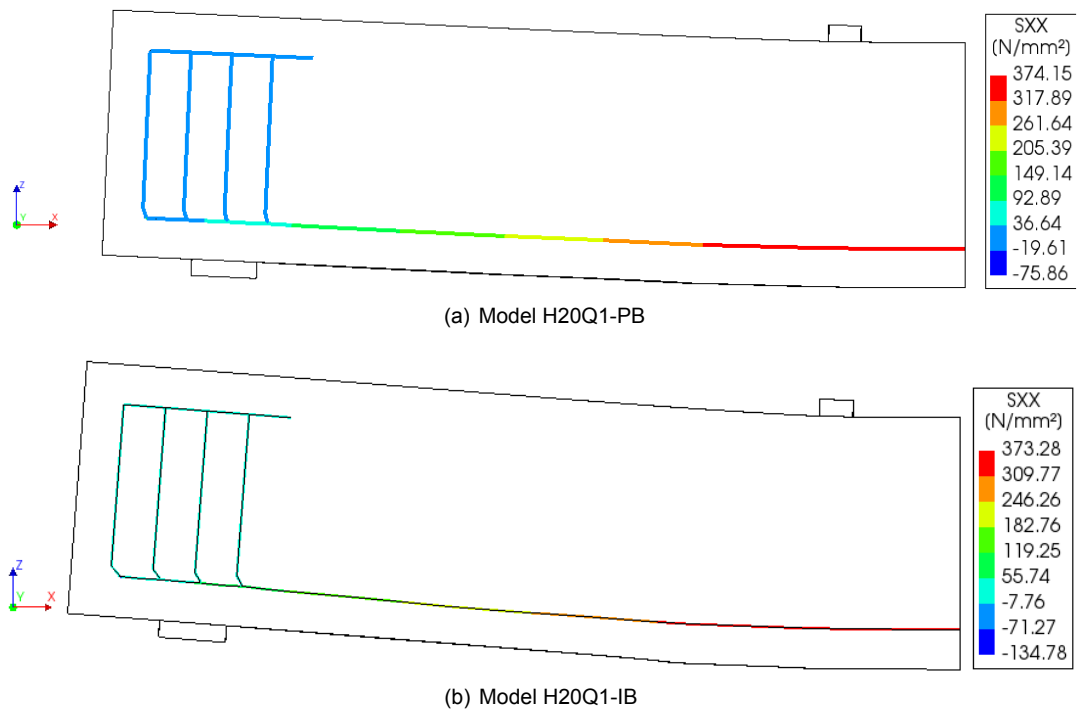


Figure 5.33: Reinforcement stresses SXX in numerical models of beam H20Q1

Figure 5.34 shows failure crack pattern for experimental beam H20Q1. The red markings for cracks indicate a possible shear flexure failure, with three shear-flexure cracks and number of small flexural cracks. Figure 5.35 shows the failure crack pattern for the numerical models for beam H20Q1. For both interface types, the numerical failure type is shear-flexure as well. There is no significant

difference in the failure crack pattern between the two interface types. Small flexural cracks are also present but are omitted to view localized cracks more clearly.

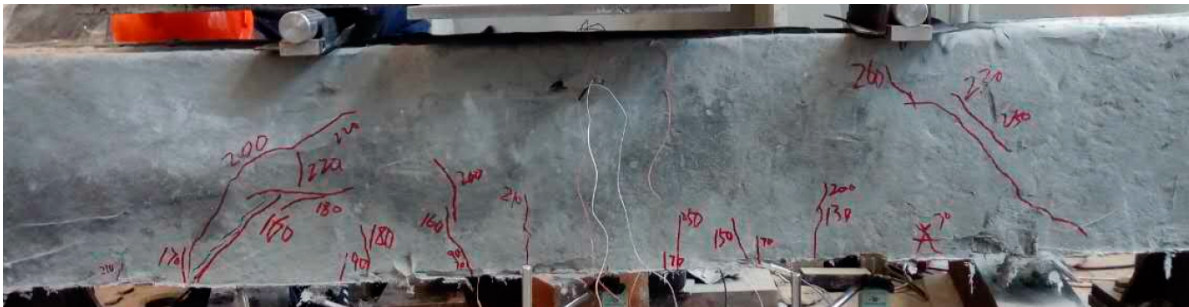
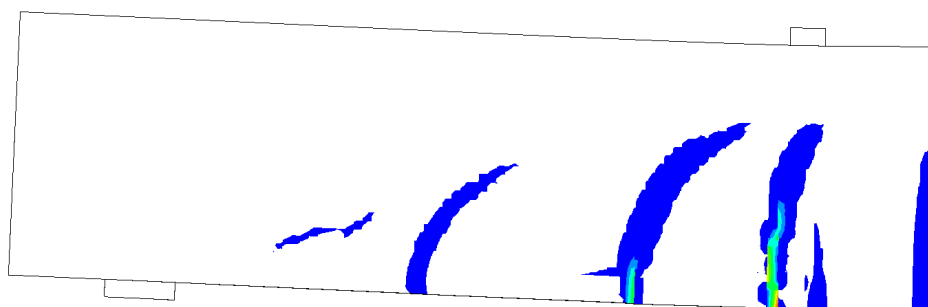


Figure 5.34: Experimental failure crack pattern of benchmark beam H20Q1

(a) H20Q1-PB - Max Crack-width $E_{cw1} = 1.38\text{mm}$



(b) H20Q1-IB - Max Crack-width $E_{cw1} = 1.33\text{mm}$

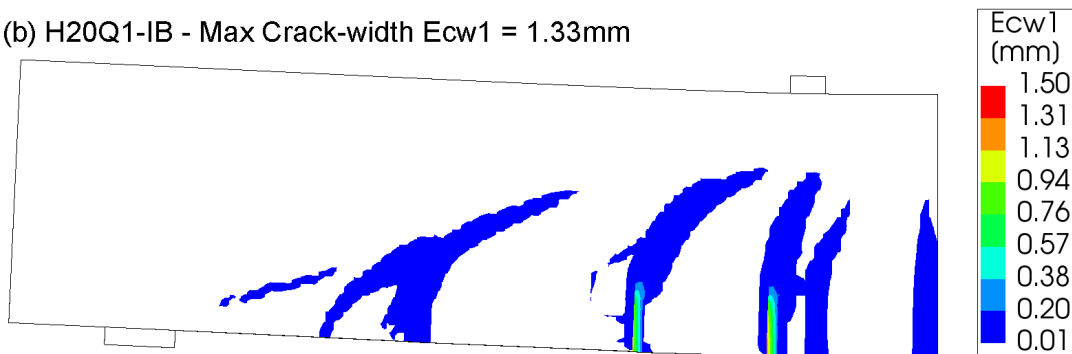


Figure 5.35: Numerical failure crack pattern of numerical models; (a) H20Q1-PB, and (b) H20Q1-IB

Beam H40Q1

Figure 5.36 shows the comparison of the load-deflection response of experimental beam H40Q1 with respective numerical models modelled using Perfect Bond (PB) and Imperfect Bond (IB) hybrid interface types. The experimental load-shear strain response measured at the hybrid interface is presented using dash lines. The authors of the benchmark study report that the experimental beam H40Q1 fails due to debonding of the SHCC layers applied on the sides of the RC beam. The cracks initiate and develop with an increase in load, then partial debonding occurs after which few cracks initiate and develop in the SHCC layers before the layers eventually completely debond at the ultimate load. Because of the failure of the interface that, in spite of doubling the SHCC layer thickness from 20mm to 40mm in H40Q1, the experimental peak load of beam H40Q1 is only 1.4% higher as compared to beam H20Q1. The experiment continues beyond 125kN load and the capacity increases by another 25kN, however, the resulting failure crack pattern is a consequence weak of hybrid interaction of SHCC and concrete due to excessive debonding.

Comparison of the experimental load-deflection response with the numerical response of model H40Q1-PB indicates that the numerical stiffness is not comparable throughout the test. For model H40Q1-PB, the hybrid interface has a perfect bond condition, i.e. no debonding of SHCC and concrete layers is modelled, contrary to experimentation. Hence, no change in stiffness is recorded in the numerical model at 120kN, and the peak load is also approximately 59% higher as compared to experiment.

The hybrid interface is modelled in model H40Q1-IB to allow for debonding of SHCC and concrete layers, as in the experiment. The numerical load-deflection response of model H40Q1-IB is almost identical to H40Q1-PB up till a load of 222kN, after which a plateau develops in load-deflection response for model H40Q1-IB. Start of plateau indicates point where significant debonding occurs, as illustrated in Figure 5.37(a), and afterwards, the reinforcement yields by the end of the plateau. Lack of debonding in model H20Q1 for IB interface but significant debonding in model H40Q1 suggests that debonding of the interface is influenced by the SHCC thickness considered. This aspect is evaluated further in the discussion section. Like for beam H20Q1, the numerical peak load in both numerical models for beam H40Q1 is also limited by poor convergence due to yielding of reinforcement (contour plots are same as Figure 5.33, thus are not presented).

Table 5.13: Peak load and failure type comparison between experimental and numerical results of hybrid beam H40Q1

R_{exp} (kN)	R_{PB} (kN)	R_{IB} (kN)	Failure _{exp}	Failure _{PB}	Failure _{IB}
150	238	226	Debonding	Flexure	Debonding

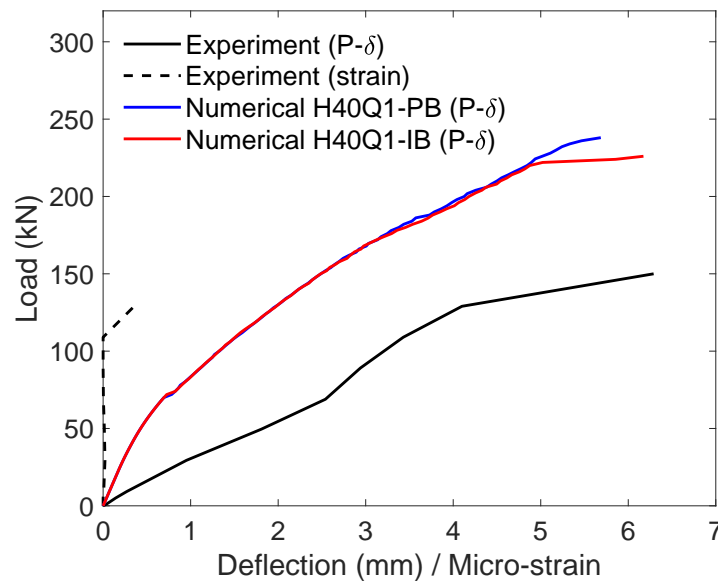


Figure 5.36: Load vs mid-span deflection comparison of numerical models H40Q1-PB and H40Q1-IB with benchmark experimental beam H40Q1

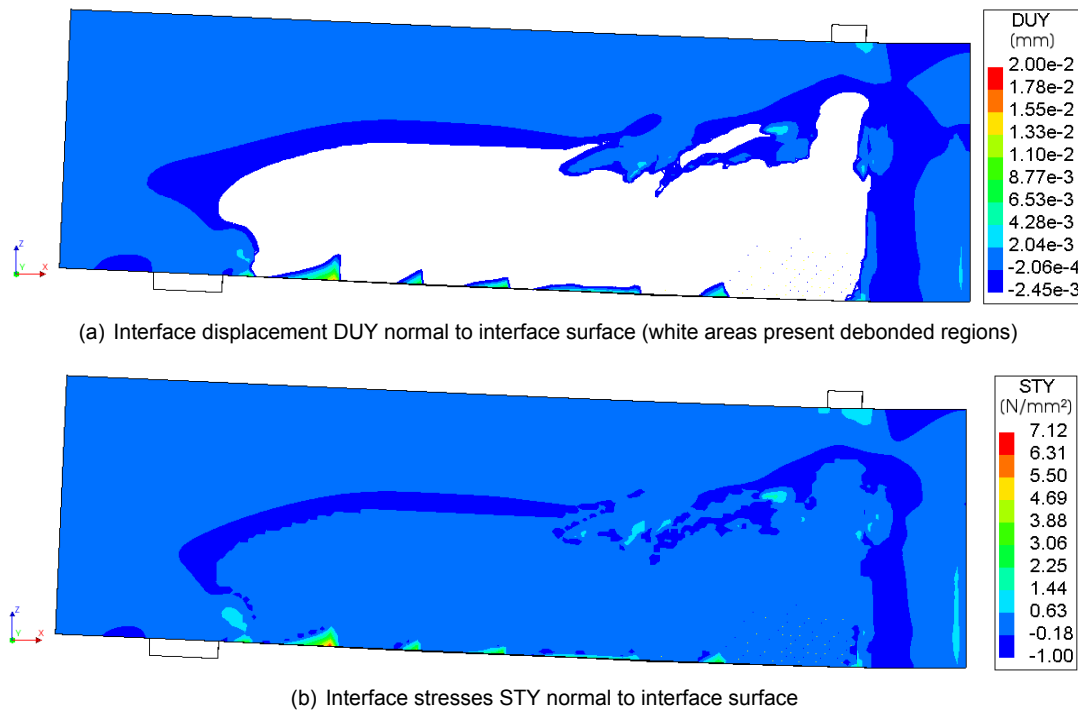


Figure 5.37: Interfacial results of numerical model H40Q1-IB

In spite of significant delamination, the peak load for the H40Q1-IB is only 5% lower from H40Q1-PB and is still 51% higher than the experimental peak load. However, the debonding in H40Q1-IB is more comparable to experiments, therefore, the numerical peak load of model H40Q1-IB should be more comparable to experiment as well, but this is not the case. This suggests that interface delamination might not be affecting the numerical peak load. This aspect is investigated in the discussion section.

Figure 5.38 shows failure crack pattern for experimental beam H40Q1. The red markings for cracks indicate a localized flexural crack and number of additional small flexural cracks. Figure 5.39 shows the failure crack patterns for the numerical models for beam H40Q1. For both interface types, the numerical failure crack pattern includes a localized flexural crack as well. This similarity is consistent with the results for H20Q1 models even though there is significant delamination at the interface in model H40Q1-IB. The influence of interface on the failure crack pattern obtained numerically is further discussed in the discussion section.

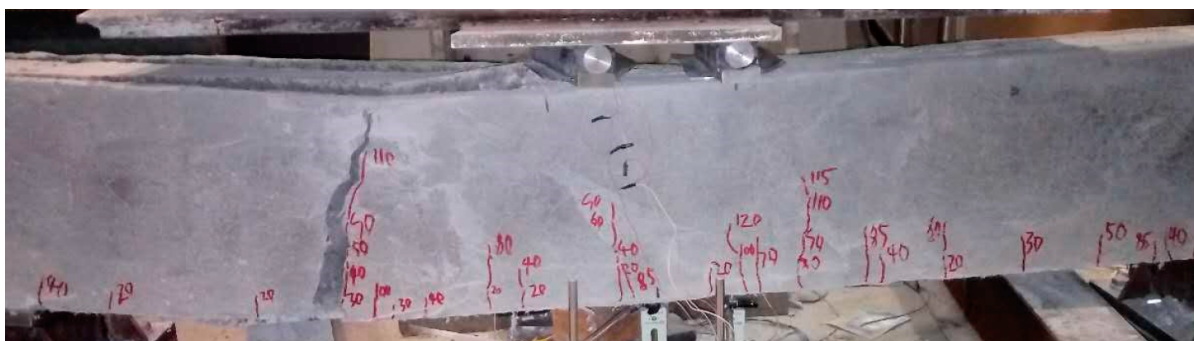


Figure 5.38: Experimental failure crack pattern of benchmark beam H40Q1

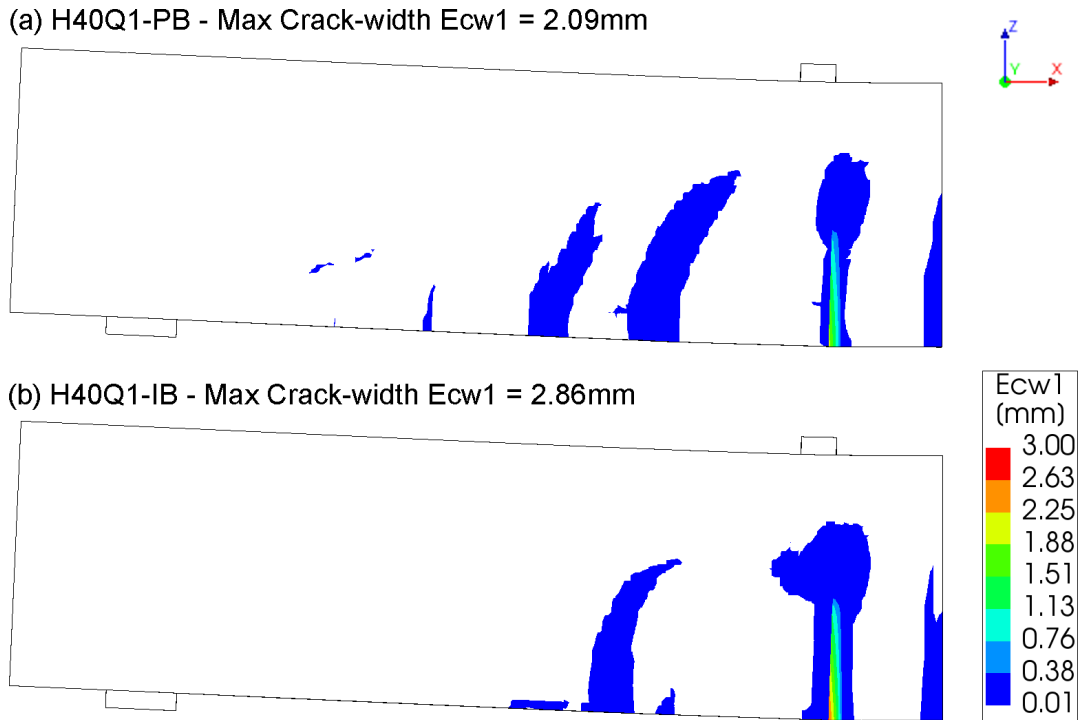


Figure 5.39: Numerical failure crack pattern of numerical models; (a) H40Q1-PB, and (b) H40Q1-IB

Beam H5Q2

Figure 5.40 shows the comparison of the load-deflection response of experimental beam H5Q2 with respective numerical models modelled using Perfect Bond (PB) and Imperfect Bond (IB) hybrid interface types. The authors of the benchmark study report that for beam H5Q2, no debonding of the SHCC layers at the interface during loading or at the ultimate failure is reported and the hybrid beam fails in shear tension. The numerical stiffness after crack localization at around 25kN is lower as compared to experiment, due to which the ultimate deflection is higher than the experiment.

Comparison of the experimental load-deflection response with the numerical response of model H5Q2-PB indicates that the numerical peak load is approximately 10% higher, which is significantly low as compared to the first two beams. The reason for this is the fact that a mesh size of 10mm is relatively coarser for models of beam H5Q2 as compared to first two beams, and therefore, the numerical peak load is not being overestimated due to mesh size. The small difference also suggests that the Perfect Bond (PB) hybrid interface condition, i.e. no slip or debonding at the interface, is appropriate to model this beam since no debonding is reported during the experiments as well.

Modelling Imperfect Bond (IB) hybrid interface in model H5Q2-IB results in almost an identical peak load as compared to model H5Q2-PB, and the numerical peak load is approximately 7.5% higher as compared to experiments. This suggests that the values of parameters for Imperfect Bond (IB) interface in the numerical model, such as tension, cohesion and friction angle (stated in Chapter 4), are similar to that in the experiment such that almost no debonding at the hybrid interface is observed, as illustrated in Figure 5.41(a). For both numerical models, the peak load is limited by poor convergence due sudden changes in plasticity, as shown in Figure 5.42.

Table 5.14: Peak load and failure type comparison between experimental and numerical results of hybrid beam H5Q2

R_{exp} (kN)	R_{PB} (kN)	R_{IB} (kN)	Failure _{exp}	Failure _{PB}	Failure _{IB}
72.6	80	78	Shear tension	Shear flexure	Shear flexure

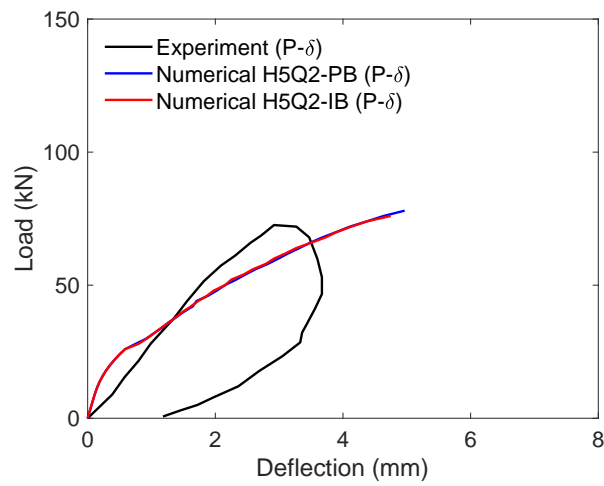


Figure 5.40: Load vs mid-span deflection comparison of numerical models H5Q2-PB and H5Q2-IB with benchmark experimental beam H5Q2

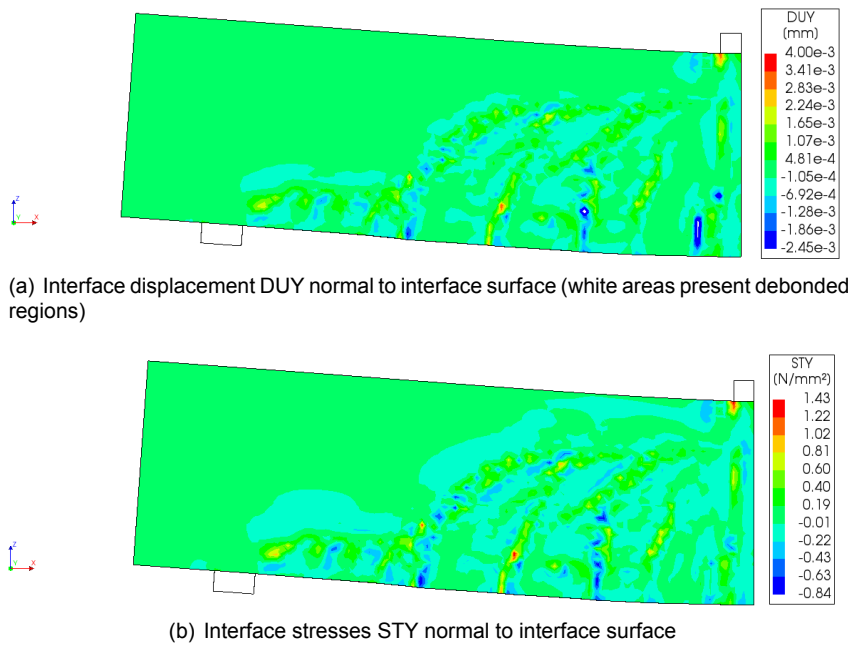


Figure 5.41: Interfacial results of numerical model H5Q2-IB

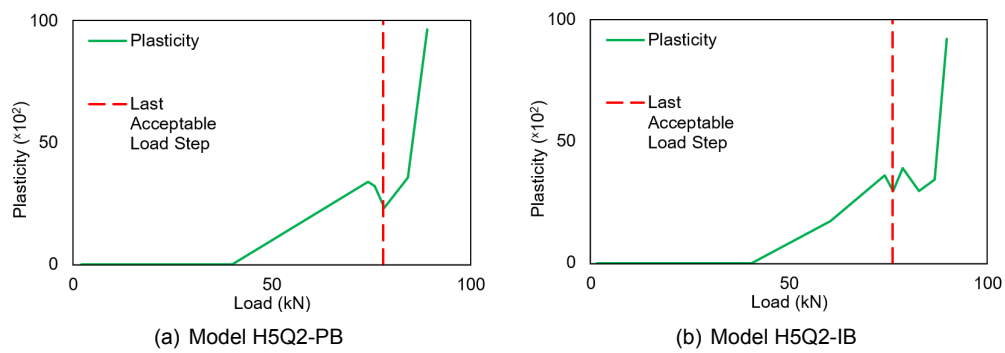


Figure 5.42: Load vs plasticity for numerical models of beam H5Q2

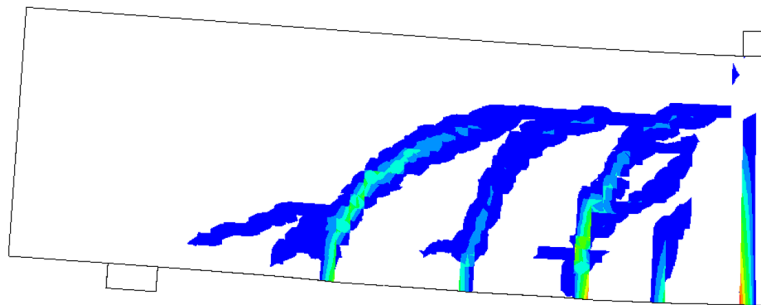
Unlike in a numerical model, it is difficult to develop a completely perfect bond in reality. Therefore, some debonding might still have occurred, although not mentioned in the benchmark study. Moreover, this debonding might be relatively higher in the experiment than that observed in model H5Q2-IB, resulting in a slightly lower experimental peak load as compared to the numerical model.

Figure 5.43 shows failure crack pattern for experimental beam H5Q2, indicating shear-tension failure. Figure 5.44 shows the failure crack pattern for the numerical models for beam H5Q2. For both interface types, the numerical failure crack pattern resembles shear flexural failure instead of shear-tension as observed in the experiment. Same failure pattern between the two numerical models is because the Imperfect Bond (IB) hybrid interface conditions are no different from Perfect Bond (PB). The numerical failure type, however, is different from the experiment. The reason is the same as for control beam model CB2-Mahaidi of the same benchmark study, i.e. the crack pattern provided in the experiment is corresponding to the ultimate failure and not the peak load as in the numerical model. Therefore, if the numerical model is analysed as such that the post-peak behaviour is also captured, then something more definitively can be said about the numerical failure crack pattern as well. This hypothesis can be backed from Figure 5.44, where, although there is a clear formation of shear-flexure cracks, part of the main diagonal crack is starting to progress along the longitudinal reinforcement as well, indicating possible shear-tension failure as observed in the experiment.



Figure 5.43: Experimental failure crack pattern of benchmark beam H5Q2

(a) H5Q2-PB - Max Crack-width $E_{cw1} = 0.84\text{mm}$



(b) H5Q2-IB - Max Crack-width $E_{cw1} = 0.80\text{mm}$

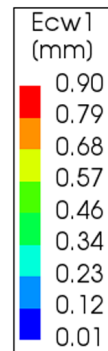
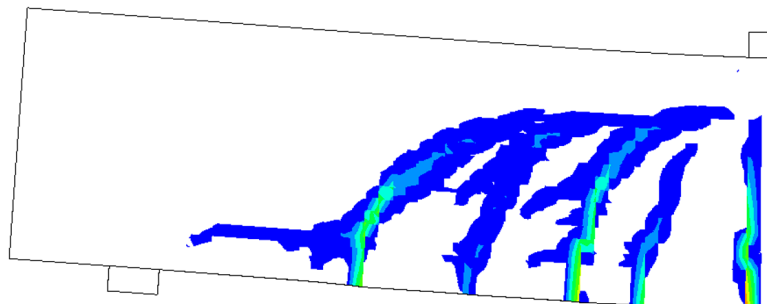


Figure 5.44: Numerical failure crack pattern of numerical models; (a) H5Q2-PB, and (b) H5Q2-IB

Beam H10Q2

Figure 5.45 shows the comparison of the load-deflection response of experimental beam H10Q2 with respective numerical models modelled using Perfect Bond (PB) and Imperfect Bond (IB) hybrid interface types. The authors of the benchmark study report that for beam H10Q2, no debonding of the SHCC layers at the interface during loading or at the ultimate failure is reported and the hybrid beam fails in shear tension. The numerical stiffness after crack localization at around 30kN is lower as compared to experiment, resulting in higher ultimate mid-span deflection as compared to the experiment.

Comparison of the experimental load-deflection response with the numerical response of model H10Q2-PB indicates that the numerical peak load is approximately 5% higher. A possible reason for a low difference is the same as for beam H5Q2, i.e. the mesh size selected is not resulting in over-estimated peak loads. The small difference also suggests that the Perfect Bond (PB) hybrid interface condition, i.e. no slip or debonding at the interface, is appropriate to model this beam since no debonding is reported during the experiments as well.

Modelling Imperfect Bond (IB) hybrid interface in model H10Q2-IB results in almost identical peak load as compared to model H10Q2-PB, and the numerical peak load is approximately 2.6% higher as compared to experiments. However, contrary to model H5Q2-IB, there is debonding in model H10Q2-IB, as illustrated in Figure 5.46(a). However, the numerical peak loads between PB and IB interface types are almost identical. Therefore, the results of model H10Q2-IB, in addition to model H40Q1-IB, clearly show that the interface delamination is not influencing the numerical peak load significantly and as the SHCC thickness is increased, more debonding in the numerical model is observed. These aspects are evaluated further in the discussion section. Like for beam H5Q2, the numerical peak load in both numerical models for beam H10Q2 is also limited by poor convergence due to sudden changes in plasticity (plots are similar to beam H5Q2 shown in Figure 5.42, thus are not presented).

Table 5.15: Peak load and failure type comparison between experimental and numerical results of hybrid beam H10Q2

R_{exp} (kN)	R_{PB} (kN)	R_{IB} (kN)	Failure _{exp}	Failure _{PB}	Failure _{IB}
91.6	96	94	Shear tension	Shear flexure	Shear flexure

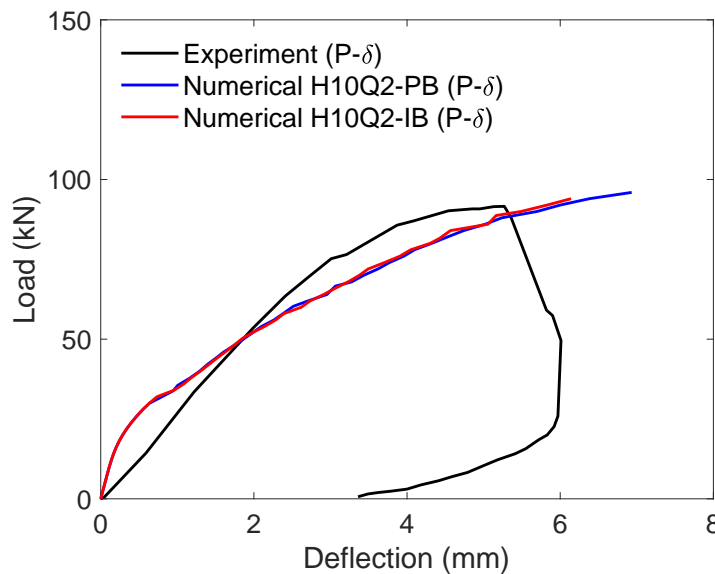


Figure 5.45: Load vs mid-span deflection comparison of numerical models H10Q2-PB and H10Q2-IB with benchmark experimental beam H10Q2

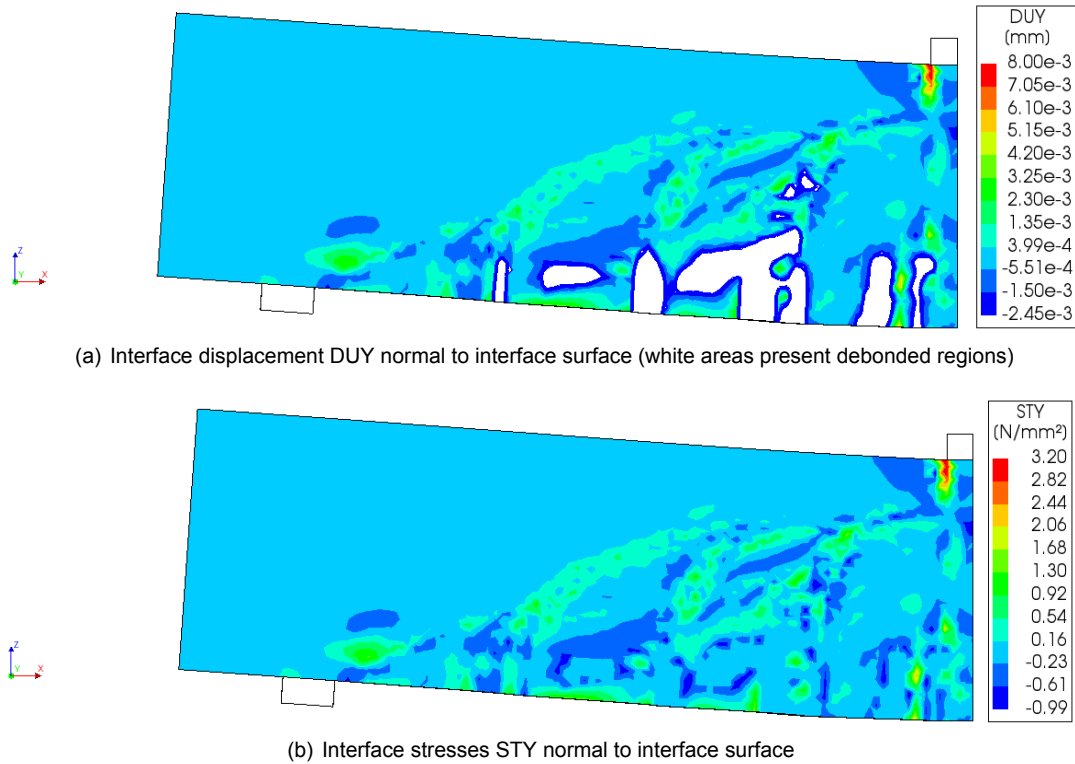


Figure 5.46: Interfacial results of numerical model H10Q2-IB

Figure 5.47 shows failure crack pattern for experimental beam H10Q2, indicating shear-tension failure. Figure 5.48 shows the failure crack patterns for the numerical models for beam H10Q2, indicating shear flexure failure. The reason for difference in experimental and numerical failure crack patterns is as provided earlier for beam H5Q2, i.e. the crack pattern provided in the experiment is corresponding to the ultimate failure and not the peak load as in the numerical model. Therefore, it is difficult to conclusively say something about the numerical failure crack pattern for this beam unless the post-peak behaviour is also modelled. Nevertheless, like beam H5Q2, part of the main diagonal crack in numerical models of beam H10Q2 is also starting to progress along the longitudinal reinforcement. Therefore, the obtained numerical failure crack patterns for both H5Q2 and H10Q2 beam are acceptable, compared to experiment.



Figure 5.47: Experimental failure crack pattern of benchmark beam H10Q2

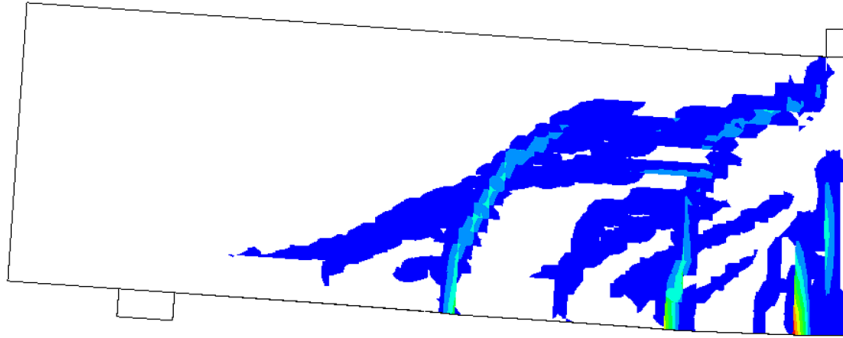
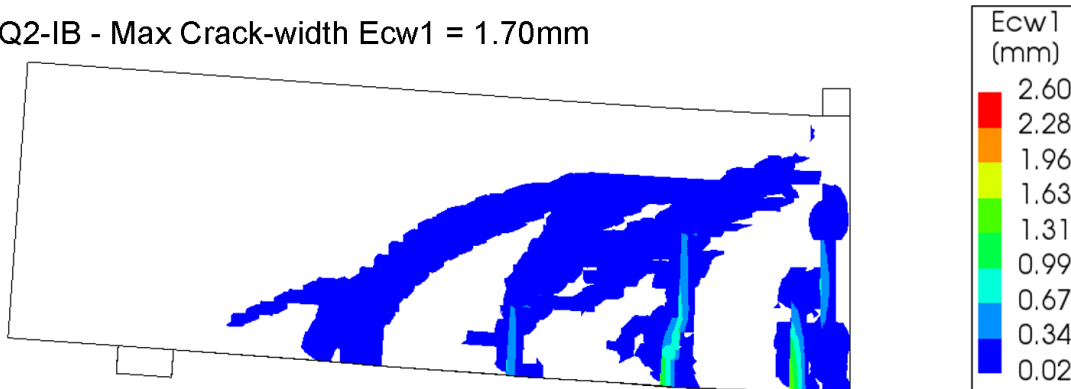
(a) H10Q2-PB - Max Crack-width $E_{cw1} = 2.55\text{mm}$ (b) H10Q2-IB - Max Crack-width $E_{cw1} = 1.70\text{mm}$ 

Figure 5.48: Numerical failure crack pattern of numerical models; (a) H10Q2-PB, and (b) H10Q2-IB

5.3.2. Discussion Modelling Phase III

From the analyses of hybrid beams, the delamination modelled using Coulomb friction model results in peak load that is not different from the case in which a perfect bond is assumed, unlike experiments in which a low peak load is obtained due to debonding of SHCC. Furthermore, the numerical failure crack pattern for hybrid beams modelled with both Perfect Bond (PB) and Imperfect Bond (IB) interface type (properties listed in Table 4.13) is identical, despite delamination in case of IB interface. These observations suggest possible incorrect behaviour of analysed hybrid beams, which could either be due to wrong inputs for mesh size or interface properties, or possible limitation of DIANA in predicting peak loads and failure crack patterns of hybrid beams accurately in case of delamination at the hybrid interface. These aspects are investigated in this section.

Comparison of Peak Load of Strengthened and Un-strengthened Beams

There are some interesting trends observed in peak loads of experimental and numerical results. Table 5.16 compares the experimental peak loads of RC beams with hybrid beams and Table 5.17 compares the numerical peak loads of RC beams with hybrid beams modelled using different hybrid interfaces.

From Table 5.16, it is observed that in experiments, the increase in capacity of RC beams strengthened using SHCC is 38-74% for smaller SHCC thickness (5-10mm) as compared to 21-28% for thicker SHCC layers (20-40mm). This is because of debonding of SHCC layers due to delamination at the hybrid interface for beams with relatively thicker SHCC layers. Similar trend for peak loads is observed in the numerical models as well, as shown in Table 5.17 for both types of hybrid interface. However, the percentage increase in strengthening in each hybrid beam model is higher in the numerical models as compared to experiments. Table 5.18 shows over-prediction of peak loads in the hybrid beam models for all SHCC thicknesses as compared to experiments. The over-prediction is more severe in hybrid beams modelled with relatively thicker SHCC layers (20-40mm).

Table 5.16: Comparison of experimental peak loads of SHCC-RC hybrid beams with RC beams

RC Beam		Hybrid Beam			Increase (%)
Beam	R_{CB} (kN)	Beam	t_{SHCC} (mm)	R_{HYB} (kN)	
CB2	53	H5Q2	5	73	38
		H10Q2	10	92	74
CB1	122	H20Q1	20	148	21
		H40Q1	40	150	28

Table 5.17: Comparison of numerical peak loads of SHCC-RC hybrid beams with RC beams

RC Beam		Hybrid Beam					
Beam	R_{CB} (kN)	Beam	t_{SHCC} (mm)	Perfect Bond		Imperfect Bond	
				R_{PB} (kN)	Increase (%)	R_{IB} (kN)	Increase (%)
CB2	51	H5Q2	5	80	57	78	53
		H10Q2	10	96	88	94	84
CB1	162	H20Q1	20	212	31	216	33
		H40Q1	40	238	47	226	40

Table 5.18: Comparison of peak loads of numerical SHCC-RC hybrid beams with experimental hybrid beams

Beam	t_{SHCC} (mm)	R_{EXP} (kN)	R_{NUM} (kN)			
			R_{PB}	Increase (%)	R_{IB}	Increase (%)
H5Q2	5	73	80	10	78	7
H10Q2	10	92	96	4	94	2
H20Q1	20	148	212	43	216	46
H40Q1	40	150	238	59	226	51

Based on the results presented for the hybrid beams, it is clear that Perfect Bond (PB) hybrid interface type results in an overestimation of numerical peak load in case of interface delamination during experimentation, as is the case for beam H20Q1 and H40Q1. The Imperfect Bond (IB) interface is defined in this thesis to allow for delamination following the stress distribution, resulting in numerical peak loads which are closer to experiments. However, as the results show, the peak loads in models modelled using IB interface only differ by approximately 2-5% as compared to models with a perfect bond. There is a possibility that the IB interface properties (listed in Table 4.13) considered are different from actual experiments (as they are referenced from other studies), still, it needs to be investigated whether modelling the interface delamination using Coulomb friction interface model can affect the peak load significantly or not. Furthermore, the mesh size might also be influencing the peak loads. Additionally, the influence of interface on stiffness, SHCC thickness and the crack pattern is also discussed.

Influence of Interface Delamination and Mesh Size on Peak Load and Stiffness

Additional numerical models of beam H20Q1, listed in Table 5.20, are analysed with variations in interface properties and mesh size. Additional interface types are listed in Table 5.19. The load-deflection response of additional analyses as compared to experiment and model H20Q1-IB is shown in Figure 5.49. Model H20Q1-IB is now denoted as H20Q1-IB-10mm.

To investigate the influence of interface delamination on peak load, beam H20Q1 is modelled using Weak Bond (WB) interface, the properties of which are listed in Table 5.19. The input values for

WB interface are half of the values considered for IB interface (properties listed in Table 4.13). The resulting load-deflection response of model H20Q1-WB-10mm is shown in Figure 5.49. By reducing the tensile strength, friction angle and cohesion values to half in WB interface, the peak load only decreases by approximately 4% in comparison to IB interface and is approximately 41% higher than the experimental peak load.

Table 5.19: Additional analysed hybrid interface types

Name	Notation	Cohesion (MPa)	$\theta_{friction}$ (rad)	Dilatancy	Tension (MPa)
Weak Bond	WB	1	0.305	0	0.5
Hypothetical Bond	HB	0.01	0.01	0	0.01

Table 5.20: Additional analyses of beam H20Q1

Beam	Interface Type	Mesh Size (mm)	Notation
H20Q1	Weak Bond	10	H20Q1-WB-10mm
	Weak Bond	20	H20Q1-WB-20mm
	Hypothetical Bond	20	H20Q1-HB-20mm

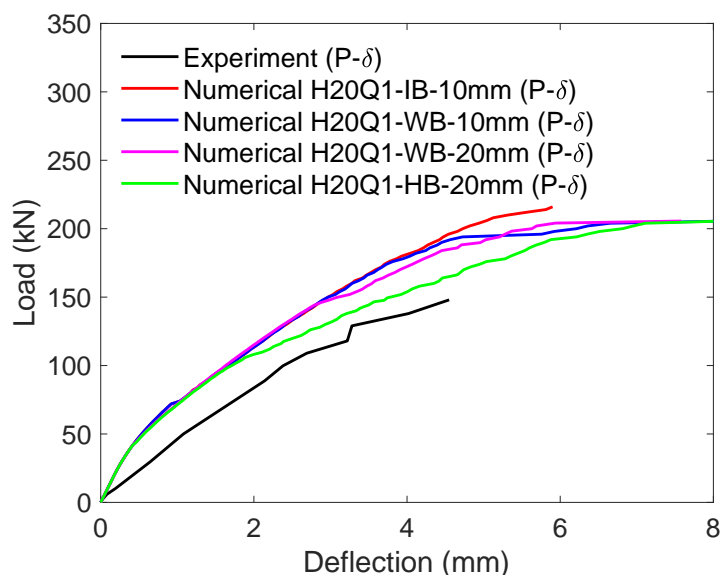


Figure 5.49: Load vs mid-span deflection comparison of additional numerical models of beam H20Q1

Figure 5.50 shows the interface delamination for models H20Q1-IB-10mm and H20Q1-WB-10mm at respective peak loads. It is observed that by reducing the interface properties in WB interface, delamination at the peak load has significantly increased, as expected, but still, the peak load difference between models H20Q1-WB and H20Q1-IB is only 4%.

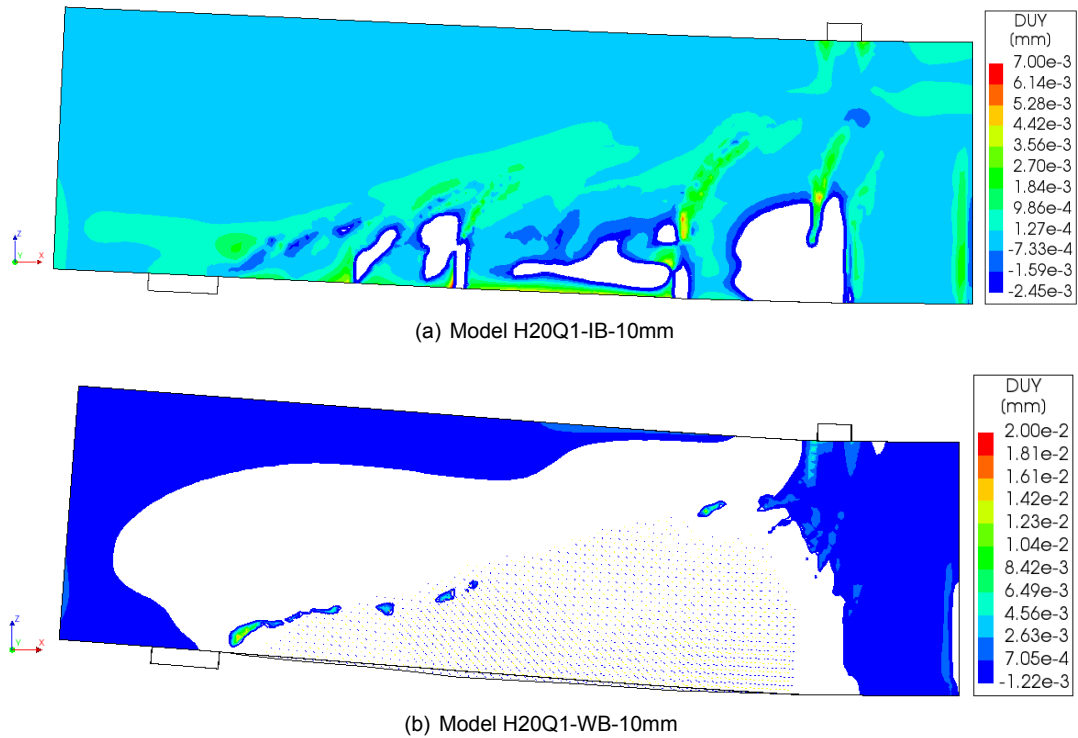


Figure 5.50: Interface displacement DUY in numerical models of beam H20Q1 with varying interface types (white areas present debonded regions)

It is concluded from Modelling Phase I that when modelling the shear behaviour of reinforced concrete (RC) beams using Al-Mahaidi shear retention function (SRF), the ideal mesh size is obtained by having 20 elements in beam height to obtain good results. Since this is not the case for hybrid beams of benchmark study 1 (30 elements in the height of beam when 10mm mesh size is used), the numerical peak loads are expected to be overestimated.

To investigate the possible influence of mesh size on peak load in hybrid beams, model H20Q1-WB is modelled with 20mm mesh size. The resulting load-deflection response of model H20Q1-WB-20mm is also shown in Figure 5.49. It is observed that unlike for RC beams, using a coarse mesh size for a hybrid beam results in almost identical peak load as compared to a fine mesh, with only a 2% difference in values. This indicates that the mesh size is not influencing the numerical peak load of the hybrid beams, unlike RC beams modelled using the same solution strategy. Figure 5.51 shows the interface displacement for models H20Q1-WB-10mm and H20Q1-WB-20mm at respective peak loads. Significant debonding due to delamination at the interface is observed when a coarse mesh size is used in model H20Q1-WB-20mm, still, the peak load is approximately 38% higher as compared to experiment.

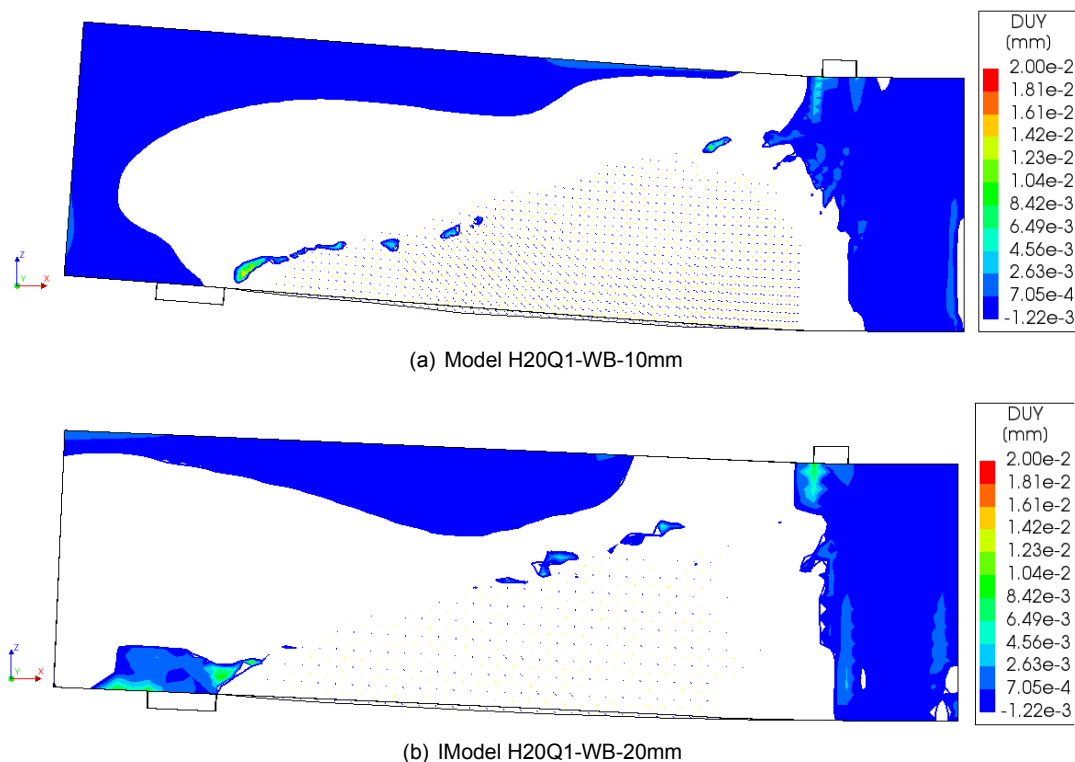


Figure 5.51: Interface displacement DUY of numerical model H20Q1-WB modelled with varying mesh sizes (white areas present debonded regions)

So far, it is observed that irrespective of increasing the mesh size and the magnitude of delamination at the hybrid interface, the peak loads in the numerical models are not comparable to experimental values. This suggests that the numerical model continues to load SHCC and concrete layers even after significant delamination at the hybrid interface, till the load step after which poor convergence due to yielding of reinforcement is observed. To investigate this aspect, beam H20Q1 is now modelled with interface properties taken close to zero, as listed in Table 5.19. This interface is called Hypothetical Bond (HB). (Note: term “Hypothetical” is used because the input interface values are extremely low as compared to hybrid interfaces constructed in reality)

The resulting load-deflection response of model H20Q1-HB-20mm is also shown in Figure 5.49. Again, the peak load is almost identical to previous numerical models even though an extremely weak interface is modelled. Figure 5.52 shows the interface delamination at a load of 100kN and peak load for model H20Q1-HB-20mm. It is observed that most of the interface has significantly delaminated till a load of 100kN, yet, the numerical model adds another 95kN to the capacity. The beam fails at approximately 195kN, where the longitudinal reinforcement yields, as shown in Figure 5.53 ($f_y = 374\text{MPa}$). This supports the hypothesis in the previous paragraph that irrespective of the magnitude of delamination, the numerical model continues to load the beam till the load step where poor convergence due to yielding of reinforcement is observed.

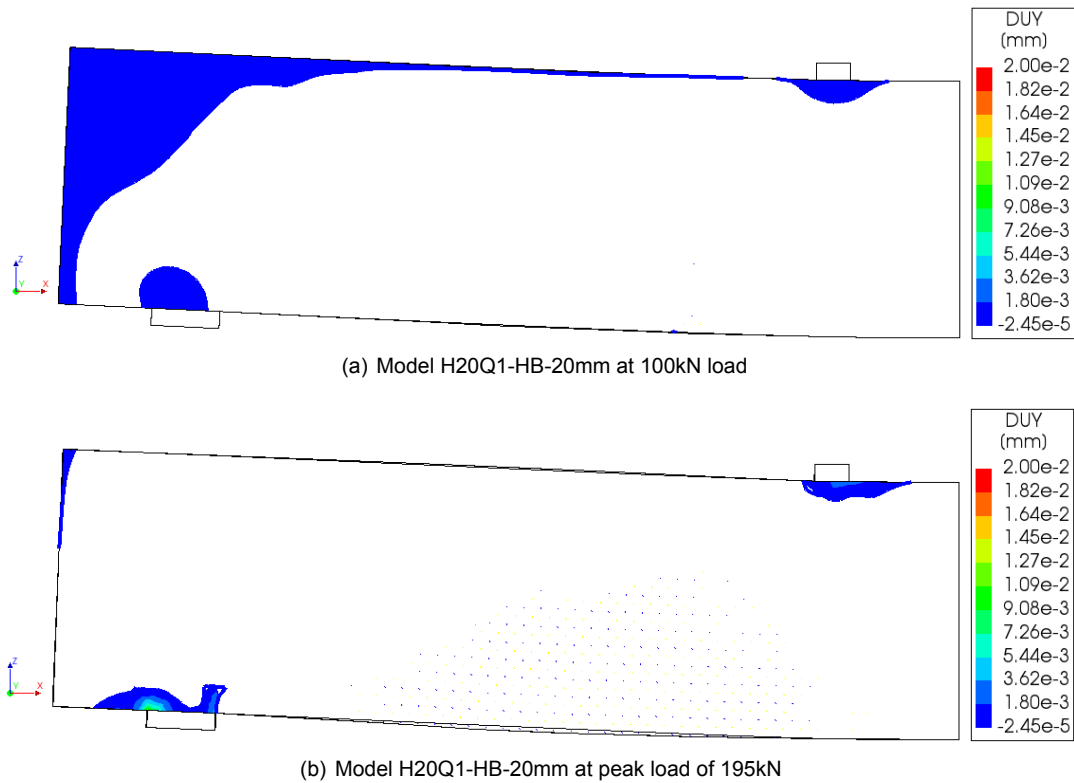


Figure 5.52: Interface displacement DUY in numerical model H20Q1-HB-20mm at different loads (white areas present debonded regions)

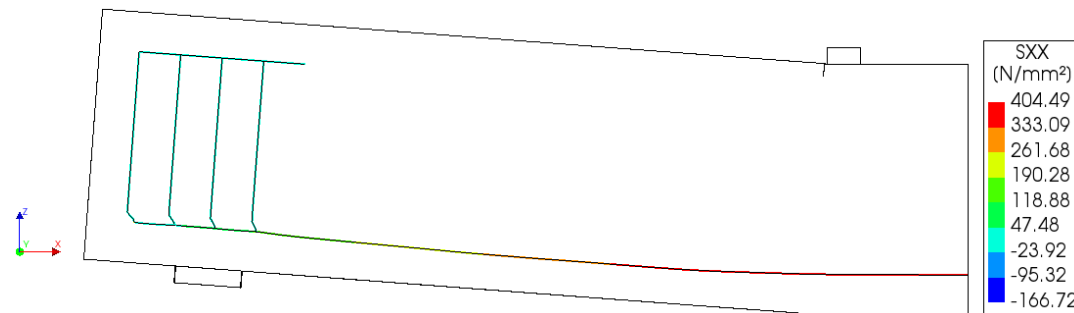


Figure 5.53: Reinforcement stresses SXX in numerical model H20Q1-HB-20mm

It is important to understand why the numerical model continues to load the beam even though the interface has almost completely delaminated. To check this, a small-scale model of SHCC and concrete layers with IB interface properties loaded in tension with eccentricity is tested, and the details are provided in Appendix D. It is observed that a numerical failure (divergence) due to interface is only possible once the SHCC and concrete layers have completely debonded due to exceeding the tensile strength of the interface. And as observed in Figure 5.52, there are parts of the interface close to edges and load and support plates which are not delaminated even till the peak load. Therefore, the model continues to load the beam, only now, the SHCC and concrete layers are being loaded separately, and the analysis is stopped at the load step after which poor convergence due to yielding of reinforcement is observed.

The numerical behaviour of interface delamination is different from the observation in experiments. As observed during experimentation for beams H20Q1 and H40Q1, once the interface partially delaminates, the experiment continues for a few load steps before the SHCC layers peel off of con-

crete. But in the numerical models, even though the interface is mostly delaminated, the numerical model continues to load the beams giving higher load capacity. Therefore, there exists limitation of DIANA in accurately modelling the selected hybrid beams when delamination at the hybrid interface is considered.

It can also be observed from the load-displacement response in Figure 5.19 that the stiffness of the numerical model reduces once the interface delaminates, like for model H20Q1-HB-20mm at around 100kN. A possible reason for this is that once SHCC layer debonds from concrete, the additional cracks that develop in the concrete layer are not restrained by the SHCC layer, thereby, resulting in excessive cracking of the concrete layer. This increased volume of cracked concrete in case of excessive delamination possibly results in lower stiffness.

Influence of SHCC Thickness on Interface Delamination

In experiments, beams H20Q1 and H40Q1 show debonding of SHCC layers at the failure load, however, in the numerical models for both beams, delamination using IB interface is only significant in model H40Q1-IB as compared to model H20Q1-IB. This difference is investigated by constructing a simplified 2D model of the quarter model of a hybrid beam, as shown in Figure 5.54.

The simplified model represents the cross-section of the quarter model of the hybrid beam, with concrete on the right and SHCC on the left. Symmetry supports are provided along the extreme edge of the concrete layer. Load and support plates are provided at the top and bottom respectively, and the model is loaded in uniaxial tension via displacement-controlled method at the top. Modelling of pure tension behaviour might be a misrepresentation of the simulated behaviour in the hybrid beams as shear is not considered, however, for now, the simplified model is studied by applying a tensile load. IB interface properties (listed in Table 4.13) are modelled, having a critical displacement of 0.00245mm, beyond which debonding of layers is observed in the hybrid beams. The displacement of the interface is measured at Point A, as shown in Figure 5.54. Two thicknesses of SHCC are evaluated; 20mm and 40mm. The respective numerical models are denoted as “SHCC-IB-20mm” and “SHCC-IB-40mm”. The model is constructed in XY plane and interface displacement is represented by DUX, which is the displacement normal to the interface. Negative values of displacement DUX represent opening at the interface. Numerical solution strategy SS2 is used to analyse the simplified models, and the material properties for SHCC and concrete are kept the same as for beams H20Q1 and H40Q1. A mesh size of 20mm is used.

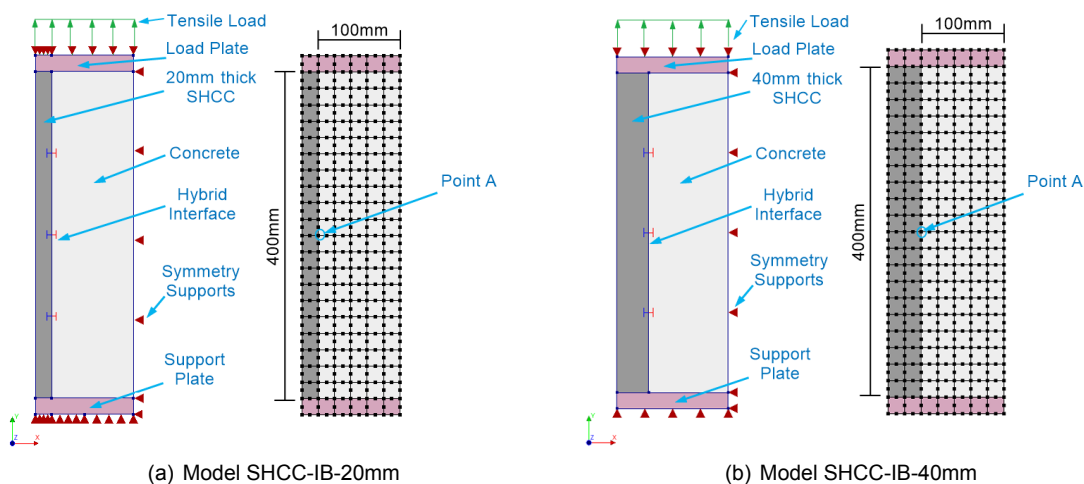


Figure 5.54: Geometry and mesh configuration of simplified models

Plot of interface displacement DUX vs load factor for the considered models is shown in Figure 5.55. The critical displacement value is denoted as “Failure Limit - IB Interface”. It is observed that when

a relatively small thickness of 20mm for SHCC is used, there is some delamination in the beginning, however, from around a load factor of 0.014 onwards, the delamination is almost zero. In contrast, for relatively high SHCC thickness of 40mm, the delamination at the interface continues to increase with increasing load before eventually the failure limit is reached at a load factor of 0.025, resulting in debonding of SHCC layer.

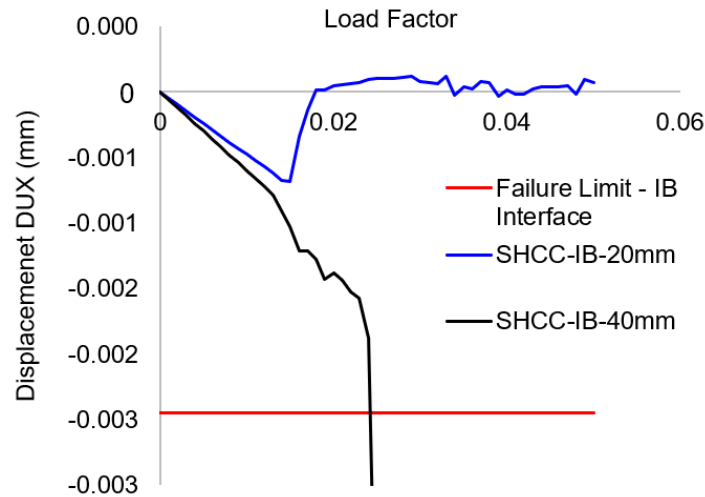


Figure 5.55: Interface displacement DUX vs load factor plot for simplified models of varying SHCC thickness

The deformation of models at load factor of 0.025 is shown in Figure 5.56. The debonding is evident in model SHCC-IB-40mm, however, the SHCC layer is not debonded from concrete in model SHCC-IB-20mm. No debonding is observed in model SHCC-IB-20mm at Point A. This explains why very little delamination is observed for hybrid beam H20Q1-IB with a thickness of 20mm of SHCC as compared to experiment.

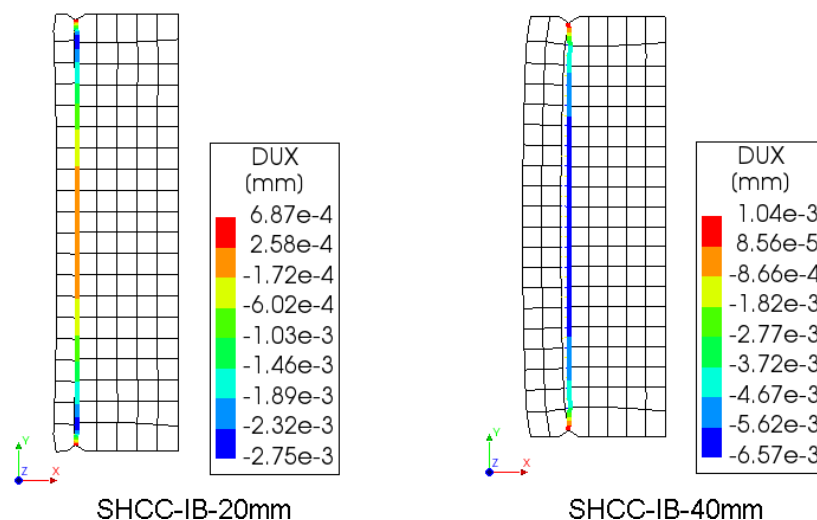


Figure 5.56: Deformation and interfacial displacement DUX at 0.025 load factor of simplified models with varying SHCC thickness

The simplified model is further tested for 20mm thickness of SHCC, only now the delamination at the interface is modelled using WB interface type (properties listed in Table 5.19). The model is denoted as “SHCC-WB-20mm”. The interface configuration of this model is similar to model H20Q1-WB-20mm, in which delamination at the interface is observed. The interface displacement DUX vs

load factor response and deformation for model SHCC-WB-20mm are shown in Figure 5.57. It can be observed that the delamination behaviour at the interface in simplified model SHCC-WB-20mm is similar to that observed in the hybrid beam H20Q1-WB-20mm.

Even though the stress-state in the simplified model is different from the actual hybrid beam, it can explain the delamination behaviour for hybrid beams modelled with varying SHCC thicknesses and interface types.

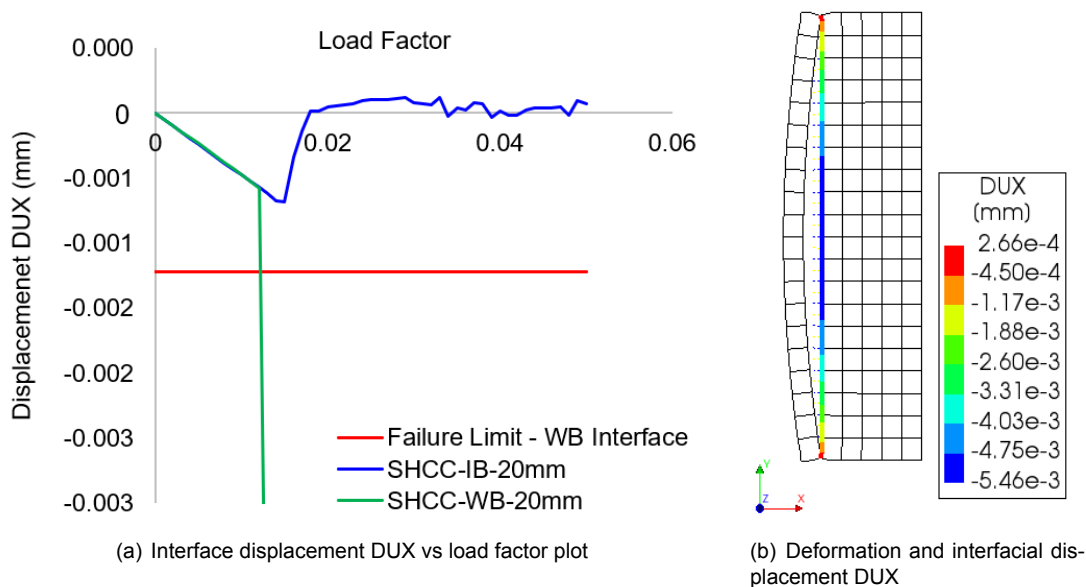


Figure 5.57: Results of simplified model SHCC-WB-20mm

Observation of increased SHCC thickness resulting in delamination failure in the numerical models is consistent with the results observed during experimentation in benchmark studies. A small SHCC thickness means that the SHCC layers can crack at lower loads and the hybrid beams fail due to excessive cracking instead of delamination, as observed in experimental beams H20Q1, H5Q2 and H10Q2. Note that cracking does lead to debonding of SHCC, but is not the governing failure parameter in the beams mentioned above. In contrast, too thick SHCC, as in H40Q1 beam, requires a higher load to crack due to increased stiffness. A consequence of this is the loss of bond strength at the hybrid interface, resulting in failure of the hybrid beam due to delamination. The same concept can be applied for the hybrid beams modelled using IB interface in this thesis. It is observed that multiple localized cracks in all but H40Q1-IB hybrid beam are observed, which suggests that SHCC is not too thick to result in failure due to delamination and can crack significantly. However, in hybrid beam H40Q1-IB, significant delamination is observed, and cracks are not well distributed.

The above described influence of the thickness of SHCC overlay on delamination is consistent with van Zijl's observation on masonry specimens strengthened using SHCC overlay of varying thickness [54]. It is reported that if the thickness of the SHCC overlay exceeds a certain threshold, then instead of cracking in SHCC overlay, delamination at the interface occurs. Characterising a "too" thick SHCC is subjective. For example, if a very weak hybrid interface is developed, then even relatively thin SHCC overlay can result in failure due to debonding. However, if a relatively strong bond is used, then exceeding a certain threshold value of SHCC thickness leads to failure due to delamination at the interface.

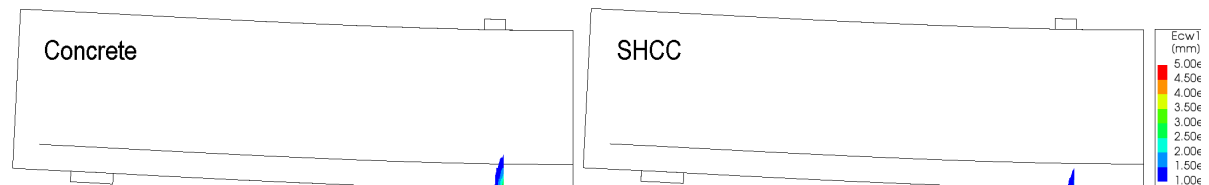
Influence of Interface Delamination on Failure Type

For the four tested hybrid beams, correct failure type is predicted in the numerical models for the two beams of benchmark study 1 (H20Q1 and H40Q1). The numerical failure type for hybrid beams of benchmark study 2 (H5Q2 and H10Q2), as reported, cannot be directly compared with the experimental results. This is because post-peak behaviour is not captured in the numerical models unlike experiments and the experimental failure crack pattern provided in the study is corresponding to the ultimate load and not the peak load as in the numerical model. Still, it can be seen in Figures 5.44 and 5.48 that the main shear flexure crack is transforming to shear tension crack, similar to experiments.

Interestingly, no significant difference in the failure crack pattern is observed when the interface type is varied between Perfect Bond (PB) and Imperfect Bond (IB) (properties listed in Table 4.13), despite of debonding of SHCC, as in model H40Q1-IB. To investigate whether delamination influences the failure crack pattern, it is important to understand how cracks are developing in the hybrid beam.

It is observed in all the hybrid beam models modelled in this thesis that cracks localize at the same load in both SHCC and concrete layers. This is illustrated in Figure 5.58, which shows cracks in concrete and SHCC layers separately at the point of localization in model H20Q1-WB-20mm at 44kN load. At the time of localization, there is no delamination of the interface and the cracks in concrete result in the cracking of adjacent SHCC elements at the interface. Therefore, the cracks localized in concrete and SHCC are identical in terms of location. As the load increases, additional elements crack in both concrete and SHCC, and already localized cracks increase in width.

(a) Crack localisation at 44kN load in concrete and SHCC



(b) Interface displacement DUY at 44kN load (no debonding)

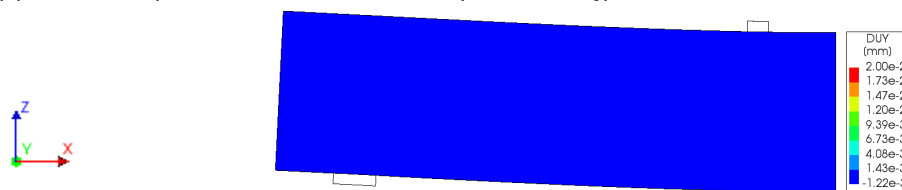
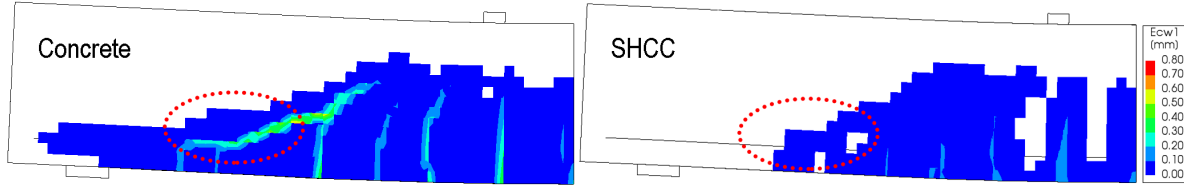


Figure 5.58: Results for H20Q1-WB-20mm at 44kN load; (a) Crack pattern at localization in SHCC and concrete layers separately (b) Interface displacement (white areas present debonded regions)

Upon loading further up till 152kN, delamination at the bottom can be observed, resulting in localized partial debonding of SHCC. An additional localized crack develops in the highlighted region in the concrete layer, however, it does not result in development of a localized crack in SHCC due to delamination at the hybrid interface.

(a) Crack pattern at 152kN load in concrete and SHCC



(b) Interface displacement DUY at 152kN load

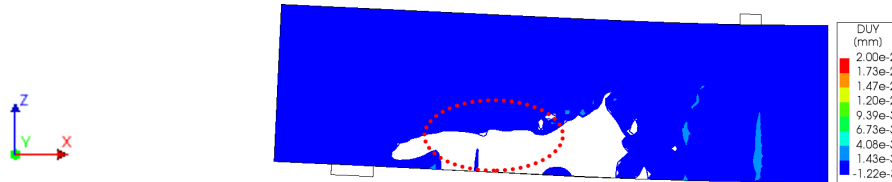
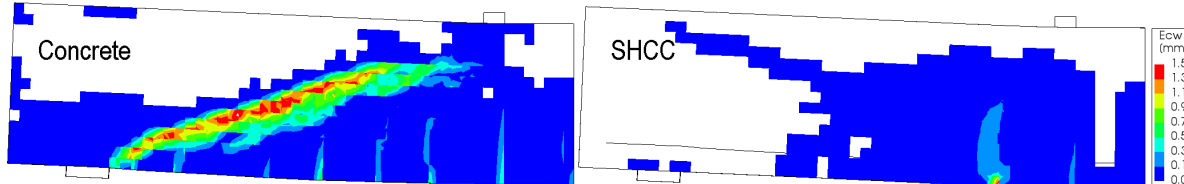


Figure 5.59: Results for H20Q1-WB-20mm at 152kN load; (a) Crack pattern at point of increased delamination (b) Interface displacement (white areas present debonded regions)

Close to peak load at 195kN, the SHCC layer further debonds, and the crack pattern remains different in SHCC layer as compared to concrete. This is because the region in which additional cracks localize in concrete is already debonded from SHCC. With increasing load, concrete cracks more and already developed cracks localize further, but due to delamination, SHCC does not develop a localized crack in the same region. However, this does not mean that the SHCC does not crack with increasing load once it is debonded from concrete.

The above discussion indicates that delamination does influence the crack pattern developed on the SHCC layer in the numerical model. This also proves that the layers continue to get loaded separately even after delamination in the numerical model.

(a) Crack pattern at 195kN load in concrete and SHCC



(b) Interface displacement DUY at 195kN load

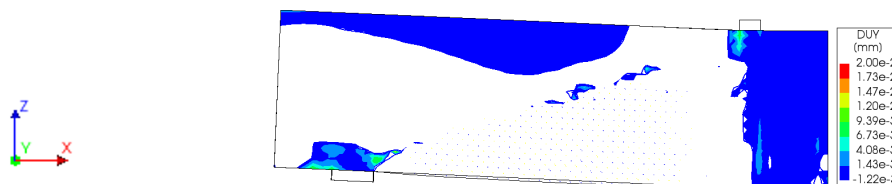


Figure 5.60: Results for H20Q1-WB-20mm at peak load of 195kN load; (a) Crack pattern (b) Interface displacement (white areas present debonded regions)

The reason why the hybrid beams modelled earlier show similar crack pattern irrespective of the interface type is the fact the load at which interface delaminates is close to the numerical capacity of the beams, and before the interface could delaminate further and concrete could develop a new crack in the delaminated region, peak load is reached and the analysis stops.

Influence of Quarter Model Configuration

A quarter of the geometry of hybrid beams is modelled in this thesis to reduce computation time. A recent study at TU Delft [5] reports that modelling of a quarter of a pile cap geometry results in an overestimation of peak load due to an initial peak that occurs because of overestimation in post-cracking stiffness. However, the quarter model is reported to be a decent approach for modelling the failure crack pattern and it also reduces computation time significantly. In order to compare the difference in results of a quarter beam model with half and full-scale models, a sample hybrid beam is analysed. The geometries of the hybrid beams are shown in Figure 5.61. The quarter model is constructed using the same approach for previously analysed hybrid beams. Perfect Bond (PB) hybrid interface condition is modelled. "Mirror" function in DIANA is used to make half-scale and full-scale models from the same quarter model.

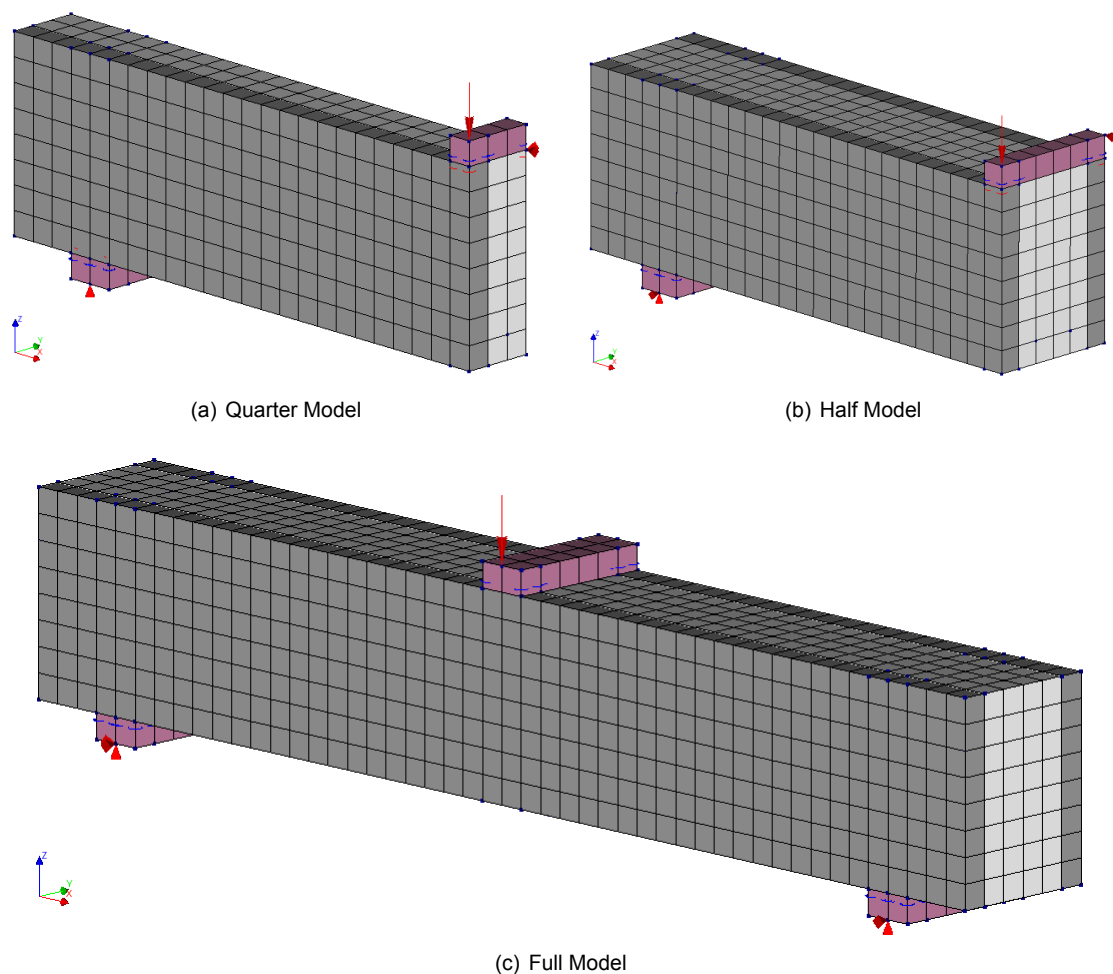


Figure 5.61: Different geometries of sample hybrid beam

Figure 5.62 shows the load-deflection response obtained for the quarter, half and full-scale models of the hybrid beam. The overall load-deflection response of the three types of geometries is identical, with only a slight difference in the peak loads observed. The quarter model gives the highest peak load as compared to the other two models. However, as observed from Figure 5.63, the failure crack patterns are almost identical. Therefore, the hybrid beams with perfect bond interface can be modelled using a quarter model, keeping in mind the slightly high peak load obtained. Hybrid beams including delamination at the hybrid interface are not assessed since they already result in inaccurate predictions of peak loads and failure patterns, as described earlier.

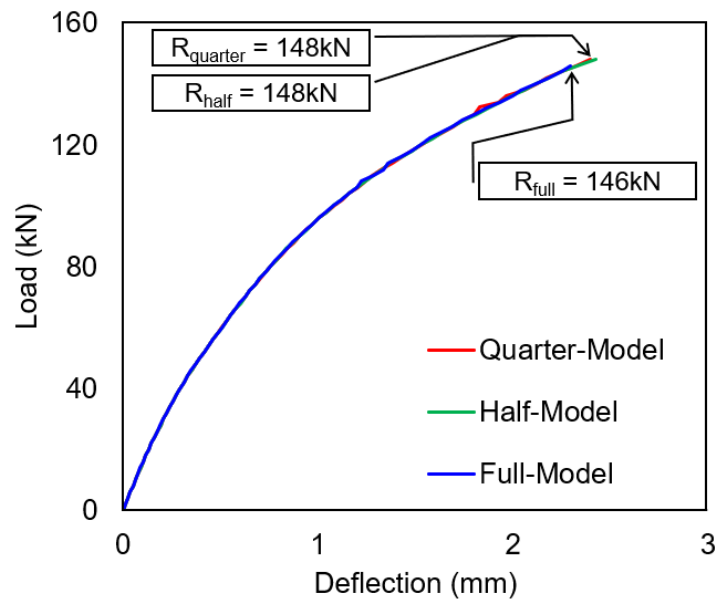


Figure 5.62: Load vs mid-span deflection comparison of quarter, half and full-scale models of a sample hybrid beam

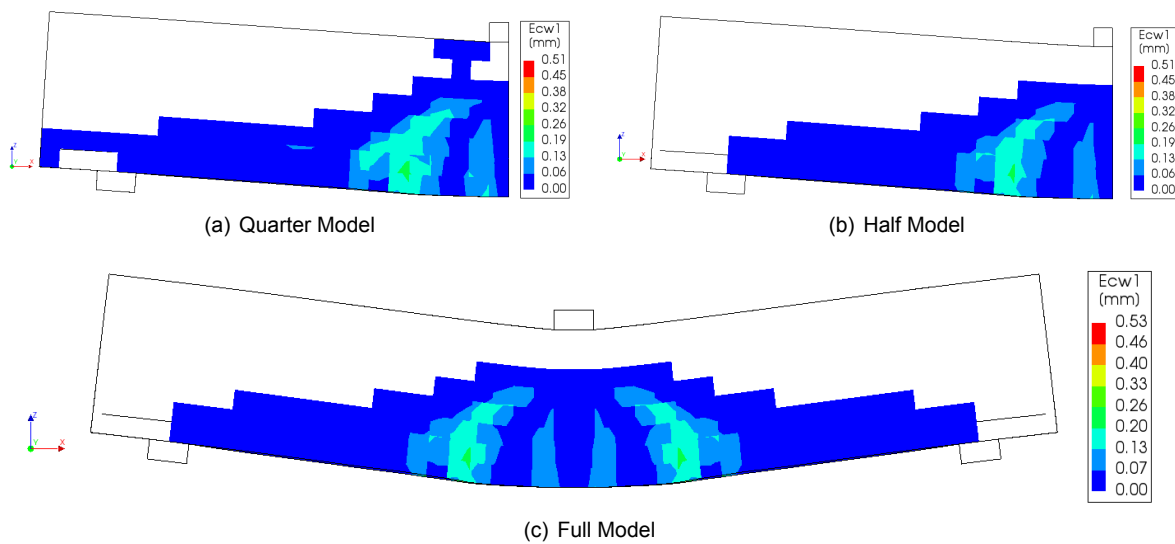


Figure 5.63: Failure crack pattern of different geometries of sample hybrid beam

5.3.3. Conclusions Modelling Phase III

1. In case of no delamination during experimentation at the hybrid interface like in beams H5Q2 and H10Q2, analysis of such hybrid beams using Al-Mahaidi shear retention function and consideration of perfectly bonded hybrid interface results in an accurate prediction of peak loads and failure type. The predicted peak loads differ by only 2% to 10% as compared to experiments. This is valid for a mesh size which results in 20 elements in the height of the beam, as described in Modelling Phase I.
2. In case of delamination during experimentation at the hybrid interface like in beams H20Q1 and H40Q1, analysis of such hybrid beams using Al-Mahaidi shear retention function and consideration of delamination at the hybrid interface using Coulomb friction model results in inaccurate prediction of peak loads and failure type due to limitation of DIANA in recognising significant delamination at the hybrid interface as reason for failure of hybrid beam. The beam can only fail numerically due to delamination once all the elements at the interface have delaminated, which is impossible to simulate. Consequently, the debonded SHCC and concrete layers are continued to be loaded till numerical failure due to poor convergence is obtained, resulting in an overestimation of peak load and wrong prediction of failure crack pattern.
3. Although numerically, delamination is observed at the hybrid interface modelled using Coulomb friction model, the inability of DIANA in recognising this as reason for failure of hybrid beam results in inaccurate prediction of peak loads of hybrid beams with increasing SHCC thickness, which is contrary to experimentation.
4. Negligible mesh size influence is observed in hybrid beams modelled for delamination due to limitation of DIANA in modelling delamination at the interface using Coulomb friction model accurately.
5. Using a quarter geometry of hybrid beams results in approximately 1% difference in peak load and almost no difference in failure crack pattern as compared to full-scale model.

5.4. Conclusions

This thesis aims to study the shear behaviour of SHCC-RC hybrid beams, focusing on the contribution of SHCC in increasing the shear capacity of reinforced concrete beams and behaviour of the hybrid interface. First, the shear behaviour of reinforced concrete beams is evaluated using two types of shear retention functions considered from the available models in DIANA FEA software. Based on the results obtained, a single shear retention function is selected to model, first, a reinforced SHCC beam and then finally, SHCC-RC hybrid beams with varying types of hybrid interface.

Shear Behaviour of Reinforced Concrete Beams

Shear behaviour of reinforced concrete beams is analysed using two numerical solution strategies, varying in the type of shear retention function considered; Damage-based and Al-Mahaidi.

- Analysis of the selected reinforced concrete beams using Damage-based shear retention function results in an accurate prediction of peak loads if a mesh size, resulting in 30 or more elements in the height of the beam, is used. In comparison, a relatively coarser mesh size leads to inaccurate prediction of peak load due to lack of consideration of aggregate interlock. The failure type is inaccurately predicted regardless of the mesh size considered due to lack of consideration of aggregate interlock as well.
- Analysis of the selected reinforced concrete beams using Al-Mahaidi shear retention function results in an accurate prediction of peak load if a mesh size, resulting in 20 elements in the height of the beam, is used. The type of shear failure is also correctly predicted, and the shear crack angle differs on average by 6.5% only as compared to experiments. Implicit consideration of aggregate interlock in the form of shear retention factor β allows beams analysed using Al-Mahaidi shear retention function to predict the failure load and failure type accurately. In comparison, a relatively fine mesh size results in an inaccurate prediction of both peak load and failure type.

Based on the numerical results, it is concluded that the numerical solution strategy consisting of Al-Mahaidi shear retention function performs better in predicting both the failure load and failure type relatively accurately.

Shear Behaviour of Reinforced SHCC Beam

Shear behaviour of reinforced SHCC beam is analysed using numerical solution strategy consisting of Al-Mahaidi shear retention function only.

- Modelling of shear behaviour of reinforced SHCC beam with a numerical solution strategy consisting of Al-Mahaidi shear retention function is not able to correctly predict the peak load and failure crack pattern. The model suffers from poor convergence due to excessive cracking along the longitudinal reinforcement, failing at a load lower than the experimental peak load. Consequently, an inaccurate numerical failure crack pattern is obtained as compared to the experiment.

From the numerical analysis, it is concluded that the numerical solution strategy consisting of Al-Mahaidi shear retention function is not able to model the shear behaviour of a reinforced SHCC beam accurately.

Shear Behaviour of SHCC-RC Hybrid Beam

Although the behaviour of a reinforced SHCC beam using the numerical solution strategy consisting of Al-Mahaidi shear retention function is not reliably modelled, still, the same solution strategy is used to analyse SHCC-RC hybrid beams since the SHCC layer in hybrid beams is not reinforced. The numerical failure load and failure type of hybrid beams are influenced by the type hybrid interface considered.

- The peak load and failure type is accurately predicted when a numerically perfect bond condition is modelled at the hybrid interface for hybrid beams exhibiting no debonding during experimentation, like beams H5Q2 and H10Q2. Accurate prediction of peak loads and failure type in such hybrid beams is in the case when a mesh size resulting in 20 elements in the height of the beam is used, as suggested in the modelling of reinforced concrete beams using Al-Mahaidi shear retention function.
- Modelling for delamination at the hybrid interface, in case of delamination during experimentation (like in beams H20Q1 and H40Q1), results in an inaccurate prediction of peak load and failure type. This is due to the inability of the numerical model in recognising significant delamination at the hybrid interface, modelled using the Coulomb friction model, as a possible reason for the failure of the hybrid beam. This is a limitation of DIANA. A numerical failure due to delamination at the hybrid interface is only possible if all the elements at the hybrid interface have delaminated, which is impossible to simulate. Consequently, the SHCC and concrete layers are continued to be loaded till numerical failure due to poor convergence is obtained, resulting in an inaccurate prediction of peak load and failure crack pattern.
- In experiments, increasing the thickness of SHCC layers from 20mm to 40mm results in only 1.4% increase in peak load because of failure due to delamination with increased SHCC thickness. However, as the numerical model is not able to recognise significant delamination at the hybrid interface (modelled using Coulomb friction) as a possible reason for the failure of the hybrid beam, the peak loads are inaccurately predicted for hybrid beams modelled with varying SHCC thicknesses as well.
- Unlike reinforced concrete beams, the influence of mesh size is negligible in hybrid beams modelled for delamination due to limitation of DIANA in modelling failure of the hybrid beam due to delamination at the interface.
- Hybrid beams with a perfect bond modelled using a quarter geometry result in a relatively higher peak load as compared to a full-scale model. However, the difference is only approximately 1%, and the failure crack pattern is almost identical in both cases. Therefore, keeping in mind the slightly high peak load, quarter models to model hybrid beams with a perfectly bond interface can be used.

From the analyses of all hybrid beams, it is concluded that the numerical solution strategy consisting of Al-Mahaidi shear retention function is only able to accurately predict the failure load and failure type of those experimental hybrid beams in which failure due to delamination is not observed. However, in case of failure due to delamination, the numerical models inaccurately predict the peak load and failure type, and the results are not reliable.

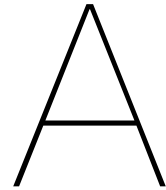
6

Recommendations

1. It is recommended to expand the benchmark reinforced concrete beams to include beams with shear span-to-effective depth ratio less than 3 in order to assess the feasibility of the defined numerical solution strategies in modelling beams failing due to brittle failure of the compressive strut.
2. In the thesis, all the beams analysed using Al-Mahaidi shear retention function are modelled using a single value of minimum shear retention factor β_{min} . As reported in the literature, change in the value of β_{min} affects the behaviour of the beam analysed. Therefore, a sensitivity study can be performed to determine the optimum value of β_{min} to model reinforced concrete beams with a shear span-to-effective depth ratio of 3, failing due to shear-tension or shear-compression.
3. This research work is the first time that SHCC-strengthened reinforced concrete beams failing in shear are modelled in DIANA. Therefore, RC beams strengthened using SHCC on sides of the beam are only evaluated. As reported in the literature, reinforced concrete beams can be strengthened using a 3-sided jacketed configuration. Evaluating the solution strategies developed in this thesis on such type of hybrid beams will also be beneficial to study.
4. The analysis of beams without transverse reinforcement is significantly influenced by the choices in a numerical solution strategy, i.e. the constitutive model, mesh size, shear retention function, reinforcement type, convergence criteria and the maximum number of iterations per load step. There are studies performed in DIANA to model reinforced concrete beams without transverse reinforcement in which these parameters are varied. However, the influence of variation of most of these parameters on hybrid beams is not studied, and only shear retention function is varied in this thesis. It will be beneficial to study shear behaviour of hybrid beams without transverse reinforcement by varying other parameters that make up a solution strategy as well.
5. For modelling micro-cracking behaviour of SHCC, generally, fine mesh size is used. In this thesis, the tensile behaviour of SHCC is defined using a multi-linear curve, which is not mesh size-dependent. Therefore, it is recommended to model reinforced SHCC beams with fine mesh sizes to assess if the micro-cracking behaviour is captured accurately or not. Furthermore, bond-slip reinforcement can be used to possibly avoid excessive cracking along the reinforcement.
6. Interface delamination in hybrid beams is modelled in this thesis using the Coulomb friction model, as implemented in DIANA FEA software package. However, the results show that the failure of the hybrid beam due to delamination is incorrectly modelled. There are additional formulations in DIANA to model the delamination behaviour at the hybrid interface, and their study will be beneficial in judging whether DIANA can be reliably used to model hybrid beams which exhibit failure due to delamination at the hybrid interface.

7. Numerical stability at the onset of cracking and capturing of post-peak response in beams failing in a brittle manner like shear is challenging to achieve. Analysis of beams using tools like arc-length and line-search in DIANA might be beneficial to use to avoid poor numerical stability and to capture post-peak response if a load-controlled analysis is performed, respectively.

Appendices



Convergences of the Numerical Models

Part I

Modelling Phase I

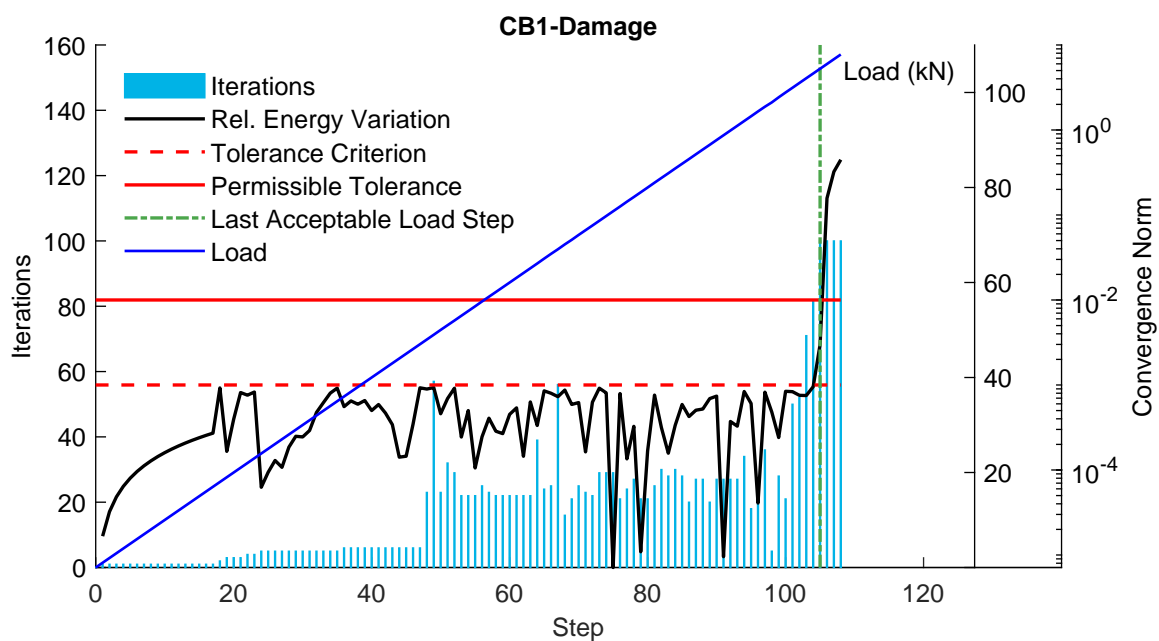


Figure A.1: Convergence plot for model CB1-Damage

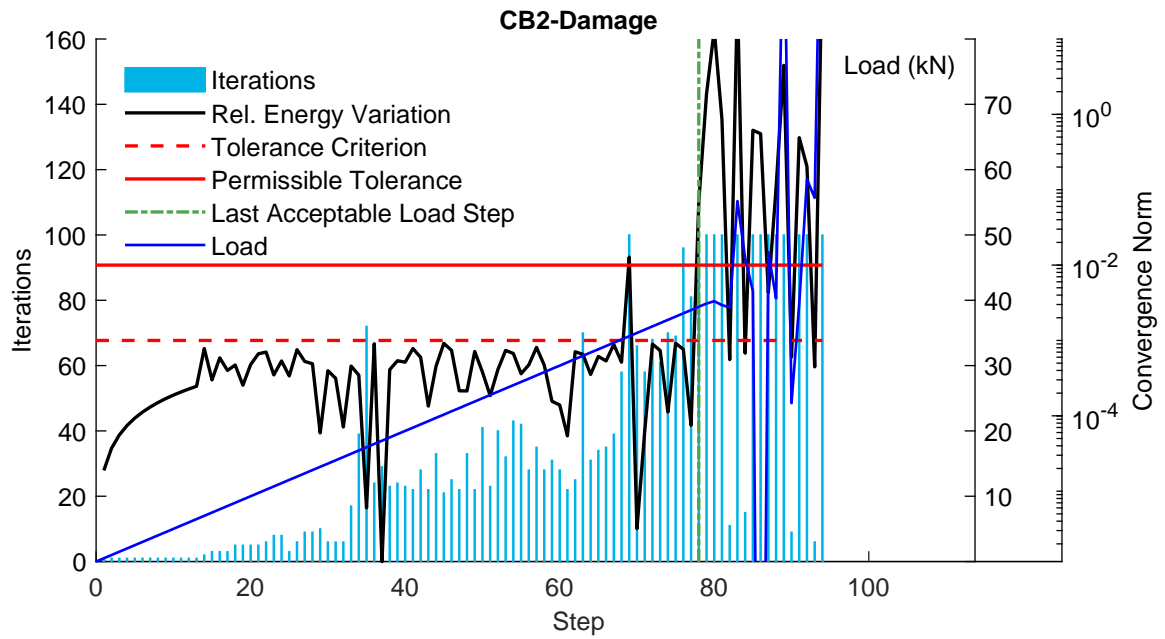


Figure A.2: Convergence plot for model CB2-Damage

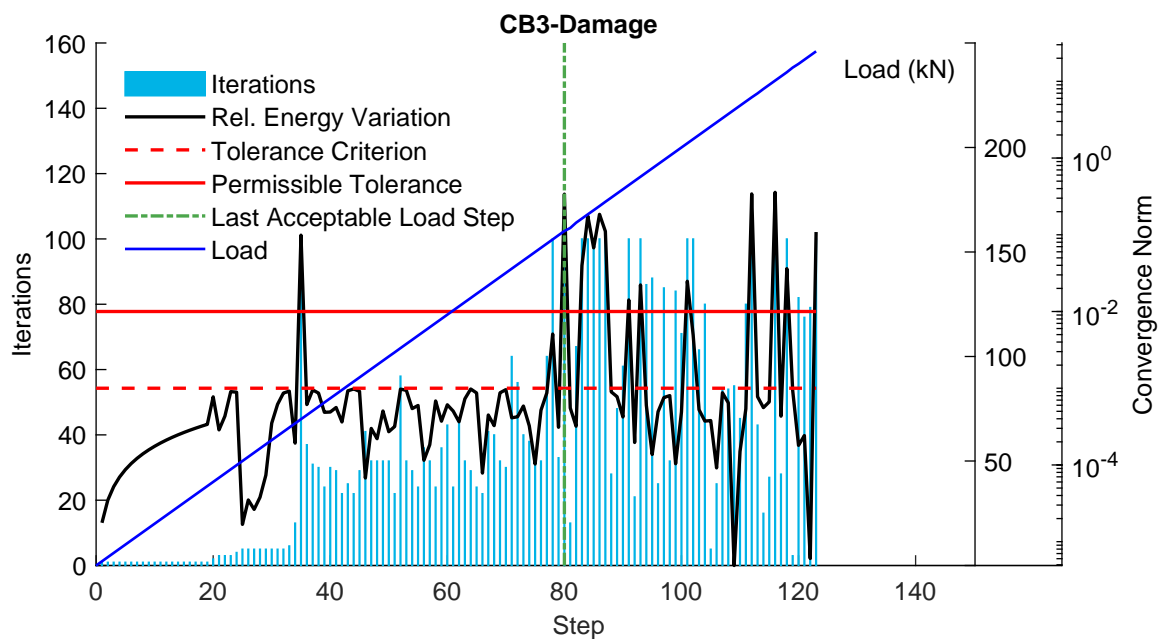


Figure A.3: Convergence plot for model CB3-Damage

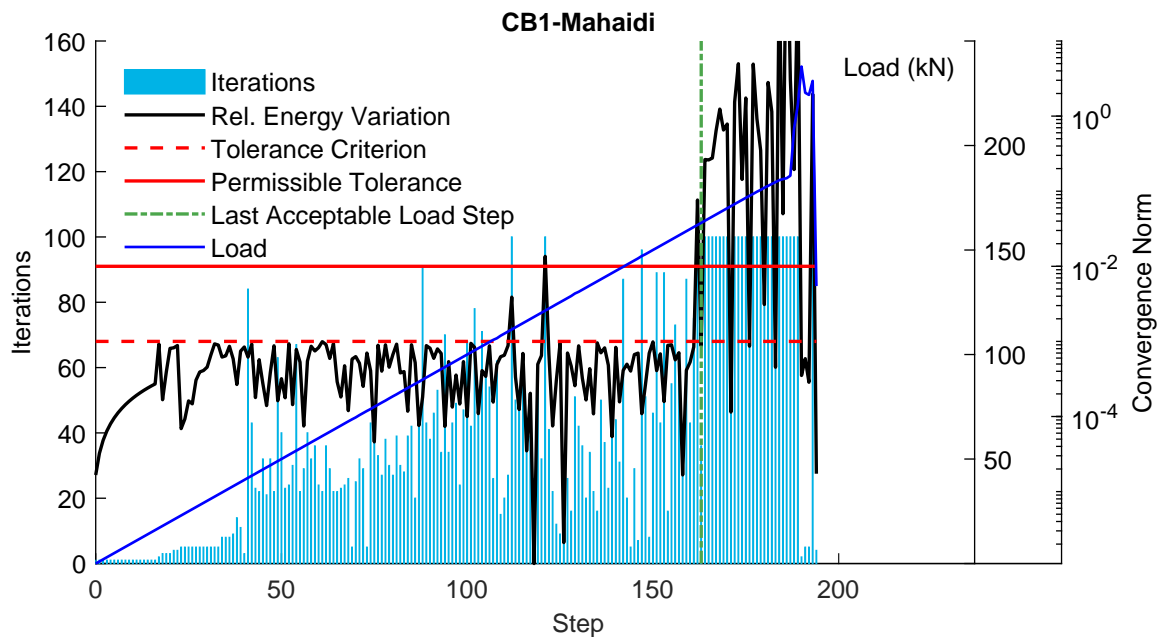


Figure A.4: Convergence plot for model CB1-Mahaidi

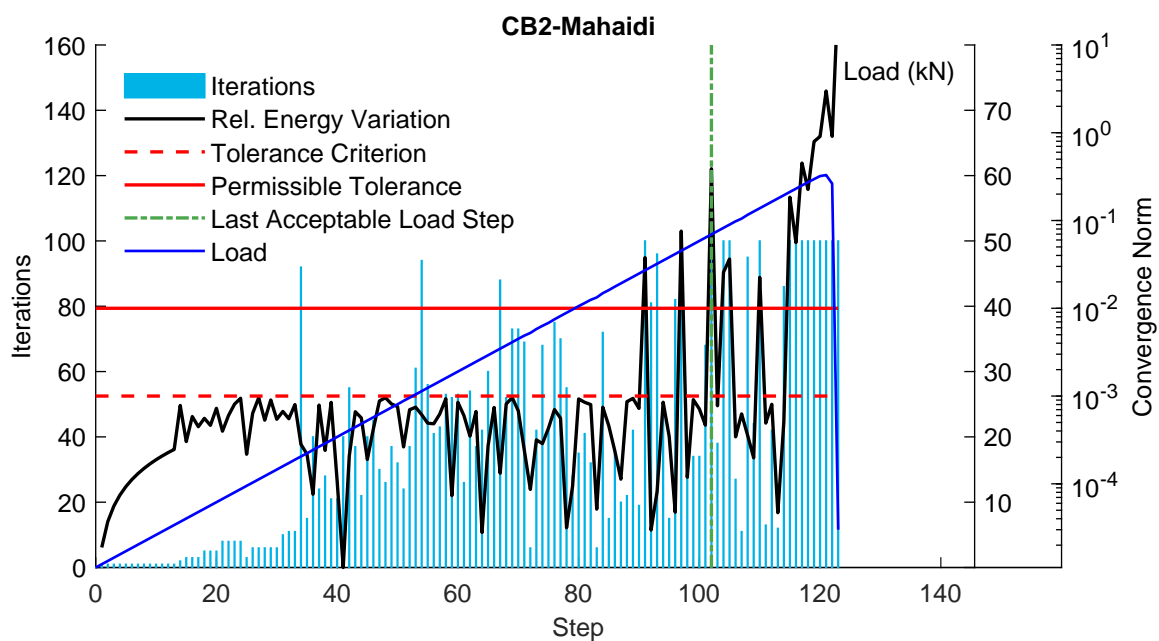


Figure A.5: Convergence plot for model CB2-Mahaidi

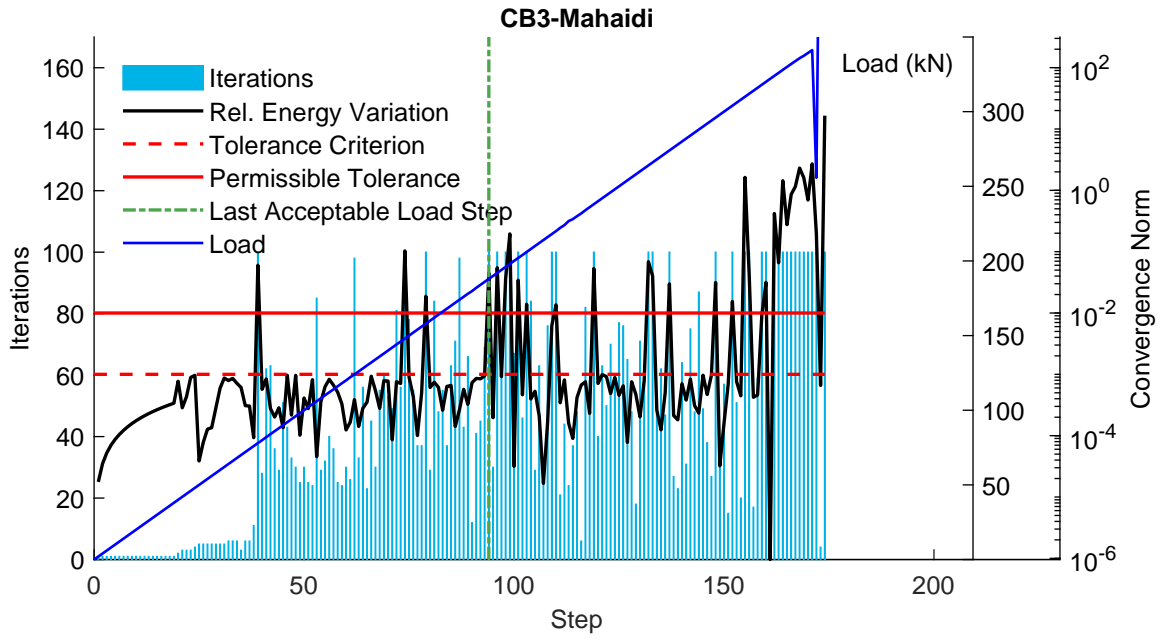


Figure A.6: Convergence plot for model CB3-Mahaidi

Modelling Phase II

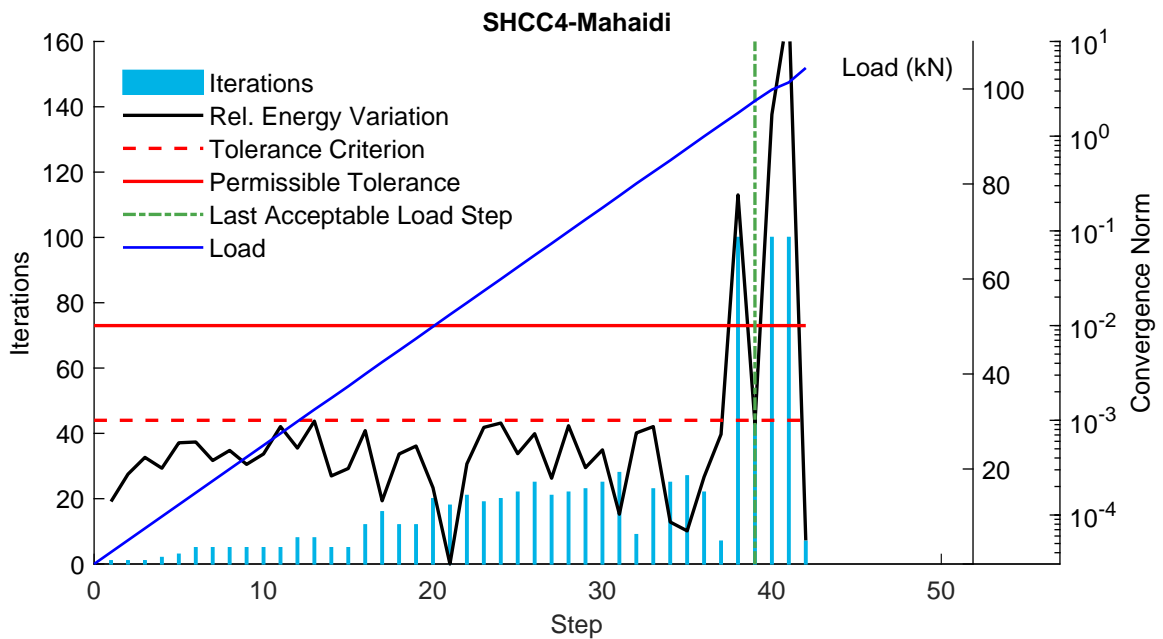


Figure A.7: Convergence plot for model SHCC4-Mahaidi

Modelling Phase III

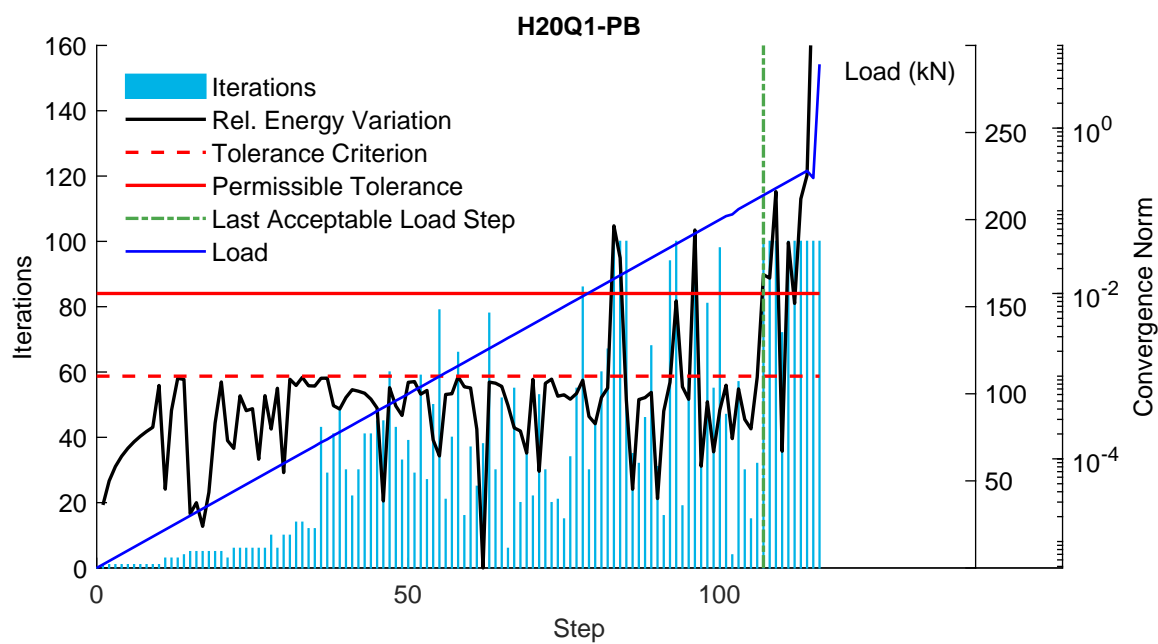


Figure A.8: Convergence plot for model H20Q1-PB

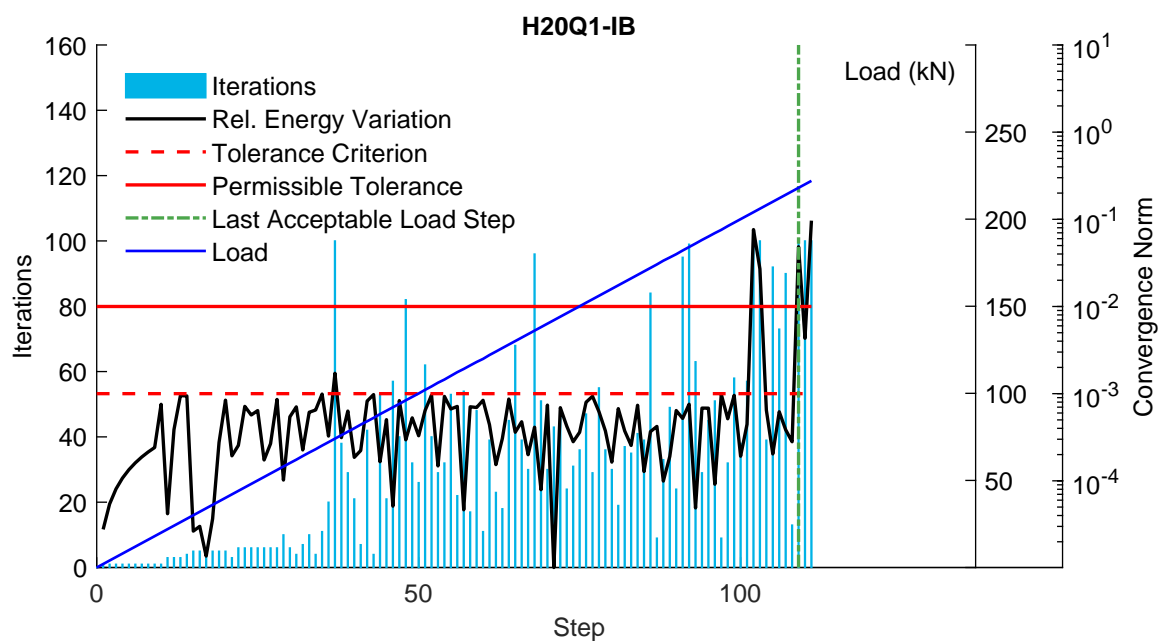


Figure A.9: Convergence plot for model H20Q1-IB

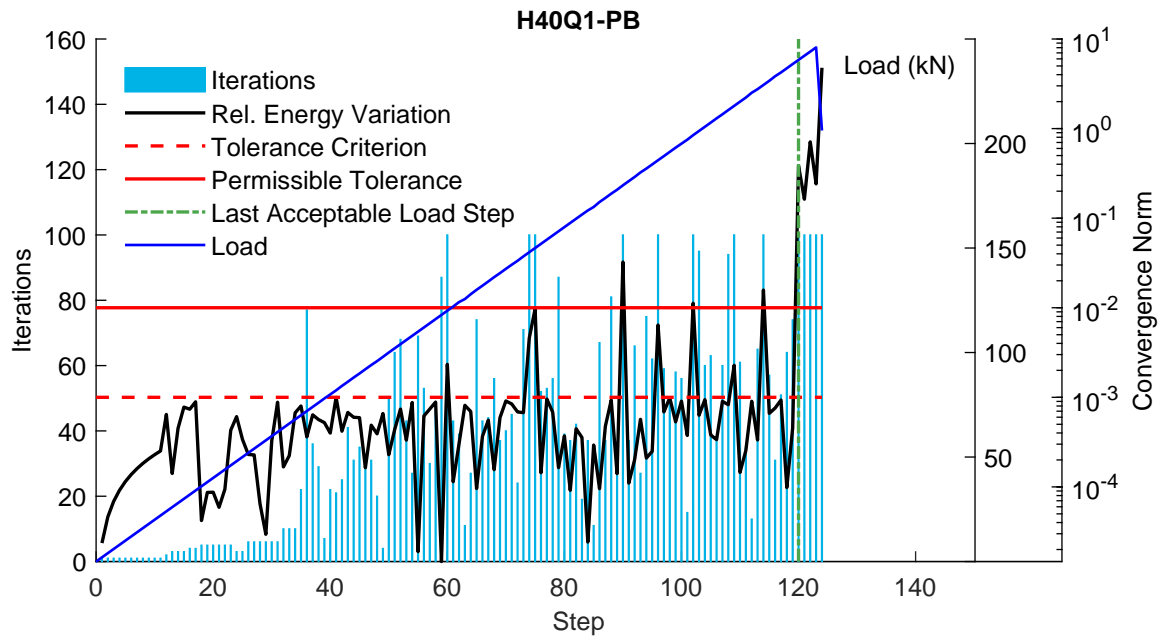


Figure A.10: Convergence plot for model H40Q1-PB

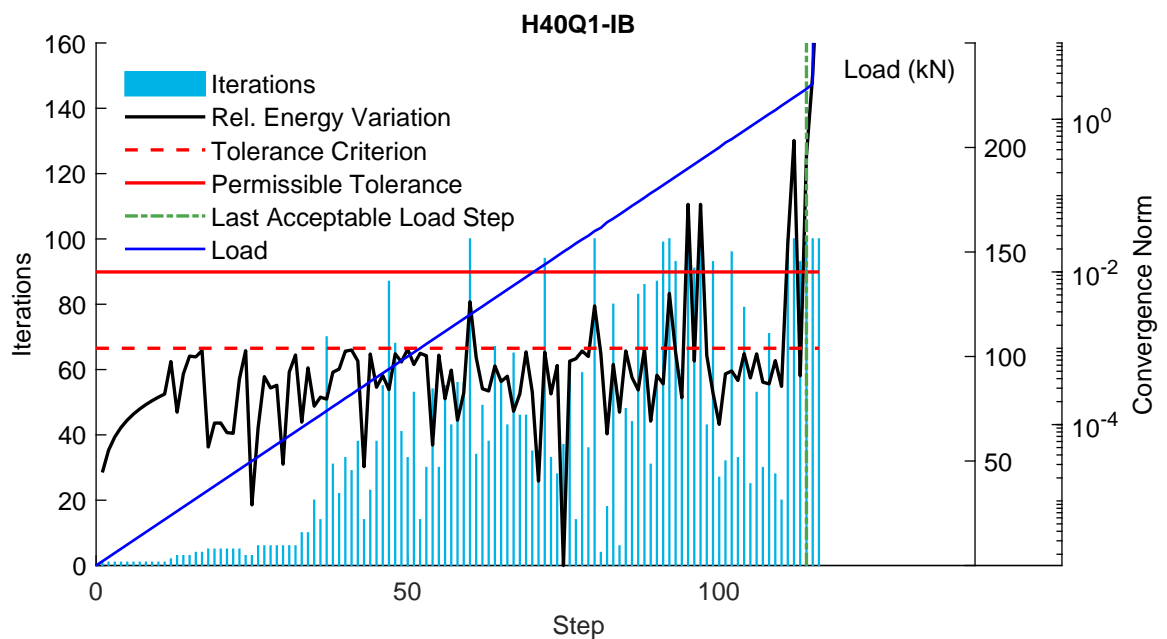


Figure A.11: Convergence plot for model H40Q1-IB

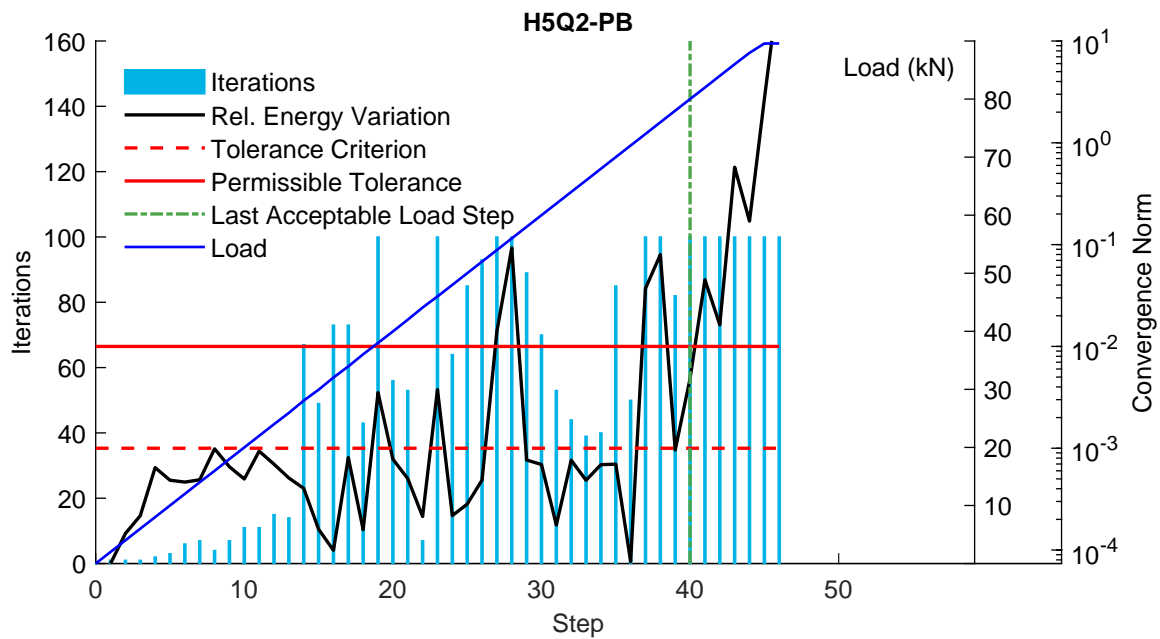


Figure A.12: Convergence plot for model H5Q2-PB

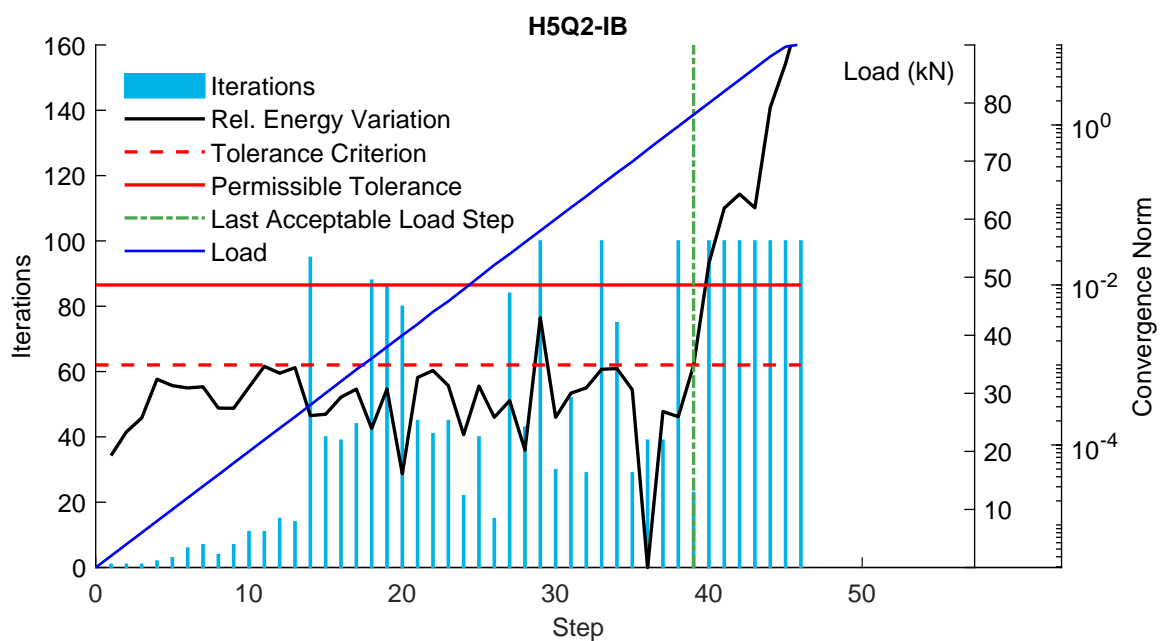


Figure A.13: Convergence plot for model H5Q2-IB

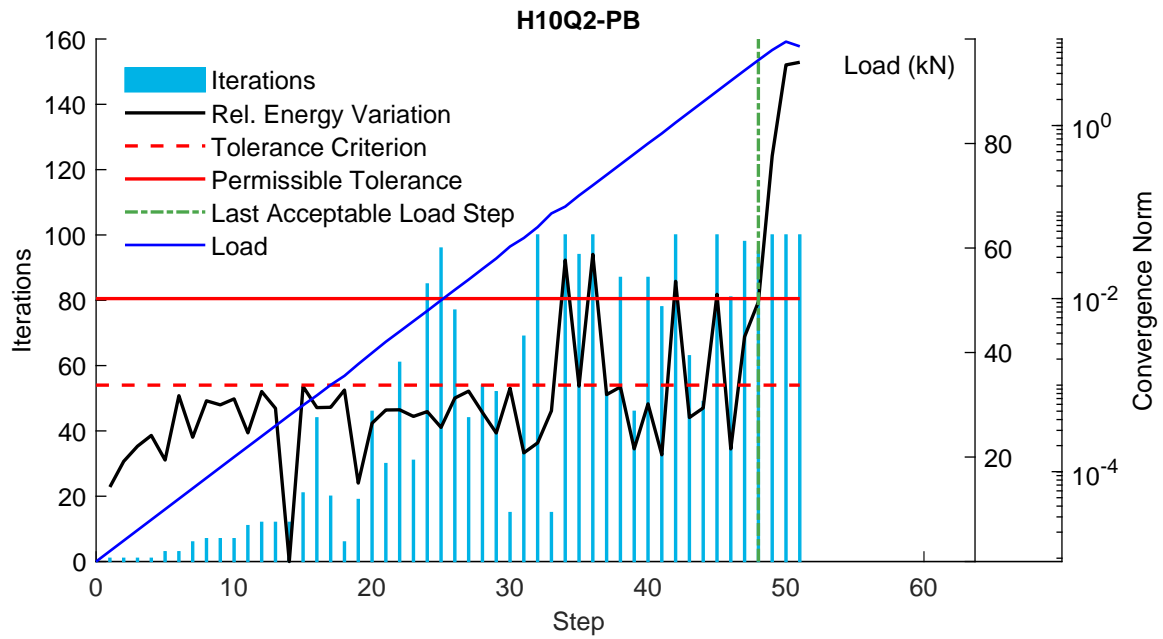


Figure A.14: Convergence plot for model H10Q2-PB

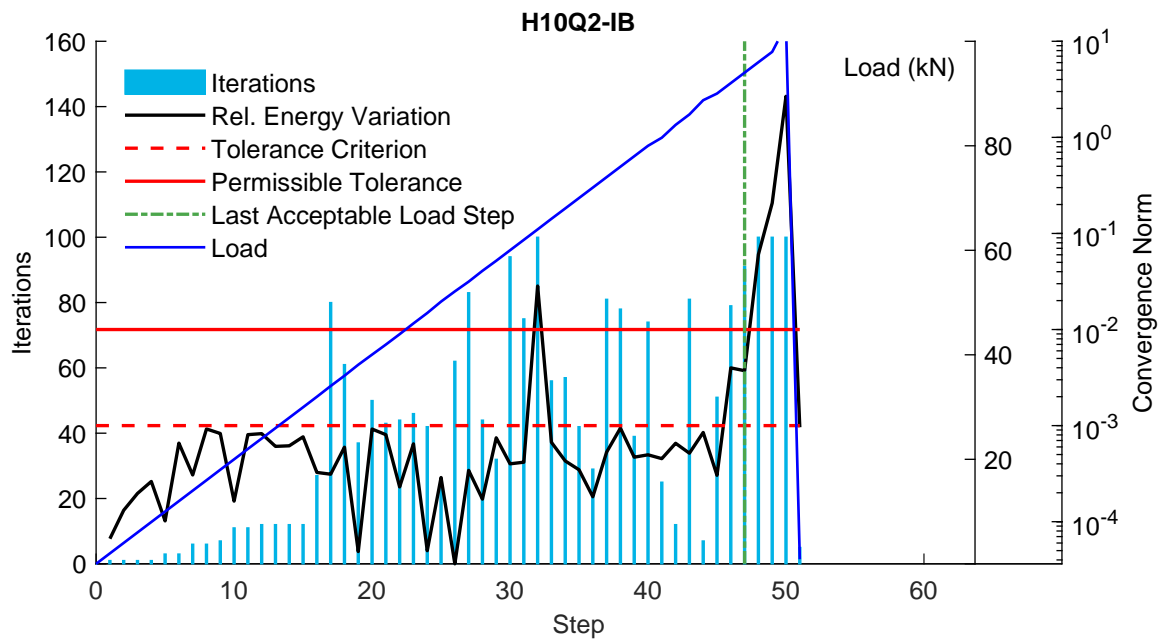


Figure A.15: Convergence plot for model H10Q2-IB

B

Poisson Ratio and Compressive Strength of SHCC

Modelling of SHCC requires input for the Poisson ratio and compressive strength. According to Zhou [66], the material properties of SHCC (ECC) vary with varying compressive strength, such as the elastic modulus, Poisson ratio and toughness.

Poisson Ratio

The Poisson ratio of SHCC in the elastic stage are plotted against compressive strength as shown in Figure B.1(a). It is observed that for strengths lower than 50MPa, the Poisson ratio increases slightly with the compressive strength. However, when the strength exceeds approximately 50MPa, the Poisson ratio stays almost constant at 0.17. As in this thesis, the SHCC compressive strengths vary, therefore appropriate values of the Poisson ratio need to be input.

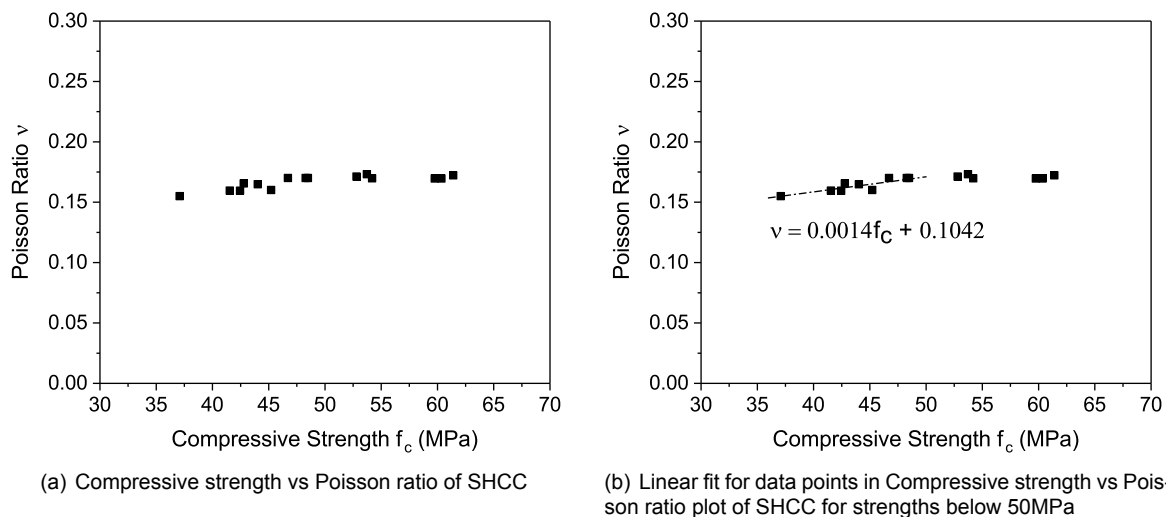


Figure B.1: Relation between compressive strength vs Poisson ratio of SHCC [66]

The compressive strengths of SHCC used in this thesis are 38MPa (design experiments), 56MPa (benchmark study 1) and 91MPa (benchmark study 2 and 4). For the benchmark studies, the Poisson

ratio of 0.17 is used as the strengths exceed 50MPa, as described above. For designed experiments, a linear best fit curve is plotted for data points below 50MPa. This is illustrated in Figure B.1(b). The obtained linear equation is used to calculate the Poisson ratio for the design experiments. The values described in Table 4.18 are based on the above theory. Note that the SHCC compressive strengths tested in [66] range between 35-60MPa, but for this thesis, it is assumed that the variation of compressive strength with the Poisson ratio remains constant after 50MPa, up to 91 MPa. This is an assumption and reality might be different.

Compressive Strength

Zhou [66] tested cylindrical SHCC specimens of varying compressive strengths in uniaxial compressive strength setup. The test setup is shown in Figure B.2(a) and the stress vs axial deformation plot is shown in Figure B.2(b). As it can be seen, the uniaxial compressive behaviour of SHCC is different from the parabolic behaviour assumed to model the compressive behaviour of regular concrete as per the NLFEA guidelines [28]. Therefore, the “Parabolic” compressive input in DIANA cannot be used to model the compressive behaviour of SHCC, instead a multi-linear curve is input. Another reason for not using the parabolic compressive input is the fact that the compressive fracture energy is also required to be input. Normally, it can be calculated using the formulas provided in the NLFEA guidelines for regular concrete, but the same formulas cannot be used for SHCC. Therefore, input of the compressive behaviour of SHCC as a multi-linear curve is a viable option.

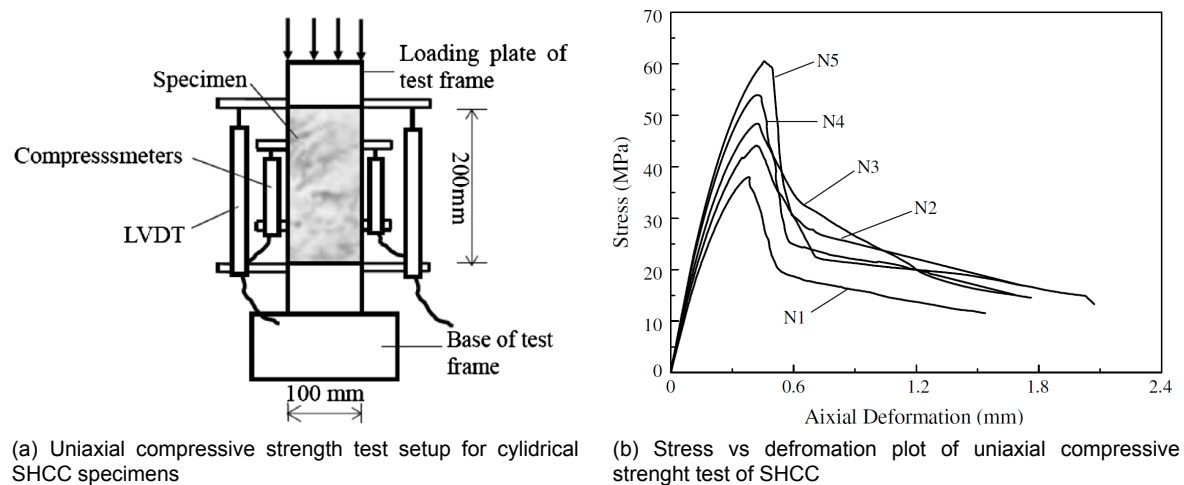


Figure B.2: Compressive strength of SHCC [66]

As described earlier, there are three types of SHCC being dealt with in this thesis based on their compressive strengths; one from Jian Zhou’s study [67] for designed experiments and two SHCC from benchmark studies. For the design experiments with f_c of 38MPa, the multi-linear compressive curve input is the same as formulation N1 tested by Zhou [66]. The input data and corresponding curves are shown in Figure B.3.

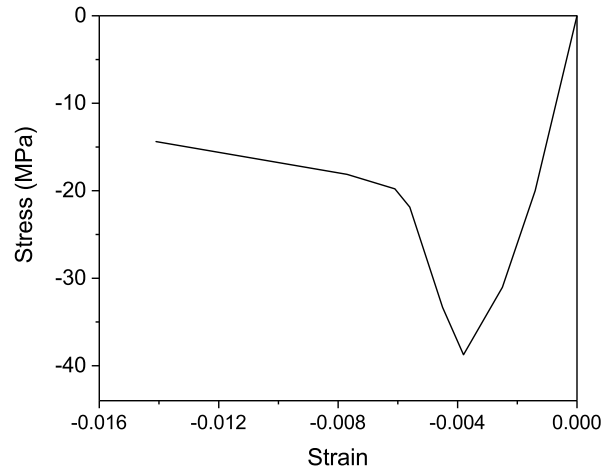


Figure B.3: Uniaxial compressive strength input for SHCC used in designed experiments

For the benchmark studies, no uniaxial compressive strength test of SHCC is performed. Therefore, the analytical model proposed by Zhou [66] is used to obtain the multi-linear compressive behaviour of SHCC of benchmark studies. The analytical model is tested by Zhou on his experimental results and good agreement between the analytical and experimental results is obtained with a coefficient of correlation ranging between 0.9 - 0.99.

The analytical model divides the multi-linear compressive curve of SHCC in to two main branches; ascending and softening. Ascending part is till the peak stress and strain, and is further divided into two parts. According to Zhou, linear elastic compressive behaviour of SHCC exists till 40% of the ultimate strength. This part of the curve is calculated using Equation B.1.

$$\sigma = E_0 \cdot \varepsilon \text{ for } 0 < \varepsilon < \varepsilon_{0.4} \quad (\text{B.1})$$

$\because \varepsilon_{0.4}$ = strain at 40% of ultimate strength and E_0 is the elastic modulus

The elastic modulus is decreased when stress exceed 40% of the peak stress. the elastic modulus is reduce using a factor α , and the stress is calculated using Equation B.2.

$$\sigma = E_0 \cdot \varepsilon \cdot (1 - \alpha) \text{ for } \varepsilon_{0.4} < \varepsilon < \varepsilon_0 \quad (\text{B.2})$$

$\because \varepsilon_0$ = strain corresponding to peak strength and α is calculated using Equation B.3

$$\alpha = a \cdot \frac{\varepsilon E_0}{f'_{cr}} - b \quad (\text{B.3})$$

The parameters “a” and “b” are 0.308 and 0.124, determined using linear regression analysis of the experimental results by Zhou. The post-peak behaviour or softening part of the curve is also divided into two parts illustrated by Equations B.4 & B.5.

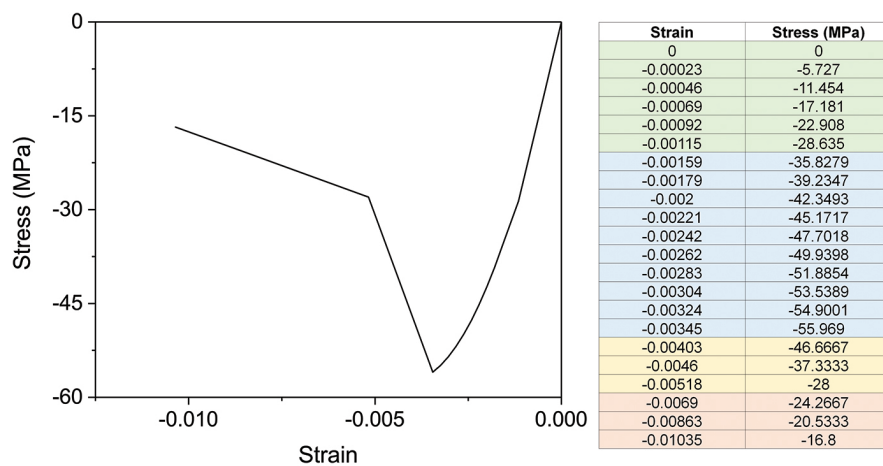
$$\sigma = m(x - x_0) + f'_{cr} \text{ for } x_0 < x < x_l \quad (\text{B.4})$$

$$\sigma = m(x - x_l) + \sigma_l \text{ for } x_l < x < x_{max} \quad (\text{B.5})$$

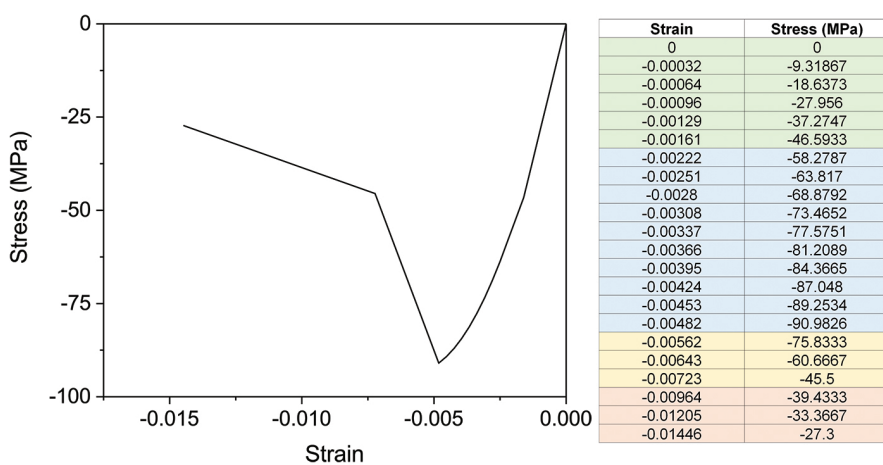
$\because x_0$ and f'_{cr} are deformation and stress at peak load and x_l and σ_l are deformation and stress in the inflection point of the softening curve. The following steps are followed to obtain the multi-linear curve,

1. With peak strength i.e. the compressive strength known, determine the corresponding strain ε_0 using Equation B.2.
2. From the peak stress and strain, determine the 40% stress and strain values.
3. With Elastic modulus known, calculate stress corresponding to strain values less than $\varepsilon_{0.4}$ using Equation B.1.
4. Calculate stress corresponding to strain values higher than 40% of the peak stress till the peak strain ε_0 using Equation B.2.
5. Determine x_0 by multiplying ε_0 with the gauge length, which is 10mm in this study.
6. Statistical analysis of the experimental results shows that $x_l = 1.5x_0$ and $\sigma_l = 0.5f'_{cr}$. Determine x_l and σ_l using these expressions.
7. In order to determine the the maximum deformation and corresponding stress, [60] suggests that $x_{max} = 3 \cdot x_{peak}$ where x_{peak} is the peak deformation which can be determined by multiplying peak strain with the gauge length, and $\sigma_{max} = 0.3 \cdot f'_{cr}$.
8. Now, a total of three points are known in the softening part of the multi-linear curve. Using " x_0, f'_{cr} " and " x_l, σ_l ", determine the slope "m" and using " x_l, σ_l " and " x_{max}, σ_{max} ", determine the slope "n".
9. Using Equations B.4 & B.5, obtain the post peak behaviour compressive stresses of SHCC corresponding to deformation values. Plot stress vs strain by converting deformations to strains using the gauge length.

The plot data and corresponding plots of SHCC of benchmarks studies are illustrated in Figure B.4.

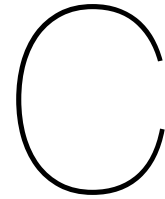


(a) Uniaxial compressive strength curve of SHCC for benchmark study 1



(b) Uniaxial compressive strength curve of SHCC for benchmark studies 2 and 4

Figure B.4: Multi-linear compressive strength input for SHCC of benchmark studies



Self-weight of SHCC

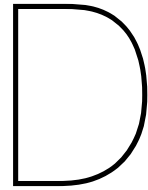
In numerical modelling, the self-weight of concrete and SHCC is considered. Self-weight of concrete is taken as 2400kg/m^3 as per NLFEA guidelines [28]. Mix design details for SHCC are not provided in the benchmark studies from which self-weight could be calculated. Therefore, an SHCC specimen of $600 \times 150 \times 150\text{mm}^3$ dimensions is cast in the Stevin lab. The mix design is shown in Table C.1. The calculations for the self-weight of SHCC are shown in Table C.2.

Table C.1: Material quantities for SHCC

Materials	Unit	Quantity
Cement (CEM III)	kg/m^3	790
Limestone	kg/m^3	790
SP	kg/m^3	2.13
Water	kg/m^3	425
PVA Fibres	kg/m^3	26

Table C.2: Self-weight calculations for SHCC

Property	Unit	Quantity
Total Volume	m^3	0.0027
Total Mass	kg	5.49
Self-weight	kg/m^3	2034



Hybrid Interface Behaviour in Tension

This analysis is performed to:

1. Describe the sign notations considered in this thesis for the interface results such as displacement and stresses, and
2. To prove the hypothesis stated in the discussion section for Modelling Phase III that the numerical model only fails once the interface has completely delaminated.

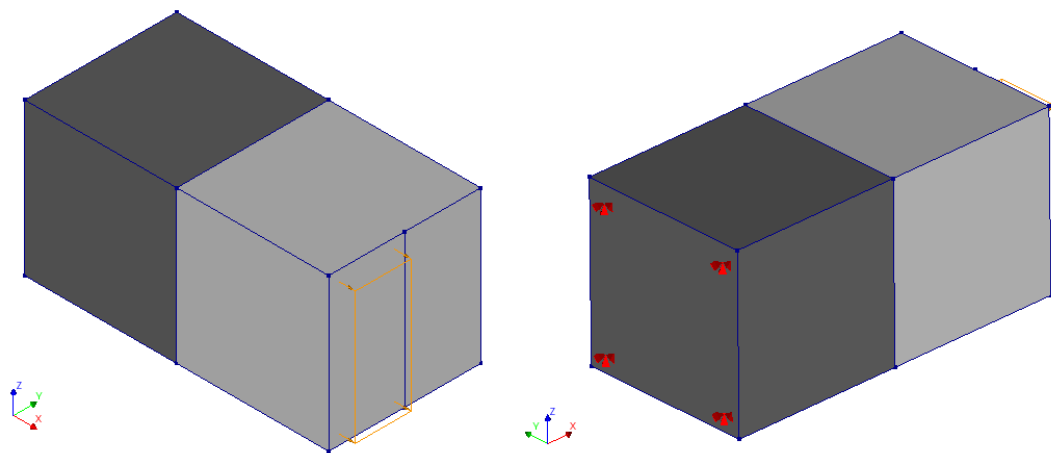


Figure D.1: 3D numerical model

Consider the numerical model shown in Figure D.1. It consists of 3D SHCC and concrete layers with Imperfect Bond (IB) surface interface defined between them. The SHCC end face of the model is restrained in all possible translational directions and an eccentric tensile load is applied on the concrete face. At the interface, the concrete edge face is assigned as “source” and SHCC face is assigned as “target” while modelling the interface. Eccentric load is applied to allow for non-uniform delamination at the interface under tension. Based on the tensile strength input of 1MPa and interface stiffness, the critical displacement at which delamination occurs is approximately 0.00245mm.

Sign Notations

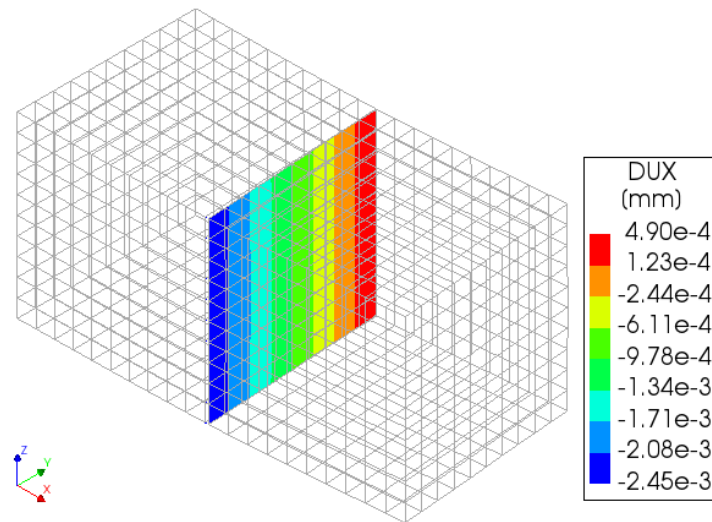


Figure D.2: Interface displacement DUX at an arbitrary load step

Figure D.2 shows the interface displacement and stresses at an arbitrary load step in the numerical model. The tensile load is applied in positive global X direction. However, the global displacement and stress values are negative. This is because for interface, the displacement and stresses are presented on the “source” face relative to the “target” face. The results are negative when “source” face moves away from the “target” face and vice versa. In this thesis, the hybrid interface is modelled in global X-Z plane and the tensile stresses and displacement are in the global Y direction. Therefore, stresses STY and displacement DUY are reported for delamination. The negative results indicate opening (debonding) at the interface as it is in tension.

Numerical Failure due to Interface

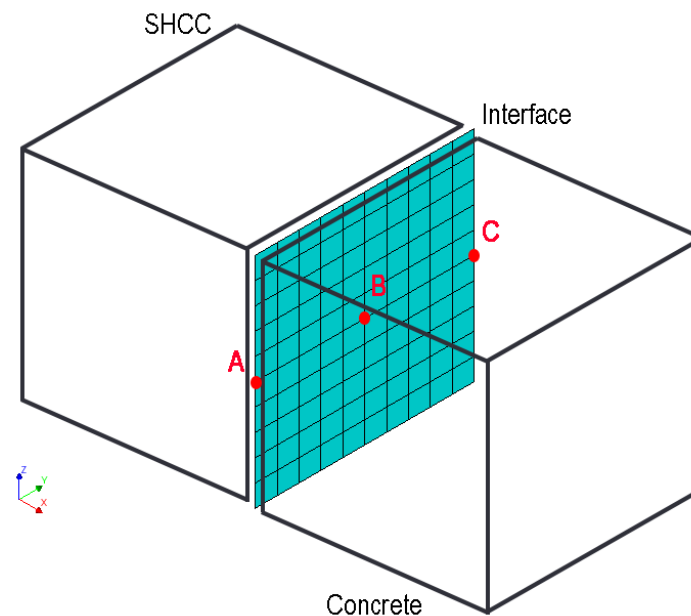


Figure D.3: Points A, B and C on interface

Consider Figure D.3. Three points are selected on the “source” face; Point A is directly loaded

under tension, Point B is in the mid of the face, and Point C is at the opposite edge of Point A and is not loaded under direct tension, but displaces along X-axis due to the eccentric tensile load applied.

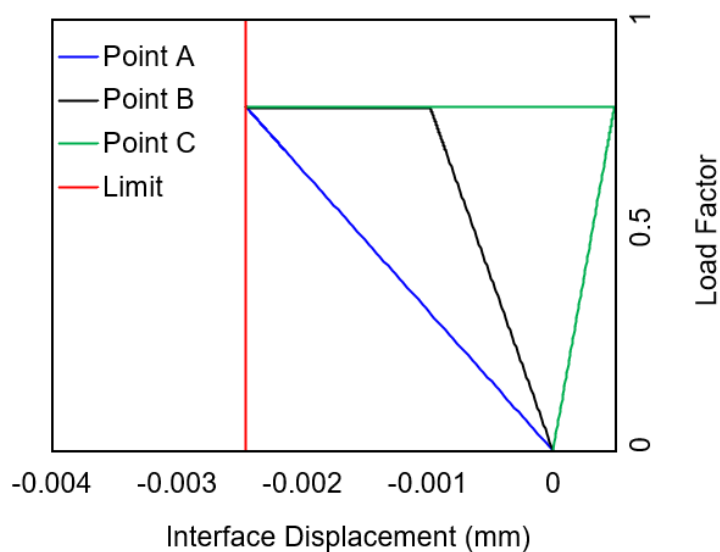


Figure D.4: Interfacial displacement vs load factor at Points A, B and C

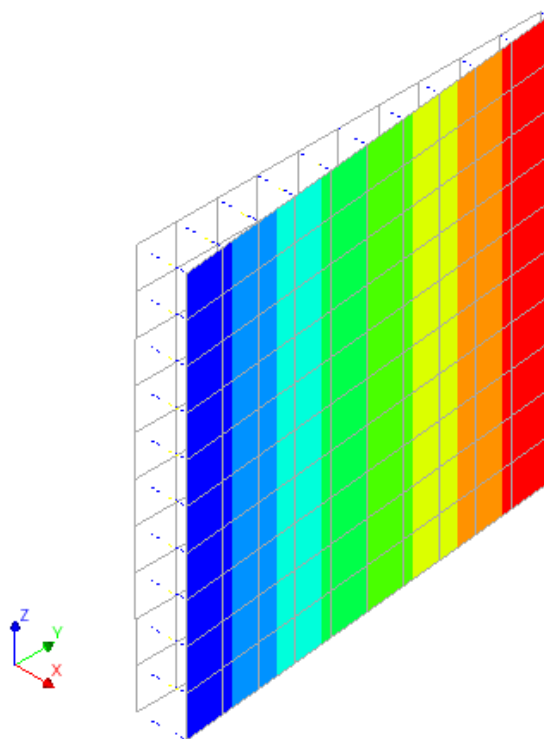
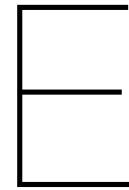


Figure D.5: Delaminated interface at the terminated load step

Figure D.4 shows the debonding at the selected points with respect to the load applied. It is observed that once the three points reach the critical displacement value of 0.00245mm, the analysis stops due to divergence. Therefore, the numerical model fails only once all the elements have exceeded the critical displacement value.



Numerical Validation of Flexural Behaviour of SHCC

The paper of Jian Zhou et al. [67] is used to validate the flexural behaviour of SHCC in DIANA.

Description of Experimental Study [67]

This study includes evaluation of the mechanical properties of Engineered Cementitious Composites (ECC) by varying the constituents of the mix design. Polyvinyl Alcohol (PVA) Fibres are used in ECC, with a length of 8mm, diameter of $40\mu\text{m}$, tensile strength of 1600MPa and the density of 1300 kg/m^3 . The fibre surface is coated with 1.2% oil by weight in order to reduce the chemical and friction bond inside the cementitious matrix. Six different mix designs using Portland Cement (PC) limestone powder and Blast Furnace Slag (BFS) are tested. Additionally, one formulation using BFS cement and limestone is also evaluated, keeping the PVA fibre percentage as 2%. This additional formulation is developed to simplify the mix design by eliminating the need to use BFS and PC separately in order to produce ECC. The results of mix M6 are used in this thesis to model SHCC since it showed the best mechanical properties. This is attributed to the fact that the PC/BFS ratio of 0.43 in M6 matches the typical value of this ratio in BFS cements. For further use, the term “ECC” in this study is replaced with “SHCC” for uniformity in the reporting terminology used for materials.

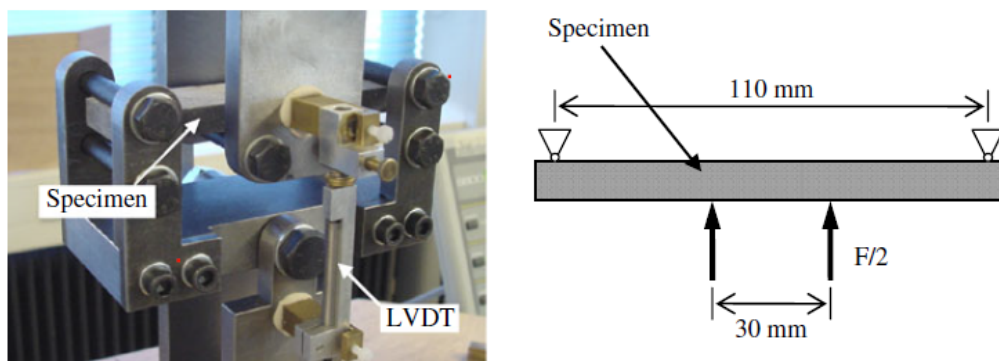


Figure E.1: Four-point bending test setup for coupon specimens

Three cubes wet cured for 28 days with the dimensions of $40\times 40\times 40\text{ mm}^3$ are used to determine the compressive strength. For mix design M6, the mean cubic compressive strength is approximately

38MPa. This study does not include the stress-strain curve from the uniaxial compressive strength test of mix M6. Therefore, the uniaxial compressive strength result reported by Cai et al. [9] is referenced to obtain the compressive stress-strain curve of SHCC, as shown in Figure E.2. The properties of mix design of SHCC reported by Cai are comparable to the mix M6 of Zhou, with the same compressive strength of approximately 38MPa. Therefore, it is used as input in DIANA. The Young's Modulus of 18500MPa is used.

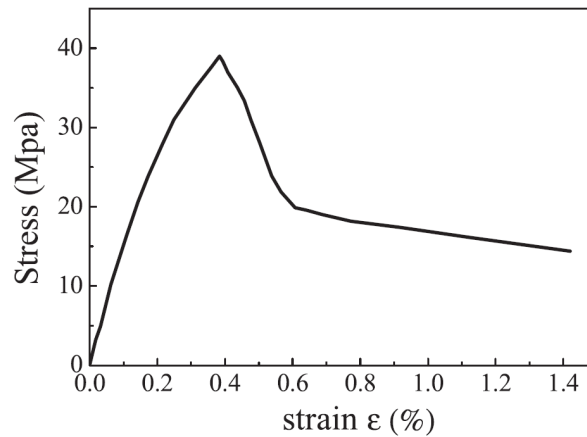


Figure E.2: Compressive stress-strain curve of SHCC

Five specimens of ECC of mix design M6 are tested for uniaxial tensile strength as shown in the Figure E.3(a). First cracking stress is approximately 3MPa. The average ultimate strain capacity is reported to be around 3.3%. Corresponding to this strain value, an average ultimate tensile stress for SHCC of about 3.7 MPa is obtained. This is calculated from the figure.

A total of five coupon specimen wet cured for 28 days with the dimensions of $120 \times 30 \times 10 \text{ mm}^3$ are subjected to four point bending test, as shown in Figure E.1. The support span of the four-point bending test set-up is 110 mm, with a loading span of 30mm. Two LVDTs are attached on both sides of the test set-up to measure the flexural deflection of the coupons. A deformation control test with a speed of 0.01 mm/s is performed. The experimental average flexural deflection capacity is approximately 3.9mm.

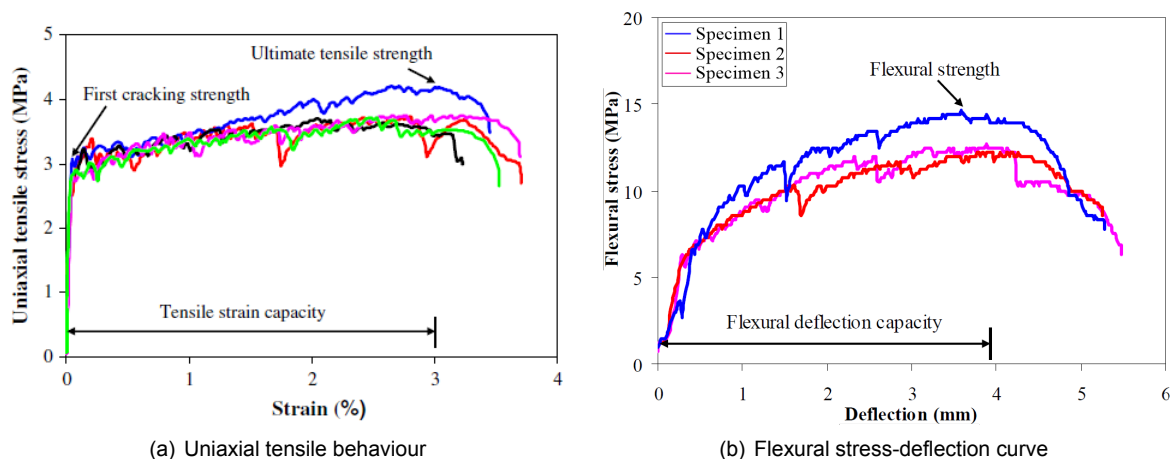


Figure E.3: Experimental tensile and flexural behaviour of SHCC

Numerical Validation of Flexural Behaviour

The stress-strain values for the uniaxial tensile behaviour of SHCC reported in the study are first assessed numerically. This is due to a lack of SHCC-specific constitutive model in DIANA i.e. a model defined for materials exhibiting strain-hardening. As described in Part I of the thesis, for modelling the tensile behaviour of SHCC, *fib* FRC model is used. However, *fib* FRC model is based on tension-softening [20]. Therefore, it is important to check whether the selected constitutive model is able to replicate the experimental results.

The reported experimental tensile behaviour of SHCC is checked by evaluating the flexural behaviour of SHCC. The coupon specimens, of the exact same dimensions as reported in the study, are modelled in DIANA and loaded in a four-point bending setup as well. The numerical flexural response of SHCC coupon is compared with the experimental results shown in Figure E.3(b). The final tensile input for SHCC is based on the comparison between the experimental and numerical flexural test results. The set-up for the numerical model and obtained results are discussed below.

Types of Model

The experimental flexural response of SHCC is compared with two types of numerical models, varying in the input stress-strain values for the tensile behaviour,

1. Model **Numerical-3.7**, which is a trilinear tensile curve based on the reported experimental uniaxial tensile strength test results by Zhou et al., having an ultimate stress value of 3.7MPa [67]
2. Model **Numerical-4.6**, which is a trilinear tensile curve whose ultimate stress value is increased to 4.6MPa based on the results obtained from using model “Exp”

Geometry of a model

A 2D model with regular plane stress elements is constructed, as shown in Figure E.4. The total length of the specimen is 120mm. The loading span is 30mm and the flexural span is 40mm, giving a total effective length of 110mm. Height of the specimen is 10mm and the width is 30mm. (Note: In the description, planar longitudinal dimensions are referred to as “length”, transverse dimension as “height” and thickness i.e. in-to the plane as “width”)

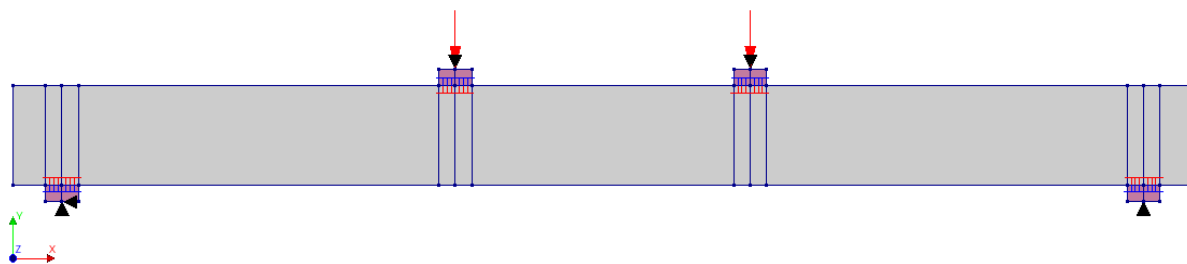


Figure E.4: Numerical model of SHCC coupon

Material model and properties

A total strain-based rotating crack model is used to model the flexural behaviour of SHCC. The multi-linear model is used for the compressive behaviour, as indicated in Figure E.5(a). The tensile behaviour of SHCC is modelled using *fib* FRC total strain curve. Two types of tensile inputs are defined as shown in Figure E.5(b); based on (1) the average values of stress-strain obtained from the uniaxial tensile strength tests performed by Zhou, (2) the adjusted input. The adjusted input is defined since the experimentally reported values are not able to give acceptable results. This aspect is discussed later in the results section of the chapter.

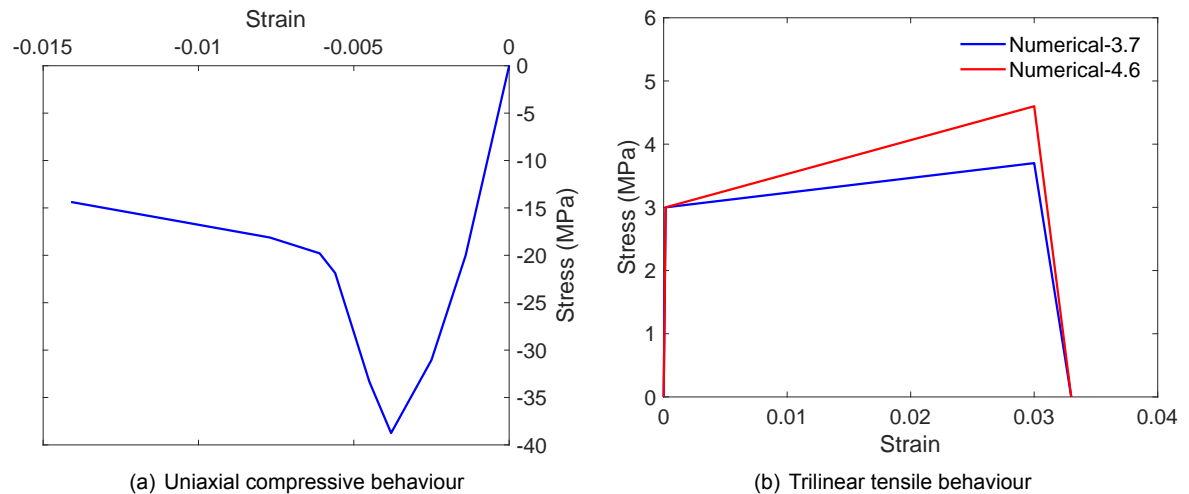


Figure E.5: Compressive and tensile input properties of SHCC

Loads and Supports

Vertex loads and supports are provided at the centre of the respective plates, as shown in Figure E.4. Plates are provided to avoid convergence issues during the analysis. The load and support plates are modelled using linear elastic steel with an Young's Modulus of 210000 MPa. To avoid the localization of stresses, a linear elastic interface is defined between the support plates and the coupon specimen. The properties of this interface are based on the properties of SHCC i.e. the normal stiffness is equal to the Young's Modulus of SHCC and the shear stiffness is equal to the Young's Modulus of SHCC divided by 1000.

Mesh and Analysis Procedure

Edge-controlled meshing with an element size of 1.67mm as per NLFEA guidelines [28] is used. Meshed model is shown in Figure E.6. Displacement-controlled analysis considering both the physical and geometrical non-linear effects is performed. Full Newton Raphson method of iteration is used for the analysis. Load steps of (0.1)50 are used to have the ability to obtain an approximate mid-span deflection of at least 4mm based on the experimental results. Maximum of 100 iterations per load step are allowed with the tolerance of the energy norm equal to 0.001 as per the guidelines [28].

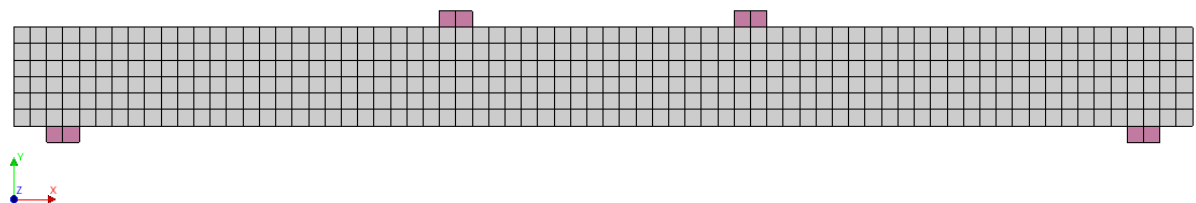


Figure E.6: Mesh configuration of SHCC coupon

Summary of Inputs

Table E.1: Summary of inputs for numerical model of SHCC coupon specimen

Geometry of the Model	
Geometry	2D
SHCC Material Model	
Material Class	Concrete and Masonry
Crack Model and Orientation	Total strain-based rotating
Tensile curve	<i>fib</i> FRC
Compression curve	Multi-linear
Load and Support Conditions	
Left support	X-Y restrained
Right support	Y restrained
Load type	Displacement-controlled
Imposed deformation	1mm
Load steps	0.1(50)
Mesh	
Element type	Regular plane stress
Element name	CQ16M
Interface element type	2D Line Quadratic
Mesh size	1.67mm
Interpolation scheme	Quadratic
Integration scheme	3x3 Gaussian (Default)
Analysis Procedure	
Iteration procedure	Newton-Raphson (Regular)
Iterations per load step	100
Convergence norm and tolerance	Energy (0.001)

Results and Conclusions

Figure E.7 compares the load-deflection response of the three experimentally tested coupon specimens with the results from the numerical models. Numerical results are shown till the last acceptable load step. The numerical response is bi-linear i.e. initial linear elastic part and non-linear part after stress exceeds from approximately 8MPa. (Note: In explanation of results in the next paragraph, the term “non-linear stiffness” means stiffness of the stress-deflection response after the linear elastic response ends)

Figure E.7 indicates that the flexural response of experimentally tested specimens 2 and 3 is similar as compared to specimen 1, having non-linear stiffness of approximately 1.01 N/mm³ and 1.24 N/mm³ respectively. The non-linear stiffness of specimen 1 is approximately 1.54N/mm³. The average experimental non-linear stiffness is approximately 1.26 N/mm³. The figure also indicates that the numerical response of both models is limited till the peak stress at which localization of cracks occur, and not post-peak softening is obtained as in experiments. The non-linear stiffness of model “Numerical-3.7”, which is based on the experimental tensile stress-strain values, is approximately 0.7 N/mm³, which is very low as compared to the tested specimen. The low non-linear stiffness can be attributed to low ultimate stress value in the tensile curve. This is assessed by increasing the ultimate stress in the tensile curve input from 3.7MPa to 4.6MPa in model “Numerical-4.6”. The corresponding

non-linear stiffness of model “Numerical-4.6” is approximately 1.1 N/mm^3 , which is close to the calculated experimental stiffnesses. And the stress-deflection response, till the peak load, is similar to specimens 2 and 3 as well.

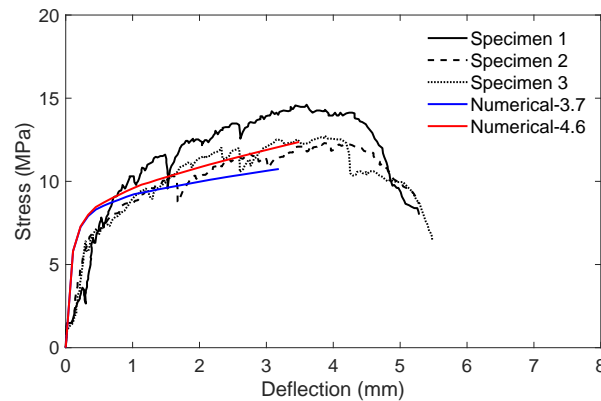
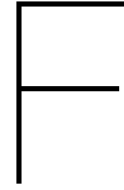


Figure E.7: Stress-deflection response from flexural test of SHCC coupon specimen

In conclusion, the reported ultimate tensile stress value of 3.7 MPa is not good enough to produce a numerical stress-deflection response that is comparable to experiments. And if the ultimate stress value is increased, as in model Numerical-4.6, the non-linear stiffness improves. However, the ultimate numerical deflection capacity for the numerical models is approximately 37% lower and softening behaviour is also not captured numerically. Therefore, even though an improved bi-linear behaviour is obtained numerically by altering the stress-strain values in the tensile curve, the selected constitutive model is unable to capture the post-peak softening behaviour. Therefore, if the stresses in the designed experimental beams tested numerically in DIANA are such that the ultimate tensile stress and strain of SHCC is exceeded, it will lead to abrupt failure of SHCC instead of a gradual failure. SHCC is continued to be modelled using *fib* FRC model considering this limitation.



Analytical Calculations for Design of Hybrid Beams

Three types of beams are designed based on the type of geometry; Control Beam (Control), and hybrid beams with 15mm and 10mm SHCC thickness on the sides (HYB15 and HYB10), respectively. Hybrid beam with SHCC thickness of 15mm (HYB15) is based on calculations for shear capacity of reinforced concrete (RC) beam using Eurocode-2 [23], described in Section F. Providing 15mm thick SHCC layer on each side of the RC beam theoretically results in hybrid beam which has a shear capacity corresponding to which crushing failure of normal concrete at the top occurs. Therefore, SHCC thickness in model HYB15 is as per design requirements. HYB10 beam with 10mm SHCC thickness is designed to investigate the response of the hybrid beam in case the SHCC is under-designed.

Geometrical Properties

The geometrical properties of reinforced concrete (RC) beam for these experiments are based on the RC control beam tested by Huang [30]. Huang concludes that beams with clear cover of 31mm from the bottom longitudinal reinforcement perform better in hybrid configuration when SHCC is applied in place of regular concrete in the tensile region. Therefore, RC beam with 31mm clear cover is selected to obtain the geometrical properties of the designed beams in this appendix. Adopting the same method of construction of hybrid beam as Huang's i.e. replacing part of regular concrete with SHCC for flexure, the SHCC here is applied on the sides for shear by replacing part of existing regular concrete with equivalently thick SHCC and no SHCC is applied in the tensile region of the hybrid beam. However, it is ensured that the total beam thickness is 150mm in the hybrid beams. This is different from the hybrid beams in the benchmark studies discussed in this thesis where SHCC is applied in addition to regular concrete. There is no constant moment region in the designed beams i.e. a three point bend test is performed instead of four-point in order to allow for shear failure. The shear spans are of 500mm length, resulting in an shear span-to-effective depth ratio (a/d) of approximately 3. No transverse reinforcement is provided in the shear spans and top longitudinal reinforcement is also not provided. The geometrical properties of the RC beam to which SHCC is applied are described in Table F.1.

Table F.1: Geometrical properties of experimental beams (mm)

Total Length	Effective Length	Total Width	Height	Effective Depth (d)	a/d
1400	1000	150	200	165	3

As mentioned earlier, the SHCC layers are applied on the sides of the reinforced concrete beam

by replacing part of the regular concrete. The thickness replaced is limited by the side clear cover i.e. 43mm on each side in order to ensure that the longitudinal reinforcement lies within regular concrete. For the design calculations, the starting thickness of SHCC is assumed to be 15mm on each side. Therefore, the width of regular concrete part of the beam is 120mm. This is illustrated in Figure F.1.

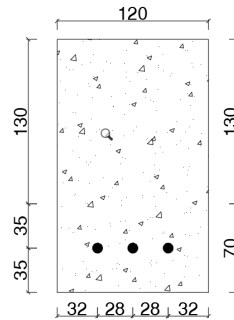


Figure F.1: Concrete cross-section for calculations

Material Properties

For the material properties of concrete and reinforcement, Huang's thesis is referenced [30], and the material properties of SHCC are referenced from the validation study performed in Appendix E. [67]. The material properties of concrete, SHCC and steel reinforcement are listed in Table F.2. All material properties are assumed to be mean values, as in the reference study. Based on the results in Appendix E, the tensile curve of model Numerical-4.6 is used for design of experiments here. The input parameters are listed in Table F.3.

Property	Symbol	Value	Unit
Concrete			
Characteristic Compressive stress	$f_{ck,cyl}$	28	MPa
Mean Compressive stress	$f_{cm,cyl}$	36	MPa
Cracking stress	$f_{ctm,fl}$	4.54	MPa
Elastic strain	ϵ_c	0.106	%
Ultimate strain	ϵ_{cu}	0.35	%
Young's Modulus	E_c	34000	MPa
SHCC			
Mean Compressive stress	$f_{cm,SHCC}$	38	MPa
Young's Modulus	E_{SHCC}	18500	MPa
Reinforcement			
Yielding stress	f_{sy}	550	MPa
Ultimate stress	f_{su}	650	MPa
Yielding strain	ϵ_{sy}	0.275	%
Ultimate strain	ϵ_{su}	5	%
Young's Modulus	E_s	200000	MPa
Reinforcement Diameter	\emptyset	8	mm
Reinforcement Area	A_s	150.76	mm ²
Reinforcement Ratio	ρ_l	0.0061	-

Table F.2: Material properties for design of experiments

Table F.3: Trilinear tensile curve of SHCC for design of experiments

	$\sigma_{SHCC,t,cr}$ (MPa)	$\varepsilon_{SHCC,t,cr}$ (%)	$\sigma_{SHCC,t,max}$ (MPa)	$\varepsilon_{SHCC,t,max}$ (%)	$\varepsilon_{SHCC,t,u}$ (%)
Average	3	0.016	4.6	3	3.3

Design Calculations

Eurocode-2 [23]

Firstly, the shear capacity of the reinforced concrete beam is calculated using the Eurocode-2 [23] as follows,

$$\mathcal{V}_{Rd,c} = 0.18 \cdot k \cdot (100 \cdot \rho_l \cdot f_{ck})^{\frac{1}{3}} = 0.99 \text{MPa} \quad (\text{F.1})$$

$$\therefore k = 1 + \sqrt{\frac{200}{d}} \leq 2$$

So the shear capacity of the reinforced concrete beam is approximately 0.99 MPa. Then, the capacity of the beams is determined as such that crushing is expected at the top of the beam i.e. $\varepsilon_{cu} = 3.5\%$.

The compression force is

$$F_{cc} = \text{coefficient} \cdot f_{cm,cyl} \cdot x \cdot b = 3.65 \cdot x \quad (\text{F.2})$$

$$\therefore \text{coefficient} = \frac{\varepsilon_{cu} - \frac{\varepsilon_c}{2}}{\varepsilon_{cu}} = 0.844$$

The force in steel reinforcement is

$$F_s = A_s \cdot f_{su} = 90.48 \text{kN} \quad (\text{F.3})$$

The force equilibrium gives,

$$F_s = F_{cc} \quad (\text{F.4})$$

$$x = 24.82 \text{mm}$$

The moment is calculated as,

$$M = F_s \cdot (d - \beta \cdot x) = 14.05 \text{kNm} \quad (\text{F.5})$$

$\therefore \beta = 0.39$, which is the distance factor.

The applied shear force is,

$$V_{Ed} = \left(\frac{4 \cdot M}{L} \right) / 2 = 28.11 \text{kN} \quad (\text{F.6})$$

$$\mathcal{V}_{Ed} = \frac{V_{Ed}}{b \cdot d} = 1.42 \text{MPa} < \mathcal{V}_{Rd,c} \quad (\text{F.7})$$

Therefore, the capacity of reinforced concrete beam alone is insufficient to provide the required resistance. Therefore, the strut inclination method, used to calculate the amount of transverse reinforcement required, is applied to determine the thickness of SHCC strips and the spacing with which they are required to be applied to obtain the required shear capacity,

The strut angle is calculated as,

$$\theta = \frac{1}{2} \cdot \arcsin \cdot \left(\frac{2 \cdot V_{Ed}}{\alpha_{cw} \cdot f_{cd} \cdot b \cdot z \cdot v} \right) = 8.83^\circ < 21.8^\circ \quad (\text{F.8})$$

$$\therefore \alpha_{cw} = 1, v = 0.6 \cdot \left(1 - \frac{f_{ck}}{250} \right), z = d - \beta \cdot x$$

Therefore, $\theta = 21.8^\circ$

The shear reinforcement is calculated as,

$$V_{Rd,s} = \frac{A_{sw}}{s} \cdot f_{ywd} \cdot z \cdot \cot(\theta)$$

The above formula is modified for SHCC as,

$$\frac{A_{SHCC}}{s} = \frac{V_{Ed}}{\sigma_{SHCC,t,cr} \cdot z \cdot \cot(\theta)} = 24.13 \text{mm}^2/\text{mm} \quad (\text{F.9})$$

Assuming that SHCC is applied as strips of 1mm length and 15mm thickness, then the total cross-sectional area is $A_{SHCC} = 2 \cdot 1 \cdot 15 = 30 \text{mm}$. The centre-to-centre spacing of SHCC strips comes out to be,

$$s = \frac{30}{24.13} = 1.24 \text{mm} \simeq 1 \text{mm}$$

Therefore, SHCC strips applied at approximately 1mm c/c spacing is theoretically sufficient to provide the required shear resistance. Note that applying SHCC strips of 1mm length at a c/c spacing of 1mm actually ends up forming a SHCC panel on the sides, as illustrated in Figure F.2. The panels are applied throughout the length of the beam.

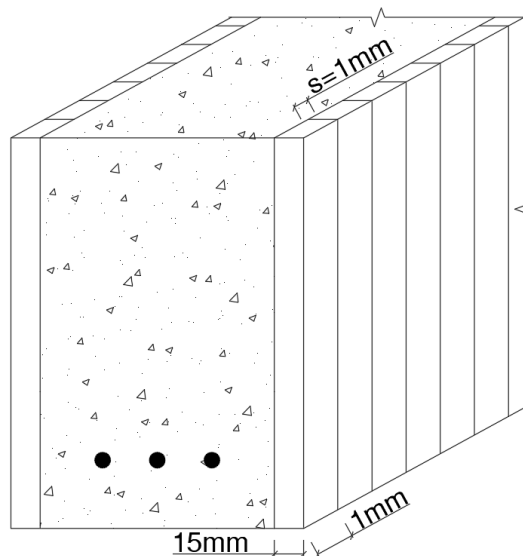


Figure F.2: SHCC side panel configuration in hybrid beam

Baghi [7]

Baghi [7] studied the strengthening of reinforced concrete beams using SHCC-FRP panels on the sides. In addition to experimentation, he also assessed different analytical techniques available at the time to predict the shear capacity of hybrid beams and proposed a simplified expression to calculate the shear resistance of SHCC panels. An underlying important assumption here is that a perfect bond exists between the substrate (regular concrete) and the overlay (SHCC). According to Baghi [7],

$$V_{SHCC} = 2 \cdot \left(\frac{2}{3} \cdot t_{SHCC,total} \cdot h_{SHCC} \cdot \tau_{SHCC} \right) \quad (F.10)$$

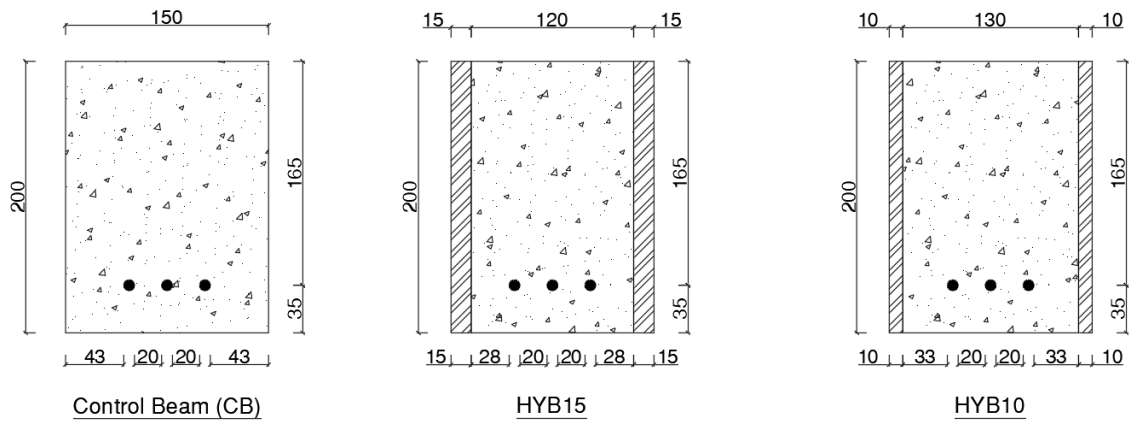
The expression is multiplied with 2 because the SHCC is assumed to be applied on both sides of the beam. In the above expression, $V_{SHCC} = V_{Ed}$, $h_{SHCC} = 200\text{mm}$ and $\tau_{SHCC} = 3.5\text{MPa}$ (assumed according to [8]). The total SHCC thickness is calculated as,

$$t_{SHCC,total} = \left(\frac{3 \cdot V_{SHCC}}{4 \cdot h_{SHCC} \cdot \tau_{SHCC}} \right) \approx 30\text{mm} \quad (F.11)$$

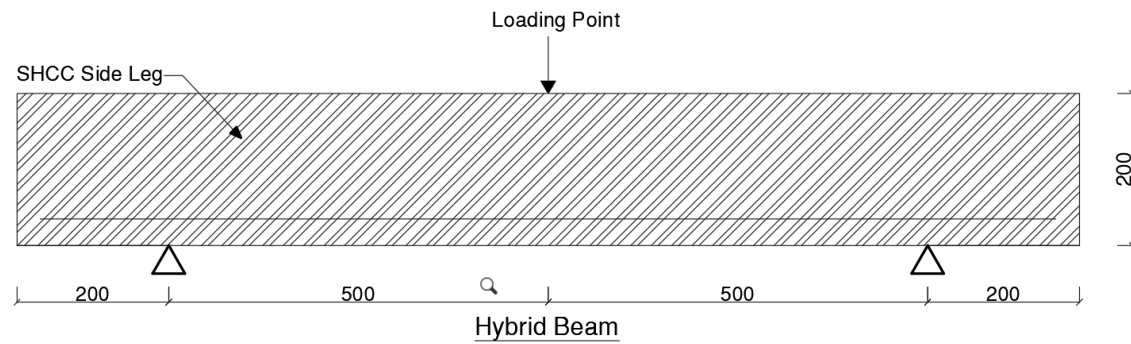
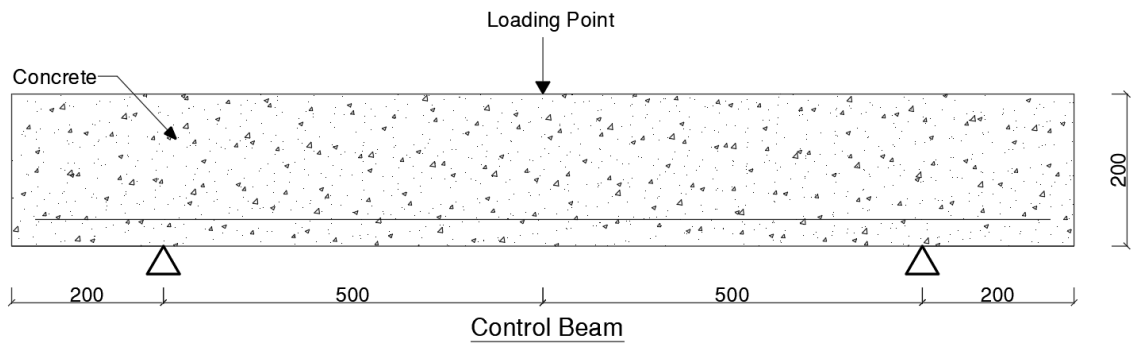
Therefore, thickness of single SHCC panel on one side of the beam is approximately 15mm, which is consistent with the value obtained using the Eurocode.

Experimental Beams

As per the above calculations, a hybrid beam with 15mm SHCC thickness is designed. Additionally, a hybrid beam with 10mm SHCC thickness is also designed to study the behaviour of the hybrid beam when it is under-designed in terms of the thickness of SHCC provided. The designed specimens are illustrated in Figure F.3.



(a) Cross-section



(b) Longitudinal-section

Figure F.3: Designed beams



Casting of Concrete Beam in a U-shaped SHCC Jacket Mould

The mould is designed to allow for easy casting of SHCC jacket without any consolidation issues. The hardened SHCC jacket is then used as a mould to cast regular concrete without any damage.

The mould is divided into two parts (in terms of its construction material); outer wooden mould, and inner styrofoam block. The outer wooden mould in combination with styrofoam is used to cast SHCC. In Step I, the regular concrete part of the specimens is replaced with styrofoam. The styrofoam is covered with tape/aluminium foil and is greased as well to prevent the development of any bond between styrofoam and cast SHCC. The styrofoam block is taped from the bottom side inside the wooden mould with two-sided tape to prevent it from moving when the wooden mould is placed on the vibration table for compaction of SHCC. The jacket for the strengthened beam is cast inverted to get the U shape, as shown in Figure G.1.

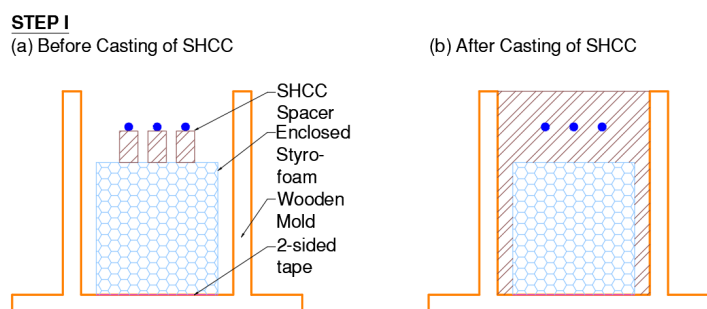
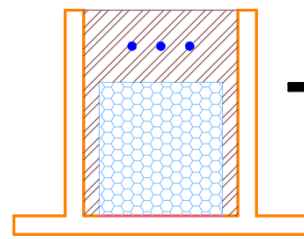


Figure G.1: Casting of U-shaped SHCC

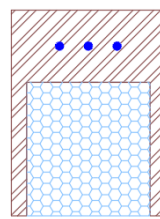
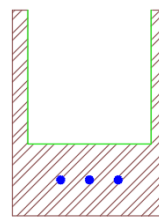
After Step I, the SHCC mould is in the form of an inverted U shape form-work. It is reverted and removed from the wooden mould. Interface can be applied in the form of sand-epoxy mix, after which regular concrete can be cast in place of the styrofoam, as shown in Figure G.2.

STEP II

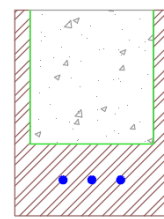
(a) Before Casting of Concrete



As in Step I

Remove Wooden
MoldRevert, remove styrofoam
and apply epoxy-sand
interface

(b) After Casting of Concrete

**Figure G.2:** Casting of Concrete in U-shaped SHCC mould

Bibliography

- [1] Belkis Filian Abad, Eva OL Lantsoght, and Yuguang Yang. Shear capacity of steel fibre reinforced concrete beams. In *Proceedings of the FIB Symposium, Krakow, Poland*, pages 27–29, 2019.
- [2] MS Abdel-Jaber, PR Walker, and AR Hutchinson. Shear strengthening of reinforced concrete beams using different configurations of externally bonded carbon fibre reinforced plates. *Materials and Structures*, 36(5):291–301, 2003.
- [3] Farshid Jandaghi Alaei and Bhushan Lal Karihaloo. Retrofitting of reinforced concrete beams with cardifrc. *Journal of Composites for Construction*, 7(3):174–186, 2003.
- [4] Tarek Alkhrdaji. Strengthening of concrete structures using frp composites. *Building Blocks - STRUCTURE Magazine*, (3):18–20, 2015.
- [5] Sali Asefa. Non-linear finite element analysis and parametric study of four-pile pile caps. 2020.
- [6] Simon Austin, Peter Robins, and Youguang Pan. Shear bond testing of concrete repairs. *Cement and concrete research*, 29(7):1067–1076, 1999.
- [7] Hadi Baghi. Shear strengthening of reinforced concrete beams with shcc-frp panels. 2015.
- [8] Hadi Baghi and Joaquim AO Barros. Shear properties of the strain hardening cementitious composite material. *Journal of Materials in Civil Engineering*, 28(10):04016093, 2016.
- [9] Jingming Cai, Jinlong Pan, and Xiangming Zhou. Flexural behavior of basalt frp reinforced ecc and concrete beams. *Construction and Building Materials*, 142:423–430, 2017.
- [10] Vladimír Cervenka, L Jendele, and Jan Cervenka. Atena program documentation. *Theory and User Manual, Cervenka Consulting, Prague*, 2005.
- [11] VLADIMIR Cervenka, J Cervenka, RADOMIR Pukl, and TEREZA Sajdlova. Prediction of shear failure of large beam based on fracture mechanics. In *International Conference on Fracture Mechanics of Concrete and Concrete Structures*, pages 1–8, 2016.
- [12] GM Chen, JF Chen, and JG Teng. On the finite element modelling of rc beams shear-strengthened with frp. *Construction and Building Materials*, 32:13–26, 2012.
- [13] Guangming Chen et al. Behaviour and strength of rc beams shear-strengthened with externally bonded frp reinforcement. 2010.
- [14] T Claus. Non-linear finite element analysis of shear critical reinforced concrete beams. *Delft University of Technology, Delft*, 2009.
- [15] Price Code. Eurocode 2: Design of concrete structures-part 1-1: General rules and rules for buildings. 2005.
- [16] RJ Cope, PV Rao, LA Clark, and P Norris. Modelling of reinforced concrete behaviour for finite element analyses of bridge slabs. *Numerical methods for nonlinear problems i*, 1980.
- [17] Tahar Hassaine Daouadji, Abderezak Rabahi, Boussad Abbes, and Belkacem Adim. Theoretical and finite element studies of interfacial stresses in reinforced concrete beams strengthened by externally frp laminates plate. *Journal of Adhesion Science and Technology*, 30(12):1253–1280, 2016.

- [18] R De Borst and P Nauta. Non-orthogonal cracks in a smeared finite element model. *Engineering Computations* 2 (3), 35-46.(1985), 1985.
- [19] Arjen de Putter. Towards a uniform and optimal approach for safe nlfca of reinforced concrete beams: Quantification of the accuracy of multiple solution strategies using a large number of samples. 2020.
- [20] BV Diana Fea. Diana 10.3 finite element analysis user's manual. *Ed. Delft, The Netherlands*, 2019.
- [21] Salvador JE Dias and Joaquim AO Barros. Shear strengthening of rc beams with nsm cfrp laminates: Experimental research and analytical formulation. *Composite Structures*, 99:477–490, 2013.
- [22] Fédération Internationale Du Béton. Model code 2010—first complete draft. *fib Bulletin*, (55):318, 2010.
- [23] *EN 1992-1-1 Eurocode 2: Design of concrete structures - Part 1-1: General rules and rules for buildings*, Brussels, 2005. EN, CEN.
- [24] Esmaeel Esmaeeli, Joaquim AO Barros, and Hadi Baghi. Hybrid composite plates (hcp) for shear strengthening of rc beams. 2013.
- [25] Panagiotis Evangeliou. Probabilistic nonlinear finite element analysis of reinforced concrete beams without shear reinforcement. 2016.
- [26] João P Firmo, João R Correia, and Luke A Bisby. Fire behaviour of frp-strengthened reinforced concrete structural elements: A state-of-the-art review. *Composites Part B: Engineering*, 80:198–216, 2015.
- [27] Sanjay Govindjee, Gregory J Kay, and Juan C Simo. Anisotropic modelling and numerical simulation of brittle damage in concrete. *International journal for numerical methods in engineering*, 38(21):3611–3633, 1995.
- [28] MAN Hendriks, A de Boer, and B Belletti. Guidelines for nonlinear finite element analysis of concrete structures (rtd: 1016-1: 2017), 2017.
- [29] Adrian KY Hii and Riadh Al-Mahaidi. An experimental and numerical investigation on torsional strengthening of solid and box-section rc beams using cfrp laminates. *Composite structures*, 75 (1-4):213–221, 2006.
- [30] Zhekang Huang. Flexural behaviour of reinforced concrete beams with a layer of shcc in the tension zone: Experimental study. 2017.
- [31] Mohamed K Ismail and Assem AA Hassan. Influence of fibre type on the shear behaviour of engineered cementitious composite beams. *Magazine of Concrete Research*, pages 1–12, 2019.
- [32] Nikhil Jayananda. Flexural behaviour of reinforced concrete beams with a layer of shcc in the tension zone: Numerical study by atena model. 2017.
- [33] D Kachlakev and DD McCurry. Behavior of full-scale reinforced concrete beams retrofitted for shear and flexural with frp laminates. *Composites Part B: Engineering*, 31(6-7):445–452, 2000.
- [34] Ahmed Khalifa, Gustavo Tumialan, Antonio Nanni, and Abdeldjelil Belarbi. Shear strengthening of continuous rc beams using externally bonded cfrp sheets. In *American Concrete Institute, Proc., 4th International Symposium on FRP for Reinforcement of Concrete Structures (FRPRCS4), Baltimore, MD*, pages 995–1008. Citeseer, 1999.
- [35] Sun-Woo Kim, Wan-Shin Park, Young-Il Jang, Luciano Feo, and Hyun-Do Yun. Crack damage mitigation and shear behavior of shear-dominant reinforced concrete beams repaired with strain-hardening cement-based composite. *Composites Part B: Engineering*, 79:6–19, 2015.

- [36] M. Kunieda and K. Rokugo. Recent progress on hpfrc in japan required performance and applications. 2006.
- [37] AP Lampropoulos, Spyridon A Paschalis, OT Tsioulou, and Stephanos E Dritsos. Strengthening of reinforced concrete beams using ultra high performance fibre reinforced concrete (uhpfr). *Engineering Structures*, 106:370–384, 2016.
- [38] Victor C Li. Engineered cementitious composites (ecc)-tailored composites through micromechanical modeling. 1998.
- [39] Richard Malm. *Predicting shear type crack initiation and growth in concrete with non-linear finite element method*. PhD thesis, KTH, 2009.
- [40] Giovanni Martinola, Alberto Meda, Giovanni A Plizzari, and Zila Rinaldi. Strengthening and repair of rc beams with fiber reinforced concrete. *Cement and concrete composites*, 32(9):731–739, 2010.
- [41] N Mitra, LN Lowes, et al. Factors influencing analytical continuum simulation of three-point bend test of a concrete notched beam. In *de The 14th World Conference on Earthquake Engineering, Beijing-China*, 2008.
- [42] Amir Mofidi, Sébastien Thivierge, Omar Chaallal, and Yixin Shao. Behavior of reinforced concrete beams strengthened in shear using l-shaped cfrp plates: Experimental investigation. *Journal of composites for construction*, 18(2):04013033, 2014.
- [43] Shozab Mustafa. Analytical and numerical study of arch action in t-beam bridges. 2019.
- [44] Vu Hong Nghiep. *Shear design of straight and haunched concrete beams without stirrups*. Technische Universität Hamburg, 2011.
- [45] Mohammadali Rezazadeh, Inês Costa, and Joaquim Barros. Influence of prestress level on nsm cfrp laminates for the flexural strengthening of rc beams. *Composite Structures*, 116:489–500, 2014.
- [46] Jan G Rots. Smearred and discrete representations of localized fracture. In *Current trends in concrete fracture research*, pages 45–59. Springer, 1991.
- [47] JG Rots. Comparative study of crack models. *Finite Elements in Civil Engineering Applications*, pages 17–28, 2002.
- [48] MAA Saafan. Shear strengthening of reinforced concrete beams using gfrp wraps. *Acta Polytechnica*, 46(1), 2006.
- [49] Abdul Aziz Abdul Samad, Noridah Mohamad, Noorwirdawati Ali, J Jayaprakash, and Priyan Mendis. Rehabilitation of continuous reinforced concrete beams in shear by external bonding of carbon fiber reinforced polymer strips for sustainable construction. In *Key Engineering Materials*, volume 708, pages 49–58. Trans Tech Publ, 2016.
- [50] Reza Sarkhosh, Joost Walraven, and Joop den Uijl. Shear-critical reinforced concrete beams under sustained loading part ii: Numerical study. *HERON*, 60(3):207, 2015.
- [51] Shantanu Singh. Influence of interface and type of strain hardening cementitious composite (shcc) on crack control in shcc-concrete hybrid beams. 2019.
- [52] SN Sinha. *Reinforced concrete design*. Tata McGraw-Hill Education, 2014.
- [53] Tihitina Tilahun Teshome. Model uncertainty of non-linear finite element analysis of reinforced concrete beams without shear reinforcement: Examining the effect of modelling strategies and modes of failure. 2019.
- [54] Gideon PAG van Zijl and Leon de Beer. Sprayed strain-hardening cement-based composite overlay for shear strengthening of unreinforced load-bearing masonry. *Advances in Structural Engineering*, 22(5):1121–1135, 2019.

- [55] Frank J Vecchio and Michael P Collins. Compression response of cracked reinforced concrete. *Journal of structural engineering*, 119(12):3590–3610, 1993.
- [56] Christian Wagner, Nick Bretschneider, Beate Villmann, and Volker Slowik. Modeling of the bond between strain hardening cementitious repair layers and concrete substrate. In *3rd International RILEM Conference on Strain Hardening Cementitious Composites*, page 279, 2014.
- [57] Guan Wang, Caiqian Yang, Yong Pan, Fawang Zhu, Kai Jin, Kefeng Li, and Antonio Nanni. Shear behaviors of rc beams externally strengthened with engineered cementitious composite layers. *Materials*, 12(13):2163, 2019.
- [58] Jiaying Wei, Chang Wu, Yixin Chen, and Christopher KY Leung. Shear strengthening of reinforced concrete beams with high strength strain-hardening cementitious composites (hs-shcc). *Materials and Structures*, 53(4):1–15, 2020.
- [59] Yuguang Yang. Shear behaviour of reinforced concrete members without shear reinforcement: a new look at an old problem. 2014.
- [60] Kequan Yu, Yao Ding, Jiepeng Liu, and Yulei Bai. Energy dissipation characteristics of all-grade polyethylene fiber-reinforced engineered cementitious composites (pe-ecc). *Cement and Concrete Composites*, 106:103459, 2020.
- [61] Yongxing Zhang, Shu Bai, Qingbin Zhang, Xueming Zhang, et al. Failure behavior of strain hardening cementitious composites for shear strengthening rc member. *Construction and Building Materials*, 78:470–473, 2015.
- [62] Yongxing Zhang, Naoshi Ueda, Hikaru Nakamura, and Minoru Kunieda. Behavior investigation of reinforced concrete members with flexural strengthening using strain-hardening cementitious composite. *ACI Structural Journal*, 114(2):417, 2017.
- [63] Yongxing Zhang, Hui Peng, and Weihua Lv. Shear stress transfer model for evaluating the fracture behaviour of shccs for rc shear strengthening. *Magazine of Concrete Research*, 70(10):512–518, 2018.
- [64] Y.X. Zhang, N. Ueda, Y. Umeda, H. Nakamura, and M. Kunieda. Evaluation of shear failure of strain hardening cementitious composite beams. *Journal of Bridge Engineering*, 16(5):577–584, 2011. doi: 10.11532/structcivil.57A.908.
- [65] Zhichao Zhang and Cheng-Tzu Thomas Hsu. Shear strengthening of reinforced concrete beams using carbon-fiber-reinforced polymer laminates. *Journal of composites for construction*, 9(2):158–169, 2005.
- [66] Jiajia Zhou, Jinlong Pan, and Christopher KY Leung. Mechanical behavior of fiber-reinforced engineered cementitious composites in uniaxial compression. *Journal of materials in civil engineering*, 27(1):04014111, 2015.
- [67] Jian Zhou, Shunzhi Qian, M Guadalupe Sierra Beltran, Guang Ye, Klaas van Breugel, and Victor C Li. Development of engineered cementitious composites with limestone powder and blast furnace slag. *Materials and Structures*, 43(6):803–814, 2010.